Study of additive's chemical structure effect on the control of fuel reactivity

Minh Duy Le

THESE DE DOCTORAT
DE L'UNIVERSITE DE LORRAINE
Préparée à
IFP ENERGIES NOUVELLES ET LRGP

Pour obtenir le grade de
DOCTEUR DE L'UNIVERSITE DE LORRAINE

ECOLE DOCTORALE N°608
Sciences et Ingénierie des Molécules, des Produits, des Procédés et de l'Énergie

Spécialité de doctorat : Génie des Procédés, des Produits et des Molécules

Par

MINH DUY LE

Portant sur

L'étude de l'influence de la structure chimique des additifs sur le contrôle de la réactivité des carburants

Travail présenté à Nancy, le 29 mai 2020

Composition du Jury

Laurent Catoire	Professeur, ENSTA Paris Tech, Institut Polytechnique de Paris	Rapporteur
Guillaume Vanhove	Maître de Conférences, PC2A, Université de Lille	Rapporteur
Nabiha Chaumeix	Directrice de Recherche, CNRS Orléans	Examinateur
Véronique Dias	Chercheuse qualifiée, Université catholique de Louvain	Examinateur
Fabrice Foucher	Professeur, PRISME, Université d'Orléans	Examinateur
Pierre-Alexandre Glaude	Directeur de Recherche, CNRS Nancy	Directeur de Thèse
Mickaël Matrat	Ingénieur de Recherche, IFP Energies Nouvelles	Encadrant IFPEN
Arij Ben Amara	Ingénieur de Recherche, IFP Energies Nouvelles	Encadrant IFPEN
Baptiste Sirjean	Chargé de Recherche, CNRS Nancy	Invité

Acknowledgements

The work presented in this manucsript was carried out thanks to a collaboration beween IFP Energies Nouvelles (IFPEN), Laboratoire Réactions et Génies des Procédés (LRGP), and Laboratoire Pluridisciplinaire de Recherche en Ingénierie des Systèmes, Mécanique, Énergétique (PRISME).

I would like to express my sincere appreciation to my supervisors at IFPEN, Dr. Mickaël Matrat, and Dr. Arij Ben Amara for giving me this opportunity to conduct this thesis. I am grateful for their help, their advice, their patience, and their positive attitudes to encourage me during my work.

I wish to show my deepest gratitude to my thesis director Dr. Pierre-Alexandre Glaude. His precious advice help me a lot to advance my work. I am also grateful for the warm welcome during my time at LRGP.

I would like to thank Professor Fabrice Foucher for his welcome and his guide during my time at PRISME. My thanks also go to Yi Yu and Bruno Moreau for their help to conduct my experiments at PRISME.

I would like also to thank Michèle Kuhwarth, Michel Chardin, and other people at IFPEN, LRGP, PRISME whose assistances were uncountable to my thesis.

My thanks also go to my friends, Luis Enrique Martinez Alvarado, Louise Ganeau, Vũ Đức Thạch Sơn, Trần Thị Thới, Trịnh Ngọc Tú, Nguyễn Mạnh Quân for sharing memorables moments with me.

After all, I wish to express my special regards to my parents, my sister, and my girl friend. Without their support I would not definitively finish my thesis. The sentence below is written in Vietnamese which is my native language so that they can fully understand my gratitude:

«Cám ơn mọi người vì tất cả »

Table of contents

Abbreviations

Φ	Equivalence ratio
BDC	Bottom dead center
BDPA	N,N'-di-sec-butyl-p-phenylenediamine
BHT	Di-tert-butyl-2,6-para cresol
CFD	Computational fluid dynamics
CFR	Cooperative fuel research
CI	Compression ignition
DCN	Derived cetane number
DIB-1	2,4,4-trimethyl-1-pentene
DTBPh	2,6-di-tert-butylphenol
E_a	Activation energy
EHN	2-ethylhexyl nitrate
EMC	Evaporation and Mixing Control
FAME	Fatty acid methyl esters
FCC	Fluid catalytic cracking
GCI	Gasoline compression ignition
HCCI	Homogeneous charge compression ignition
IAE	International Energy Agency
IC	Internal combustion
IDT	Ignition delay time
IPN	Isopropyl nitrate
IQT	Ignition quality testing
LLNL	Lawrence Livermore National Laboratory
LRGP	Laboratoire Réaction et Génie des Procédés
LTC	Low-temperature combustion
MMT	Tricarbonyl manganese methylcyclopentadienyl
MON	Motor octane number
MPRR	Maximum Pressure Rise Rate
NTC	Negative temperature coefficient
OPDA	N',N'-di-sec-o-phenylenediamine
OBHP	Octadecyl-3-(3,5-di-tert-butyl-4-hydroxyphenyl) propionate
P	Pressure
PAH	Polycyclic aromatic hydrocarbon
P_c	Compression pressure
PFR	Plug flow reactor
PRF	Primary reference fuel
PSR	Perfectly stirred reactor
RCM	Rapid compression machine
RMG	Reaction mechanism generator
RON	Research octane number
ROP	Rate of production
SACI	Spark assisted compression ignition
SI	Spark-ignition
ST	Shock tube
T	Temperature
T_c	Compression temperature
TDC	Top dead center
TEGDN	Tetraethylene glycol dinitrate
TEL	Tetraethyl lead
TMT	Tetramethyl tin
TPP	triphenylphosphine

Chapter 1: Introduction

1.1 Generalities about engine-fuel adequacy

According to the reference scenario of the International Energy Agency (IAE), the global demand for energy is expected to increase by 40% between 2007 and 2030 [1]. Fossil fuels will account for more than three-quarters of the demand increase. Half of the consumption of this energy source is dedicated to transport. In this sector, the internal combustion (IC) engine actually remains a major application (around 97%). Its use is related to a societal issue of first order: the pollutant emissions. Three main areas are being explored to mitigate the emissions: the search for an innovative combustion system; the optimization of engine performance; and the addition of a bio-based increasing neutral CO_2 emissions.

Two conventional IC engines are spark-ignition (SI) engine and compression ignition (CI) engine. The CI engine is powered by compression [2]. The combustion begins, following the injection of the fuel, by self-ignition thanks to the high temperatures and pressures in the combustion chamber. To do this, a significant compression rate is required. The operating principle of the conventional SI engine, whose injection is indirect, is different from that of the CI engine. The fuel is premixed with air and then injected into the combustion chamber [2]. In the SI engine, combustion begins when the compressed mixture of air and fuel is ignited by a spark. These two conventional engine possess undeniable advantages but face increasingly restrictive limitations to improve efficiency while limiting emissions [3, 4].

To overcome the main drawbacks of conventional IC engines, low-temperature combustion (LTC) [5] has proved to be a promising method to increase engine efficiency. LTC is studied in diverse forms such as homogenous charge compression ignition (HCCI) [6], gasoline compression ignition (GCI) [7], reactivity controlled compression ignition (RCCI) [8], spark assisted compression ignition (SACI) [9], etc.. The development of these new combustion systems aims to take advantage of the benefits of each traditional engine while pushing the operating limits of thermal engines.

Fuel-engine adequacy is the key parameter to increase the engine performance while getting a benefit from an emissions reduction. Specifically, the reactivity is one of the most important characteristic of fuels ensuring the fuel-engine adequacy. An example of project on engine fuel adequacy is "Co-optima" [10] which is ongoing in the United States (US). This project involves academic partners and transport manufacturers. It aims to assess the key properties of fuels affecting the engine performance. This guides the combustion system developments by considering fuel formulation. This task is actually a major item because of the higher volume of various alternative fuels. These fuels come from, for example, plants, food waste and from processes such as Fisher-Tropsh [11] or hydrotreatment of vegetal oils (HVO). These alternative fuels are responsible for potentially significant changes in fuel reactivity. As a result, the fuel formulation must evolve to meet the fuel-engine adequacy.

1.1.1 Standards for fuel reactivity

Fuel remain reactive in both liquid and gas phase. Before being consumed by the combustion in the engine, the fuel reactivity through its stability is of first order. Fuel can oxidize in the liquid phase in several places such as the tank, the fuel circulation system or the injector under different pressure and temperature [12]. The incorporation of biofuels such as fatty acid methyl esters (FAME) can reduce the oxidation stability of fuel. The autoxidation of fuel results in undesirable products, including deposits. The last compounds can reduce engine performance by affecting several components of engine such

as the pump, the injector filtering system (see Figure 1), etc.. Additionally, deposits can affect the combustion of fuels. Kupoyama et al. [13] observed that deposits are responsible for pre-ignition in a low-speed, high-load SI engine.

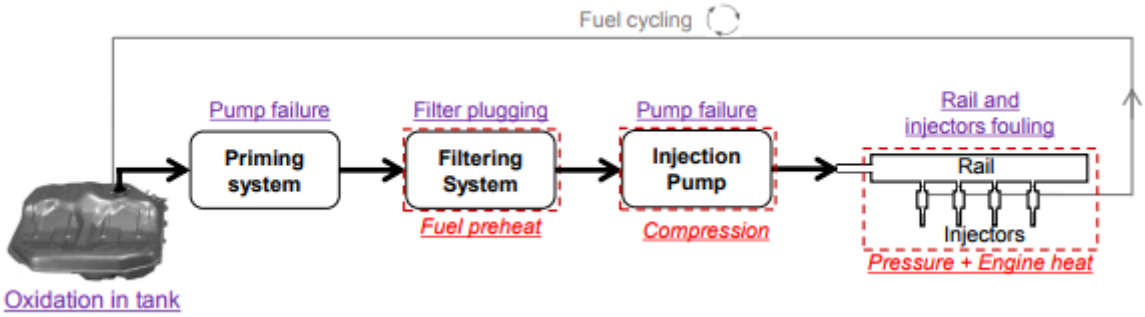

Figure 1: Impact of deposits on engine operation [14].

In the combustion chamber in engines, the gas-phase reactivity of fuels need to be carrefully controlled. The fuel employed in CI engines must be prone enough to self-ignition, i.e. have high gas-phase reactivity. On the otherhand, to prevent undesired combustion phenomenon such as knock and/or pre-ignition, the gas-phase reactivity of fuel used for SI engines are necessarily low. Besides, the commercialization of LTC engines is still limited due to the incomplete control of combustion. For example, the combustion phasing of the HCCI engine is difficult to manage when operating at variable loads and speeds [15]. Engine developments regarding gasoline combustion also investigate lean operation. This combustion mode operates at low temperatures, which can result in low nitrogen oxides (NO_x) and soot emissions. The main disadvantages of lean combustion are over-frequent misfire and engine instability [16]. All these above techniques expect an in-depth comprehension of fuel chemical reactivity since the fuel itself controls the auto-ignition which remains a key parameter for combustion emissions.

To facilitate the fuel formulation, some standards considering fuel reactivity has been employed. The induction period is one of the characteristic parameters often used to assess the oxidation stability of fuels. This parameter is the time that it takes for hydroperoxides and oxidation products to begin to accumulate (see Figure 2). For practical use, the induction period is a period during which a quantity of fuel or oxidant has been consumed by liquid-phase oxidation. This parameter is measured by several experimental methods such as autoclave [14], Rancimat [17] or PetroOxy [18] .

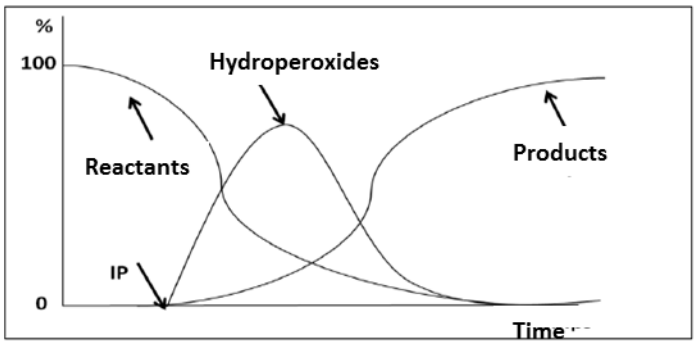

Figure 2: Simplified representation of hydroperoxide and oxidation products formation during the autoxidation of fuels [12].

To regulate the gas-phase reactivity of fuels, two standard measurements named as cetane number and octane number are employed for CI engines and SI engines respectively. The fuel used for Ci

engines is known as diesel fuel. The cetane number of diesel fuel is obtained by comparing, on a standardized engine, the behavior of the fuel with that of two reference hydrocarbons: hexadecane (cetane number of 100) and 1-methylnaphthalene (cetane number: 0). A fuel has an cetane number of "X" when it has the same self-ignition property as a mixture of "X" % vol. of *n*-cetane and (100-X) % vol. of 1-methylnaphthalene. Currently, 1-methylnaphthalene is replaced by 2,2,4,4,6,8,8-heptamethylnonane (isocetane) with a cetane number of 15. The minimum value of the cetane number of commercial diesel fuels varies with different countries (or regions) and are presented in Table 1.

Table 1 : Mimimum values of the cetane number in different geographic areas

Region	Minimum value of cetane number	Standard
Europe	51	EN 590 [19]
North America	40	ASTM D975 [20]

The cetane number is an important indicator of diesel fuel quality. The higher the cetane number, the shorter the auto-ignition time. The last parameter is the time between the injection of fuel and the first identifiable increase in pressure in the engine combustion chamber [2]. Suppes et al. [21] concluded that the engine operating with fuels having a high cetane number started easier in cold conditions and produced less NO_x. Indeed, the diesel fuel with lower cetane number makes the auto-ignition period longer. The long auto-ignition delay promotes the homogenization stage of the fuel in the combustion chamber. The longer homogenization generates a high temperature that favors the formation of NO_x.

The standard method for measuring a fuel's cetane number is EN ISO 5165/ ASTM D613 [22]. A four-stroke, single-cylinder, indirect injection engine is used in this method. The engine is called cooperative fuel research (CFR) engine. This engine operates at a constant speed (900 rpm) and its compression rate ranges from 8 to 36. This method is suitable for measuring diesel fuels with a cetane number between 30 and 65. A similar method to ASTM D613 is the DIN 51773 method [23]. This method is widely used in Europe. Like the ASTM D613, a four-stroke, single-cylinder, indirect injection engine is used in this method. The engine also operates at a constant speed (1000 rpm) and its compression rate is set at 18.2. The measurable range of cetane number is from 40 to 75. The disadvantages of these two previous methods are their high cost of operation and a large amount of fuel used for each measurement. Due to these reasons, different alternative methods have been developed. They are based on measures of derived cetane number (DCN). The principle of these methods is to measure the time it takes for a fuel to self-ignite in a constant volume combustion chamber. Then, the cetane number of the targeted fuel is deducted by correlations. Currently, there are three standardized DCN methods: ignition quality testing (IQT) known as EN 15195/ASTM D6890 [24], fuel ignition testing (FIT) known as EN 16144/ASTM D7170 [25], cetane ignition delay (CID) known as EN 16715/ASTM D7668 [26].

Gasoline fuel are used for SI engines. The quality of a gasoline fuel related to its gas-phase reactivity is represented by its octane number. The development of SI engines deals with several abnormal combustion phenomena such as pre-ignition and engine knocking. These undesirable phenomena limit potential gains in the efficiency associated with down-sizing engines [27]. Pre-ignition is defined as the self-ignition of the load before the action of the engine spark plug. In the literature, the origin of this phenomenon is associated with the presence of a hot spot that can be generated for example by the projection of incandescent deposits into the combustion chamber [13]. Other mechanisms are mentioned, such as the intake of a lubricant/fuel mixture that can generate early self-ignition [28]. The role of fuel in this process is still not clear, but the literature highlights correlations between certain fuel properties and the appearance of pre-ignition. Regarding the knocking, this phenomenon is

related to the self-ignition of some of the fresh gases outside the envelope of the flame front. It results from a local increase in pressure and temperature that allows the air-fuel mixture to self-ignite. These abnormal combustion phenomena are the cause of motor incidents that can go as far as breaking [2]. Therefore, the gasoline used for SI engines must resist the self-ignition, i.e., its octane number must be high (> 95).

There are two types of octane number: research octane number (RON) and motor octane number (MON). The RON and MON values of a fuel are obtained by comparing the reactivity of the target fuel with that of a mixture of two reference hydrocarbons: *n*-heptane and 2,2,4-trimethylpentane also called isooctane. For example, a fuel has an octane number (RON or MON) "X" when it has the same resistance to self-ignition as a mixture consisting of X% vol. of isooctane and (100-X) % vol. *n*-heptane. Generally, the RON and MON values of a fuel are different and are not sufficient to predict the trend of this fuel in terms of the appearance of engine knock [29]. For this reason, alternative parameters have been proposed in the literature. For example, the OI (Octane index) is defined by:

$$OI = (1 - K) \times RON + K \times MON \qquad (Eq. 1)$$
$$OI = RON - K \times S$$

with :

- S = RON –MON, the sensitivity of fuel
- K: an engine and operating condition dependent coefficient

The K and S values depend solely on the operating conditions of the engine. For supercharged engines, K takes a negative value between 0 and -1 [30]. The value of S is often between 6 and 13 [2].

The RON and MON values of a fuel are measured on a CFR engine using two standard methods: the ASTM D2699/EN ISO 5164 method [31] and the ASTM D2700/EN ISO 5163 method [32] respectively. The differences between these two methods are the intake air temperature and the engine speed. These last two values for MON measurement are 149 °C and 900 rpm. They are much higher than those for RON measurement: 52 °C and 600 rpm, which are thus linked to less severe conditions.

To sum up, standards are employed to regulate fuel reactivity in both liquid and gas phases. The induction period represents the oxidation stability of fuels. Cetane number and octane number indicate the reactivity quality of diesel fuel and gasoline fuel respectively in the gas phase.

1.1.1. Use of fuel additives

Nowadays, engine development is focusing on new innovative engines and alternative biofuels. Fuel combustion should maximize engine efficiency while reducing exhaust emissions. Chemical reactivity is one of the key parameters that must be carefully taken into account to formulate fuels. It needs to be adjusted to suit the application. For diesel fuel, a high cetane number (> 51) is desired i.e., it is necessary to increase its gas-phase reactivity. On the other hand, for gasoline fuel, its octane number must be high (RON > 95) to avoid undesirable phenomena such as engine knock and potentially pre-ignition. Oxidation stability is also an important criterion to evaluate fuel quality. Over time, fuels can oxidize during several phases: storage, transport or even supply to the combustion chamber via the injection system [2]. Fuel autoxidation results in the formation of undesirable products such as oxygenated molecules, deposits, gums, etc. [12]. These products can damage the engine fuel distribution system [33] or induce abnormal combustion [13]. Thus, fuels must be resistant to autoxidation, i.e. the reactivity of fuels in the liquid phase must be weakened.

As a result, the fuel formulation must evolve to meet the fuel-engine adequacy. To do this, there are two global methods: (1) the modification of the base fuel and (2) the use of additives. The first method must take into account the introduction of variable chemical constituents, especially with different biofuels depending on geographical origin and policy choices. The former method is therefore expensive and complex. The latter method is more relevant. Indeed, the use of additives is the solution that has been preferred for several decades to address the diversification of fuels and even to improve their properties. For example, 2-ethylhexylnitrate (EHN) has been used since the 1970s to increase the diesel fuel cetane number [34]. Antioxidants such as di-tert-butyl-2,6-para cresol (BHT) [35] are added to fuels to prevent their degradation over time. The advantage of using additives is therefore undeniable but complex in a context where the fuel-engine adequacy must be continuously optimized.

In order to control fuel reactivity, several additives can be used. An additive usually refers to a molecule exhibiting an effect at very low concentration. This doping level is generally lower than 1% mol. To better understand the impact of additives on fuel reactivity, it is necessary to consider the possible effects on the gas-phase reactivity over a wide range of temperatures. Once in the combustion chamber, the fuel undergoes a rapid rise in pressure and temperature that helps to increase sharply its reactivity. A radical mechanism is followed [12, 36]. A similar mechanism is actually reported for liquid phase oxidation [12] and for low-temperature gas phase combustion [36]. This implies that additives dedicated to one phase could impact the other on several aspects. Literature is limited on these "multi-effects" of additives as the additive use remains mostly on trial and error approach. The efficiency of additives depends also on the fuel and the presence of contaminants or other additives. Indeed, more than 20 types of additives are likely to be added to fuels [33] and potential antagonistic or synergistic effects could be observed.

From a chemical point of view, not every molecule can be used as an additive. In the literature, when considering reactivity enhancing or inhibiting additives, some chemical functions are identified. Some alkyl nitrates are used as cetane boosters [37] while many hindered phenols are employed as antioxidants [38]. For example, the effect of the cetane booster EHN is reported in the literature by Ghosh et al. [39]. This study confirms that the effect of EHN on the cetane number of diesel fuel depends not only on its concentration but also on the reactivity of the base fuel (see Figure 3). However, there are few robust kinetic models which can properly simulate the effects of this additive. Figure 4 shows the effect of EHN on the combustion of a reference fuel, which is a *n*-heptane/isooctane mixture [40]. It presents the ratio between the ignition delay times (IDT) of the doped and neat fuels. It is observed that the simulation-experiment agreement is unsatisfactory. This indicates that the kinetic model of this additive has to be improved for further applications such as Computational fluid dynamics (CFD) simulations of engines.

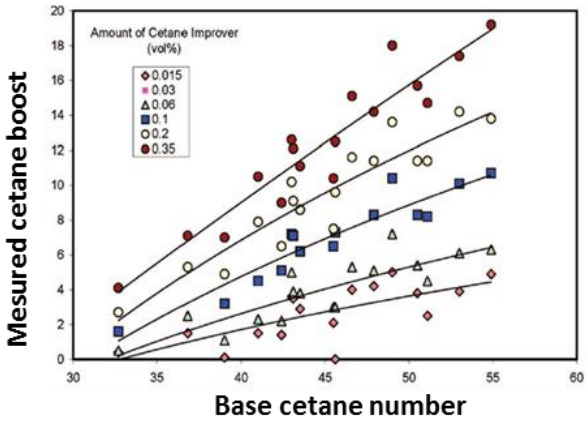

Figure 3: EHN Cetane boosting effect of EHN on different initial cetane numbers of diesel fuels [39].

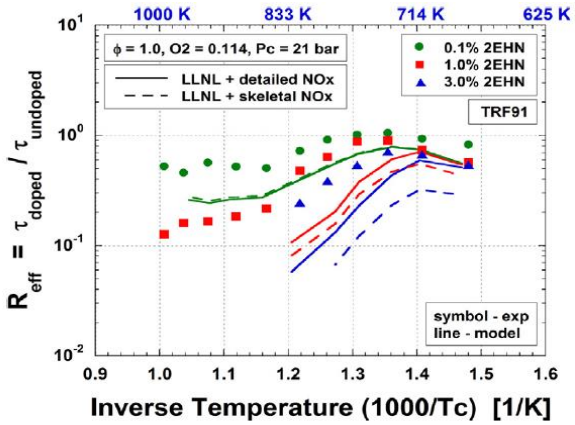

Figure 4: Simulation of the inhibiting effect of EHN on the IDT of a reference fuel (a *n*-heptane/isooctane mixture) with a detailed kinetic model [40].

Consequently, fundamental experimental data about the effect of fuel additives are required not only to approach real engine operating conditions but also to explore the additive effect on different thermodynamic conditions and with different fuels.

1.2 Objective of the study

Understanding the chemical effect of additives is necessary to improve their efficiency and even to provide additional means to develop new combustion systems with alternative fuels. In this context, this thesis aims to (1) better understand the chemical effect of fuel additives; and (2) estimate some potential effects of additives in various thermodynamic conditions and base fuels thanks to the developed and validated kinetic models. The former task includes establishing effective experimental and numerical methods to investigate the chemical effect of fuel additives.

To achieve the objective, this thesis consists of four steps.

First, a literature study is carried out to identify additives that have significant effects on fuel reactivity in both the gas and liquid phases. This step also enables choosing a reference fuel in which the potential effects of these additives are studied.

Then, a detailed kinetic model is developed to model the effect of additives on the gas-phase reactivity of the reference fuel. This step is carried out by the data assembly from the literature and establishment of dedicated sub-models.

In parallel, some experiments are conducted to exploit the effect of additives. Indeed, the gas-phase reactivity of fuel can be characterized by various parameters: the IDT as well as burning velocity. These parameters must be carefully considered to optimize the engine performances regardless of the engine type. For example, in a compression ignition engine, a fuel with a short IDT is preferred to promote the start of combustion. At the same time, fuels used in a spark-ignition engine must resist enough to the self-ignition and their flame velocity must be sufficiently high to avoid detonations in the engine. The experimental devices used in this thesis are therefore a shock tube (ST) as well as a rapid compression machine (RCM) to measure the IDT of fuels over a wide range of temperatures. Additionally, the laminar burning velocity of the fuel is measured in a flat flame burner. The experiments in the burner were conducted by Matieyendu Goussougli [41], an intern at Laboratoire

Réaction et Génie des Procédés (LRGP) in Nancy, France. The obtained experimental results help to validate the developed kinetic models in this thesis.

The chemical effect of additives on the combustion properties including the ignition delays and the flame speed is eventually characterized.

This manuscript consists of six chapters. Following this introduction, the chapter two is dedicated to presenting the state of the art on the use of fuel additives in both gas and liquid phases. The selection of the surrogate fuel and the additives to be studied is discussed in the chapter three. The considered experimental methods are also shown. The development of the detailed kinetic model is described in the chapter four. Then experimental and numerical results obtained during this thesis are illustrated in the chapter five. The validated kinetic model is used to predict the effect of the investigated additives on different base fuels in various conditions.

Chapter 2: Literature study

2.1 Chemical mechanism of fuel oxidation

The liquid-phase oxidation mechanism involves a radical mechanism similar to one of the gas-phase oxidation. The two mechanisms are described in this section.

2.1.1 Liquid-phase oxidation

The oxidation stability of fuel is one of the major concerns for engine-fuel adequacy [14]. In the liquid phase, the slow oxidation of fuels can impact their physical-chemical properties. Indeed, this phenomenon leads to the formation of oxygenated products such as acids or alcohols which can transform into deposits. Formed deposits can damage the fuel distribution and injection systems. They can also initiate abnormal combustion by delivering particles with variable physicochemical properties into the combustion chamber. Figure 5 demonstrates the predominant role of peroxide decomposition in the liquid-phase reactivity of fuel.

- Initiation :

$$RH \xrightarrow{Initiator} R\bullet$$

$$ROOH \rightarrow RO\bullet + HO\bullet$$

$$2ROOH \rightarrow ROO\bullet + RO\bullet + H_2O$$

- Propagation :

$$R\bullet + O_2 \rightarrow ROO\bullet$$

$$ROO\bullet + RH \xrightarrow{abstraction} ROOH + R\bullet$$

$$ROO\bullet + RH \xrightarrow{addition} ROOR + H\bullet$$

$$ROOH \xrightarrow{decomposition} alcohols, carbonyls, epoxides, olefins, free\ radicals \ldots$$

- Termination :

$$R\bullet + R\bullet \rightarrow Products$$

$$R\bullet + ROO\bullet \rightarrow Products$$

$$ROO\bullet + ROO\bullet \rightarrow Products$$

Figure 5: Simplified mechanism of the liquid-phase oxidation of hydrocarbon [12].

The initiation step of autoxidation corresponds to the departure of a hydrogen atom from the parent hydrocarbon to form a free radical. This step has several sources: thermal decomposition, a reaction with a chemical initiator (e.g. metal ions) or radiation. If hydroperoxides already present in the fuel, they can break down into free radicals and contribute to the initiation stage. Subsequently, the propagation stage consists of the formation and the decomposition of hydroperoxides to form oxidation products such as alcohols, carbonyls, epoxides, etc. Finally, the termination step represents the recombination of free radicals to form stable products which potentially contribute to the formation of fuel deposits.

2.1.2 Gas-phase oxidation

The combustion of hydrocarbons in the gas phase follows a radical mechanism. Generally, three combustion regimes corresponding to three temperature intervals: low (T < 800 K), intermediate (800 -950 K) and high (T > 1000 K), are often presented to describe the combustion of hydrocarbons.

Combustion at low température (T < 800 K)

Figure 6 represents the simplified oxidation scheme of alkanes. In this temperature range, the initiation stage is an H-atom abstraction reaction by oxygen to form a radical R and HO_2. Then, the radical R can react with oxygen to form a peroxyl radical ROO. The last radical can form hydroperoxide species symbolized as QOOH by isomerization reactions which are in this case related to the migration of a hydrogen atom. These QOOH molecules can follow several types of reactions to produce oxygenated compounds and lighter radicals. The formation of hydroperoxides is a key step of combustion at this range of temperature because they feed the radical pool by releasing OH and other small radicals thanks to its degenerate branching steps.

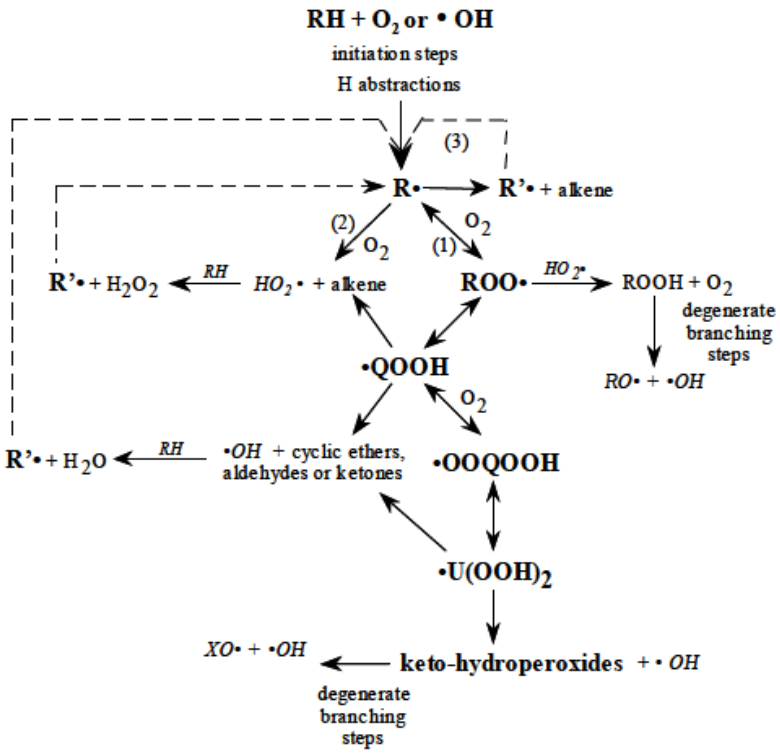

Figure 6: Simplified oxidation scheme of alkanes at low temperature(T < 800K) [36]

Combustion at intermediate temperature (800 K < T <950 K)

Under this condition, it is observed that the IDT, i.e., the reactivity of alkanes decreases with temperature. This phenomenon is named as Negative Temperature Coefficient (NTC). It is the result of the displacement of the thermochemical equilibrium R + O_2 = ROO back to the formation alkyl radical, which then reacts principally to form alkenes and cyclic ethers (see Figure 6). The formation of hydroperoxides decreases sharply. For this reason, the reactivity of hydrocarbons decreases.

This combustion behavior, which is specific to alkanes and molecules containing alkyl chains, is not representative for all hydrocarbons, for example, toluene does not have a NTC zone [42]. The toluene molecule is very stable thanks to the aromatic ring. It is seemly unreactive at low temperatures (T < 750 K) [43]. NTC behavior is then not observed for this molecule.

Combustion at high temperature (T > 1000 K)

At high temperatures, the break of C-C bonds is favored, which leads to the formation of small molecules. In addition to the reaction RH + O_2 = R + HO_2, the initiation steps include the unimolecular decomposition of the initial hydrocarbon: RH = R' + R ''. Under this condition, the chain-branching reaction H + O_2 = OH + O is responsible for the reactivity of hydrocarbons.

2.2 Effect of additives on the reactivity of fuels

In order to control the fuel reactivity, additives are employed. Their doping level is low (less than 1% mol.). This part presents the state of the art of the use of fuel additives in both gas and liquid phases.

2.2.1 Use of fuel additives in liquid phase

To improve the oxidation stability of fuel, several types of antioxidants are employed. Depending on their mode of action, they are divided into three groups: free radical scavengers, hydroperoxide decomposers, and metal deactivators. The first two types of antioxidants are used to reduce the reactivity of peroxy ROO radicals and ROOH hydroperoxides, i.e. to slow down of the propagation stage of the autoxidation of fuel. The last type of antioxidant is able to disable metal ions and thus to limit the initiation step of the autoxidation of fuels containing traces of metals.

2.2.1.a Free radical scavenger

The mode of action of free radical scavengers (AH) is presented in Figure 7. First, the antioxidant AH reacts with peroxy radicals ROO to form the corresponding hydroperoxides and the radical A. This step prevents the reaction between the parent fuel RH and radicals ROO. Therefore, the formation of radicals R, which is a key player in the liquid-phase oxidation of fuel, is limited. Then, the new radical A can react with oxygen to give a radical peroxy AOO. This radical can react with either HR, AH or another radical AOO to form stable products. The reaction of AOO with HR limits the efficiency of the antioxidant because it also contributes to the formation of radical R.

$$
\begin{aligned}
AH + ROO\bullet &\rightarrow ROOH + A\bullet \\
A\bullet + O_2 &\rightarrow AOO\bullet \\
AOO\bullet + RH &\rightarrow AOOH + R\bullet \\
AOO\bullet + AH &\rightarrow AOOH + A\bullet \\
AOO\bullet + AOO\bullet &\rightarrow produits\ stables
\end{aligned}
$$

Figure 7: Simplified mechanism of free radical scavengers [44].

The antioxidants that follow this mode of action must have a labile hydrogen atom to facilitate the reaction with ROO• radicals. Thus, the most common chemical compounds used free radical scavengers are substituted phenols and aromatic amines. Nagpal et al. [35] studied the effect of some phenolic and amine antioxidants: N,N'-di-sec-butyl-p-phenylenediamine (BPDA), N',N'-di-sec-o-phenylenediamine (OPDA), BHT, 2,6-di-tert-butylphenol (DTBPh) in cracked naphthas (see Table 2) (naphtha is a petroleum cut obtained by the distillation of crude oil). The doping levels of the additives were between 10 and 60 ppm. The induction period of fuels was measured by the ASTM D525 method [45]. The result showed that these additives actually increased the induction period of fuels by 300 to 2000 minutes. It was also observed that the efficiency of antioxidants depended on the base fuel. BPDA

was more effective for fluid catalytic cracking (FCC) naphtha A and BHT, on the other hand, was more effective for visbreaking naphtha B.

Table 2: Composition of the neat fuels investigated in the study of Nagpal et al.[35] and efficiency of antioxidants

Characteristic	FCC naphtha A	FCC naphtha B	Visbreaking naphtha A	Visbreaking naphtha B	Coker naphtha
Composition of neat fuel (% vol.)					
- Aromatic	9.4	4.9	7.2	5.3	4.3
- Olefin	64.9	61.9	36.6	42.9	47.3
- Saturated hydrocarbons	25.7	33.2	56.2	51.8	48.4
Induction period of neat fuel (min)	104	22	39	108	131
Additive dose required to raise the induction period to 480 min (ppm)					
- BDPA	15.0	46.5	77.0	21.0	7.5
- OPDA	26.5	40.5	>80.0	>80.0	11.0
- BHT	20.0	48.6	37.5	10.0	18.0
- DTBPh	23.5	61.5	24.0	11.0	9.0

The performance of free radical scavengers depends on temperature. This observation was confirmed by the study by Diaby et al. [46]. These authors tested the effect of an antioxidants named octadecyl-3-(3,5-di-tert-butyl-4-hydroxyphenyl) propionate (OBHP) in squalane. The last compound is an iso-alkane whose raw formula is $C_{30}H_{62}$. Without additives, the autoxidation of the squalane at 180°C did not present an induction period for a 60-hour test. By adding OBHP at a doping level of 0.5 % vol., a 20-hour induction period was observed (see Figure 8.a). On the other hand, this induction period disappeared at a higher temperature (205°C) (see Figure 8.b). This can be explained by the stability of antioxidants. At high temperatures, antioxidants decompose to form free radicals which promote the fuel autoxidation.

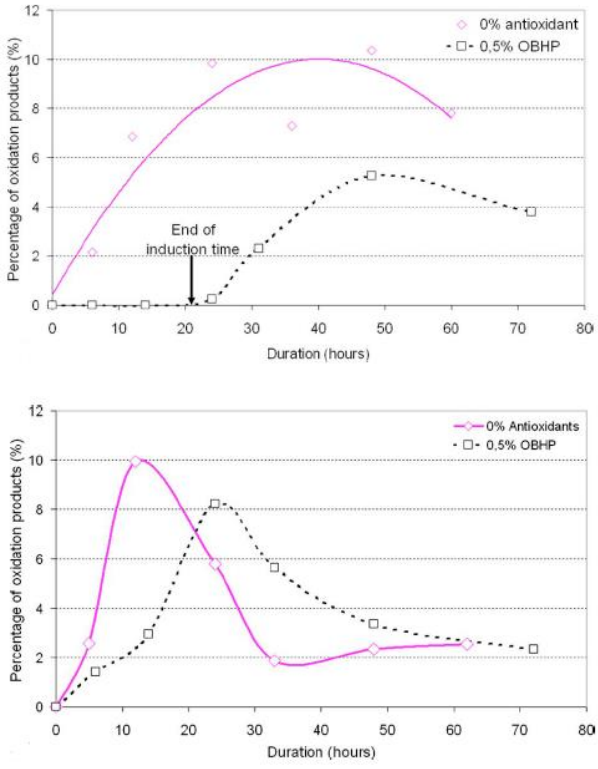

(a)

(b)

Figure 8: Effet of OBHP on the autoxydation of squalane at (a) 180°C et (b) 205°C. This figure is adopted from the work of Diaby et al. [46]

The result of the above study also suggests the potential impact of free radical scavengers on the combustion of fuels. As the temperature of the combustion chamber is much greater than the one of the fuel distribution and injection systems, this type of antioxidants may modify the gas-phase reactivity of the fuel.

McCormick et al. [47] studied phenolic antioxidants that could replace BHT as 4-methylanisole, phenol, p-cresol, 2.4-xylenol, guaiacol, 4-methylguaiacol, 4-methylacetophenone, 4-propylphenol and 4-propylguaicol. These additives can be produced from lignocellulosis-biomass, which is a natural source. It was observed that 2,4-xylenol was the most effective antioxidant. This compound slightly improved the fuel octane index (from 85.8 to 89 at a doping level of 2% vol.). Further experimental studies need to be carried out to figure out the impact of free radical scavengers on the ignition property of fuel.

2.2.1.b Hydroperoxide decomposer

The mode of action of hydroperoxide decomposers (symbolized as A) is presented below [48] :

$$A + ROOH \rightarrow A = O + ROH$$

This type of antioxidant slows down the autoxidation of fuels by reacting with hydroperoxides formed by the parent fuel. The most well-known hydroperoxide decomposers are phosphines (PR_3), phosphites ($P(OR)_3$), tertiary amines (NR_3), and sulphides (R_2S) [48, 49]. The global reactions of these additives with hydroperoxide are presented in Table 3.

Table 3: Global reaction representing the antioxidant characteristic of some hydroperoxide decomposers

Antioxidant	Reaction
Phosphine	$PR_3 + ROOH \rightarrow O = PR_3 + ROH$
Phosphite	$P(OR)_3 + ROOH \rightarrow O = P(OR)_3 + ROH$
Amine tertiaire	$NR_3 + ROOH \rightarrow O = NR_3 + ROH$
Sulfide	$SR_2 + ROOH \rightarrow O = SR_2 + ROH$

Tommaso et al. [48] studied the effect of triphenylphosphine (TPP) on the autoxidation of diethyl ether. The experiments were carried out in an autoclave at 100°C. The efficiency of this additive was compared to that of BHT, which is a conventional antioxidant. The results showed that TPP was much less effective than BHT. Generally, the doping level of TPP needed to be about 100 times larger than one of BHT to obtain a similar effect.

Zabarnick et al. [49] were interested in the antioxidant effect of hexyl sulfide. This additive was studied in two fuels: the Exxsol D110, which is a paraffinic petroleum cut, and the jet fuel F-2747. The liquid-phase oxidation of fuels was carried out in a spherical reactor at 140°C and 1 atm. Hexyl sulfide was introduced into fuels at a doping level between 3000 mg/L and 7000 mg/L. This antioxidant improved the oxidation stability of the jet fuel F-2747 (see Figure 9). On the other hand, it was ineffective for the solvent Exxsol D110 (see Figure 10). Then, BHT was introduced into the solvent D110 to study the interaction of hexyl sulfide with a substituted phenol because the jet fuel F-2747 contained a small amount of this type of compound. A synergistic effect was observed when both two additives (hexyl sulfide and BHT) were added to the solvent Exxsol D110 (see Figure 11). For this synergistic effect to be observable, the doping level of additives had to be high enough. For example, with BHT at 30 mg/L, the synergetic effect was observed only for a doping level of hexyl sulfide superior to 9900 mg/L (see Figure 12). Similarly, by keeping the concentration of hexyl sulfide at 10000 mg/L, the synergetic effect was observed only for a doping level of BHT higher than 20 mg/L (see Figure 13).

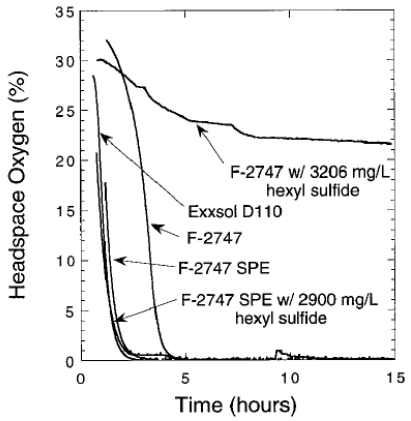

Figure 9: Headspace oxygen varying with time for the autoxidation of the jet fuel F-2747 with/without hexyl sulfide [49].

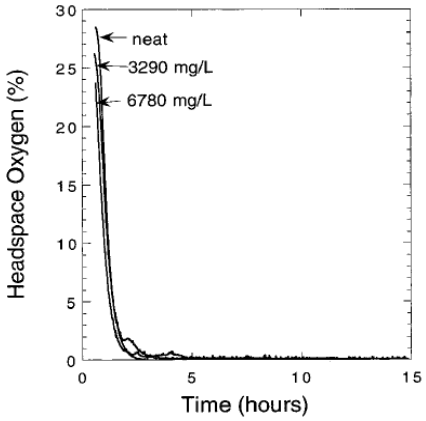

Figure 10: Headspace oxygen varying with time for the autoxidation of the solvent D110 with/without hexyl sulfide [49].

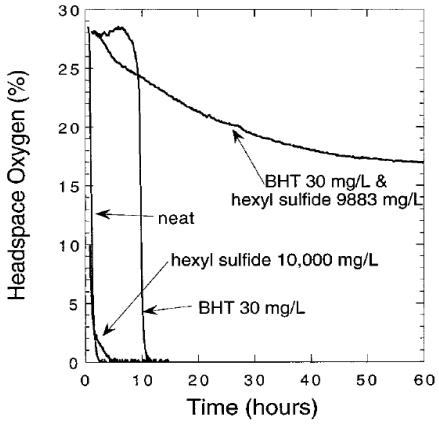

Figure 11: Headspace oxygen varying with time for the autoxidation of the solvent D110 with/without additives (hexyl sulfide and BHT) [49].

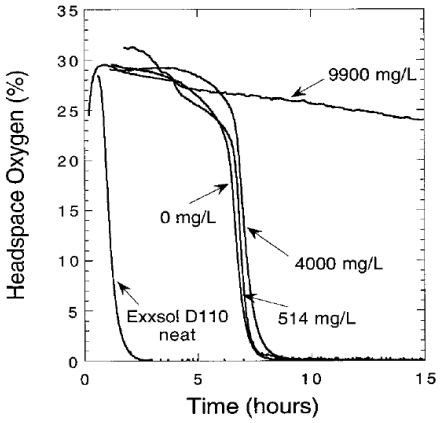

Figure 12: Headspace oxygen varying with time for the autoxidation of the solvent D110 with/without BHT (30 mg/l) at various doping levels of hexyl sulfide [49].

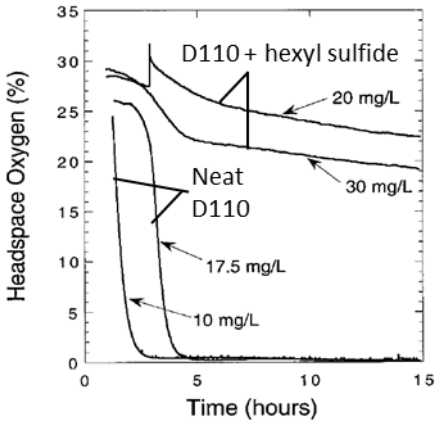

Figure 13: Headspace oxygen varying with time for the autoxidation of the solvent D110 with/without hexyl sulfide (10000 mg/l) at various doping levels of BHT.

Zabarnick et al. [49] also proposed a reaction mechanism to support their observations. The main reactions in the propagation stage of the liquid-phase oxidation of a hydrocarbon are:

$$(1)\ R\bullet + O_2 = ROO\bullet$$
$$(2)\ RH + ROO\bullet = R\bullet + ROOH$$
$$(3)\ ROOH = RO\bullet + OH\bullet$$

Without a free radical scavenger, the rate of the reaction (2) is faster than that of the reaction (3), so the global oxidation rate of a hydrocarbon depends little on the decomposition of ROOH. Therefore, the addition of a hydroperoxide decomposer (hexyl sulfide) is not effective in improving the oxidation stability of the solvent Exxsol D110. In the presence of a free radical scavenger, the rate of the reaction (2) is slowed down, so the global oxidation rate of a hydrocarbon depends much more on the rate of the reaction (3). Thus, the employment of hexyl sulfide, in this case, is very effective because this antioxidant would slow down the decomposition of hydroperoxides. The result of the study of Zabarnick et al. [49] shows that hydroperoxide decomposers are only effective in the presence of free radical scavengers.

2.2.1.c Metal deactivator

The oxidation stability of fuel may be affected by the presence of metals originating from several sources. Commercial fuels may already contain some traces of metals. In the engine, the lubricant additive package [50] and the aging of mechanical parts can also contribute to the amount of metals presented in fuel such as iron or copper. These metals, especially transition metals, catalyze the decomposition of hydrocarbons (noted as RH) and hydroperoxides (noted as ROOH) into free radicals [51]. As a result, metals diminish the fuel oxidation stability. The mode of action of metals on hydrocarbon autoxidation is presented below [51]:

(a) $$RH \xrightarrow{metals} R\bullet$$

(b) $$ROOH + M^{n+} \rightarrow RO\bullet + M^{(n+1)+} + OH^-$$

(c) $$ROOH + M^{(n+1)+} \rightarrow ROO\bullet + M^{n+} + H^+$$

In the case that the metal is a strong oxidizer, for example, Pb^{4+}, the reaction (b) is favored. On the other hand, if the metal is a strong reducing agent, for example, Fe^{2+}, the reaction (c) is supported. Transitional metals such as copper, cobalt, manganese, etc. can play an oxidizing and reducing role at the same time. Thus, in the presence of transition metals, reactions (a), (b) and (c) are simultaneously favored.

The impact of metal on the fuel autoxidation can be remarkable even at a very low amount (in the order of µg/l). Teixeira et al. [52] studied the effect of several metals as copper (Cu), iron (Fe), nickel (Ni), lead (Pb), zinc (Zn) on the oxidation stability of gasoline fuel. Metals were introduced into the fuel at a doping level from 0.25 to 3 g/l. The oxidation stability of fuel was evaluated by the method ASTM D381 [53], which measured the amount of deposits formed after a fixed storage period from a few days to a few weeks. Copper was observed to be the most active metal. The presence of this metal increased the amount of deposits (from 2 to 10 times) at all doping levels. The effect of iron was also remarkable. Meanwhile, nickel and zinc activities were limited and lead activity was negligible.

To avoid the harmful activity of metals on the oxidation stability of fuels, metal deactivators are used. The mode of action of metal deactivators is the chelation. This type of antioxidant forms complexes with metals in the fuel (see Figure 14), which limits the interaction between metals and hydrocarbon molecules.

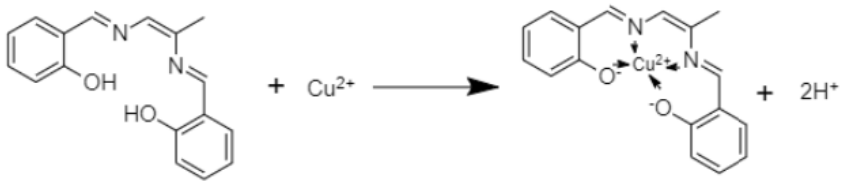

Figure 14: Reaction of N,N'-disalicylidine-1,2-propane diamine with copper cation[54].

2.2.1.d Conclusions

The three main types of antioxidants studied in the literature are free radical scavengers, hydroperoxide decomposers, and metal deactivators. The modes of action of these types of antioxidants are different.

The autoxidation of fuel in the liquid phase follows a radical mechanism similar as in the gas phase. It consists of three steps: initiation, propagation, and termination. Free radical scavengers and hydroperoxide decomposers influence the propagation stage, while metal deactivators impact the initiation stage.

Unlike free radical scavengers, hydroperoxide decomposers and metal deactivators are only effective under certain conditions. Hydroperoxide decomposer shows its efficiency only in the presence of a free radical scavenger and metal deactivator is effective if metals are incorporated into the target fuel. The efficiency of the antioxidant also depends on temperature and base fuels. However, the effect of these parameters remains little discussed in the literature.

Free radical scavengers are the most studied and commercially employed in daily life. As temperature influences the activity of free radical scavengers, this type of antioxidant potentially modifies the gas-phase reactivity of fuels. To our best knowledge, no detailed kinetic models were developed in the literature to address the issue. Thus, experimental and numerical investigations are necessary to better understand the impact of free radicals scavengers on the combustion of fuel.

2.2.2 Use of fuel additives in gas phase

To adjust the gas-phase reactivity of fuels, two types of additives has been employed: cetane boosters which can enhance the fuel reactivity, and octane boosters which are used to reduce the fuel reactivity. The following sections present the cetane boosters and octane boosters that have been studied in the literature.

2.2.2.a Cetane booster

Cetane boosters are chemical compounds being capable of increasing the cetane number of fuels. The formulation of an additive must incorporate several constraints [21] such as (a) its efficiency in improving ignition properties; (b) the risks associated with storage and transport; (c) the cost of using the additive. The two types of cetane boosters often studied in the literature are organic additives and nanoparticles.

Nanoparticle additives

Nanoparticles have been examined in the literature for their performance in improving the cetane number of diesel fuels. From a chemical point of view, nanoparticle additives are often metal oxides, for example, Al_2O_3 and CeO_2. The size of the nanoparticles is between 20 and 100 nm. In the literature studies, the doping level of nanoparticles is around 100 ppm.

Nanoparticles of aluminum oxide (nano Al_2O_3) have been the subject of several studies. Basha et al. [55] studied the effect of nanoparticles of aluminum oxide having a medium diameter of 51 nm in an emulsion containing 85% diesel and 15% water by volume. The addition of nano Al_2O_3 (from 25 to 100 ppm) increased the cetane number of the fuel-water emulsion from 5 to 7 units. Gumus et al. [56] determined that the doping level of nano Al_2O_3 (diameter of 27-43 nm) should be higher than 50 ppm to obtain a quantifiable effect (an increase of 0.5 units) on boosting cetane number of a diesel fuel having a cetane number of 53.8. In addition, Saraee et al. [57] observed that the addition of nano Al_2O_3 (diameter of 40 nm) slightly increased engine power. Another type of nanoparticle used as a cetane booster is cerium dioxide (nano CeO_2). Arul Mozhi Selvan et al. [58] examined the effect of 32-nm diameter CeO_2 nanoparticles (doping level of 25 ppm) in a diesel fuel whose cetane number was 46. This study showed a positive impact of nano CeO_2 on the cetane number of the diesel fuel.

The mode of action of nanoparticle cetane booster is little discussed in the literature. Saraee et al. [57] explained their experimental observation by the oxidation of carbon deposits thanks to Al_2O_3 nanoparticles. Nano Al_2O_3 contributes as an additional source of oxygen for the fuel combustion. The fuel IDT reduction by adding nanoparticle additives is explained by the homogeneity of fuel-air mixture enhanced with nanoparticles [59]. This type of compound promotes the atomization of diesel fuel by lowering the viscosity. Therefore, in the presence of nanoparticles, the fuel is better mixed with air and the combustion improved. The chemical effect of nanoparticles on combustion is little discussed and not clear in the literature [60]. Beside, a problem often encountered with nanoparticle additives is the instability of fuel-nanoparticle mixtures. Indeed, nanoparticles in the fuel can sediment over time. Gumus and at. [56] demonstrated the need for the use of a surfactant to enhance the stability of the diesel-A_2O_3 fuel mixture (see Figure 15). The addition of the Darvan-C surfactant could slow down the sedimentation rate of Al_2O_3 nanoparticles.

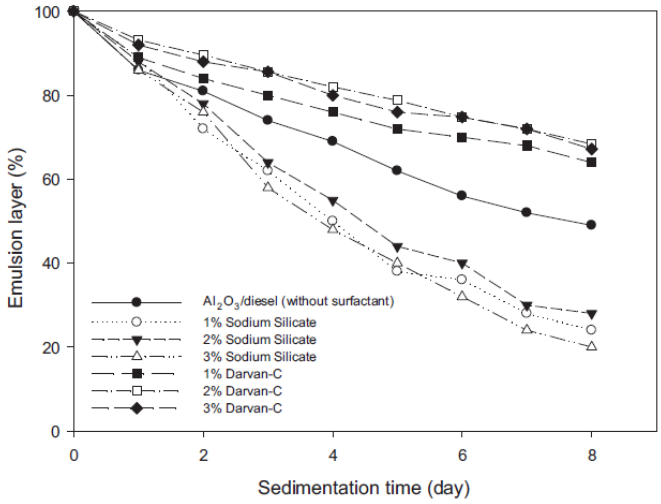

Figure 15: Sedimentation speed of nano Al_2O_3 in the presence of two types of surfactants: Darvan-C and sodium silicate at different concentrations [56].

Organic additives

The other type of cetane booster is represented by organic additives. Organic cetane boosters mainly refer to two chemical functions: nitrates (-O-NO_2) and peroxides (RO-OR'). These types of compounds are known for their ease of decomposing into smaller radicals which can accelerate the combustion of fuels [34]. Indeed, the bond energies of the RO-NO_2 and RO-OR' are very low compared to conventional bonds: C-C, C-C, C-O, C-H, O-H (see Table 4). This allows nitrates and peroxides compounds to dissociate at low temperatures to form radicals and thus enhance fuel reactivity.

Table 4 : Bond energy of several types of chemical bonds

Type of chemical bond	Bond energy (kcal/mol)	Ref.
RO-NO_2	33	[61]
RO-OR'	40	[62]
C-C	90	[63]
C=C	170	[63]
C-O	90	[63]
C-H	100	[63]
O-H	105	[63]

Since the 1950s [37], organic nitrates have been known for their efficiency in improving the cetane number. Robbins et al. [37] tested the performance and stability of several additives: nitrates (26 compounds), nitroalkanes (5 compounds) and peroxides (9 compounds) to improve the cetane number of a diesel fuel. All compounds are listed in Table 5. By calculating the average gain on cetane number by adding additives at doping level of 1.5% vol. into different diesel fuels, Robbins et al. indicated that nitrates were more effective than peroxides in boosting cetane number. The efficiency of additives saturated despite the increase in their doping level. This work also highlighted the loss of efficiency (from 27% to 90% of their initial efficiency) of these additives after 6 months of storage in containers exposed directly under the sun.

Table 5: List of additives investigated experimentally in the study of de Robbins et al.[37].

Nitrates	2-Chloroethyl nitrate, 2-ethoxyethyl nitrate, isopropyl nitrate, 1,3-dinitrate -2-dimethyl propane, trimethylal propane trinitrate, butyl nitrate, mixed amyl nitrate, primary amyl nitrate, secondary amyl nitrate, isoamyl nitrate, secondary hexyl nitrate, primary hexyl nitrate, 2-ethylhexyl nitrate, *n*-heptyl nitrate, *n*-octyl nitrate, *n*-nonyl nitrate, cyclohexyl nitrate, ethylene glycol dinitrate, diethylene glycol dinitrate, dipropylene glycol dinitrate, propylene lycol dinitrate, ethylene propylene diglycol dinitrate, glycol dinitrate, dilycol dinitrate, triglycol dinitrate, tetraglycol dinitrate
Nitroalkanes	Nitromethane, nitroethane, 1-nitropropane, 2-nitropropane, nitrobenzene
Peroxides	Butyl peroxyde, caproyl peroxyde, heptylyl peroxyde, chaulmoogryl peroxyde, oleyl peroxyde, stearyl peroxyde, lauroyl peroxyde, triacetone peroxyde, acetyl benzoyl peroxide

In history, amyl nitrate was first used as a commercial cetane booster. It was later replaced by hexyl nitrate in the 1960s and by the EHN from 1978 [34]. The last additive is widely used because of its excellent cost-efficiency. Ghosh et al. [39] noted that the efficiency of EHN increased not only with its doping level but also with the initial value of the cetane number of the targeted fuel (see Figure 16).

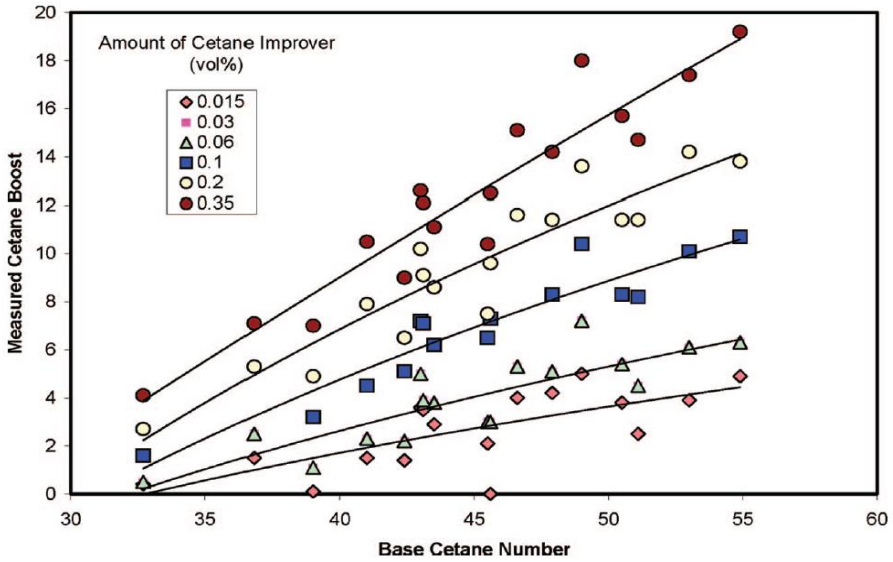

Figure 16: Cetane number boosting effect of EHN in different diesel fuels. Figure adopted from the work of Ghosh et al. [39].

In an effort to replace EHN, some other nitrates have been studied. Among these compounds, tetraethylene glycol dinitrate (TEGDN) was considered in several studies. This cetane booster was studied by Suppes et al. [64]. Its efficiency was compared with that of EHN in two fuels: the fuel (1) which was a mixture of *n*-hexane and ethanol in proportion 3:1 by volume and the fuel (2) which was a diesel fuel whose cetane number was 42. The IDT was measured in a constant-volume combustion chamber. The results showed that at a doping level of 1% vol., TEGDN reduced the IDT of both fuels. Compared to EHN, TEGDN was less effective, which is inconsistent with other literature studies. For example, Robbins et al. [37] reported that TEGDN was 50% more effective than EHN and Russell et al. [65] indicated that TEGDN was 300% more effective than the EHN. The inconsistency in observations of TEGDN performance can be explained by its poor fuel solubility [21].

Peroxides have also been studied as cetane boosters in the literature. Di-tertiary-butyl peroxide (DTBP) was studied by Nandi et al. [34]. This additive was added at several doping levels (0.1 to 1.25% vol.) in different diesel fuels whose initial cetane number were between 26 and 60. The cetane number of fuels was measured by the ASTM D613 method. In general, the results showed that the efficiency of DTBP was about 80% of one of EHN. Additionally, Hashimoto et al. [66] tested the performance of the cumene hydroperoxide in a mixture of *n*-heptane and toluene. The cetane number of the fuel increased by 12 units (from 35 to 47) by the addition of cumene hydroperoxide at 1% mol..

Recently, several studies have focused on cyclic peroxides. Rode et al. [67] studied the cetane boosting effect of dimers (tetraoxanes) and trimers of peroxides (hexaoxoanes) at doping levels of 500 ppm and 1000 ppm. The structures of the investigated additives are presented in Table 6. Peroxides **3a, 4a, 4c, 4d** with acyclic lateral chains were more effective (from 1 to 6 units of cetane number gain) compared to EHN. However, peroxides **3b, 4b** containing cyclic lateral chains were less effective than EHN. This was explained by the stability of the cyclic structure.

Table 6: Chemical structures of cyclic peroxides studied by Rode et al.[67].

Compound	Nomenclature	Chemical structure
3,3,6,6-tetrapropyl-1,2,4,5-tetraoxane	**3a**	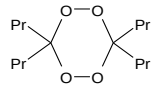
Dicyclohexyl-1,2,4,5-tetraoxane	**3b**	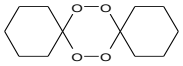
3,3,6,6,9,9-hexapropyl-1,2,4,5,7,8-hexaoxonane	**4a**	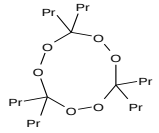
Tricyclohexyl-1,2,4,5,7,8-hexaoxonane	**4b**	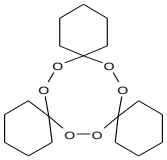
3,6,9-tributyl-3,6,9-trimethyl-1,2,4,5,7,8-hexaoxonane	**4c**	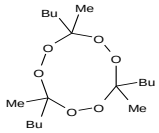
3,6,9-trihexyl-3,6,9-trimethyl-1,2,4,5,7,8-hexaoxonane	**4d**	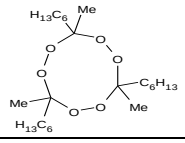

The general mechanism of organic additives has been reported in the work of Hashimoto et al. [66] (see Figure 17). According to this mechanism, additives decompose thermally to produce alkoxy radicals. Then, by reactions of β-scission, alkoxy radicals form alkyl radicals and an unsaturated compound (aldehyde or ketone). These alkyl radicals can react with O_2 to form peroxyl radicals that accelerate the oxidation of the diesel fuel.

- The reaction of deomposition of fuel additives

Nitrates, nitrites : $RO - NO_x \rightarrow RO\bullet + NO_x$ (1)

Peroxides : $RO - OR \rightarrow 2RO\bullet$ (2)

- The reaction of β-scission of alkoxy radicals

$RO\bullet \rightarrow R'\bullet + (aldehyde\ or\ ketone)$ (3)

- The reaction of addition to O_2

$R'\bullet + O_2 \rightarrow R'O_2\bullet$ (4)

Figure 17: Simplified mechanism describing the chemical effect of peroxides and nitrates additives on the gas-phase reactivity of fuels [68].

The above mechanism was supported by the work of Hartmann et al. [69]. These authors performed a ST study of *n*-heptane doped with EHN at high pressure (40 bar) from 690 to 1275 K. The impact of EHN on the IDT of the fuel was the largest in the low range of investigated temperature (770 - 1000 K).

A kinetic model was constructed in this study to identify the origin of the EHN effect. By simulations, Hartmann et al. [69] suggested that the reactivity-promoting effect of EHN related to the formation of highly reactive heptyl radicals during the thermal decomposition of EHN.

EHN was also investigated experimentally in a RCM at 21 bar from 675 to 1025 K by Goldsborough et al. [40]. The targeted fuels were mixtures of *n*-heptane, toluene, and isooctane. It was found that the EHN effect increased non linearly with doping levels. This effect was largest at T > 770 K. A significant difference was observed between the experiments and simulations results. Goldsborough et al. [40] indicated that together with 3-heptyl radical, a "NO_2-NO" loop involving reactions of nitrogen oxides (NO_x) with small radicals (H, HO_2) could generate OH radicals contributing to the EHN promoting effect. The result of this study suggests that the simplified mechanism of Hashimoto et al. [66] is not sufficient to well explain the effect of nitrate additives which can be partly linked to the nitrogen oxides chemistry. A detail nitrogen oxides chemistry must be included in the kinetic model to simulate better the promoting effect of EHN.

In order to better assess the effect of cetane boosters, some works aimed to identify the relationship between the efficiency of additives and their characteristics such as their chemical structure and thermal stability. Yonei et al. [68] were interested in the dependence of the efficiency of cetane boosters on their chemical structure. By calculating the bond dissociation energy of cetane boosters and molecules that have no effect on the cetane number of fuels thanks to quantum chemistry calculation, Yonei et al. proposed that the bond dissociation energy limit of cetane boosters should be included between 10-50 kcal/mol.

Oxley et al. [70] studied the relationship between thermal stability and the efficiency of several cetane boosters: EHN, isopropyl nitrate (IPN), TEGDN, DTBP and tricarbonyl manganese methylcyclopentadienyl (MMT). The additives studied were classified in an increasing order of thermal stability as follows: DTBP < EHN < TEGDN < IPN < MMT. This order changes for their efficiency as cetane boosters: MMT < IPN < DTBP < EHN < TEGDN. Therefore, no correlation was found between thermal stability and the efficiency of cetane boosters. Oxley et al. [69] proposed some explanations for this observation. MMT was ineffective as a cetane booster because its chemical structure was not conducive to the formation of reactive radicals. The species released by the decomposition of MMT are mainly carbon monoxide and methylcyclopentadiene. Similarly, the main decomposition product of IPN is acetone, which is a relatively stable compound. IPN is also an ineffective cetane booster. The major products of DTBP decomposition are 2-butanone and acetone which are stable against oxidation. In comparison with IPN, DTBP breaks down more easily than IPN through the relatively weak O-O bond scission. Therefore, this compound is more effective than IPN as a cetane booster. On the other hand, EHN and TEGDN can produce many reactive radicals thanks to their molecular structure. Therefore, they are the most effective cetane boosters. This publication highlighted the importance of the structure of cetane boosters on their efficiency. Cetane boosters efficiency is indeed related to their ability to promote radicals formation. Important parameters are: (1) the type of functional chemical group, (2) the size of the carbon chain. Additionally, the size of the carbon chain plays an essential role. It must be long enough to encourage the formation of reactive radicals and to ensure its safe operation. Indeed, the molecule with a short carbon chain can be very unstable and dangerous such as methyl nitrate [71].

According to the above studies, the performance of cetane boosters depends mainly on their chemical structure through the carbon chain and functional chemical group. Their molecular structure should be conducive to the formation of free reactive radicals. In the case of nitrate cetane booster, this literature review suggests that their promoting effect may be related to the nitrogen oxides chemistry. A detail sub-mechanism of nitrogen oxides chemistry has to be incorporated in kinetic models to better

simulate the experimental studies of nitrate cetane booster, e.g., the works of Hartmann et al. [69] and Goldsborough et al. [40].

2.2.2.b Octane booster

To avoid knocks in SI engines, octane boosters are introduced in gasoline fuel. The formulation of octane boosters takes into account several important factors such as (a) the ability to reduce engine knock; (b) the absence of undesirable effects for the engine such as corrosion or deposit formation; and (c) the stability of the fuel-additive mixture.

Historically, the use of octane boosters began in 1916 with the use of iodine [72]. This additive is effective but has been rarely used in practice due to economic constraints. Moreover, iodine reacts with metals such as copper, zinc, and iron. As a result, the use of iodine damages the metal pipes and the combustion chamber in engines. The discovery of the effect of iodine has initiated the search for other effective organic octane boosters. In 1919, Boyd et al. [72] noticed the efficiency of aniline as an octane booster. However, the oxidation of aniline gives a bad smell and this molecule can severely corrode metals. These constraints limited the use of aniline. Then, in the early 1920s, organometallics, especially lead and then manganese containing molecules, were successfully tested and used until the 1970s. Arising environmental constraints with the addition of post-treatment system triggered the transiton from organometallic compounds to oxygenated ones. Indeed, lead was identified as a poisoning agent of oxidation catalysts. It should also be mentioned the health concern related to the emission of lead in the environment. As a comment, it should be mentioned that the addition of organometallics is not always negative for the activity of the post-treatment system. Studies have shown that the presence of metals from, for example, lubricants could increase the activity of the catalyst [73]. In this section, the state of the art on the study of octane boosters including organometallic additives and organic additives is presented. Besides, the impact of these organometallics is also discussed with regard to their effect on the velocity of flame propagation. This point will be discussed below because the flame velocity is an essential parameter in the context of engine knock [74].

Organometallic additives

An organometallic is a chemical compound containing one or more covalent bonds between a carbon atom and a metal. These additives are added to fuels at a doping level of about ml/L. The most effective ones often contain a transition metal, for example, lead or iron. In the 1920s, the dominant organometallic additive on the market was tetraethyl lead (TEL). The relative efficiency of TEL compared to other octane boosters is presented in Table 7. It is observed that TEL is more useful than other additives. However, the use of TEL was discontinued since the 1970s because of its toxicity to human health and to oxidation catalysts in the post-treatment system [72]. Then, other organometallics have also been tested such as iron pentacarbonyl or nickel carbonyl in an effort to replace TEL.

Table 7: Relative antiknock efficiency of various compounds. The efficiency of aniline is conventionally defined as 1 [72].

Octane booster	Relative efficiency (%)
Tetraethyl lead	118
Tetraphenyl lead	73
Iron pentacarbonyl	50
Nickel carbonyl	35
Diphenyl amine	1.5
Aniline	1.0
Ethanol	0.1

The octane number boosting effect of organometallic has been characterized with a standard method [72]. However, fundamental studies such as RCM or ST investigations about the effect of organometallic are scarce in the literature. Ferrocene is a highly efficient octane booster [75]. This molecule has an atom of iron stored between two cyclopentadienyl groups. Though the use of ferrocene decreases because of the formation of iron deposits on the spark plug, this additive is still being employed in several countries within an acceptable doping level (less than 38 mg Fe/l) [76]. The studies on ferrocene are still limited. Most experimental researches on this additive in the literature were realized in flame studies [77, 78]. To our knowledge, there is only one study of ferrocene in a RCM. Recently, Fenard et al. [75] conducted experiments in a RCM at relatively low temperatures (< 850 K) to investigate the effect of ferrocene on the combustion of isooctane and 3-hexene. It was observed that ferrocene increased the IDT of two fuels under the investigated conditions. This effect increased with doping levels of ferrocene. In the case where two-stage ignitions were observed, ferrocene only showed its inhibiting effect on the main ignition event.

In addition to the use as octane booster, organometallics have been known as effective flame inhibitors. Koshiba et al. [79] studied some metallocenes for their flame inhibitor effect. A metallocene (see Figure 18) is an organometallic compound in which a transition metal is surrounded by two cyclopentadienyl ligands (Cp). Different metallocenes were examined: the chromocene ($CrCp_2$), the manganocene ($MnCp_2$), the ferrocene ($FeCp_2$), the colbaltocene ($CoCp_2$), and the nickelocene ($NiCp_2$). The performance of these additives was studied on the combustion of filter papers absorbing *n*-pentane in the presence of these metallocenes. The result of this study showed that metallocenes slowed the speed of the combustion (from 60% to 100%) of filter papers. The order of efficiency of the additives was determined as: $CrCp_2 > MnCp_2 > FeCp_2 > CoCp_2 > NiCp_2$ (least effective).

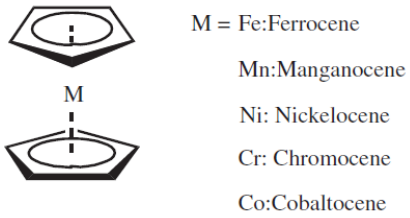

Figure 18: Chemical structure of metallocenes in the study of Koshiba et al.[79].

Reinelt et al. [80] studied the inhibitor effect of iron pentacarbonyl ($Fe(CO)_5$) in a methane-air flame by varying the equivalence ratio from 0.9 to 1.1. The performance of this additive increased with the equivalence ratio. For a Φ of 1.1, 100 ppm of iron pentacarbonyle reduced the flame speed by 50%. On the other hand, the efficiency of this additive saturated at the highest doping level (200 ppm).

Similar additives to $Fe(CO)_5$ were also examined. Linteris et al. [81] studied the inhibitor effect of tetramethyl tin (TMT) and methylcyclopentadienyl manganese tricarbonyl (MMT) in a methane-air flame. Flame velocity was measured under the following conditions: the intake temperature ranged from 298K to 353K and Φ = 0.9 - 1.1. MMT was more effective than TMT. Indeed, 3000 ppm of TMT reduced the flame velocity by 40% while 400 ppm of MMT lowered the flame speed by 50%. MMT was also found to be half as effective as iron pentacarbonyl.

The chemical effect of organometallic additives has not been fully elucidated in the literature. Most studies agreed that the inhibiting effect of organometallics related to their ability to decelerate the widening of the radical pool of the fuel combustion [82]. Benson et al. [82] proposed a "chain debranching" mechanism to explain the octane number boosting effect of lead-containing additives in the gas phase:

$$Pb + HO_2 = PbO + OH$$
$$PbO + HO_2 = PbOH + O_2$$
$$PbOH + H = Pb + H_2O$$

Global reaction: $$2HO_2 + H = H_2O + OH + O_2$$

In this mechanism, lead plays a catalytic role in transforming two active radicals HO_2 and H into stable species: H_2O, O_2 and a radical OH. As a result, the gas-phase reactivity of fuel decreases.

By analogy with the point of view of Benson et al. [82], Fenard et al. [75] proposed that the inhibiting effect of ferrocene would be due to the conversion of HO_2 and H_2O_2 into unreactive species on the surface of iron oxide particles. According to Fenard et al., the oxidation of ferrocene formed gaseous iron atoms which could be rapidly oxidized into gaseous iron oxides. The latter compounds could aggregate into iron oxide particles, on the surface of which the catalytic reaction would occur.

Similar mechanisms have also been proposed to explain the flame inhibitor effect of other organometallics. Wlokas et al. [83] developed a kinetic model to simulate the effect of iron pentacarbonyl in a hydrogen-oxygen flame. The reaction paths of $Fe(CO)_5$ under different conditions is displayed in Figure 19.

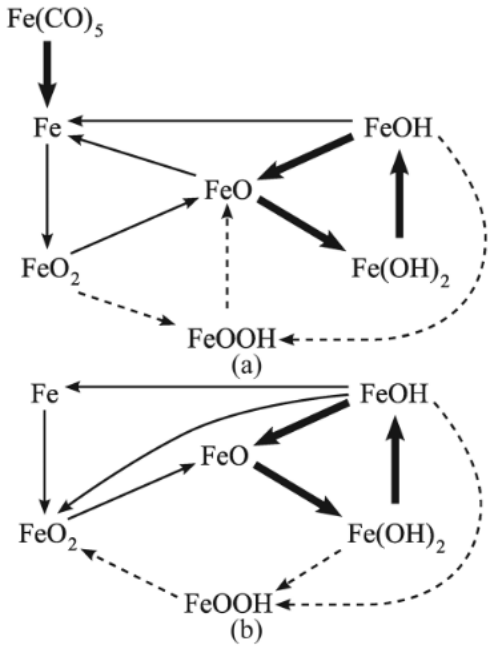

Figure 19: Reaction flux of the iron species in the early flame at 15 mm (a) and 65 mm (b) height above the burner (HAB) and 170 ppm $Fe(CO)_5$. The line thickness represents the intensity of flux. The FeOOH branch was removed in the final reduced mechanism developed by Wlokas et al. [83]. This figure is adopted from [83]

The flame inhibitor effect of $Fe(CO)_5$ is illustrated by two cycles of reactions: the recombination of H atoms and the recombination of O atoms (see Figure 20). Iron species (FeOH, Fe) plays a catalytic role in transforming active radicals (H, O) into stable molecules (H_2, H_2O, O_2). The review of chemical mechanisms of organometallics in the literature suggests that an organometallic can present both effects: octane number booster and flame inhibitor. This statement is at least valid in the case of ferrocene, which is effective both as an octane booster [75] and as a flame inhibitor [79].

Combination of H atoms:	Combination of O atoms:
$FeOH + H = FeO + H_2$	$Fe + O_2 + M = FeO_2 + M$
$FeO + H_2O = Fe(OH)_2$	$FeO_2 + O = FeO + O_2$
$Fe(OH)_2 + H = FeOH + H_2O$	$FeO + O = Fe + O_2$
Global reaction:	Global reaction:
$FeOH + H + H = FeOH + H_2$	$Fe + O + O = Fe + O_2$

Figure 20: Two catalytic cycles allowing the recombination of hydrogen and oxygen atoms in the presence of iron species [83].

Despite the chemical effect of organometallic octane booster is not fully clarified in the literature, it is obvious that the efficiency of organometallics depends on their chemical structure: nature of the metal and ligand. As shown in Table 7, tetraethyl lead is a better octane booster than tetraphenyl lead. Cumming et al. [84] found that chromium hexacarbonyl ($Cr(CO)_6$) was an additive that promotes engine knock. The addition of $Cr(CO)_6$ at 0.1 g/l reduced the octane number of fuel (from 67 to 62.5). Meanwhile, the iron pentacarbonyl ($Fe(CO)_5$) was a very effective octane booster [72]. It was proposed that the effect of $Cr(CO)_6$ was due to chromium multiple levels of oxidation. Chromium can form either monoxide (CrO), sesquioxide (Cr_2O_3), trioxide (CrO_3), or peroxide (CrO_4). Therefore, a balance between these oxides, for example, $Cr_2O_3 \rightarrow 2CrO + O$ could be favored. This balance would act as an additional supply of oxygen and then promote the combustion of fuel.

To summarize, according to the above studies, the effect of organometallic octane boosters may be due to the ability of metals to catalyze the reactions of the combination of free reactive radicals into stable products. Further investigations are necessary to validate this proposition. The inhibiting effect of organometallics importantly depends on the chemical structure of organometallics including metal and ligand. In addition, some organometallics are effective in reducing flame velocity.

Organic additives

The other type of octane booster is organic additive. The main organic octane boosters studied in the literature are aromatic amines and oxygenated compounds. Nowadays, aromatic amines are no longer used. This is related to some main issues [72] which are: the olfactory nuisance during combustion, the corrosion of metals and the formation of deposits which can damage the injection system of an engine. The most commonly used oxygenated octane boosters are ethanol, methyl tert-butyl ether, and ethyl tert-butyl ether. However, they present a significant impact only at very high doping levels (5% - 100% vol.) in fuels [85]. Consequently, oxygenated octane boosters are not discussed in this literature review.

The reactivity inhibitor effect of aromatic amines has been studied in the literature. Brown et al. [86] examined the anti-knock effect of 104 aromatic anilines in a fuel containing 40% *n*-heptane, 20% diisobutylene, 20% toluene and 20% isooctane by volume. The most effective amines were N-methyl-p-phenylenediamine, N-methylaniline, p-ethylaniline, and N-methyl-m-toluidine. Cullis et al. [87] investigated the inhibiting effect of nine amines: monomethylamine, dimethylamine, trimethylamine, trimethylamine, monoethylamine, diethylamine, triethylamine, aniline, N-methylaniline and N-dimethylaniline on the combustion of *n*-heptane in a closed reactor at a pressure of 100 - 800 mmHg, from 236 to 340 °C. The temperature and pressure histories of the reactor were recordeded by the corresponding sensors. The authors observed that amines could slow the spread of cool flames. The most effective amines according to this work were dimethylamine and N-methylaniline.

Cullis et al. [87] proposed a mechanism (see Figure 21) to explain the inhibiting effect of amines. The efficiency of aromatic amines is due to the ability to form stable products with free radicals. For this reason, the fuel reactivity was reduced in the presence of amine additives. According to this mechanism, aromatic amines were only effective at low temperatures (T < 800 K) where radical peroxides were dominantly formed during the combustion of fuels.

- The main reaction of propagation of the combustion of *n*-heptane (AH is an intermediate species containing a labile H atom):

$$RO_2\bullet \rightarrow AH + HO\bullet$$

$$RO_2\bullet + AH \rightarrow ROOH + A\bullet$$

$$AH + O_2 \rightarrow AO_2H$$

$$RH + HO\bullet \rightarrow R\bullet + H_2O$$

$$R\bullet + O_2 \rightarrow RO_2\bullet$$

- The interaction between AH and aromatic amines (InH) :

$$AH + InH \rightarrow PH$$

- The molecules PH can react with peroxide radicals following two different ways (a) and (b):

$$RO_2\bullet + PH \rightarrow ROOH + P\bullet\ (stable\ radicals) \text{(a)}$$

$$RO_2\bullet + PH \rightarrow stable\ products \text{ (b)}$$

Figure 21: Mechanism of aromatic amines employed as octane booster [87].

2.2.2.c Conclusions

Two main types of additives are introduced to modify the reactivity of fuels in the gas phase: cetane boosters and octane boosters.

Two types of cetane boosters which are the most studied in the literature are organic additives and nanoparticles.

Organic compounds containing the chemical functions as nitrates and peroxides can be used as cetane boosters. Their efficiency depends on two parameters: (1) the nature of the functional chemical group; and (2) the size of the carbon chain. It seems that in general cyclic peroxides are more effective than nitrates, which are more effective than acyclic peroxides. In addition, the performance of cetane boosters may vary according to the type of fuel. Additionally, physical characteristics such as the solubility of additives can also be of the first order to discuss the effect of an additive. Actually, EHN is the dominant commercial cetane booster. Despite the wide use of this additive, its chemical effect has not been fully understood. This literature review suggests the promoting effect of EHN, and/or other nitrate cetane boosters, may relate partly to the nitrogen chemistry.

Few nanoparticles have been used to improve the cetane number of diesel fuels. Some metal oxides (Al_2O_3, CeO_2) in the form of nanoparticles were examined. However, the efficiency of these additives remains rarely discussed in the literature, particularly concerning a potential chemical effect.

The performance of cetane boosters appears to be related to two factors: the capacity of producing free radicals in the case of organic additives and the ability to better homogenize the fuel-air mixture in the case of nanoparticles. The chemical effect of nanoparticles remains little discussed in the literature.

The use of octane boosters is intended to reduce the gas-phase reactivity of gasoline fuels. Two types of octane boosters are commonly studied in the literature: organometallic additives and organic additives. The efficiency of an octane booster depends on several factors such as its chemical structure, the experimental condition (pressure, temperature, etc.) and the chemical composition of the fuel.

The performance of an octane boosters related to the capacity of reducing radical pool. The mode of action of the two types of additive is different. Organometallics are supposed to play a catalytic role in converting highly active radicals such as H or HO_2 into more stable species. Meanwhile, aromatic amines can react with peroxide radicals to form stable products. Fundamental experiment studies in ST and/or RCM are essential to better understand the chemical effect of octane booster.

Generally, organometallic additives are much more effective (4 to 100 times) than organic octane boosters. Organometallics are active over a higher temperature range compared to aromatic amines. The presence of a catalytic cycle seems to give it a significant advantage over amines which can only interact with peroxide radicals. The last compound exists dominantly during the combustion of fuel only at low temperatures ($T < 800$ K).

The use of organometallic boosters with fuel is often limited because of their toxicity to humans and to the catalysts used in post-treatment system [72]. Organometallics present usually both effects: reactivity inhibitor effect and flame inhibitor effect, for example, iron pentacarbonyl [72] and ferrocene [75, 78]. A more detailed comprehension of the chemical effect of organometallic can promote the search for a new efficient and safe organometallic octane boosters from the knowledge of existant effective organometallic flame inhibitor, for example, metallocenes [79].

To sum up, the performance of additives in the gas phase varies with different fuels. This mainly relates to the chemical interaction of the additive with the fuel. This aspect can be clarified by a detailed kinetic model. In the literature, there are kinetic models that have been developed to simulate the effect of additives. However, the use of these models is still limited to understand the effect of additives because of the notable disagreement between simulation and experiment results in literature studies. This aspect is even valid for a common commercial cetane booster as EHN. More fundamental experimental studies in academic equipment like ST and/or RCM are essential to better understand the chemical effect of fuel additives. This helps to build robust kinetic models of fuel additives. The last element is very useful and powerful in CFD simulations which help to investigate different types of combustion systems as HCCI, GCI, etc. in various thermodynamic conditions and fuels. In addition, the in depth comprehension of fuel additives promotes the new design of fuel additives which can contribute to the development of more efficient and cleaner IC engines.

2.3 Conclusions

Engine-fuel adequacy is a key parameter to optimize engine performance while reducing exhaust emissions. Today, the diversification of engines in LTC conditions such as HCCI, SACI or GCI as well as the incorporation of biofuels results in an evolution of engine/fuel adequacy. Understanding the fuel reactivity is required. Indeed, the fuel itself is the main parameter regarding combustion but also the oxidation stability of this fuel. Therefore, controlling the reactivity of the fuel in both phases, gas and liquid is essential. For this reason, fuel additives have been studied and commercially employed in recent decades.

The state of the art on the use of additives in the gas and liquid phase is presented. Indeed, a radical mechanism is followed during the oxidation of the fuel regardless of the considered phase [12, 36]. This leads to the formation of similar products at least in the first moments of oxidations. For example, peroxides are formed during the autoxidation and the low-temperature combustion ($T < 800$ K) of fuel. Thus, an additive that impacts the liquid-phase reactivity of fuel can potentially influence the gas-phase reactivity of this fuel and vice versa.

In the gas phase, cetane boosters and octane boosters are respectively used to increase and decrease the fuel reactivity. As their effect is different, their mode of action is undoubtedly different. Cetane boosters are able to expand the radical pool while octane boosters are used to reduce this pool. Nitrates and organometallics are the most efficient cetane boosters and octane boosters respectively, which have been studied. In the literature, few kinetic models have been constructed to simulate the effect of additives. However, the use of these models is still limited to understand the effect of additives in various thermodynamic conditions and different base fuels. This limitation appears in the remarkable difference between the experiments and simulations results presented in the relevant studies. Thus, further investigation is necessary to better clarify the interaction between the additives and the fuels.

For the liquid phase, antioxidants such as free radical scavengers, hydroperoxide decomposers, and metal deactivators are employed to enhance the oxidation stability of fuel. Free radical scavengers are the most commonly used among these types of additives. The mode of action of this type of antioxidant is to trap free radicals formed during fuel autoxidation. This mode of action is similar to that of aromatic amines which are used as octane boosters. This aspect presents again the potential effect of free radical scavengers on the gas-phase reactivity of fuel. Like gas-phase additives, the lack of detailed kinetic models limits our understanding regarding the additives effect in the liquid-phase.

The development of detailed kinetic models is therefore essential not only to characterize the effect of gas-phase additives but also to evaluate the potential impact of antioxidants on the fuel combustion. For this reason, more fundamental studies including experimental studies with devices such as ST, RCM and burner are essential to better understand the chemical effect of fuel additives. This helps to build some robust kinetic models of fuel additives. These models enable numerical simulations which help to investigate several engine types being developed such as SACI, GCI, etc. in various thermodynamic conditions and fuels. In addition, the in-depth comprehension of fuel additives effect promotes novel molecule design which can contribute to the development of more efficient and cleaner IC engines.

Some academic equipment have been employed to study fuel additives as shock tube, rapid compression machine and burner. These experimental techniques enable the measurement of ignition delay times and flame speeds of hydrocarbons. In the next chapter, the research methodology of this study is presented. The strategy of choosing an additive-fuel system to be studied is introduced. The experimental methods used to investigate the effect of the chosen additives are then described.

Chapter 3: Materials and experimental methods

This chapter describes the selection of the surrogate fuel-additives system to be studied in this thesis. The effect of additives on the gas-phase reactivity of the surrogate fuel is experimentally investigated in three academic equipment including a shock tube (ST), a rapid compression machine (RCM), and a heat flux burner. Operating principles, as well as detail descriptions of these devices, are presented.

3.1 Surrogate fuel-additives system

The chemical composition of diesel and gasoline fuels is complex [88, 89]. It is really difficult to determine the detailed chemistry of commercial fuels. To facilitate IC engine research, surrogate fuel is employed. This kind of fuel contains one or several reference hydrocarbons such as *n*-heptane, isooctane, toluene, etc. The surrogate fuel is formulated to reproduce one or some specified properties to be examined of commercial fuel. This chapter describes the methodology of the choice of the surrogate fuel employed in this thesis. This surrogate fuel is designed to enable the study of the effect of additives on some distinct phenomena of fuel ignition as two-stage ignition and negative temperature coefficient (NTC).

As presented in the bibliography, two types of additives presenting high impact on the gas-phase reactivity of fuel are cetane boosters and octane boosters. Additionally, an antioxidant as a free radical scavenger in the liquid phase can present a potential effect on the combustion of fuel. For this reason, three additives representing three types of fuel additives (cetane booster, octane booster, antioxidant) are studied in this thesis. The selection of these additives is further described in this chapter.

3.1.1 Selection of the surrogate fuel

This chapter provides an overview of surrogates proposed in the literature. Two types of surrogates are presented in this section: diesel surrogate and gasoline fuel surrogate. Based on the review of the surrogates proposed in the literature, the surrogate fuel to be studied in this thesis is formulated.

3.1.1.a Diesel surrogate

Diesel fuel contains mainly compounds of three chemical families: paraffins, cyclo paraffins, and aromatics [90]. The paraffins consist of straight-chain and iso-paraffins which are slightly branched. The cyclo paraffins are principally 1-ring cyclohexanes with multiple alkyl side chains. 2-ring cyclohexanes and heavier cyclo-paraffins are also present at a lower ratio in comparison with 1-ring cyclohexanes. The aromatics inlude alkylbenzens, substituted 2-ring aromatics (naphthalenes) and multi-ring aromatics. For this reason, diesel surrogates are made up of one or several molecules selected from these chemical families.

The *n*-heptane has been used as a diesel fuel surrogate [4] thanks to its self-ignition behavior similar to that of diesel fuel. The cetane number of *n*-heptane is about 55 [90] which is close to that of commercial diesel in Europe, which is about 51 [19]. Moreover, detailed kinetic models for *n*-heptane combustion are available in the literature [91–93]. Despite of some advantages, the use of *n*-heptane as a mono-component diesel surrogate is not recommended due to its significantly lower density compared to diesel fuel. The *n*-hexadecane is another single-component surrogate used by Poon et al. [94]. This surrogate was chosen for the similarity of evaporation properties with diesel fuel. A reduced combustion mechanism was developed for this surrogate. However, due to the significant discrepancy from the IDT of the target diesel fuel, the use of this mono-component surrogate remains limited.

To better describe the combustion behavior of diesel fuel, multi-component surrogates were considered. A surrogate containing 30% toluene and 70% *n*-heptane by volume was used in the study of Gustavsson and Golovitchev [95]. This work aimed to replicate the effect of the chemical structure of diesel fuel on the soot formation. The surrogate correctly simulated the IDT of the diesel fuel but its application for the prediction of soot formation was inadequate.

A surrogate made up of three compounds: *n*-decane, *n*-butylcyclohexane, and *n*-butylbenzene was oxidized by Natelson et al. [96] in a pressurized flow reactor at 0.8 MPa, from 600 K to 800 K, and at Φ = 0.3. This surrogate was found to be more reactive than the target diesel fuel. The addition of an iso-paraffin in the surrogate was proposed to lower its reactivity.

A four-component surrogate (29% *n*-hexadecane, 16.4% heptamethylnonane, 8.1% naphthalene, 36.5% decalin by volume) was proposed by Puduppakkam et al. [97]. The purpose of this study was to simulate the combustion in a diesel engine by FORTE CFD software. This surrogate was formulated to imitate the physical properties of the target diesel fuel (see Table 8). A detailed kinetic model of this surrogate was reduced for use in CFD simulations. The results of simulations were compared with experimental results carried out on a BMW diesel engine. The simulation reproduced reasonably the rate of formation of exhaust gas including CO, CO_2, NO_x, soot and the IDT.

Table 8: Physical properties of the target diesel fuel and the surrogate fuel proposed by Puduppakkam et al. [97].

Property		**Diesel fuel**		**Surrogate fuel**
		Measured by Puduppakkam et al.	Typical value	
Cetane number		52.2		54.3
H/C ratio			1.8	1.87
Lower heating value (MJ/kg)			43	43.7
Threshold sooting index				25.7
Liquid density (kg /m^3)		835		827
Temperature 10% masse evaporated (K)		490		487
Temperature 50% masse evaporated (K)		547		515
Temperature 90% masse evaporated (K)		622		560
Composititon (%vol)	Aromatics	15 - 40	8.1	
	n- and iso-alcanes	25 - 50	55.4	
	Naphthenes	15 - 60	36.5	
Carbon number range			10 - 17	10 -16

To list hydrocarbons which can be used to build diesel surrogates, Farrell et al. [90] performed a review. The data in Table 9 were collected in the literature. By considering the reactivity as well as the physical properties of examined compounds, Farrell et al. proposed that a mixture of four components (*n*-decane, isooctane, methylcyclohexane, and toluene) could be used as an adequate diesel surrogate.

According to this literature review, single-component or bi-component surrogates may be sufficient to reproduce the reactivity of diesel fuels. Tri-component or tetra-component surrogates should be employed in cases where several characteristics of a diesel fuel such as physical properties or soot formation tendencies need to be reproduced.

Table 9: Diesel fuel surrogate components evalution by Farrell et al.[90].

	Understanding of mechanism		Property information	
Fuel	**Low and intermediate temperatures (T < 900 K)**	**High temperatures (T > 900 K)**	**Thermo-physical**	**Transport**
Linear alkanes				
n-heptane	A	A	A	A-
n-decane	B	A-	A	A
n-dodecane	B	B	A	A
n-hexadecane (*n*-cetane)	C	C	B+	B
Branched-chain alkanes				
2,2,4-trimethyl-pentane(isooctane)	A-	A	B+	B
2,2,4,4,6,8,8-heptamethylnonane (iso-cetane)	C	C	B-	C+
Cycloalkanes				
Methylcyclohexane	C	C	B+	B
Ethyl/propyl/butyl cyclohexane	D	D	B	C
Decahydronaphthalene (decaline)	D	D	B	B-
Single-ring aromatic				
Toluene	C	C	A	B+
Ethyl/propyl/butyl benzene	C	C	B	B
n-decylbenzene	D	D	D	D
Multi-ring aromatic				
Tetralin	D	C	B+	B-
1-methylnaphtalene	C	C	B	C

Legende				
	A	**B**	**C**	**D**
Understanding of mechanism	Detailed mechanism(s) validated over wide range	Mechanism(s) reported, but with modest discrepancies or limitations	Mechanism(s) reported, but with major discrepancies or limitations	No mechanism reported
Thermo-physical properties	Equation of state available (desity to 0.3%)	Sufficient data for model (density to 3%)	Limited data only	Extremely limited/no experimental data, predictive model feasible
Transport properties	Correlations available for viscosity and thermal conductivity (5%)	Data available for models (5-10%)	Limited viscosity and/or thermal conductivity data	Extremely limited/no experimental data, predictive model feasible

3.1.1.b Gasoline surrogate

Like diesel surrogates, the components of gasoline surrogates belong to the principal chemical families included in gasoline fuel such as linear, branched-chain and cyclic alkanes, aromatics, olefins and oxygenated comounds which are in small proportion [2].

Primary reference fuel (PRFs) are the simplest surrogates for gasoline fuel. A PRF is a mixture of *n*-heptane and isooctane. By definition, a PRF"xx" consists of xx% isooctane and (100-xx) % *n*-heptane by volume. This type of surrogate was studied in many works [98].

Other multi-component surrogates were also proposed in the literature. Gauthier et al. [99] suggested a three-component surrogate containing 63% isooctane, 20% toluene and 17% *n*-heptane by volume. A shock tube study under various conditions of temperatures (850 K - 1280 K), of pressures (15 bar - 25 bar), and of equivalence ratios (0.5 -2) showed that this surrogate was able to represent the combustion property of the target gasoline fuel. Kim et al. [100] developed a reduced kinetic model of this surrogate. The simulations performed by Kim et al. [100] were consistent with the results obtained by Gauthier et al. [99]. Potential polycyclic aromatic hydrocarbon (PAH) and soot formations by this surrogate were taken into account in the reduced kinetic model developed by Wang et al. [101]. Satisfactory agreements were observed between the simulations and experimental data such as IDT and premixed flame velocity.

To mimic the composition of gasoline fuels, alkenes (i.e. olefins) were introduced into gasoline fuel surrogates. Kukkadapu et al. [102] conducted RCM experiments with a research-grade gasoline fuel named RD387 at 20 and 40 bar, from 650 to 950 K, and at $\Phi = 0.3 – 1$. The simulation of IDT of this gasoline fuel was conducted by adopting a surrogate fuel containing 16% *n*-heptane, 57% isooctane, 23% toluene and 4% 2-pentene by volume thanks to the mechanism developed by Mehl et al. [42]. Kukkadapu et al. obtained satisfactory agreements between simulation and experiments on IDT of the gasoline fuel. Andrae et al. [103] developed a detailed kinetic model of a surrogate whose composition was 51.0% isooctane, 18.0% *n*-heptane, 26.4% toluene, and 4.6% DIB-1 (2,4,4-trimethyl-1-pentene) by volume. By comparing the simulations with the experimental data, this surrogate reproduced well the gas-phase reactivity of the target gasoline fuel except in the range of intermediate temperatures (750K – 900 K). The addition of DIB-1 was found to increase the reactivity of toluene, as well as the reactivity of the considered surrogate fuel at high temperatures.

To summarize, the most common compounds used to build gasoline fuel surrogates in the literature are *n*-heptane, isooctane, and toluene. To match the composition of gasoline fuel, some alkenes are introduced into surrogates. This addition globally results in better reproducing the gas-phase reactivity of the target fuel.

3.1.1.c Target surrogate fuel

To investigate the effect of additives, a target surrogate fuel is considered in this study. Two steps to define the surrogate fuel are (1) the choice of constituents and (2) the determination of the fraction of each constituent.

The first step follows a few constraints. The surrogate is designed to enable the study of additive impact on some specific phenomena of hydrocarbon combustion as two-stage ignition and NTC behavior. This aspect has been little discussed in the literature. Additionally, the chemical composition of the surrogate should not be too complicated to facilitate the modelization of fuel additives and then the comprehension of the chemical effect of the fuel additives considered in this thesis. A binary surrogate is thus preferred.

As shown in the above sections (see sections 3.1.1.a and 3.1.1.b), three chemical families including linear alkanes, branched-chain alkanes and aromatics are usually selected to formulate surrogates. Our surrogate is built with these types of hydrocarbons. Among these chemical families, the most commonly selected molecules are *n*-heptane, isooctane, and toluene. Advantageously, the chemistry of these molecules is well detailed in the literature [42, 104–106]. It is, therefore, preferable to build the surrogate from these compounds.

n-Heptane represents linear alkanes. The choice of *n*-heptane for the formulation of the surrogate is supported by the study of Westbrook et al. [107]. According to this work, the combustion of linear alkanes from *n*-heptane to *n*-hexadecane follows similar mechanisms. However, from a modeling point of view, the number of intermediate species to be treated is much lower for *n*-heptane than for other alkanes [107]. Thus, *n*-heptane is included in the surrogate of this thesis.

The second component of the surrogate is toluene. The choice between isooctane and toluene for the second constituent of the surrogate is based on several elements. NTC behavior is observed in the case of isooctane and *n*-heptane and not for the combustion of toluene [42]. Then, a mixture of toluene and *n*-heptane facilitates more the understanding of the additive effect on NTC behavior than a blend of isooctane and *n*-heptane. Additionally, as presented in the work of Mehl et al. [42], a mixture of toluene and *n*-heptane presents both two-stage ignition phenomena and NTC behavior. This feature meets correctly the need of the construction of the surrogate in this thesis. Finally, the reactivity of toluene at low temperatures (T < 900 K) has not been well understood in the literature due to the stability of toluene as discussed in the study of Zhang et al. [108]. The choice of toluene as a constituent of the surrogate helps to contribute to the comprehension of the chemical reactivity of toluene in blends at low temperatures.

The second step to define the surrogate is the determination of the fraction of each constituent. Table 10 shows the publications in the literature investigating the gas-phase reactivity of toluene/ *n*-heptane mixtures.

Table 10: Composition of toluene/ *n*-heptane blends studied in the literature.

Mix.	Composition (% vol.)		RON	Experimental method	T (K)	P (bar)	Φ	Ref.
	n-Heptane	Toluene						
1.	90	10	≈ 12	ST	700 - 1200	40	0.5, 1	[109]
2.	60	40	≈ 48	ST	800 - 1050	40	0.5, 1	[109]
3.	50	50	-	ST, RCM	650 - 1450	10, 30	0.5, 1, 2	[110]
4.	35	65	84	ST	620 - 1180 (900 – 1150 at 10 bar)	10, 30, 50	0.3,1	[111]
5.	25	75	-	ST, RCM	650 - 1450	10, 30	0.5, 1, 2	[110]
6.	10	90	-	ST, RCM	650 - 1450	10, 30	0.5, 1, 2	[110]

Recently, Malliotakis et al. [110] did a great effort to measure the IDT of various mixtures of toluene and *n*-heptane under different conditions of pressures (10 – 30 bar), of temperatures (650 – 1450 K), and of equivalence ratios (0.5 – 2). Experiments were conducted in a ST and a RCM. The volume fractions of toluene in these mixtures were 50%, 75%, and 90%. Previously, Herzler et al. [111] measured the IDT of a mixture containing 35% *n*-heptane and 65% toluene by volume at different pressures in a ST. Due to the limitation of the ST, the IDT of this mixture were not measured at low temperature (T < 900 K) at a pressure of 10 bar.

The mixture proposed by Herzler et al. [111] is considered in this thesis. The experiments performed in a RCM in this study complemented the IDT measurements under conditions which were not investigated by Herzler et al. This contributes to the comprehension of toluene reactivity at low temperatures (T < 900 K). In addition, this *n*-heptane / toluene mixture has a RON value of 84, which corresponds to grade of low-octane gasoline fuel. This type of fuel can be used in LTC engines like GCI engine [7]. Therefore, the study of this *n*-heptane / toluene mixture generates a source of experimental and numerical results for engine development.

To conclude, the target surrogate fuel selected in this thesis is a mixture of 35% *n*-heptane and 65% toluene by volume. The chemical structures of *n*-heptane and toluene are presented in Figure 22.

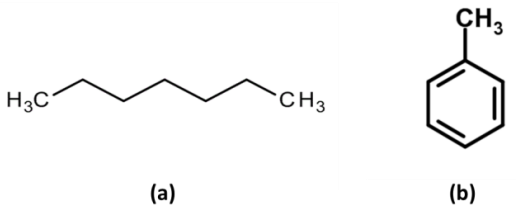

Figure 22: Chemical structures of (a) *n*-heptane and (b) toluene.

3.1.2 Selection of fuel additives

The aim of this thesis is to study the chemical effect of additives on the gas-phase reactivity of fuel. To do this, three types of additives presenting an effect on fuel reactivity are identified as cetane booster, octane booster, and antioxidant, respectively. A molecule is selected for each type of additive. To facilitate the choice of additives, the chemical structure of these additive must allow the construction of a detailed kinetic model.

Choice of a cetane booster: 2-ethylhexyl nitrate

The two main types of cetane boosters are organic additives and nanoparticles. As the effect of nanoparticles remains little discussed in the literature, organic additives are selected to study the effect of cetane booster. Among organic additives, EHN presents a significant effect on the combustion of fuel and is also the conventional additive used in daily life. Its cetane number boosting effect was reported in the literature [37, 39]. However, the chemical effect of this additive is not yet fully understood. Hartmann et al. [69] performed a ST study of *n*-heptane doped with EHN at high pressure (40 bar) from 690 to 1275 K. By simulation, Hartmann et al. suggested that the reactivity-promoting effect of EHN relates to the formation of highly reactive heptyl radicals during the thermal decomposition of this additive. More recently, EHN was experimentally and numerically investigated in a RCM at 21 bar from 675 to 1025 K by Golsborough et al. [40]. The fuels were mixtures of *n*-heptane, toluene, and isooctane. Goldsborough et al. [40] indicated that together with 3-heptyl radical, a "NO_2-NO" loop involving reactions of nitrogen oxides (NO_x) with atoms and small radicals (H, HO_2) could generate OH radicals contributing to the EHN effect. The result of this study suggests that the effect of nitrate additives can importantly link to the nitrogen chemistry. To clarify this aspect, EHN is therefore selected in this study. This helps to examine more reliably the effect of this conventional cetane booster in different conditions during engine simulations. The chemical structure of EHN is presented in Figure 23.

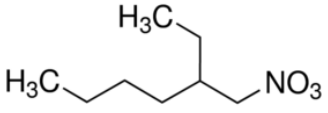

Figure 23: Chemical structure of EHN.

Choice of an octane booster: ferrocene

To choose the octane booster, organometallics are preferred because they are much more effective than organic additives [72]. It is observed that iron pentacarbonyl is a high-performance octane booster (only less effective than lead-based compounds). Iron-based additives are therefore considered. In the literature, two iron-based compounds were studied for their effect on octane number. The first one is iron pentacarbonyl [72] and the second one is ferrocene [75, 112]. Although these molecules may present undesirable effects to engine such as the formation of deposits on the plug of SI engines [72, 76, 113], these additives can still be employed at an acceptable doping level (38 mg Fe/l) in some regions [76]. Because pentacarbonyl is highly toxic to human health [114], ferrocene is selected in this thesis. Recently, Fenard et al. [75] conducted experiments in a rapid compression machine (RCM) at relatively low temperatures (< 850 K) to investigate the effect of ferrocene on the combustion of isooctane and 3-hexene. This study suggests that the chemical effect might be related to the reactions of HO_2 and H_2O_2 on the surface of iron oxide particles. The inhibiting effect of ferrocene was underestimated by the kinetic model proposed in this study. The difference between experimental and simulation results shown in the study of Fenard et al. [115] suggests that further investigations on ferrocene are necessary to explain the inhibiting effect of this additive. This thesis contributes to fulfill this task. Moreover, as discussed in the literature review, organometallics present usually both effects as reactivity inhibitor and flame inhibitor [72] [75, 78]. A more detailed comprehension of the chemical effect of ferrocene can promote the search for a new efficient and safe organometallic octane boosters from the knowledge of existent effective organometallic flame inhibitor, for example, metallocenes [79]. The chemical structure of ferrocene is presented in Figure 24.

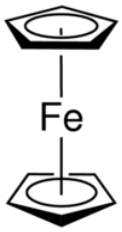

Figure 24: Chemical structure of ferrocene.

Choice of free radical scavenger: 2,4-xylenol

Antioxidants are divided into three types: free radical scavengers, hydroperoxide decomposers, and metal deactivators. Among these antioxidants, free radical scavenger is most commonly used to enhance the oxidation stability of fuel. The effect of this type of antioxidant varies with temperatures [46]. As the temperature of fuel increases sharply from the distribution system to the combustion chamber through the injection system, it is important to investigate the effect of free radical scavenger on the gas-phase reactivity of fuel to ensure the performance of engine.

One of the conventional free radical scavengers is BHT. Its effectiveness as an antioxidant was highlighted in the literature [35]. However, its chemical structure is complex. A phenolic antioxidant with a simpler structure than BHT is desired to enable the realization of a detailed kinetic model. Recently, McCormick et al. [47] studied phenolic antioxidants that could replace BHT. They were 4-methylanisole, phenol, p-cresol, 2,4-xylenol, guaiacol, 4-methylguaiacol, 4-methylacetophenone, 4-propylphenol and 4-propylguaicol. All these compounds can be produced from a natural and renewable source. It was observed that 2,4-xylenol (see Figure 25) was the most effective antioxidant. In addition, this compound slightly improved the octane number of examined fuel (from 85.8 to 89 at a doping level of 2% vol.). 2,4-xylenol can be used as a multifunctional fuel additive. This aspect

motivates the selection of 2,4-xylenol in this thesis. The chemical structure of 2,4-xylenol is shown below:

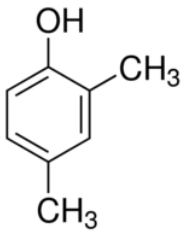

Figure 25: Chemical structure of 2,4-xylenol.

To synthesize, the three additives selected in this thesis are EHN, ferrocene, and 2,4-xylenol. The effect of these additives on surrogate reactivity is studied using several experimental methods described in the next section.

3.2 Experimental methods

Figure 26 presents all the experimental devices used in this thesis to study the effect of additives on fuel combustion. Indeed, the gas-phase reactivity of a fuel can be characterized by two parameters such as the ignition delay time (IDT) and the laminar burning velocity.

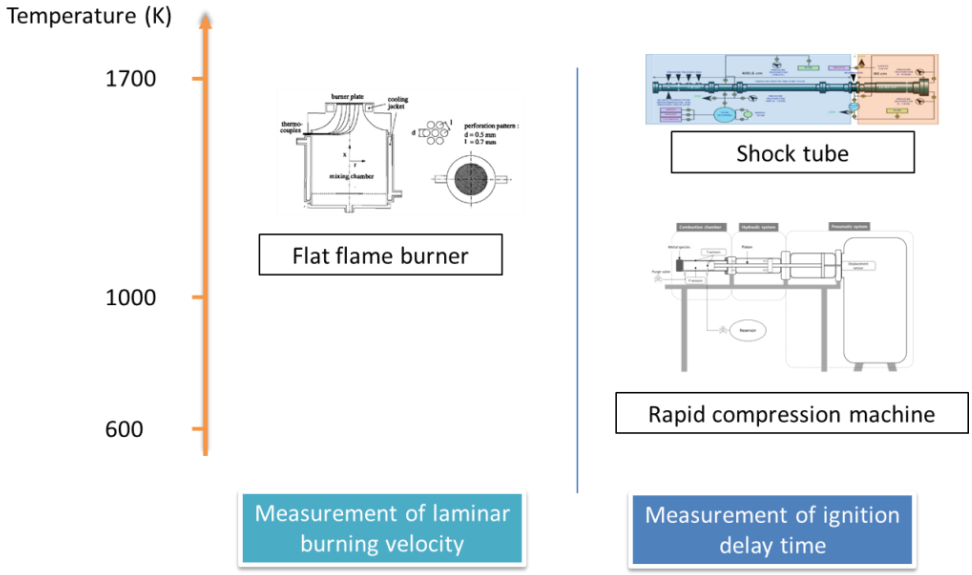

Figure 26: Presentation of experimental devices considered in this thesis with the corresponding range of operating temperatures.

A shock tube (ST) and a rapid compression machine (RCM) are employed to measure IDTs over a wide range of temperature (600 to 1700 K). Once a fuel is brought to reacting conditions (P, T, Φ), it takes a specific period of time until the fuel really ignites, when a sharp rise of pressure is observed. This period defines the IDT of the fuel in the studied conditions. This property depends importantly on temperatures and the considered reactive mixture including chemical composition, equivalence ratio, and dilution ratio. In practice, the absolute value of IDT is defined specifically according to each experimental method. While ST is used to capture fuel reactivity at high temperature (T > 900 K) [116], RCM helps to characterize fuel autoignition in a lower temperature range (T < 900 K) [117]. Experiments in ST addresses high-temperature reactivity of fuel, in which decomposition reactions are preferred. On the other hand, RCM helps to investigate the low-temperature and intermediate-

temperature reactivity of fuel. In these last ranges of temperature, some particular phenomena of fuel oxidation appear, such as NTC and cool flames. The impact of additives on key reactions involving peroxides can be investigated. Though peroxides are the major actor of fuel chemistry at low temperature, this aspect remains little discussed in the literature.

Flame velocity is an important property of fuel which helps to control combustion in engines. In this thesis, the impact of fuel additives on the laminar burning velocity of the surrogate fuel is investigated in a heat flux burner, a flat flame burner which allows to measure the burning velocity in stabilized flame conditions

The data obtained from these experimental equipment are both fundamental and essential to validate the developed kinetic models. Then, the validated models allow understanding the chemical effect of additives.

Initially, the manipulations in a ST were carried out at *Laboratoire Réactions et Génie des Procédés* (LRGP), Nancy. Besides, the experiments in a flat flame burner at LRGP were performed by Goussougli et al. [41]. Then, the experiments in a RCM were conducted at the *Pluridisciplinaire de Recherche en Ingénierie des Systèmes, Mécanique, Énergétique* (PRISME) laboratory in Orleans. Operating principles, as well as detail descriptions of these setups, are further presented.

3.2.1 Shock tube

The combustion of fuel in an IC engine is complex and related to fuel chemistry at highly different conditions (P, T, Φ). ST is an academic experimental equipment that helps to investigate the fuel reactivity at high temperatures (T > 1000 K). The operating principle and detail description of the ST of LRGP are presented in this section.

3.2.1.a Operating principle

A shock tube is a system permitting heating adiabatically a gas mixture by the effect of shock waves in a very short time. The simplified diagram of a shock tube is presented in Figure 27.

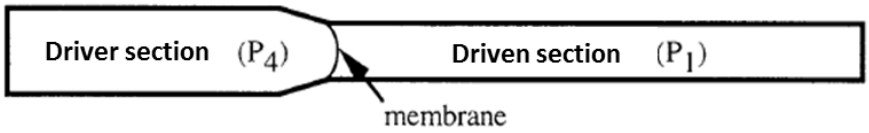

Figure 27: Simplified diagram of a shock tube [118].

A shock tube consists of two parts separated by a membrane. They are called driver and driven sections. The driven section of the tube is filled with the fuel gas mixture, initially at low pressure P_1 (about hundreds of Torr). The driver section of the tube contains compressed high pressure driver gas at about several bar. Driver gas is usually an inert gas. The initial temperature of gases in the whole tube is the ambient temperature ($T_4 = T_1 = T_{ambient}$). After the rupture of the membrane, a series of pressure waves are generated. They compress into a shock wave propagating toward the driven section at a supersonic velocity. The driver gas propagates also toward the driven section at a lower velocity than that of the shock wave. The temperature and pressure of the propagating driver gas rise by the effect of the shock wave. A discontinuity surface is then formed between the propagating driver gas and the fresh driven gas and move toward the driven section at the same velocity of the propagating driver gas. Simultaneously, a rarefaction wave moves back to the driver section at a subsonic speed. Due to the effect of the rarefaction wave, the temperature (T_3) and the pressure (P_3) of the driver gas decrease. In the driven section, the incident shock wave is reflected by the wall at the end of the tube. The reflected shock wave compresses and heats the fuel gas mixture to the desired

condition of combustion (P_5, T_5) at the moment of the contact with the discontinuity surface. The shock tube principle is summarized in Figure 28. Table 11 resumes the indexing of the state (pressure and temperature) of various gases involved in the shock tube test.

Table 11: Indexation of different states (pressure and temperature) of the various gases involved in shock tube experiments

Index	Designation
P_1, T_1	Initial fuel gas mixture
P_2, T_2	Driver gas propagating behind the incident shock wave
P_3, T_3	Driver gas between the discontinuity surface and the end of the driver section
P_4, T_4	Initial driver gas
P_5, T_5	Fuel gas mixture at the desired condition behind the reflected schock wave

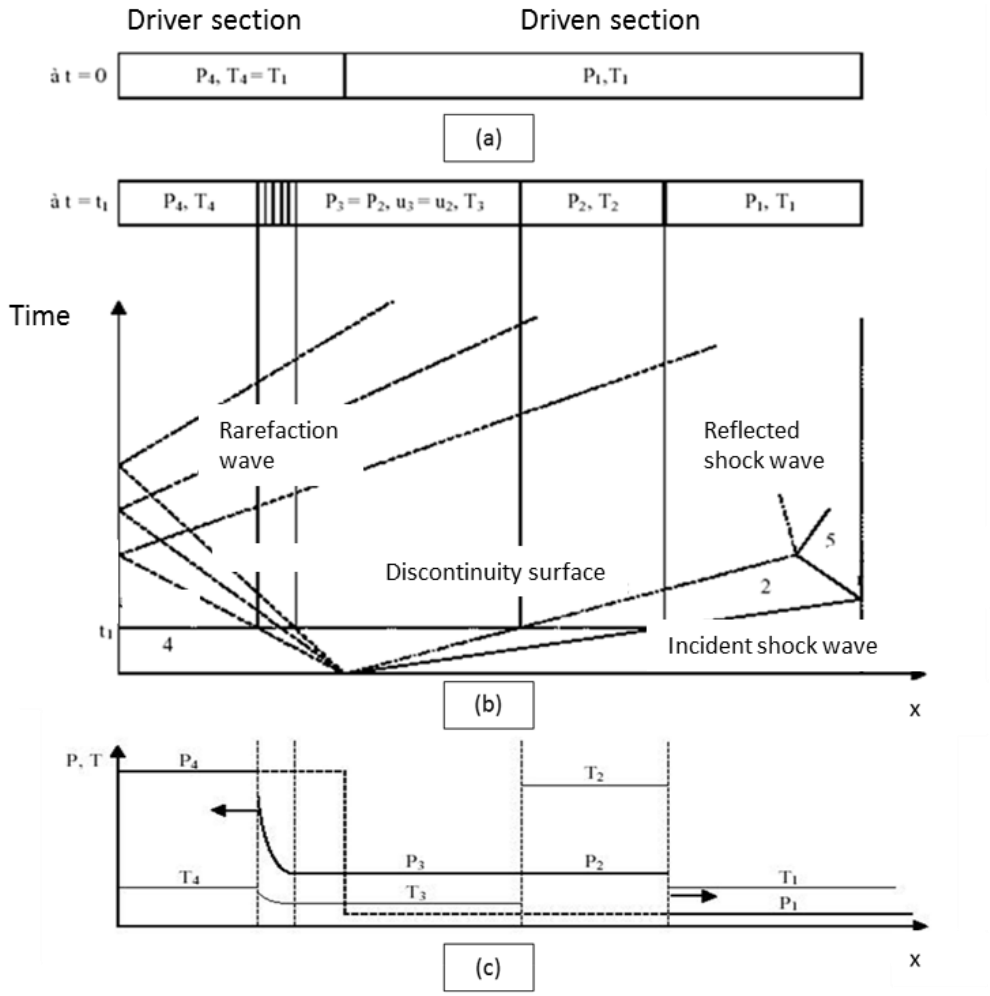

Figure 28: Principe of a shock tube. (a) Tube before the rupture of the membrane. (b) Propagation of the shockwave, the discontinuity surface, and the rarefaction wave as a function of time. (c) Profiles of pressure and temperature in the whole tube at the moment t_1 after the rupture of the membrane [118].

The intensity of the shock wave depends mainly on the speed of sound in the gases of two sections and the ratio of their specific heat. Strong shock wave can be achieved by using a driver gas allowing a high speed of sound. For this reason, the density of driver gas is low. On the contrary, a heavy gas is used as a diludant of the fuel gas mixture to be studied [119].

3.2.1.b Experimental set-up

Several studies have employed LRGP shock tube to measure the IDT of hydrocarbons whose carbon atom number varies between 1 and 7 [118, 120–122] . A photo of this shock tube is presented in Figure 29.

Figure 29: Photo of the LRGP schock tube.

Figure 30 presents the detail diagram of the LRGP shock tube used in this thesis.

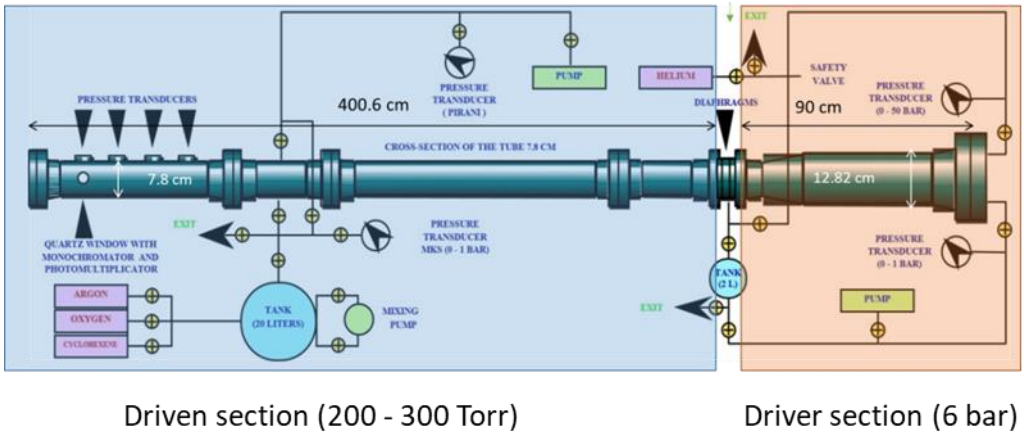

Figure 30: Detail diagram of the shock tube in LRGP, Nancy

The driven section of the tube has a length of 400.6 cm and an inner diameter of 7.8 cm. It is connected with two pumps which help to vacuum the driven section before the fill of a fuel gas mixture for a new test. The fuel gas mixture is prepared in a tank which provides the desired amount of fuel mixture in the driven section for each experiment. Four pressure sensors are attached to the inner wall of the tube. They are placed near the end of the tube. The distance between two consecutive sensors is 15 cm. The known distance between the positions of the sensors permits to deduce the speed of the shock wave. Based on this speed, the initial conditions (temperature, pressure, chemical composition) of the fuel gas mixture, and the thermodynamic properties of involved gases, the state (P_5, T_5) of the gases behind the reflected shock wave is calculated using a solver program based on equations of the conservation of mass, momentum and energy [123].

A monochromator (Ealing 82415) and a photomultiplier (Hamamatsu E 717-21) are used to tracks the emission of excited OH* radical at the wavelength of 306 nm.

The driver section of the shock tube has a length of 90 cm and an inner diameter of 12.82 cm. As the driven section, it is connected to a vacuum pump. Helium is used as the driver gas.

The intermediate compartment (length of 5.2 cm; inner diameter of 5.8 cm) is located between the driver and driven sections. It contains two 75µm-thick terphane membranes that can resist to a maximum pressure of about 4 bar. This part is connected to a vacuum pump. Additionally, this compartment is linked to a vacuum chamber. The opening of the connexion with the vaccum chamber allows the rupture of membranes by a sudden lowering of the pressure in the intermediate compartment.

The measurement of IDT is carried out behind the reflected shock wave at 10 mm from the end of the tube which is the position of the last pressure sensor. Ignition is monitored by the emission of OH* radicals. The effects of walls on the time of self-ignition are considered negligible as measured IDT are really short, i.e. between 10 µs and 1 ms.

3.2.1.c Experimental procedure

The driven part of the tube is prepared as follow. Initially, the entire tube is pumped using the three pumps to reach a vacuum condition (< 10^{-3} Torr). Then, the driven section of the tube is cleaned by introducing about 200 Torr of argon. After a few minutes, argon is purged and the driven section is reestablished vacuum (< 10^{-3} Torr). After that, 100 to 300 Torr of reactive gas mixture are introduced into the driven section for each experiment. This pressure is regulated to achieve the desired initial temperature of combustion (T_5). The gas mixture to be studied is previously prepared by the partial pressure method in a tank connected to the driven section. The gas mixtures are daily prepared for a total pressure of 800 Torr.

The intermediate compartment is then filled with helium at a pressure of about 3 bar. The preparation of each manipulation on the shock tube is finalized by filling 6 bar of helium in the driver section.

Once the tube is isolated, the shot is triggered by the opening of the valve allowing the very fast rupture of membranes. The shock wave then forms rapidly in the driven section of the tube at a distance of about 50 cm from the second membrane. This wave propagates to the end of the tube where it reflects to bring the reactive gas mixture to a high temperature (800 to 2000 K) and a pressure of up to 11 bar. The rise of the wall temperature does not exceed a few degrees Celcius because the gas is rapidly cooled by mixing with helium.

Time-based signal recordings from the four pressure sensors (see Figure 31) are used to calculate the speed of the shock wave. Each of the four curves has a first jump corresponding to the passage of the incident shock wave and a second one corresponding to that of the reflected shock wave. The time that elapses between the first jumps of two successive curves corresponds to the passage of the incident shock wave. The average of these three times (100 - 200 µs) is then provided in the calculation program.

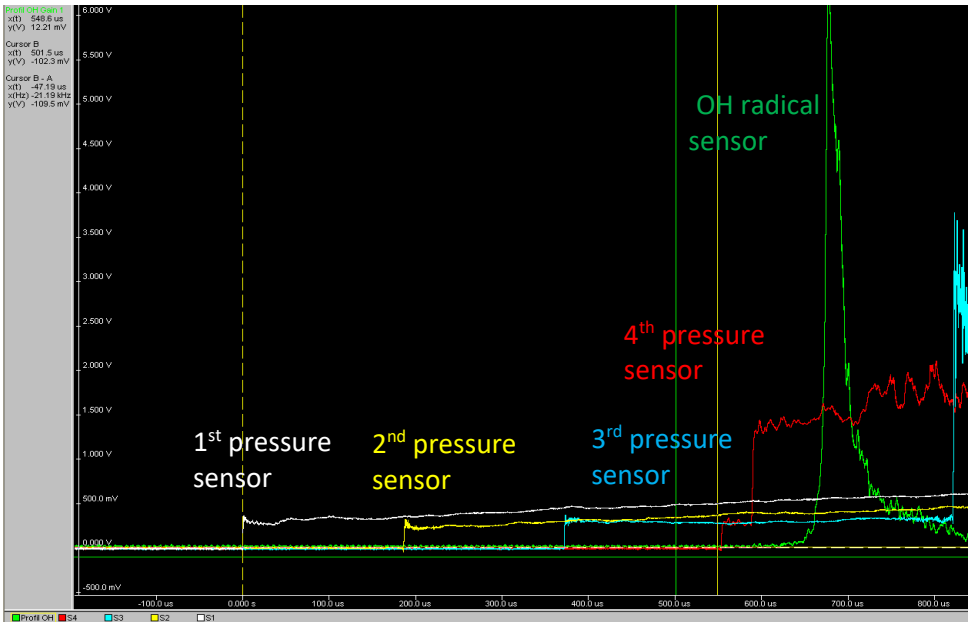

Figure 31: Typical profiles of pressure and OH radical during a ST experiment.

Figure 32 shows the determination of the IDT of each experiment. It is defined as the time elapsed between the second jump of the pressure curve of the last pressure sensor and the first 10% increase of the total signal of OH radicals. This criterion is often used in the literature. The measurable IDT varies from 10 to about 1000 µs. The condition of combustion (T_5, P_5) is determined by solving the conservation equations of mass, momentum, and energy. These equations are given in Appendix A2.

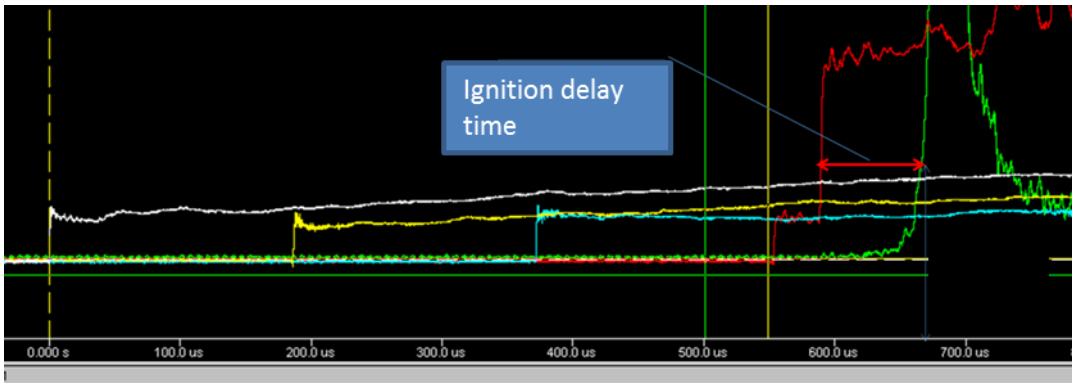

Figure 32: Determination of IDT for a ST test.

3.2.2 Rapid compression machine

Since the earliest researches dedicated to IC engine development, rapid compression machines (RCM) have been employed to explore the combustion properties of fuels at engine-relevant conditions [124]. In this thesis, experimental measurements of IDT of fuel at relatively low temperatures (T < 1000 K) are conducted in the RCM of the University of Orleans. The operating principle and details description of this RCM are presented in this section.

3.2.2.a Operating principle

RCM is an equipment permitting the compression of a fuel gas mixture to the desired condition (P_c, T_c) of combustion in a short time (about several ms) thanks to the movement of a piston. While ST is used to capture fuel reactivity at high temperatures (T > 1000 K) [116], RCM helps to characterize fuel

autoignition in a lower temperature range (T < 1000 K) [117] as presented in Figure 33. The data obtained from RCM are valuable to understand fuel reactivity at LTC-combustion conditions.

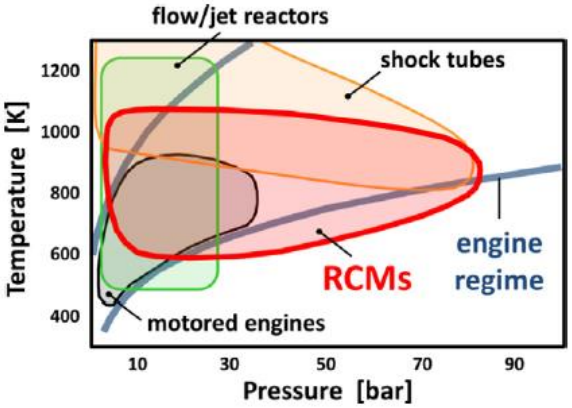

Figure 33: Temperature-pressure diagram of typical working conditions for experimental equipment and IC engines. This figure is adopted from the work of Goldsborough et al. [117].

The single-piston RCM of the University of Orleans has three main parts: the combustion chamber, the hydraulic system, and the pneumatic system. A simplified diagram of the considered RCM is presented in Figure 34. The pneumatic system provides the motive power for the piston to compress the fuel gas mixture in the combustion chamber. At the top dead center (TDC) position, the piston is locked nearly immediately by the hydraulic system.

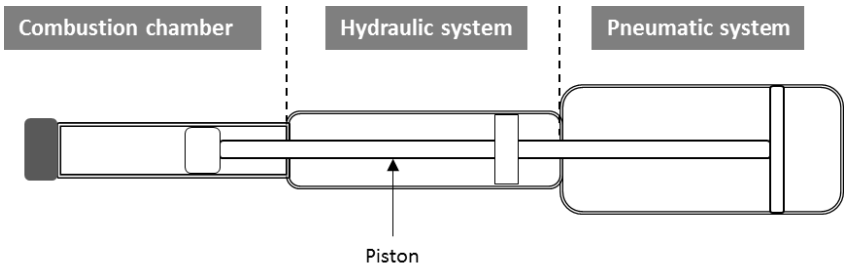

Figure 34: Three main parts of the RCM of the University of Orleans.

The condition (P_c, T_c) of the combustion of RCM experiments depends principally on several factors as intake condition (T_0, P_0, chemical composition) of fuel gas mixture and compression ratio. Value of P_c is experimentally recorded by pressure sensors. The temperature of the combustion chamber varies importantly from near 400 K (before piston movement) to near 900 K (when piston stops) and reaches to several thousand K during the combustion of fuel. Thus, it is really difficult to experimentally obtain the value of T_c. For experiments at the RCM of the University of Orleans, this value is calculated thanks to the isentropic relation, where γ is the ratio of specific heats of gas mixture:

$$\int_{T_0}^{T_c} \frac{\gamma}{\gamma - 1} \frac{dT}{T} = ln\left(\frac{P_c}{P_0}\right) \qquad (Eq. 2)$$

As the RCM is employed to explore autoignition chemistry of fuels, physical effects need to be mitigated as much as possible. To this, several factors must be carefully considered while building a RCM such as the gas compression process and crevice volume of piston [117].

Ideally, the compression process of RCM should be likely spontaneous as in the case of ST to limit heat exchange and chemical reactions. However, a really high-speed piston is not feasible in practice. Thus, RCM design must be undertaken in care to optimize the period of compression of the RCM. A typical

parameter noted as t_{50} is usually used to characterize the compression phase of RCM. This parameter is defined as the period necessary for the rise of P_c from $P_{c,max}/2$ to $P_{c,max}$ ($P_{c,max}$ is the value of P_c at the TDC). As explained by Goldsborough et al. [117], the value t_{50} of RCM is informative since it indicates the duration of gas mixture being at near-TDC conditions. This value is required to be short especially in the case of IDT measurements of very reactive mixtures. The t_{50} of the RCM of the University of Orleans is 4 ms. Another parameter needs to be well controlled is the piston rebound. Once the piston of RCM stops, it can slightly move back in the expansive direction. This phenomenon is called piston rebound. Cassel et al. [125] showed that a small variation of the combustion chamber at TDC could importantly affect the gas mixture temperature and then make experimental results difficult to be interpreted. In the RCM of this thesis, the pneumatic method is used to drive the piston while the hydraulic system is employed to stop pistons movements. The latter method is effective to suppress piston rebounds as suggested in the literature [117].

During the compression process, vortex formation can be observed. This results from the non-desired movement of gas boundary layers. Figure 35 represents the mechanism of vortex formation while a flat piston is employed. The actual design of RCM follows several suggestions in the literature [126, 127] to use creviced piston to suppress vortex formation. This helps to maintain the post-charge homogeneity.

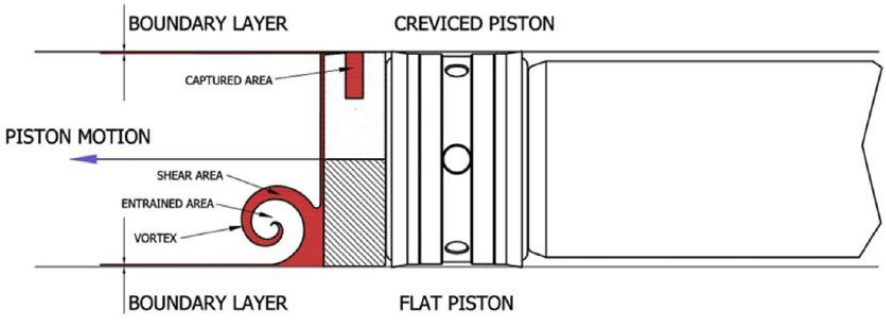

Figure 35: Vortex formation in the case of flat piston. This figure is entirely adopted from the work of Sung et al. [128].

3.2.2.b Experimental set-up

The RCM of the University of Orleans has been used to investigate the combustion properties of ammonia [129]. The photo of this machine is shown in Figure 36.

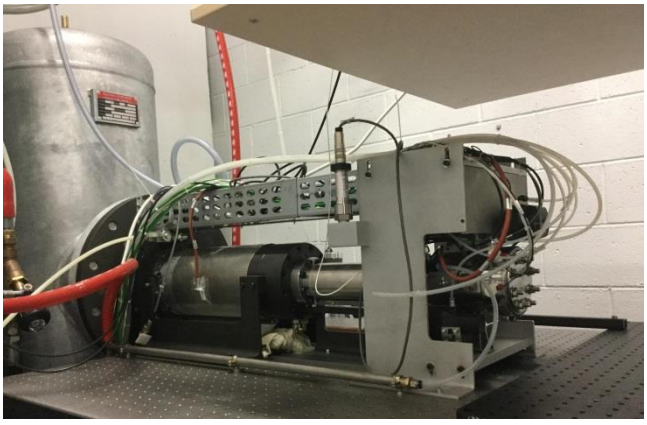

Figure 36: Photo of the RCM of the University of Orleans.

Figure 37 illustrates a simplified diagram of the RCM used in this thesis.

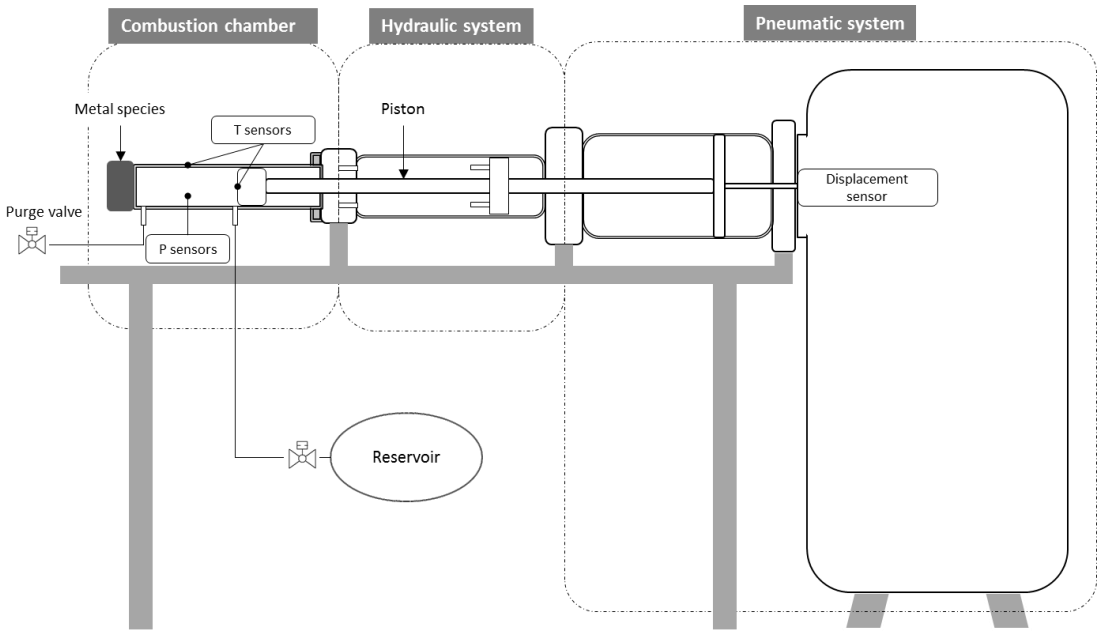

Figure 37: Simplified diagram of the RCM of the University of Orleans.

Reacting mixtures are prepared in a reservoir. Mass flows rates of gases comprising N_2, O_2 are regulated by Bronkhorst Cori-flow M13.

The piston of the RCM is pneumatically powered by pressurized air (7 bar) stocked in a big tank. A hydraulic system is employed to immediately lock the piston at TDC. The pressure of oil used in this system is regulated by a hydraulic pump. A vacuum pump is used to get a vacuum condition in the combustion chamber before each experiment.

The stroke and the bore of the piston of the RCM have a length of 300 mm and 50 mm respectively. This piston has a crevice volume of 9.94 cm^3. The displacement of the piston is recorded by a sensor Penny & Giles ICS 100. The duration of each compression process is about 33 ms. The volume of the combustion chamber varies from 12.96 cm^3 to 57.53 cm^3. This volume is adjusted by the incorporation of some metal rings at the endpoint of the RCM. The variation of the combustion chamber enables the change in the compression ratio between 8.9 and 20.7. The latter parameter along with the intake temperature (T_0) and intake pressure (P_0) help to achieve the desired initial conditions (P_c, T_c) of the combustion at TDC. The intake pressure is measured by a Keller PAA-33X/80794 piezoresistive transducer while the pressure history of the combustion chamber is registered thanks to a AVL QH32C piezoresistive transducer. The intake temperature corresponds to the initial temperature of the combustion chamber and the piston. The temperatures including intake temperature and the temperature of the reservoir are controlled by K thermocouples. The errors of measurement of in-cylinder pressure, intake pressure, intake temperatures, and mass flow rate are ± 1%, ± 1 mbar, ± 2 K and ± 1% respectively.

All operations of the RCM comprising piston movement, vacuum check, work of hydraulic pump, regulations of intake temperature, intake pressure, and temperature of the reservoir are automatically proceeded thanks to a central computer.

The important characteristics of the RCM of the University of Orleans are summarized in Table 12.

Table 12: Main characteristic of the RCM of the University of Orleans.

Parameter	Value
Compression time	35 ms
Time $P_{c,max}/2$ to $P_{c,max}$ (t_{50})	4 ms
Piston acceleration/deceleration time	15/5 ms
Crevice volume	9.94 cm^3
Compression ratio	8.9; 12.9; 20.7
Stroke, bore	300 mm, 50 mm

3.2.2.c *Experimental procedure*

Before each experiment in the RCM, the fuel gas mixture is prepared in the reservoir. The liquid fuel is introduced into the reservoir by a syringe. It is the unique manual step in this experimental procedure. All other steps are carried out thanks to the central computer. After the introduction of the liquid fuel, N_2 and O_2 are added in the reservoir to obtain the desired gas mixture. A mechanic agitation during 30 minutes is conducted to ensure the homogeneity of mixtures. The temperature of this reservoir is maintained at 80°C to avoid condensation of fuels. All mixtures are prepared on the day of manipulation.

The compression piston is returned to the bottom dead center (BDC) position thanks to the pneumatic system. The combustion chamber is cleaned by air and then set in vacuum condition thanks to the vacuum pump. The temperatures of the combustion chamber and the compression piston are fixed at a targeted value which varies from 50 to 120 °C.

The fuel gas mixture is then aspired into the combustion chamber at a requested P_0 varying from 200 to 1200 mbar. The IDT measurement is now ready to start. A signal from the central computer is sent to the pneumatic system to push brutally the driving piston toward the TDC position. The fuel gas mixture is compressed by the piston movement. The fuel ignition occurs in the combustion chamber at the TDC position.

Figure 38 illustrates a typical pressure history of the combustion chamber during a RCM experiment. At low temperature (T < 750 K), two-stage ignitions can be observed. In this thesis, the main IDT is defined as the time between the end of the compression and the Maximum Pressure Rise Rate (MPRR), which is the maximum value of *dP/dt* calculations. In the case of two-stage ignition, the 1st-stage IDT is defined as the time between the end of compression and the first distinguishable peak of *dP/dt* calculations. The measurable IDT by this RCM ranges from 1 to 200 ms.

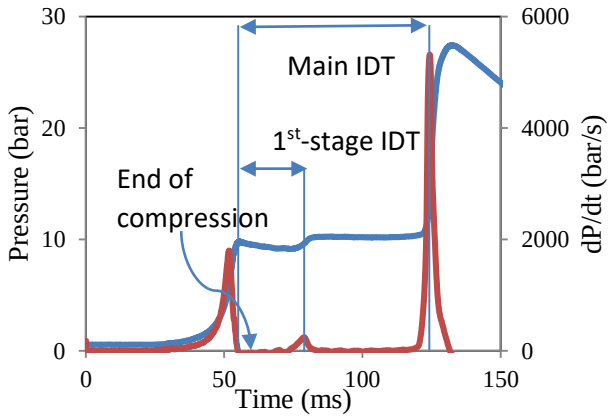

Figure 38: Typical pressure (blue line) and *dP/dt* (red line) profiles in RCM experiment. Experimental conditions: surrogate fuel, Φ = 0.5, 705 K, 10 bar.

For each measurement in RCM, three repetitions were conducted. The standard deviations of 1st-stage IDT and main IDT in this work are ±10% and ±5% respectively. Under each condition, very good repeatability of P_c is observed as presented in Figure 39.

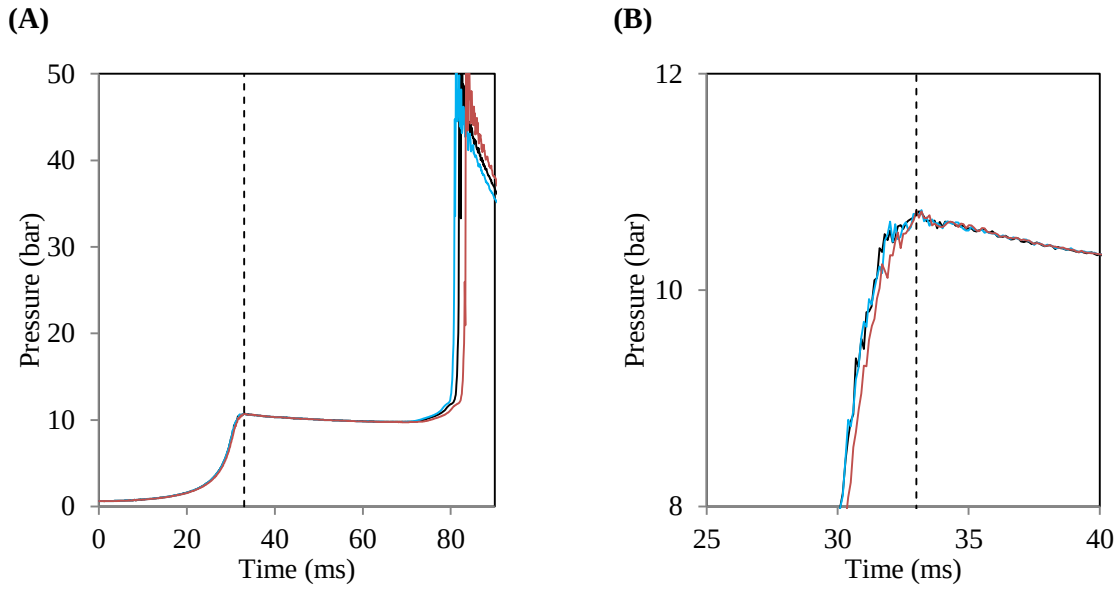

Figure 39: Pressure histories of three successive RCM tests (solid lines with different colors) for the neat surrogate fuel at P_c = 10 bar, T_c = 675 K, Φ = 1. End of compression: vertical dashed line. (A): whole range of time. (B): zoom in the range of time near the end of compression.

3.2.2.d Simulation of RCM experiments

Experiments conducted in ST and flat flame burner can be considered as adiabatic. Simulations of experimental results of ST and flat flame burner are relatively simple and performed in 0-D closed homogeneous reactor model and 1-D pre-mixed burner model respectively in CHEMKIN-PRO [130]. Simulations of RCM experiments are more complex. RCM experiments involve two phases: compression phase and combustion phase. IDT measured in a RCM can be simulated by using a homogenous reactor model with two common approaches. The first method named "frozen chemistry" assumes that no reactions occur during the compression process. The thermodynamic inputs of this simulation method are conditions (P_c, T_c) at the TDC. The second method entitled "all-simu" considers the chemical reactivity of the gas mixture during the piston movement. The intake pressure (P_0) and the piston initial temperature (T_0) are used as the initial thermodynamic conditions for modeling. The heat loss during a RCM test is taken into account by using an "effective volume" for both two simulation methods. This corresponds to a volume profile obtained by conducting non-reactive experiments where O_2 is replaced by N_2. This implies that the initial conditions (P_0, T_0) are similar to those of reactive experiments. The non-reactive pressure trace is then used in a calculation of the adiabatic core hypothesis to deduce the volume profile as described by Tanaka et al. [131]. Both simulation methods were adopted in this study in order to discuss their applicability. The simulation results obtained thanks to the 0-D closed homogenous reactor model in CHEMKIN-PRO [130] are discussed further.

3.2.3 Heat flux burner

This section is dedicated to presenting the principle of the burner used in this thesis to measure the laminar burning velocity of fuels. Fundamental characteristics of flame velocity are also presented.

3.2.3.a Genaralities about flame

There are two types of flame: premixed flames and diffusion flames. These flames are distinguished by the formation of gas mixture. In the case of premixed flames, fuel is mixed with the oxidant (usually air) before the flame. However, in diffusion flames, the mixture of fuel and oxidant is completed by diffusion in opposite directions from the fuel and from the oxidant to the reaction zone [132].

Flames can be generated under two flow regimes: laminar and turbulent. In a laminar flow, two nearby fluid particles at a given moment remain close to each other until the following moments. Meanwhile, no apparent organization is observed in turbulent regime. Fluid flow is characterized by a dimensionless number called Reynolds number. This number depends on speed of flow, density, and viscosity of fluid. Reynolds number represents the relative importance of the inertial forces associated with velocity and the friction forces associated with viscosity. If the latter is dominant (Reynolds number < 2000), the fluid layers maintain their cohesion and the flow is laminar. Otherwise, the flow is in a turbulent regime. The formula for this number is presented in Eq.3 with u is the velocity of the fluid (m/s), L is a characteristic linear dimension (m), and v is the kinematic viscosity of the fluid (m^2/s).

$$Re = \frac{uL}{\nu} \qquad (Eq.3)$$

This thesis focuses on laminar premixed flames. This type of flame has often a very small thickness that is considered zero at first approach. The flame is thus represented by a discontinuity surface separating the fresh gases from the hot burnt gases, called the "flame front". The velocity of flame front is considered as the rate of propagation of flame. In an ideal case where a flat flame of a burner is perfectly stabilized, the velocity of the flame front has no tangential component and corresponds to the normal velocity noted as S_L. The latter is regarded as the fundamental velocity of the laminar flame (see Figure 40) [132]. The velocity of flame depends importantly on fuel, oxidant, pressure and initial temperature [133].

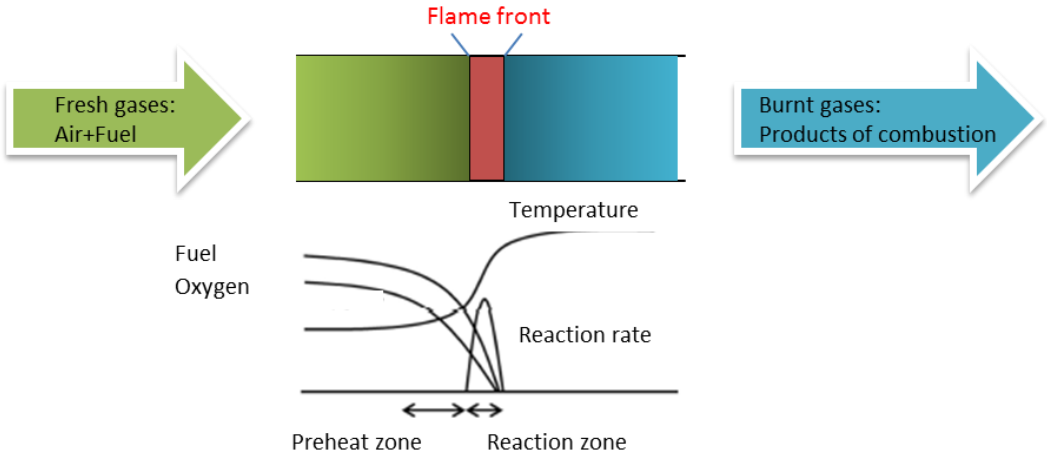

Figure 40: Structure of a laminar flame [133].

From a chemical point of view, flames correspond to the gas-phase oxidation of fuel at high temperatures (T > 900 K) in which decomposition reactions dominate [133]. The formed radicals emit visible radiations which are responsible for the appearance of flame.

By definition, the fundamental velocity S_L of flame is calculated by considering a flat surface of flame perpendicular to the gas flow. For this, the considered flame is laminar, steady, plane, unstretched, and adiabatic. Among these characteristics, the two most important factors are flame stretch and flame adiabaticity. Flame stretch is quantified as the fluctuation of the flame area. A flame is

considered adiabatic only if the heat released by fuel oxidation is used entirely to heat the adjacent fresh gas without any exchange with environment.

To measure laminar burning velocity of fuels, several methods are proposed in the literature. They differ according to different experimental equipment. In this study, a heat flux burner is employed. The operating principle, as well as the detail description of this burner, are further presented.

3.2.3.b Operating principle

The burner used in this thesis is an adiabatic flat flame burner named heat flux burner. This type of burner has been developed in several studies such as Van Maaren et al. [135], Dyakov et al. [136], Konnov et al. [137].

To stabilize the flame, this type of burner compensates for thermal losses by convective heat flows from the burner surface to flame front. The heat exchange is thus zero and it can be proved that the velocity of gases corresponds to the adiabatic laminar burning velocity [133]. Figure 41 represents a typical figure of this type of burner.

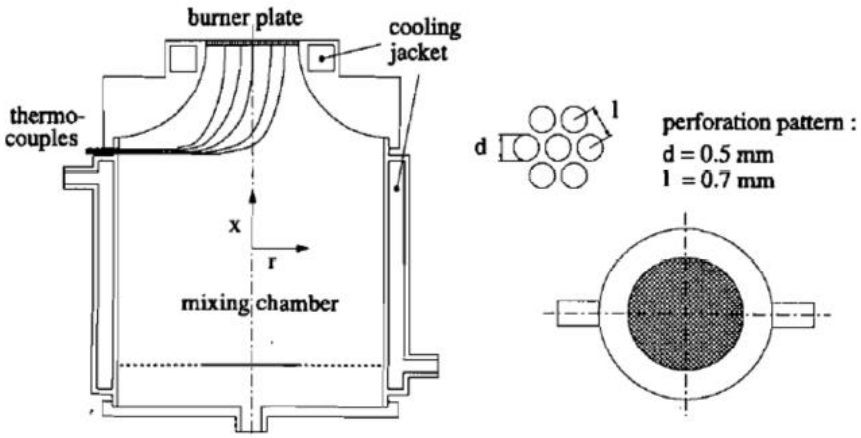

Figure 41: Diagram of an adiabatic flat flame burner [135].

The burner has a perforated plate at the head of the mixing chamber. A series of thermocouples is placed on its radial axis in the form of a diverging spiral. The temperature of the plate is kept higher (about 50 K) than that of the combustion chamber. This helps to reward thermal losses of flames.

In the condition of an adiabatic flame, the temperatures of all thermocouples are similar. If the velocity of gases is less than the adiabatic burning velocity, the heat exchange, which is the difference between the absolute value of heat loss of burner to environment and the heat gain of the burner from the heated perforated plate, is negative. In this case, the flame approaches the burner whose center is warmer than its periphery. The flame is then stabilized at subadiabatic condition. Conversely, if the speed of the fresh gases is higher than the adiabatic burning velocity, the flame moves away from the burner whose center is colder than its periphery. The flame is stabilized at superadiabatic conditions. To summarize, the velocity of the adiabatic flame is determined by adjusting the gas flow to obtain a uniform temperature profile at any point in the perforated plate of burner. Thus, the velocity of adiabatic flame S_L (cm/s) is calculated by the equation Eq.4.

$$S_L = \frac{Q_v}{S} \qquad (Eq.4)$$

With :

- Q_v: volumetric flow of fresh gas (cm^3/s)
- S: area of the perforated plate of burner (cm^2)

3.2.3.c *Experimental set-up*

The burner used in this thesis is similar to the one presented in Figure 41. The perforated plate of the burner is made of brass. Its diameter is 30 mm and its thickness is 2 mm. Each perforation has a diameter of 0.5 mm and the step between the holes is 0.7 mm as suggested by Van Maaren et al. [135]. Eight K-type thermocouples with a diameter of 0.5 mm are placed in the holes on the surface of the plate. These thermocouples are positioned on the radial axis of the plate surface at different distances and angles from the center to the periphery of the plate.

Figure 42 represents the whole experimental set-up used to measure the flame velocity of fuel in this study.

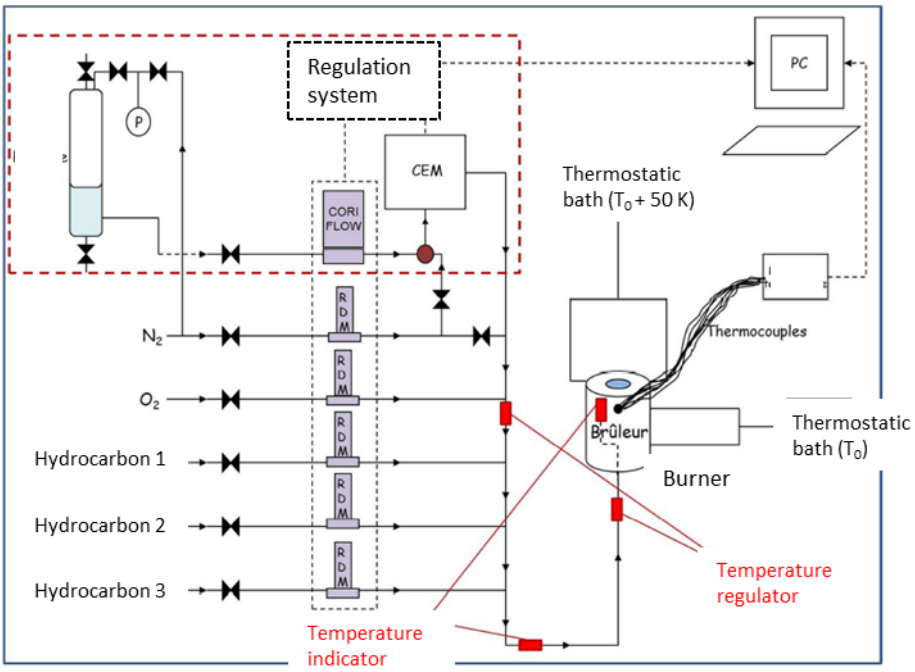

Figure 42: Diagram of the experimental set-up employed to measure flame velocity in this thesis.

The liquid fuel mixture is put in a stainless steel reservoir and pressurized by nitrogen. The volumetric flow of liquid fuel is regulated by a "Coriflow" liquid flow meter by Bronkhorst® High-Tech. The advantage of this type of flow meter is its capability to measure massic flow without the acquaintance of physics-chemical data specific to the fuel. Then the liquid fuel is vaporized into the Evaporation and Mixing Control (EMC) system. The vapors released from the EMC join the airflow to form the reactive gas mixture. Temperature regulators are placed in the pipes connecting the flow meters with the burner. They allow the pipes to be slightly heated to avoid condensation of liquid fuel. Temperatures of the mixing chamber and burner plate are controlled by thermostatic baths. A computer is used to regulate flow meters and track the temperature of thermocouples placed on the burner plate. The uncertainty in measured laminar burning velocity is about 1 m/s.

3.2.4 Experimental matrix

All chemical compounds used in this thesis come from Sigma-Aldrich®. Characteristics of these compounds such as density and purity are presented in Table 13.

Table 13: Principal characteristics of chemical compounds employed in this thesis.

Compound	CAS number	Density (g/ml) at 25°C	Purity
Toluene	108-88-3	0.865	99.8%
n-Heptane	142-82-5	0.684	99%
EHN	27247-96-7	0.963	97%
2,4-Xylenol	105-67-9	1.011	98%
Ferrocene	102-54-5	1.490	98%

Table 14 presents the experimental matrix for the study of the effect of additives in the ST and the flat flame burner in this thesis. Four fuels are considered. First, the "surrogate" fuel containing reference hydrocarbons: toluene and *n*-heptane. Next, "srgt_EHN" "srgt_2,4-xylenol" and "srgt_ferrocene" fuels are considered to study the effect of additives: EHN, 2,4-xylenol, and ferrocene respectively. EHN and 2,4-xylenol are introduced into fuels at a dosage of 1% weight basis. This kind of doping level was used by Hartmann et al. [69] while studying the promoting effect of EHN in a ST and a flat flame burner. As a concentration limitation is applied for the use of ferrocene in fuels [76], the effect of this additive is examined at a concentration of 0.1% by mass.

Table 14: Fuel matrix investigated in the ST and in the flat flame burner in this thesis.

Fuel	Chemical compound included in fuel			Composition (% mass)			Composition (% molar)		
	C1	C2	C3	C1	C2	C3	C1	C2	C3
Surrogate	Toluene	*n*-Heptane	-	70.10	29.90	-	71.86	28.14	-
Srgt_EHN	Toluene	*n*-Heptane	EHN	69.40	29.60	1.00	71.47	27.99	0.54
Srgt_2,4-xylenol	Toluene	*n*-Heptane	2,4-xylenol	69.40	29.60	1.00	71.30	27.92	0.78
Srgt_ferrocene	Toluene	*n*-Heptane	Ferrrocene	70.10	29.80	0.10	78.13	28.12	0.05

Table 15 represents the experimental matrix dedicated to the study of the effect of additives in the RCM in this thesis. Similar to the matrix for the ST and the flat flame burner, four fuels are considered as "surrogate", "srgt_EHN", "srgt_2,4-xylenol", and "srgt_ferrocene". However, the doping levels of fuel additives are modified. To facilitate the comparison of the effect of different additives on specific behaviors of fuel combustion as two-stage ignition and NTC, dopant concentrations are calculated based on the molar basis. The doping levels of EHN and 2,4-xylenol are 0.1 and 1% mol.. Meanwhile, the dosage of ferrocene is fixed at 0.01 and 0.1% mol. since this additive is limited in terms of practical concentration [76].

Table 15: Fuel matrix investigated in the RCM in this thesis.

Fuel	Chemical compound included in fuel			Composition (% mol)		
	C1	C2	C3	C1	C2	C3
Surrogate	Toluene	*n*-Heptane	-	71.86	28.14	-
Srgt_EHN_A	Toluene	*n*-Heptane	EHN	71.14	27.86	1.00
Srgt_EHN_B	Toluene	*n*-Heptane	EHN	71.79	28.11	0.10
Srgt_2,4-xylenol_A	Toluene	*n*-Heptane	2,4-xylenol	71.14	27.86	1.00
Srgt_2,4-xylenol_B	Toluene	*n*-Heptane	2,4-xylenol	71.79	28.11	0.10
Srgt_ferrocene_A	Toluene	*n*-Heptane	Ferrrocene	71.79	28.11	0.10
Srgt_ferrocene_B	Toluene	*n*-Heptane	Ferrrocene	71.86	28.13	0.01

3.3 Conclusions

To investigate the effect of additives, a surrogate fuel is considered in this study. Based on the suggestions of the literature, this surrogate is selected as a mixture of 35% *n*-heptane and 65% toluene by volume. The RON of this fuel is 84. This surrogate is employed to investigate the effect of fuel additives at various conditions (P, T, Φ) especially on some specific phenomena of combustion as two-

stage ignition and NTC. This also contributes to the comprehension of toluene reactivity at low temperatures (T < 900 K) which has not been fully understood in the literature.

Three additives targeted in this thesis are EHN, ferrocene, and 2,4-xylenol. They represent respectively three types of additive being able to affect the gas-phase reactivity of fuel as cetane boosters, octane boosters, and free radical scavengers. The effect of these additives is experimentally and numerically investigated in three devices including ST, RCM, and heat flux burner. These devices permit to examine the impact of additives on the combustion properties of fuel, which are fundamentally represented by two parameters as ignition delay time and laminar burning velocity. Moreover, these various experimental devices enable the study of the effect of fuel additives on fuel chemistry at a wide range of temperatures covering from near 675 K to near 2000 K. The last aspect remains little discussed in the literature.

To simulate the experimental results of the effect of additives, a detail kinetic model is developed based on the literature data. This model includes the chemistry of the surrogate fuel and two additives (EHN and ferrocene).

In the next chapters the construction and the validation of the kinetic model are shown. Then, the experimental results are presented and discussed with simulation results. The latter results are obtained thanks to the kinetic model developed in this thesis. Two simulation methods of RCM experiment are carefully discussed to justify their performance. After that, main key chemical reactions representing additives effect are shown. In the end of this chapter, the validated model is employed to predict the effect of the considered additives at different thermodynamic condition (P, T, Φ) on various type of fuels.

Chapter 4: Kinetic modelling

A detailed kinetic model is developed in this thesis to simulate the effect of the studied additives on the combustion of the surrogate fuel. This model consists of sub-mechanisms of the surrogate fuel and two additives, EHN and ferrocene. As the inhibiting effect of 2,4-xylenol is small as observed by McCornick et al. [47], the development of a sub-mechanism for this additive is not considered in priority. The structure of the proposed new kinetic model is graphically summarized in Figure 43. This model contains three main parts: the sub-mechanism of the surrogate fuel, the chemistry of NO_x, and the sub-mechanisms of both additives EHN and ferrocene. The construction of each part is described further in this chapter.

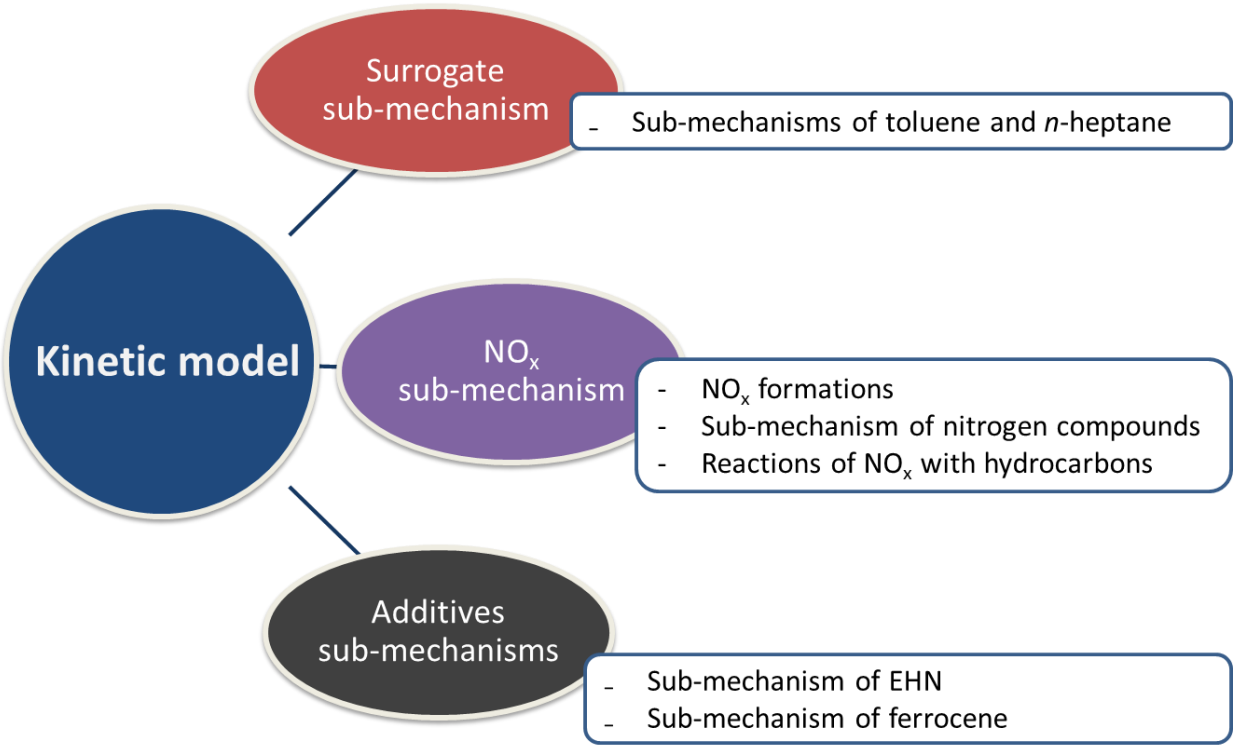

Figure 43: Structure of the kinetic model developed in this study.

4.1 Sub-mechanism of the surrogate fuel

The sub-mechanism of the combustion of the surrogate fuel is adopted from the model of Lawrence Livermore National Laboratory (LLNL) [42], which contains the detailed chemistry of toluene and *n*-heptane oxidation. This model was validated against various experimental data collected in rapid compression machine, shock tube, and jet stirred reactor covering a wide range of conditions relevant to IC engines (3 – 50 atm, 650 – 1200 K, stoichiometric mixtures). Recently, Yuan et al. [105, 106] and Zhang et al. [138] made great efforts to develop detailed kinetic models of toluene and *n*-heptane respectively. To compare the performance of the model of LNLL with these recent models, experimental data of toluene and *n*-heptane oxidation in a perfectly stirred reactor (PSR) were simulated. These experiments were conducted at 10 bar, $\Phi = 1$, and from 550 to near 1000 K by Moréac et al. [43]. Figure 44 illustrates the simulation results. It was found that the profile of *n*-heptane was well simulated by both the model of LLNL and the model of Zhang et al. [138]. In the case of toluene, its reactivity at temperatures from 900 to 950 K was overpredicted by the model of LLNL and better simulated by the recent model developed by Yuan et al. [105, 106]. As the surrogate fuel contains

dominantly toluene, an update of the sub-mechanism of this compound is performed to improve the performance of the reference model [42].

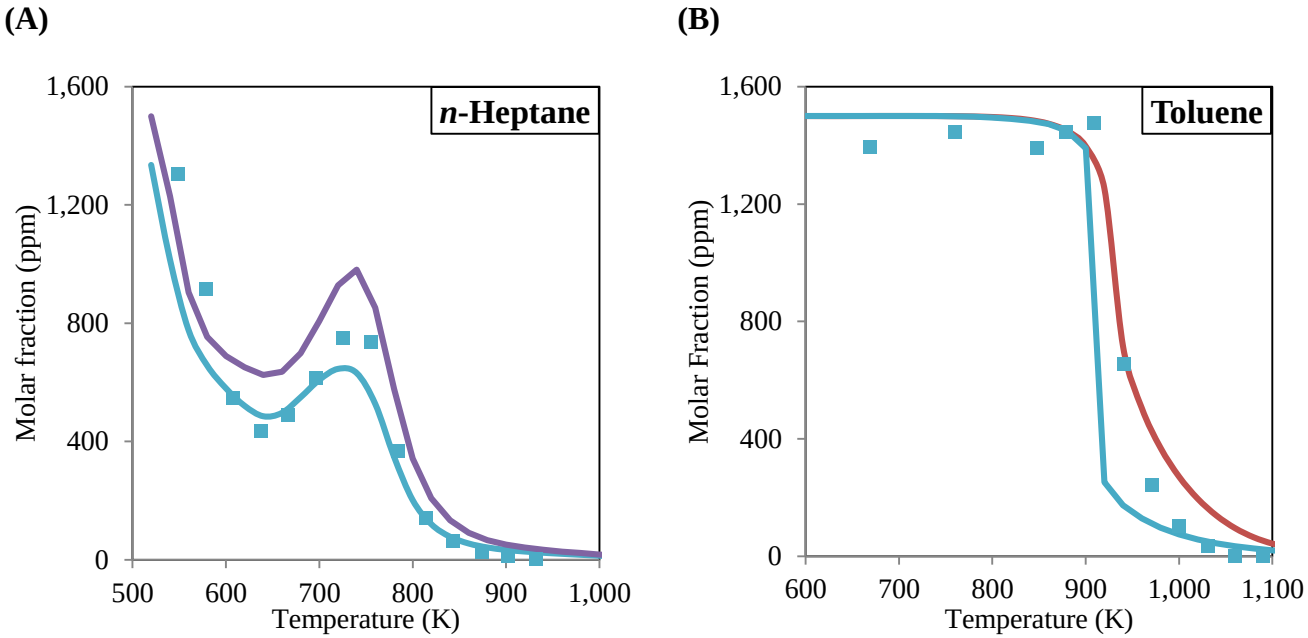

Figure 44: Species profiles of fuel at 10 atm, Φ = 1, from 500 to 1100 K. Symbols: experimental results from Moréac et al.[43]. (A): *n*-heptane. (B) toluene. Blue lines: simulations conducted with the model of LLNL [42]. Purple line: simulations conducted with the model of Zhang et al. [138]. Red line: simulations conducted with the model of Yuan et al. [105, 106].

The toluene sub-mechanism is updated following mostly the study of Yuan et al. [105, 106]. The updated sections include some elementary reactions of toluene and its derived radicals and of molecular products, e.g., benzyl, methylphenyl, benzene and its derivatives (phenyl, phenol, etc.), and small unsaturated compounds C_2-C_4. The sensitivity of 1,3-cyclopentadiene (CY13PD) and cyclopentadienyl radical (CY13PD5J) chemistry on the toluene reactivity was highlighted by Yuan et al. [106]. Therefore, the CY13PD sub-mechanism is updated according to recent data by the group of Mebel [139–141]. This last part is also important for the development of the sub-mechanism of ferrocene since this additive involves two cyclopentadienyl fragments in its chemical structure. The most important updates, i.e. new added reactions or new rates constants for existing reactions in the reference model [42], are listed in Table 16 and described in this section.

Table 16: Updated reactions of toluene

Reaction		A	n	E_a	Ref.
R1	$C_6H_5CH_3 = C_6H_5CH_2 + H$	2.78×10^{15}	0.17	91168	[142]
R2	$C_6H_5CH_3 = C_6H_5 + CH_3$	1.95×10^{27}	-3.16	107447	[142]
R3	$C_6H_4CH_3 + H = C_6H_5CH_3$	1.00×10^{14}	0.00	0	[105]
R4	$C_6H_5CH_3 + H = C_6H_5CH_2 + H_2$	6.77×10^{0}	3.98	3384	[143]
R5	$C_6H_5CH_3 + H = C_6H_4CH_3 + H_2$	3.91×10^{8}	1.80	16352	[144]
R6	$C_6H_5CH_3 + OH = C_6H_5CH_2 + H_2O$	1.77×10^{5}	2.39	-602	[145]
R7	$C_6H_5CH_3 + OH = C_6H_4CH_3 + H_2O$	1.36×10^{4}	2.69	620	[145]
R8	$C_6H_5CH_3 + O_2 = C_6H_5CH_2 + HO_2$	2.18×10^{7}	2.50	46045	[146]
R9	$C_6H_5CH_3 + O_2 = C_6H_4CH_3 + HO_2$	1.70×10^{7}	2.00	51633	[147]
R10	$C_6H_5CH_3 + H = C_6H_6 + CH_3$	2.40×10^{13}	0.00	5123	[147]
R11	$C_6H_5CH_3 + OH = C_6H_5OH + CH_3$	7.83×10^{2}	2.88	3221	[145]
R12	$C_6H_5CH_3 + OH = HOC_6H_4CH_3 + H$	3.14×10^{1}	3.36	4719	[145]
R13	$C_6H_5CH_3 + O = OC_6H_4CH_3 + H$	1.66×10^{7}	1.80	3974	[105]
R14	$C_6H_5CH_2 + O = C_6H_5CH_2O$	2.28×10^{14}	0.00	0	[148]
R15	$C_6H_5CH_2 + HO_2 = C_6H_5CH_2OOH$	3.70×10^{37}	-16.33	-67470	[149]
R16	$C_6H_5CH_2 + O_2 = C_6H_5CH_2O + O$	6.30×10^{12}	0.00	40000	[150]
R17	$C_6H_5CH_2OO = C_6H_5CH_2 + O_2$	4.17×10^{36}	-7.07	32200	[151]
R18	$C_6H_5CH_2O = C_6H_5CHO + H$	3.04×10^{32}	-6.66	21880	[152]
R19	$C_6H_5CH_2O = C_6H_6 + CHO$	2.57×10^{31}	-6.21	25760	[152]
R20	$C_6H_5CH_2O = C_6H_5 + CH_2O$	4.59×10^{43}	-9.51	39050	[152]
R21	$C_6H_5CH_2OO = C_6H_5CHO + OH$	3.88×10^{68}	-17.73	58456	[147]
R22	$C_6H_5CH_2OO + H = C_6H_5CH_2O + OH$	3.80×10^{14}	-0.19	1890	[153]
R23	$C_6H_4CH_3 + O_2 = O_2C_6H_4CH_3$	1.00×10^{13}	0.00	0	[42]
R24	$C_6H_4CH_3 + O_2 = OC_6H_4CH_2 + OH$	4.35×10^{23}	-3.36	8980	[42]
R25	$C_6H_4CH_3 + O_2 = OC_6H_4CH_3 + O$	2.44×10^{18}	-1.60	5040	[154]
R26	$C_6H_4CH_3 + O_2 = o\text{-}C_6H_4O_2 + CH_3$	2.00×10^{14}	0.00	9000	[105]
R27	$C_6H_6 + O = C_6H_5 + OH$	2.00×10^{13}	0.00	14700	[155]
R28	$C_6H_6 + OH = C_6H_5 + H_2O$	2.34×10^{4}	2.68	733	[145]
R29	$C_6H_6 + HO_2 = C_6H_5 + H_2O_2$	1.44×10^{13}	0.00	30997	[156]
R30	$C_6H_5 + O = C_5H_5 + CO$	9.00×10^{13}	0.00	0	[147]
R31	$C_6H_5 + OH = C_6H_5O + H$	5.00×10^{13}	0.00	0	[147]
R32	$C_6H_5 + HO_2 = C_6H_5O + OH$	5.00×10^{12}	0.00	0	[147]
R33	$C_6H_5 + O_2 = C_6H_5O + O$	2.60×10^{13}	0.00	6120	[147]
R34	$C_6H_5 + O_2 = C_6H_5O_2$	1.86×10^{13}	-0.22	-711	[147]
R35	$C_6H_5 + O_2 = o\text{-}C_6H_4O_2 + H$	3.00×10^{13}	0.00	9000	[105]
R36	$CY13PD + H = CY13PD5J + H_2$	7.20×10^{13}	0.00	3500	[105]
R37	$CY13PD + O = CY13PD5J + OH$	4.77×10^{4}	2.70	1106	[105]
R38	$CY13PD + OH = CY13PD5J + H_2O$	3.08×10^{6}	2.00	0	[105]
R39	$CY13PD + HO_2 = CY13PD5J + H_2O_2$	1.10×10^{4}	2.60	12900	[105]
R40	$CY13PD + O_2 = CY13PD5J + HO_2$	4.00×10^{13}	0.00	37150	[105]
R41	$CY13PD5J + O_2 = CYPDONE + OH$	8.77×10^{1}	3.11	23496	[141]
R42	$CY13PD5J + O_2 = CJCXCCXO + CO$	7.86×10^{8}	0.64	23700	[141]
R43	$CY13PD5J + O = CYPDONE + H$	2.92×10^{10}	0.72	-380	[140]
R44	$CY13PD5J + O = C_4H_5\text{-}N + CO$	4.85×10^{14}	-0.26	5560	[140]
R45	$CY13PD5J + OH = C5H5O13 + H$	2.55×10^{31}	-4.98	16090	[139]
R46	$CY13PD5J + OH = CYC5H4OH + H$	1.75×10^{26}	-3.49	16630	[139]
R47	$CY13PD5J + OH = C_4H_6 + CO$	2.69×10^{34}	-6.07	15340	[139]

Rate expression: $k = AT^n \exp\left(\frac{-E_a}{RT}\right)$ in cm³, mol, cal, s units.

4.1.1 Sub-mechanism of toluene

Unimolecular decomposition of toluene

Toluene follows three different decomposition reactions (R1 – R3) to produce benzyl ($C_6H_5CH_2$), phenyl (C_6H_5), and methylphenyl ($C_6H_4CH_3$) radicals, respectively. The rate constant of R1 and R2 were numerically calculated by Klippenstein et al [142] using the transition state theory (TST) and master equation. Because of the lack of experimental and numerical data, the rate constant of R3 was estimated by Yuan et al. [105] by analogy with a similar reaction of benzene [157].

Ipso-addition and H-atom abstraction of toluene

During combustion, toluene is importantly consumed by H-atom abstractions (R4 – R9). These reactions produce benzyl and methylphenyl radicals. The rate constant of R4 was experimentally investigated by Oehlschlaeger et al. [143] while the one of R5 was estimated by Bounaceur et al. [144]. The kinetic of H-atom abstraction reactions of toluene by OH radical (R6, R7) was experimentally measured by Seta et al. [145]. Among the reactions of O_2 with toluene, the rate constant of R8 was determined by Oehlschlaeger et al. [146] by shock tube experiments. The kinetic parameters of R9 were proposed by Keita et al. [147] by analogy with a similar reaction between benzene and O_2 [158].

Besides H-atom abstraction reactions, toluene can undergo some ipso-additions, which are substitution reactions (R10 – R13) by small radicals as H, OH, and O. The rate constant of reaction R10 is adopted from the work of Keita et al. [147]. The reactions of toluene and OH radical produce phenol in reaction R11 and cresol in reaction R12. The rate constants of these reactions considered in the model were measured by Seta et al. [145]. Similar to OH radical, O atom can react with toluene to form methylphenoxyl radical ($OC_6H_5CH_3$) in reaction R13. The kinetic parameters of this reaction were estimated by Yuan et al. [105] based on a similar reaction between benzene and O atom [159].

Oxidation reactions of benzyl radical

Benzyl radical can be oxidized by O-atoms, OH, HO_2 radicals, and O_2 as illustrated in reactions R14 – R20. The reaction R14 is taken from the model developed by Narayanaswamy et al. [148]. The rate constant of reaction R15 was theoretically calculated by da Silva et al. [149]. The oxidation of benzyl radical by O_2 (R16, R17) produces two products: benzoxyl radical ($C_6H_5CH_2O$) and benzylperoxy radical ($C_6H_5CH_2OO$). The rate constant of reaction R16 is adopted from the numerical work of Brezinsky et al. [150] and the one of R17 is collected from the study of Murakami et al. [151].

Reactions of $C_6H_5CH_2O$ and $C_6H_5CH_2OO$ radicals

$C_6H_5CH_2O$ can decompose to benzaldehyde (C_6H_5CHO), benzene (C_6H_6) and phenyl (C_6H_5) radical via three reactions (R18 – R20). The rate constants of these reactions were theoretically calculated by da Silva et al. [152]. Besides, the H-atom abstractions of $C_6H_5CH_2O$ with H, O, OH radicals, and O_2 [148] forming benzaldehyde are included in the model.

$C_6H_5CH_2OO$ can form benzaldehyde by releasing OH radical (R21). The rate constant of this reaction is adopted from the model of Keita et al. [147]. In addition, $C_6H_5CH_2OO$ reacts with H radical and produces $C_6H_5CH_2O$ (R22). This reaction was theoretically investigated by da Silva et al. [153].

Oxidation reactions of methyl phenyl radical

In the reference model [42], $C_6H_4CH_3$ reacts with O_2 via four reactions R23 – R26. While the rate constant of R23 and R24 are kept similar to that in the reference model, the rate constant of R25 is

collected from the numerical study of da Silva [154] as suggested by Yuan et al. [105]. Moreover, the reaction R26 between $C_6H_4CH_3$ and O_2 forming benzyne peroxyl radical (o-$C_6H_4O_2$) is adopted from the work of Yuan et al. [105].

4.1.2 Sub-mechanism of benzene

H-atom abstraction of benzene

Benzene (C_6H_6) forms exclusively phenyl radical (C_6H_5) via H-atom abstraction reactions (R27 – R29) with small reactive radicals as O, OH, HO_2. The rate constant of reaction R27 is adopted from the kinetic model of Alzueta et al. [155]. Seta et al. [145] investigated experimentally the reaction between benzene and OH radicals in a shock tube. By transition-state theory (TST) calculations, they confirmed that the dominant reaction between these two compounds is an H-atom abstraction reaction and proposed a rate constant for this reaction. This rate constant is used for reaction R28. The kinetic parameter of reaction R29 is taken from the theoretical study of Altarawneh et al. [156].

Oxidation of phenyl radical

Phenyl radical can be oxidized by O_2 and several radicals, such as O, OH, HO_2 via reactions R30 – R35. O atom can open the carbon ring of benzene to form CO and a linear compound C_5H_5. O_2, OH, and HO_2 radicals can react with phenyl radical to produce phenoxy radicals. Besides, phenyl radical can yield phenyl peroxy radical ($C_6H_5O_2$) or ortho-benzoquinone (o-$C_6H_4O_2$). The rate constants of the reactions R30 – R34 are adopted from the model of Keita et al. [147] and the one of reaction R35 is collected from the model of Yuan et al. [105, 106].

4.1.3 Sub-mechanism of 1,3-cyclopentadiene

H-atom abstraction of 1,3-cyclopentadiene

All reactions involving 1,3-cyclopentadiene (CY13PD) in the kinetic model developed in this thesis are collected from the model of Yuan et al. [105, 106]. 1,3-cyclopentadiene can undergo H-atom abstraction reactions (R36 – R40) to produce cyclopentadienyl radical (CY13PD5J).

Oxidation of cyclopentadienyl radical

The oxidation reactions (R41 – R46) of cyclopentadienyl radical by O_2, O and OH radicals are adopted from the latest studies. Oleinikov et al. [141] performed ab initio calculations and solved the RRKM-Master Equation to compute rate constants and product branching ratios of reactions between cyclopentadienyl radical and O_2. These authors found that the principal products were cyclopentadienone (CYPDONE) and OH radical via the reaction R41 and $CH_2CH=CHCH=O$ (CJCXCCXO) and CO via the reaction R42. By applying a similar method as Oleinikov et al. [141], Ghildina et al. [140] numerically investigated the oxidation of cyclopentadienyl radical by O atom. According to this work, the most favourable reactions are R43 producing cyclopentadienone and H atom and R44 forming a butadienyl radical and CO. Recently, Galimova et al. [139] also investigated theoretically the reactions between cyclopentadienyl and OH radical. It was found that this reaction could lead to the products as alkoxycyclopentadienyl (C5H5O13) and H atom via the reaction R45, hydroxycyclopentadienyl (CYC5H4OH) and H atom via the reaction R46, and 1,3-butadiene and CO via the reaction R47.

4.2 Sub-mechanism of nitrogen oxides

Different studies on EHN in the literature proposed different explanations of EHN impact on fuel reactivity. Hartmann et al. [69] suggested that EHN effect is due to the chemical reactivity of 3-heptyl radical. Goldsborough et al. [40] indicated that together with 3-heptyl radical, a "NO_2-NO" loop involving reactions of nitrogen oxides (NO_x) with small atoms and radicals (H, HO_2) could generate OH radicals contributing to the promoting effect of EHN. These explanations suggest that the detailed nitrogen chemistry must be considered to simulate EHN promoting effect properly. Consequently, the kinetic model in this study includes a detailed nitrogen oxides mechanism. The main parts of this mechanism are the formation of NO_x, the chemistry of small carbon-chain nitrogenous compounds (C_1-C_3) and the coupling reactions between NO_x with hydrocarbons (C_1-C_7). Several important reactions of nitrogen oxides sub-mechanism are listed in Table 17.

Table 17: Important reactions involving nitrogen oxides

Reaction		A	n	E_a	Ref.
R48	$NO + N = N_2 + O$	9.40×10^{12}	0.14	0	[160]
R49	$N + OH = NO + H$	3.80×10^{13}	0.00	0	[160]
R50	$N + O_2 = NO + O$	5.90×10^{9}	1.00	6280	[160]
R51	$CH + N_2 = NCN + H$	3.00×10^{11}	0.00	13600	[160]
R52	$CN + N = C + N_2$	5.90×10^{14}	-0.40	0	[160]
R53	$C_2 + N_2 = CN + CN$	1.50×10^{13}	0.00	41730	[160]
R54	$NCN (+M) = C + N_2 (+M)$	8.90×10^{14}	0.00	62100	[160]
R55	$NCN + H = HCN + N$	2.20×10^{11}	0.71	5322	[160]
R56	$NCN + H = HNC + N$	7.10×10^{-4}	4.62	2408	[160]
R57	$NCN + O = CN + NO$	2.50×10^{13}	0.17	-34	[160]
R58	$NCN + OH = HCN + NO$	7.10×10^{10}	0.56	5985	[160]
R59	$NCN + OH = NCO + NH$	2.20×10^{19}	-2.00	7339	[160]
R60	$NCN + O_2 = NO + NCO$	1.30×10^{12}	0.00	23167	[160]
R61	$NCN + NO = CN + N_2O$	1.90×10^{12}	0.00	6280	[160]
R62	$NO + O + (M) = NO_2 (+M)$	1.30×10^{15}	-0.75	0	[160]
R63	$NO + HO_2 = NO_2 + OH$	2.05×10^{12}	0.00	-497	[160]
R64	$H + HONO = NO + H_2O$	4.30×10^{9}	1.00	4100	[161]
R65	$H + HONO = NO_2 + H_2$	1.90×10^{3}	2.80	1400	[161]
R66	$H + HNO_2 = NO_2 + H_2$	2.30×10^{4}	2.80	-2000	[161]
R67	$CH_3 + HONO = NO_2 + CH_4$	3.60×10^{-4}	4.40	-0.4	[161]
R68	$CH_3 + HNO_2 = NO_2 + CH_4$	2.20×10^{3}	2.80	-2900	[161]
R69	$CH_3NO_2 + H = HNO_2 + CH_3$	3.30×10^{12}	0.00	3730	[160]
R70	$CH_3NO_2 + H = HONO + CH_3$	3.27×10^{12}	0.00	3730	[160]
R71	$CH_3NO_2 + H = CH_3NO + OH$	1.40×10^{12}	0.00	3730	[160]
R72	$CH_3NO_2 + H = CH_2NO_2 + H_2$	4.90×10^{13}	0.00	9220	[160]
R73	$C_2H_5NO_2 = C_2H_5 + NO_2$	3.82×10^{61}	-14.83	70656	[162]
R74	$C_2H_5NO_2 = C_2H_4 + HONO$	1.38×10^{73}	-18.60	70472	[162]
R75	$CH_3CHNO_2 = CH_3CNO + OH$	1.31×10^{83}	-21.07	86572	[162]
R76	$CH_3CHNO_2 = C_2H_4 + NO_2$	9.15×10^{76}	-18.85	77069	[162]
R77	$CH_3CHNO_2 = CH_2CH + HONO$	7.28×10^{69}	-16.95	70951	[162]
R78	$CH_3CHNO_2 = CH_2CHNO + OH$	1.28×10^{67}	-16.01	65796	[162]
R79	$CH_3CHNO_2 = CH_2CHNO_2 + H$	2.75×10^{76}	-18.41	77419	[162]

Rate expression: $k = AT^n \exp\left(\frac{-E_a}{RT}\right)$ in cm³, mol, cal, s units.

4.2.1 Formation of nitrogen oxides

The reactions of formation of NO_x were collected from the recent review of Glarborg et al. [160] and the work of Fuller et al. [161]. In this review, the authors indicated that nitric oxide (NO) could be formed via three ways including thermal NO, prompt NO and the fuel-N as presented in Figure 45.

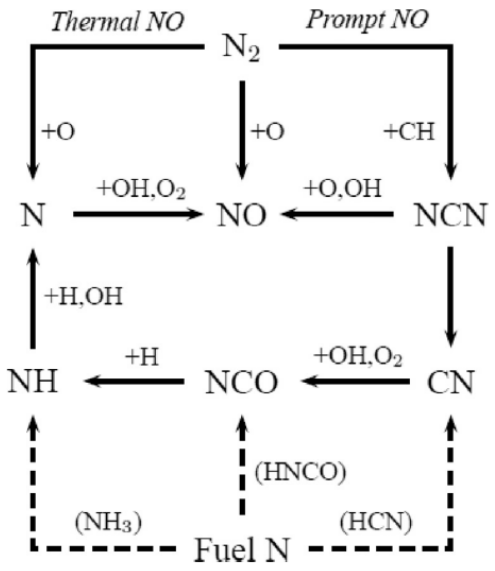

Figure 45: Simplified reaction path diagram presenting the principal steps in the formation of NO via thermal NO, prompt NO and fuel-N. This figure is adopted from Glarborg et al. [160].

In the mechanism of the thermal NO proposed by Zeldovich [163], N_2 in the air of combustion is oxidized by O atoms (reaction R48) in the initial step. As this reaction has a high activation energy (E_a = 75 kcal/mol), the thermal NO pathway plays a role only at high temperature [163]. N atom formed by the reaction R48 is then quickly transformed into NO by OH and O_2 (reactions R49 – R50).

During combustion, N_2 can be attacked by CH_x radicals (x < 4) to produce some intermediates which can form NO by several successive reactions. This mechanism proposed first by Fenimore is known as the prompt NO pathway. In this mechanism, the most important step is the reaction R51 between CH radical and N_2 producing NCN and H atom [160]. Glarborg et al. [160] summarized the most important reactions (R51 – R61) of the prompt NO. The attack of O atom, OH radicals and O_2 on NCN in reactions R57, R58 and R60, respectively, generate NO.

The last mechanism of the formation of NO involves the nitrogen contained in fuels. This mechanism is known as Fuel-N. The nitrogen content in fuel is found in several forms as amines, nitrates, nitrites, etc. These nitrogen compounds can form directly NO, NO_2 and/or via some important intermediate compounds as ammonia (NH_3), hydrogen cyanide (HCN), and isocyanic acid (HNCO) [160].

During combustion, NO_2 can be produced from the oxidation of NO by O and HO_2 radicals as presented in reactions R62 – R63.

In combustion processes, whose peak temperature is below 1800 K, NO_2 can abstract an H atom and be converted into two isomers as nitrous acid (HONO) and nitryl hydride (HNO_2) [161]. Recently, Fuller et al. [161] investigate numerically the reactions of H and CH_3 with HONO and HNO_2. Thanks to transition-state theory calculations, possible reaction channels are determined. For H + HONO system, the dominant products are NO + H_2O (R64) and NO_2 + H_2 (R65). In the case of H + HNO_2, the H-atom abstraction channel producing NO_2 + H_2 (R66) is exclusively favoured thanks to its very low activation

energy. For the same reason, both systems CH_3 + HONO and CH_3 + HNO_2 produce principally CH_4 + NO_2 via H-atom abstraction channel (R67 – R68). All above reactions are included in the model in this study.

4.2.2 Reactions of small carbon-chain nitrogen compounds (C_1-C_3)

Nitrogen compounds are produced thanks to combinations of NO_2 and hydrocarbon radicals. Experimental and theoretical data about these compounds are still scarce.

The sub-mechanism of nitromethane (CH_3NO_2) was collected from the model presented in the review of Glarborg et al. [160]. By the attack of H atom, nitromethane can be transformed into HONO, HNO_2, CH_3NO, and CH_2NO_2 (reactions R69 – R72).

The reactions of nitroethane ($C_2H_5NO_2$) presented in the work of Zhang et al. [162] based on their previous work [164] were entirely included in our model. These authors conducted the pyrolysis of nitroethane in a plug flow reactor at low pressure from 682 to 1423 K. These authors calculated theoretically the rate constant of the decomposition reactions of nitromethane (reactions R73 – R74) and its derived radical CH_3CHNO_2 (reactions R75 – R79) formed via H-atom abstractions. The adoption of these rate constants resulted in a better prediction of species profiles obtained during the pyrolysis of nitroethane in comparison with the previous model of nitroethane presented in [164].

The sub-mechanism of the two nitropropane isomers (1-nitropropane and 2-nitropropane) was built based on the reaction scheme of nitroethane. This sub-mechanism was validated against the experimental data of 2-nitropropane reported by Zhang et al. [165].

4.2.3 Reactions involving nitrogens oxides and hydrocarbons (C_1-C_7)

Thanks to the review of Glarborg [160] and the work of Anderlohr et al. [166], the reactions involving nitrogen oxides and hydrocarbons can be grouped into seven types of reactions (R_I – R_{VII}) as shown in Table 18. It has been proved experimentally that NO_x can impact the reactivity of hydrocarbons [43, 167]. NO_2 can abstract an H atom from the parent fuel (RH) to form the alkyl radical R. NO_2 is transformed into HONO via this reaction pathway (R_I). NO_2 has a radical character thanks to its original electronic structure [161]. NO_2 can then combine with free radicals to form nitro compounds via combination reactions (R_{II}) and/or to produce alkoxy radicals (RO) and NO as reactions of substitutions (R_{III}). During the combustion of hydrocarbons, NO can be converted into NO_2 by reactions (R_{IV}) with peroxyl radicals (ROO). Anderlohr et al. [166] proposed a global reaction (R_V) representing reactions of NO with OOQOOH radicals. Also, a similar global reaction (R_{VI}) was suggested by these authors to treat reactions of NO with aldehydes (RCHO). Last, free radicals can react with nitroxyl (HNO) to produce NO as presented in reactions R_{VII}.

Table 18: Reactions between NO_x and hydrocarbons

Name	Reactions
R_I	RH + NO_2 = R• + HONO
R_{II}	RNO_2 = R• + NO_2
R_{III}	R• + NO_2 = RO• + NO
R_{IV}	ROO• + NO = RO• + NO_2
R_V	•OOQOOH + NO → OH + 2HCHO + olefin + NO_2
R_{VI}	RCHO + NO_2 → R• + CO + HONO
R_{VII}	R• + HNO = NO +RH

In the present model, the reactions of NO_x with small hydrocarbons (C_1-C_2) were entirely collected from the recent review of Glarborg et al. [160]. The interactions between NO_x and heavier hydrocarbons (C_3-C_7) were adopted from the study of Anderlorh et al. [166]. The sensitizing effect of NO_x on

hydrocarbon oxidation has been investigated in the literature [167–171]. These studies highlighted the importance of reactions R + NO_2 = RO + NO (R_{III}) and RO_2 + NO = RO + NO_2 (R_{IV}) on the sensitizing effect of NO_x. The most important reactions of NO_x impacting the oxidation of *n*-heptane and toluene are presented in Table 19. The rate constant of reaction R80 between HO_2 and NO was first experimentally measured over a wide range of temperature 232 – 1271 K in a flow tube reactor by Howard et al. [172]. The rate constant reported by these authors was k = 2.11 x 10^{12} x exp(477/RT) (units: cal, mol, s, K). This result was supported by the more recent experimental study of Bardwell et al. [173] and the theoretical study of Chen et al. [174]. Bardwell et al. [173] conducted experiments in a turbulent flow tube at low temperatures 183-300 K in a pressure range of 75 to 220 Torr. The rate constant of R80 was found pressure independent and agreed well with the rate reported by Howard et al. [172]. Chen et al. [174] determined the reaction pathway of R80 at 300 K thanks to quasi-classical trajectory calculations. HOONO was found to be the principal intermediate which further decayed into NO_2 and OH. The calculated rate constant of R80 at 300 K was in good agreement with the measurement reported by Howard et al. [172]. In our model, the rate constant of R80 reported in the review of Glarborg et al. [160] is adopted. This value is included in the uncertainty range of the rate constant reported in [172].

The rate constant of reaction R81 between CH_3O_2 and NO was both experimentally and theoretically investigated in the literature. Bacak et al. [175] measured the global rate constant of the reaction CH_3O_2 + NO_2 → *Products* in a turbulent flow tube reactor from 193 to 300 K in a pressure range of 100 to 200 Torr. These authors reported a rate constant k = 1.05 x 10^{12} x exp(864/RT) (units: cal, mol, s, K). The branching ratio of the formation of CH_3 and NO_2 was found to be 100 ± 10 %. This result was supported by the study of Butkovskaya et al. [176]. These authors tried to experimentally determine the branching ratio of methyl nitrate formation in the CH_3O_2 + NO reaction. The experiments were conducted in turbulent flow reactor over the pressure and temperature ranges 50 – 500 Torr and 223 – 300 K, respectively. The branching ratio of methyl nitrate formation was determined as a value of 1 % in the considered conditions. Also, the theoretical study of Lesar et al. [177] confirmed the most dominant products of CH_3O_2 + NO reaction were CH_3O and NO. In our model, the rate constant of R81 reported in the review of Glarborg et al. [160] is adopted. This value is similar to the global rate constant reported by Bacak et al. [175].

The rate constant of reaction R82 between $C_2H_5O_2$ and NO was experimentally measured by Maricq et al. [178] over the temperature range 220 – 335 K. These authors reported an A-factor and an activation energy (E_a) of 1.87 x 10^{12} ± 9 x 10^{11} and -656 ± 217 respectively (units: cal, mol, s, K). This result was supported by the experimental work of Ranschaert et al. [179]. These authors determined also the minor formation of ethylnitrate whose branching varied from 0.006 to 0.02. In our model, the rate constant of R82 proposed in the model of Rasmussen et al. [168] is adopted. This value is included in the uncertainty range of the rate constant reported in [178].

To our knowledge, the rate constant of reaction R83 between $C_7H_{15}O_2$ and NO was not directly examined in the literature. In our model, the rate constant of R83 is adopted from the model of Anderlohr et al. [166]. These authors estimated this rate constant by multiplying the rate constant rate of reaction CH_3O_2 and NO reported in [180] by a factor of 1.8. Also, no data in the literature are found for the reaction R84 between $C_6H_5CH_2$ and NO_2. The rate constant of this reaction is based on the rate constant of the reaction of alkyl radicals (R) with NO_2: R + NO_2 = RO + NO proposed by Anderlohr et al. [166].

Table 19: Rate constant of reactions of NO_x with radicals (R_{III}, R_{IV}) and NO with aldehydes (R_{VI}).

Reaction		A	n	E_a	A-factor modification	Ref.
Reactions of $R/RO_2 + NO_x$						
R80	$HO_2 + NO = OH + NO_2$	2.05×10^{12}	0.00	-497		[160]
R81	$CH_3O_2 + NO = CH_3O + NO_2$	1.40×10^{12}	0.00	-715		[160]
R82	$C_2H_5O_2 + NO = C_2H_5O + NO_2$	1.60×10^{12}	0.00	-755		[168]
R83	$C_7H_{15}O_2 + NO = C_7H_{15}O + NO_2$	4.70×10^{12}	0.00	-358		[166]
R84	$C_6H_5CH_2 + NO_2 = C_6H_5CH_2O + NO$	4.00×10^{13}	0.00	0		This work
Reactions of $RCHO + NO_2$						
R85	$CH_3CHO + NO_2 \rightarrow CH_3 + CO + HONO$	4.20×10^{-10}	6.68	8300	x 5	[166]
R86	$C_2H_5CHO + NO_2 \rightarrow C_2H_5 + CO + HONO$	4.20×10^{-10}	6.68	8300	x 5	[166]
R87	$n\text{-}C_3H_7CHO + NO_2 \rightarrow n\text{-}C_3H_7 + CO + HONO$	4.20×10^{-10}	6.68	8300	x 5	[166]
R88	$n\text{-}C_4H_9CHO + NO_2 \rightarrow n\text{-}C_4H_9 + CO + HONO$	4.20×10^{-10}	6.68	8300	x 5	[166]
R89	$n\text{-}C_5H_{11}CHO + NO_2 \rightarrow n\text{-}C_5H_{11} + CO + HONO$	4.20×10^{-10}	6.68	8300	x 5	[166]

Rate expression: $k = AT^n \exp\left(\frac{-E_a}{RT}\right)$ in cm^3, mol, cal, s units.

By simulations, it was found that the reactions of aldehydes with NO_2 were sensible to predict the effect of NO on *n*-heptane oxidation. The kinetic parameters of this type of reactions were estimated by Anderlorh et al. by analogy with the reaction of CH_2O and NO_2 calculated by Xu et al. [181]. The A-factor of the reactions of aldehydes with NO_2 proposed by Anderlohr et al. were multiplied by 5 in order to better simulate the impact of NO on *n*-heptane oxidation presented in the study of Moréac et al. [43]. These reactions are presented in Table 19.

4.3 Sub-mechanism of 2-ethylhexyl nitrate and ferrocene

4.3.1 Sub-mechanism of 2-ethylhexyl nitrate

The past studies on EHN [40, 69, 182] agree on the main decomposition steps of this molecule. At first, NO_2 is released thanks to N-O bond scission, which is the weakest bond in EHN molecule. Together with NO_2, the 2-ethylhexyloxy (EHO) radical is formed. The detail chemistry of EHO is still unknown. A recent study of *n*-butyl nitrate (NBN) thermal decomposition was conducted by Morin et al. [183]. NBN decomposition formed butoxy radical (C_4H_9O) and NO_2. The most favourable channels of C_4H_9O reaction were its decomposition to propyl radical (C_3H_7) and formaldehyde (CH_2O) and its isomerization to hydroxybutyl radical (C_4H_8OH). Interestingly, the dominant transformation of C_4H_8OH was its back isomerization to C_4H_9O and then decomposition to C_3H_7 and CH_2O. The NBN decomposition can be described as a unique reaction NBN → $C_3H_7 + CH_2O + NO_2$. A similar reaction is then adopted in this study to describe the decomposition of EHN as presented in Table 20. The decomposition products of EHN are 3-heptyl radical (C_7H_{15}-3), CH_2O and NO_2. The rate constant of this reaction is estimated according to the experimental works on EHN decay of Pritchard et al. [184] and Bornemann et al. [182]. The reactions of 3-heptyl radical and CH_2O was included in the reference model [42].

Table 20: Rate constant of the decomposition reaction of EHN

Reaction		A	n	E_a	Ref.
R90	EHN → C_7H_{15}-3 + CH_2O + NO_2	2.50×10^{15}	0	42000	[182, 184]

Rate expression: $k = AT^n \exp\left(\frac{-E_a}{RT}\right)$ in cm^3, mol, cal, s units.

4.3.3 Sub-mechanism of ferrocene

The ferrocene sub-mechanism was built based on the literature. It consists of three groups of reactions including ferrocene decomposition, reactions of small radicals (H, O, OH, HO_2) with ferrocene and reactions of iron species. The first two groups of reactions were adopted from the work of Fenard et al. [75]. The ferrocene decomposition was described as a two-step decomposition. First, ferrocene ($FeC_{10}H_{10}$) released a cyclopentadienyl radical (CY13PD5J) to produce FeC_5H_5. The rate constant of this reaction was adopted from the work of Lewis et al. [185]. The second step was a dissociation to produce Fe and CY13PD5J. The kinetic of this reaction was estimated by Hirasawa et al. [78]. The rate of the reactions of smalls radicals with ferrocene was estimated by Fenard et al. [75] based on literature data [78, 186, 187]. Table 21 summarizes all the reactions involving ferrocene and FeC_5H_5 in the current study. Iron species reactions including iron (Fe), iron oxides (FeO, FeO_2), iron hydroxides (FeOH, $Fe(OH)_2$) and other iron compounds (FeOOH, FeH) were adopted from the study of Rumminger et al. [188]. Additionally, the kinetic model includes the reaction of Fe with NO_2 [189] and CO_2 [190]. The reactions of the nucleation of Fe atoms from the work of Wen et al. [191] were added in the kinetic model.

Table 21: Rate constant of reactions of ferrocene assembled from the literature

Reaction		A	n	E_a	Ref.
R91	FeC10H10 = FeC5H5 + CY13PD5J	2.19×10^{16}	0	91400	[185]
R92	FeC5H5 = Fe + CY13PD5J	2.00×10^{16}	0	77800	[78]
R93	FeC10H10 + HO2 → FeC5H5 + CYPDONE[a] + H2O	4.00×10^{12}	0	10000	[75]
R94	FeC10H10 + OH → FeC5H5 + C5H5OH[b]	1.10×10^{13}	0	−1040	[75]
R95	FeC10H10 + O → FeC5H5 + CYPDONE + H	2.00×10^{13}	0	2000	[75]
R96	FeC10H10 + H → FeC5H5 + CY13PD[c]	1.00×10^{13}	0	12300	[75]
R97	FeC5H5 + HO2 → Fe + CYPDONE + H2O	2.00×10^{12}	0	10000	[75]
R98	FeC5H5 + OH → Fe + C5H5OH	1.10×10^{13}	0	−1040	[75]
R99	FeC5H5 + O → Fe + CYPDONE + H	2.00×10^{13}	0	2000	[75]
R100	FeC5H5 + H→Fe + CY13PD	1.00×10^{13}	0	300	[75]

Rate expression: $k = AT^n \exp\left(\frac{-E_a}{RT}\right)$ in cm3, mol, cal, s units. [a]Cyclopentadienone. [b]2,4-Cyclopentadien-1-ol. [c]1,3-Cyclopentadiene

Chapter 5: Results and discussions

This chapter is dedicated to presenting the validation of the kinetic model and the experimental and numerical results. First, the validation of the kinetic model over a large set of literature experimental data is presented. The reactivity of the surrogate fuel is then shown. Thereafter, the effects of the three additives considered in this thesis on the IDT and the laminar burning velocity of the surrogate fuel are discussed. The method employed to simulate RCM experiments is explained. The main chemical effects of the additives are presented. Finally, the impact of additives on the gas-phase reactivity of various fuel at different conditions are predicted thanks to the validated kinetic model.

5.1 Kinetic model validation

The developed kinetic model was validated using a large set of experimental data. This includes ignition data in shock tube (ST) as well as species profiles measured in plug flow reactor (PFR) and perfectly stirred reactor (PSR). The comparison was performed in order to validate the different sub-mechanisms: the reactivity of aromatic compounds including toluene, benzene and 1,3-cyclopentadiene [105, 192–194], the toluene/ *n*-heptane mixtures reactivity [109, 111], the nitrogen chemistry [43, 162, 165, 168, 169, 195–198] and the effect of EHN [69]. The used experimental data are presented in Table 22.

Table 22: Summary of experimental studies used for the validation of the kinetic mechanism

Reactor	Fuel	Equivalence ratio	Temperature (K)	Pressure (atm)	Ref.
PFR[a]					
	Methane/ NO/ NO_2	1.20	600-900	50	[168]
	Methane/ NO_2	4.00	870-1225	2	[195]
	Nitroethane	Pyrolysis	680-1425	7×10^{-3}	[162]
	1,3-Cyclopentadiene	Pyrolysis	820-1225	1	[192]
	1,3-Cyclopentadiene	1.03	1198	1	[193]
PSR[b]					
	Ethane/ NO	1.00	825-1100	1	[169]
	n-Heptane/ NO	1.00	550-1000	10	[43]
	Benzene	1.00	980-1300	1	[194]
	Toluene	1.00	900-1200	10	[105]
	Toluene/NO	1.00	640-1100	10	[43]
	Toluene/*n*-heptane/NO/NO_2	0.20	550-950	10	[196]
ST[c]					
	Nitromethane	Pyrolysis	1180	6	[197]
	Nitromethane	1.00-2.00	875-1110	9-14	[198]
	2-Nitropropane	Pyrolysis	975-1100	5	[165]
	Toluene/ *n*-heptane	0.30-1.00	840-1200	10-50	[111]
	Toluene/ *n*-heptane	1.00	710-1200	40	[109]
	n-Heptane/ EHN	1.00	700-1200	40	[69]

[a] Plug flow reactor. [b] Perfectly stirred reactor. [c] Shock tube.

Compared to the reference model of LLNL [42], the developed model in this thesis simulates better the reactivity of aromatic compounds as illustrated in Figure 46, Figure 47, and Figure 48. Simulations of the experimental data of toluene reported by Moréac et al. [43] are presented in Figure 46. These experiments were conducted at 10 bar, Φ = 1, and from 550 to near 1000 K [43]. A better prediction

of toluene reactivity is observed especially in the temperature range 900 - 1000 K by using our new model in comparison with the LLNL reference model [42].

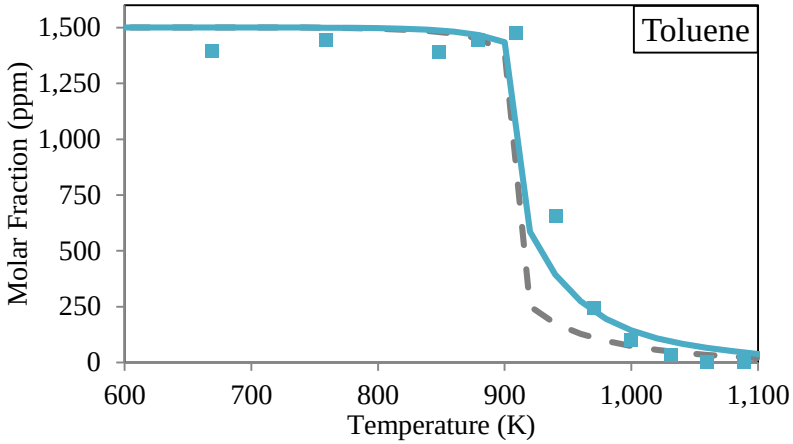

Figure 46: Species profiles of toluene at 10 atm, Φ = 1, from 500 to 1100 K in a perfectly stirred reactor [43]. Symbols: experimental results. Blue lines: simulations with the model of this thesis. Dashed lines: simulations with the model of LLNL [42].

Figure 47 presents the species profiles obtained during experiments in a PFR of 1,3-cyclopentadiene (C_5H_6) [193]. The model LLNL overestimates the reactivity of C_5H_6 at long residence times which is correctly simulated by the model of this thesis. Besides, the formation of benzene (C_6H_6) is well predicted by the developed model.

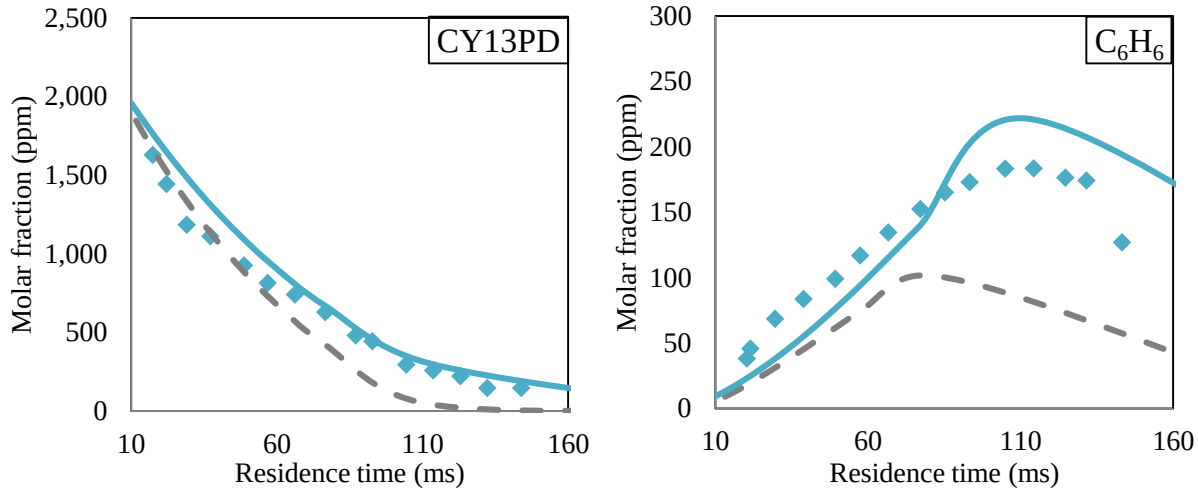

Figure 47: Species profiles of 1,3-cyclopentadiene (CY13PD) and benzene (C_6H_6) at 1198K, 10 atm, Φ = 1 during oxidation of1,3-cyclopentadiene in a plug flow reactor [193]. Symbols refer to experimental results. Solid lines represent simulations results performed with the model of this thesis. Dashed lines represent simulations results performed with the reference model of LLNL [42].

Figure 48 shows the consumption of benzene and the formation of 1,3-cyclopentadiene during the oxidation of benzene in a PSR at 1 atm, Φ = 1, from 980 – 1300 K [194]. The performance of the model of this thesis is remarkably better than that of the reference model [42].

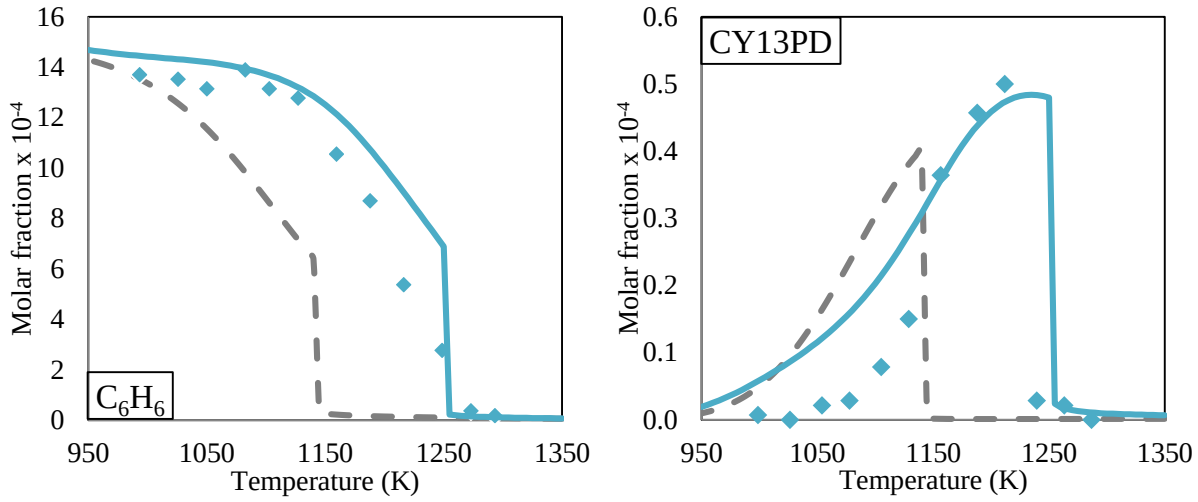

Figure 48: Species profiles of 1,3-cyclopentadiene (C_5H_6) and benzene (C_6H_6) at 1 atm, Φ = 1 during oxidation of of benzene in a perfectly stirred reactor. Symbols refer to experimental results [194]. Solid lines represent simulations results performed with the model of this thesis. Dashed lines represent simulations results performed with the reference model of LLNL [42].

The validation confirms also a good performance of the kinetic model to reproduce the reactivity of toluene and *n*-heptane mixtures [109, 111] as shown in Figure 49 and Figure 50.

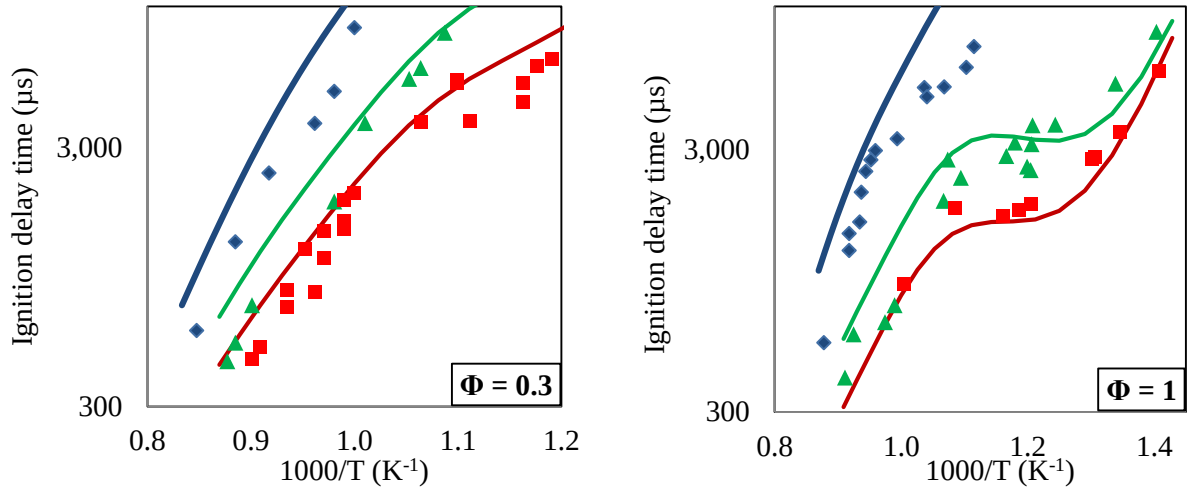

Figure 49: Ignition delay time of the mixture of *n*-heptane (35% vol.) and toluene (65% vol.) in air (Φ = 0.3 and 1) at different pressures: 10 bar (blue), 30 bar (green) and 50 bar (red). Symbols: experimental results. Lines: simulations results. Experiments conducted by Herzler et al.[111].

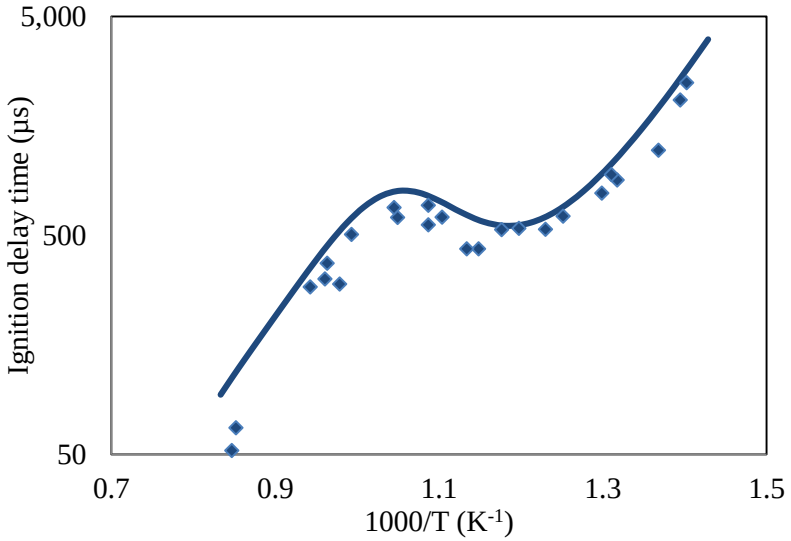

Figure 50 : Ignition delay time of the mixture of *n*-heptane (90% vol.) and toluene (10% vol.) in air (Φ = 1) at 40 bar. Symbols: experimental results. Lines: simulations results. Experiments conducted by Hartmann et al.[109].

About the simulation of the nitrogen chemistry, the model reliably predicts the NO_x effect on fuel reactivity. Moréac et al. [43] studied the impact of NO on the oxidation of *n*-heptane and toluene by conducting experiments at 10 atm from 550 to 1090 K in a PSR. Figure 51 presents the modeling results for this data set.

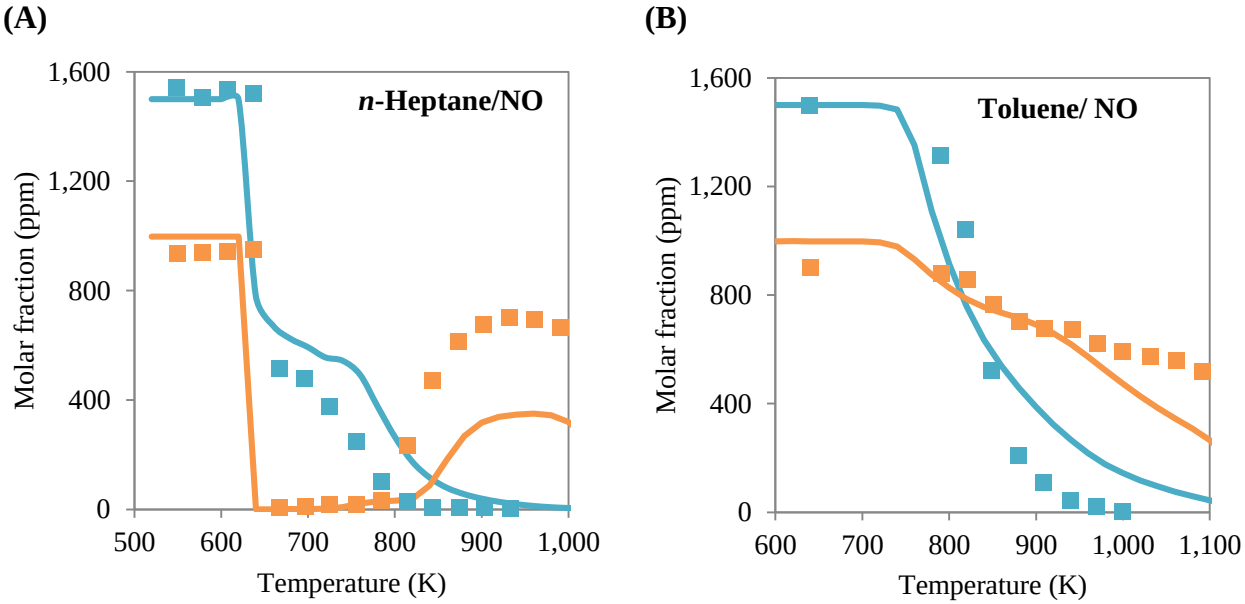

Figure 51: Species profiles of fuel (blue) and NO (orange) at 10 atm from 500 to 1100 K [43]. Symbols: experimental results. Lines: simulations results. (A): initial fuel mixture: *n*-heptane/ 500 ppm NO. (B) initial fuel mixture: toluene/ 500 ppm NO.

Figure 52 illustrates the modeling of the ignition delays for *n*-heptane doped with 1% mass. EHN at 40 bar and Φ = 1. The kinetic model provides longer IDT in doped and undoped cases especially at low temperature (T < 1000 K). The EHN promoting effect is reasonably simulated along with the temperature.

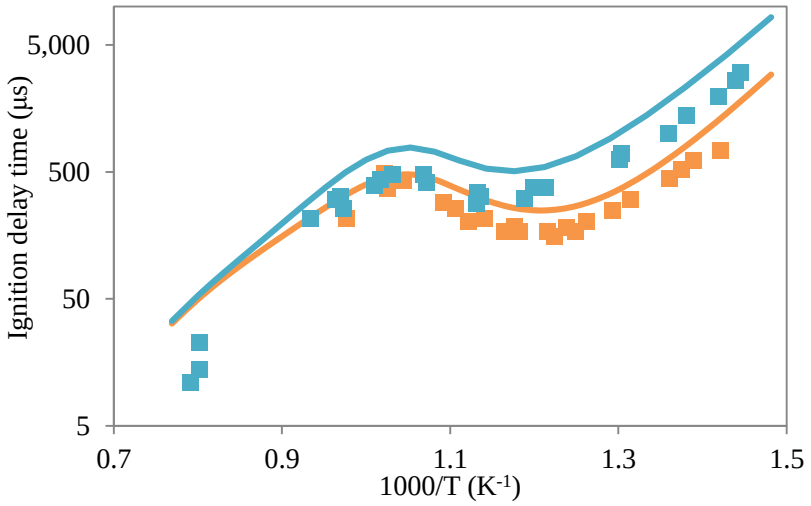

Figure 52: Measured (symbols) and simulated IDT (lines) of the neat *n*-heptane (blue) and doped *n*-heptane with 1% mass EHN (orange) at P = 40 bar, Φ = 1[109].

The modeling of other experimental data listed in Table 22 are presented in Appendix A1. The validation step demonstrates a satisfactory agreement regarding the entire data set employed.

5.2 Gas-phase reactivity of the surrogate fuel

The results of experiments performed on the ST, the RCM, and the flat flame burner with the neat surrogate fuel are illustrated and compared with the simulations in this section.

5.2.1 Ignition delay time of the surrogate fuel at T < 1000 K

5.2.1.a RCM Experiments results

RCM experiments were performed at 10 bar from 675 to 960 K for two equivalence ratios 0.5 and 1 in air as summarized in Table 23. The stoichiometric and lean conditions were investigated. The latter is considered of interest for LTC combustion engines [6, 7]. The investigated temperature range is of interest regarding the LTC systems [40].

Table 23: Experimental conditions of RCM tests performed with the surrogate fuel.

P (bar)	T (K)	Φ	Composition (% mol.) of fuel gas mixture		
			Fuel	Oxygen	Nitrogen
10	675 - 1000	0.5	1.09	20.77	78.14
		1.0	2.15	20.55	77.30

The ignition delay times of the neat surrogate fuel in these conditions are presented in Figure 53. At the stoichiometry, a NTC behavior is observed from 790 K to nearly 885 K while this phenomenon does not appear in lean condition. *n*-Heptane oxidation enables the NTC behavior as described by Battin-Leclerc et al. [36]. At both equivalence ratios, two-stage ignitions occur in the lowest temperature range (T_c < 790 K). In lean conditions, the IDT of the neat surrogate are longer, up to 4 times than those in stoichiometric conditions.

The two simulation methods of RCM experiments described in section 2.2.2.d reproduce reasonably well the experimental results including two-stage ignitions and NTC phenomenon. The “all-simu” method predicts shorter IDTs than the “frozen chemistry” method because of the chemical reactivity during the compression process, which is taken into account. Since the difference between simulations

obtained from both methods is small, it suggests that they can be applied similarly to model the IDT of the neat surrogate fuel. In general, the surrogate fuel reactivity is correctly characterized by the proposed kinetic model.

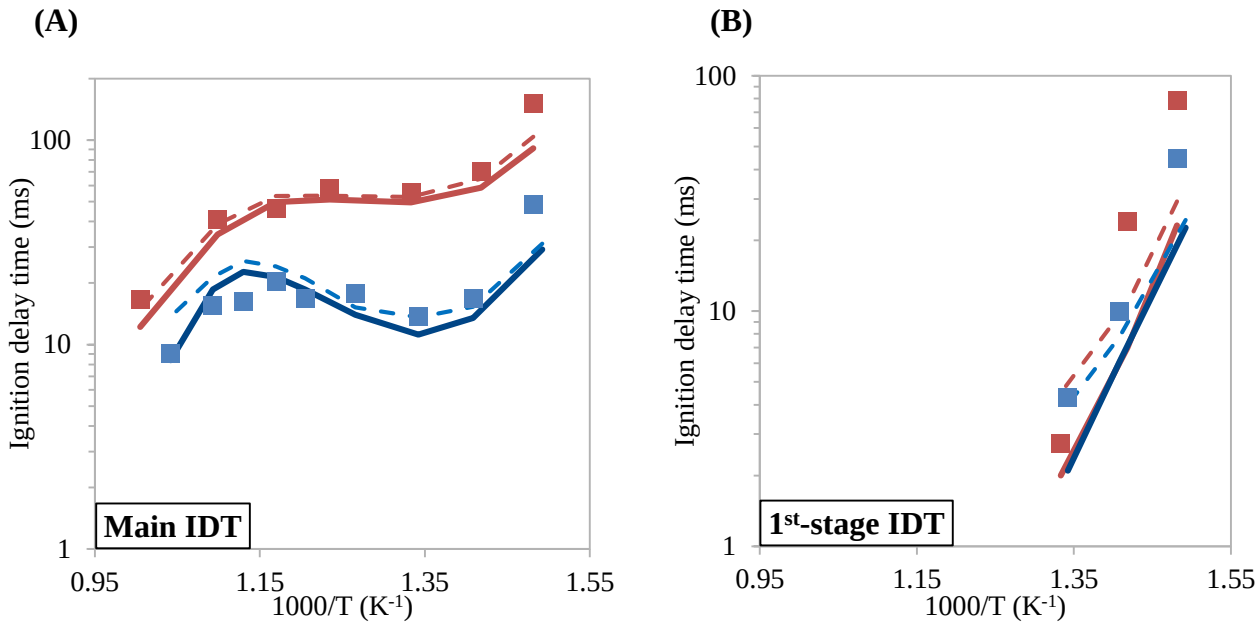

Figure 53: Measured and simulated 1st-stage ignition and main IDT of the neat surrogate fuel at 10 bar and Φ = 0.5 (red) and 1 (blue). Symbols refer to experimental data. Solid lines and dashed lines are used to illustrate modeling work performed with the "all-simu" method and the "frozen chemistry" method, respectively.

5.2.1.b Reaction pathway of the surrogate fuel

In order to investigate the combustion mechanism of the surrogate fuel combustion, rate of production (ROP) analyses were carried out at three different temperatures "T_c": 675 K, 745 K, and 915 K at P_c = 10 bar and Φ = 1. Figure 54 illustrates the main reaction pathways of the surrogate fuel. In these conditions, *n*-heptane reactivity follows mainly the low temperature oxidation scheme [36]. *n*-Heptane produces four isomers of heptyl radical by H-abstraction reactions. With addition of molecular oxygen, these heptyl radicals produce the corresponding heptyl peroxy radicals ($C_7H_{15}OO$). The peroxy radicals can release HO_2 radicals to form heptenes and/or follow isomerisations to produce hydroperoxyalkyl radicals ($C_7H_{14}OOH$). The latter compound can undergo a decomposition to form cyclic ethers and/or an addition to oxygen molecules to give peroxyhydroperoxyheptyl radicals ($OOC_7H_{14}OOH$). The formation of unsaturated species, here heptene, and cyclic ethers contribute to the NTC behavior [36]. Only at the highest T_c (915K), *n*-heptane can form *n*-propyl/*n*-butyl radicals and *n*-pentyl/ethyl radicals by unimolecular decompositions. Under this condition, heptyl radicals can undergo β-scission to mainly form *n*-propyl radical and 1-butene. On the other hand, toluene reactions are quite similar on the whole range of T_c. A small quantity of toluene reacts with H atoms to form benzene and methyl radicals (CH_3). Toluene forms primarily benzyl radical ($C_6H_5CH_2$) by H-atom abstractions. This radical can then add to O_2 to form benzyl peroxy radical ($C_6H_5CH_2OO$). This species is not much reactive compared to isomers of heptyl peroxy radicals because of the lack of an easy intramolecular isomerization. Once formed, $C_6H_5CH_2OO$ dominantly yields back $C_6H_5CH_2$ by releasing O_2. Beside the reaction $C_6H_5CH_2 + O_2 = C_6H_5CH_2OO$, another important channel of the consumption of $C_6H_5CH_2$ is the combination with HO_2 which produces benzoxyl radical ($C_6H_5CH_2O$): $C_6H_5CH_2 + HO_2 = OH + C_6H_5CH_2O$. This radical is more reactive than the benzyl peroxy radical since it can form phenyl radical (C_6H_5) and carbon monoxide (CO) by several H atom release steps. This mechanism is illustrated with the reactions presented in Table 24. These reactions were adopted from the recent validated toluene model of Yuan et al. [105].

Table 24: Rate constant of reactions of benzoxyl radical

Reactions		A	N	E_a	Ref.
R_I	$C_6H_5CH_2O = C_6H_5CHO + H$	1.68×10^{22}	-2.90	20760	[152]
R_{II}	$C_6H_5CHO = C_6H_5CO + H$	4.00×10^{15}	0.00	83700	[144]
R_{III}	$C_6H_5CO = C_6H_5 + CO$	3.98×10^{14}	0.00	29400	[144]

Rate expression: $k = AT^n \exp\left(\frac{-E_a}{RT}\right)$ in cm^3, mol, cal, s units.

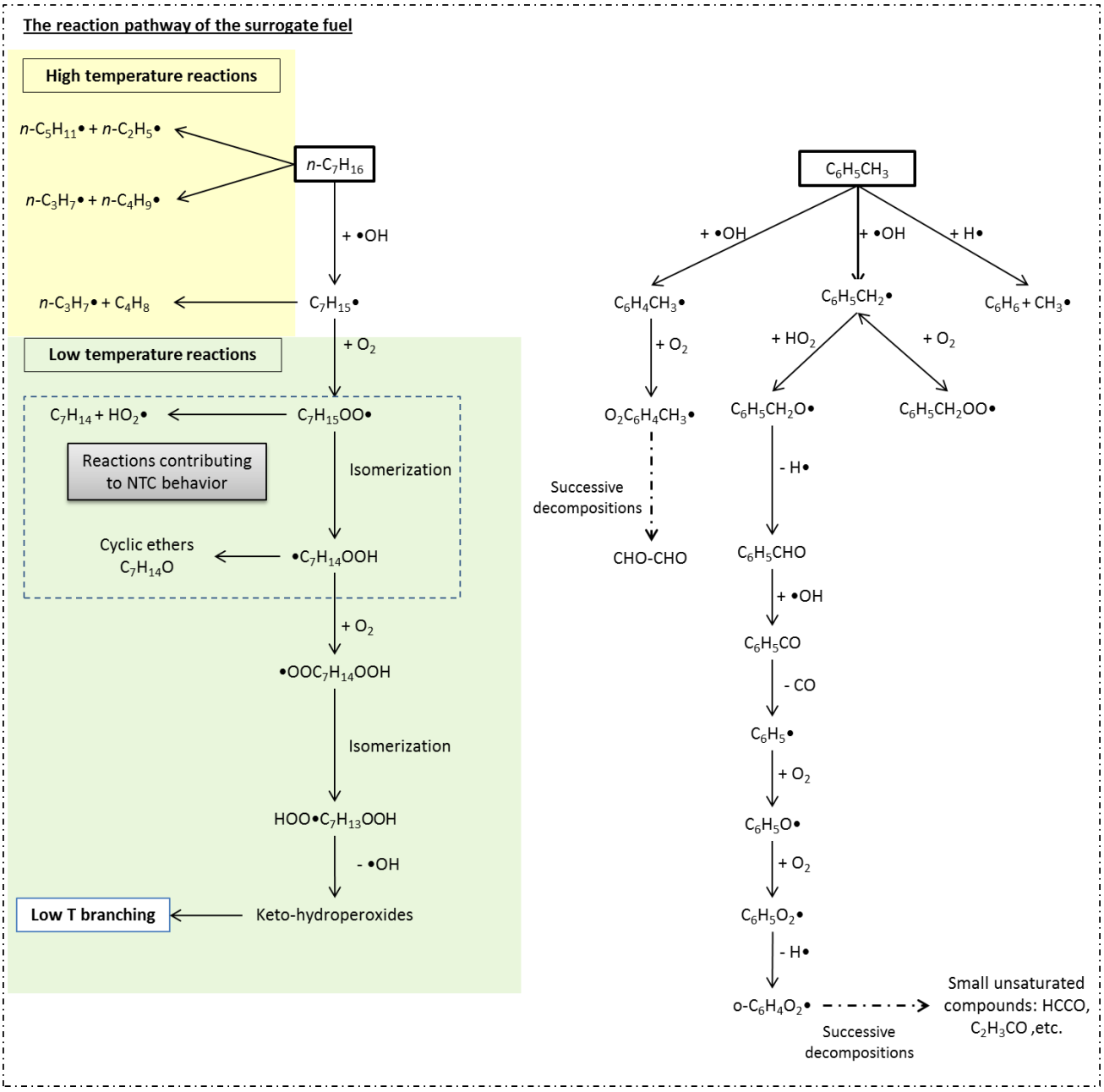

Figure 54: Reactions pathway of the surrogate fuel at 10 bar, Φ = 1 from 675 to 915 K.

5.2.2 Ignition delay time of the surrogate fuel at T > 1000 K

5.2.2.a Shock tube experiments results

Experiments in the ST were carried out at a pressure close to 10 atm. This shock tube does not allow measurements outside of a temperature range of 1350 to 1600 K for fuels considered in this thesis. Indeed, for a given shock tube geometry, the measurable range of temperature depends on the fuel IDT. The interactions between shock waves, rarefaction waves and discontinuity interfaces increase instability overtime on pressure and temperature. The measure becomes impossible beyond a certain period of time. Table 25 summarizes the experimental conditions performed on the ST with the surrogate fuel.

Table 25: Experimental condition of tests on the ST performed with the surrogate fuel.

P (atm)	T (K)	Φ	Composition (% mol.) of fuel gas mixture		
			Fuel	Oxygen	Argon
10	1350 - 1600	1	0.50	4.78	94.72

The preparation of the reactive mixtures was carried out in a tank at 25°C using the partial pressure method. The considered fuel was diluted in argon at a ratio of 0.5%. Oxygen was added to the tank to obtain the desired equivalence ratio. As the saturation vapor pressure at 25°C of toluene (28.4 torr) is less than one of *n*-heptane (38.4 torr), the composition of the surrogate fuel in the gas phase differs from that of this fuel prepared in the liquid phase because of the liquid-vapor equilibrium. The composition of the surrogate fuel introduced into the shock tube was additionally reassessed by the calculation of this equilibrium thanks to the UNIFAC model [199] in PRO II software [200]. The result of the calculation is presented in Table 26. The simulations of the measured IDT of the surrogate fuel in Figure 55 were conducted with the calculated gas-phase composition.

Table 26: Composition of the surrogate fuel.

Fuel		Surrogate fuel experimentally prepared in the liquid phase	Surrogate fuel numerically calculated in the gas phase at 25°C
Composition (% mol.)	**Toluene**	71.9	56.7
	***n*-Heptane**	28.1	43.3

Figure 55 shows the IDT of the surrogate fuel at 10 atm from 1350 K to 1600 K at stoichiometric condition. As expected, two-stage ignitions and NTC are not observed. The IDT of the surrogate fuel varies linearly inversely with temperature. The measured IDT of the surrogate fuel at this condition is ranging from 10.6 and 362.8 µs. The simulation results agree satisfactorily with the experiments.

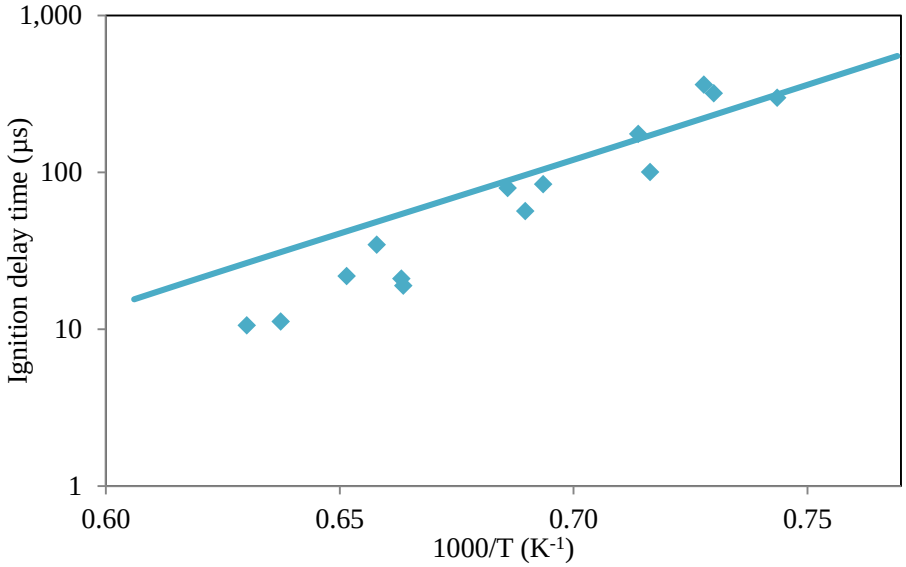

Figure 55 : Ignition delay times of the surrogate fuel at 10 atm, Φ = 1. Symbols: experiments. Solid lines: simulations.

5.2.2.b *Reaction pathway of the surrogate fuel*

To investigate the reaction pathway of the surrogate fuel in the condition of ST experiments, i.e. at high temperature (T > 1350 K), ROP analyses were carried out at 1400 K, P = 10 bar and Φ = 1. Figure 56 illustrates the main reaction pathways of the surrogate fuel in the examined condition.

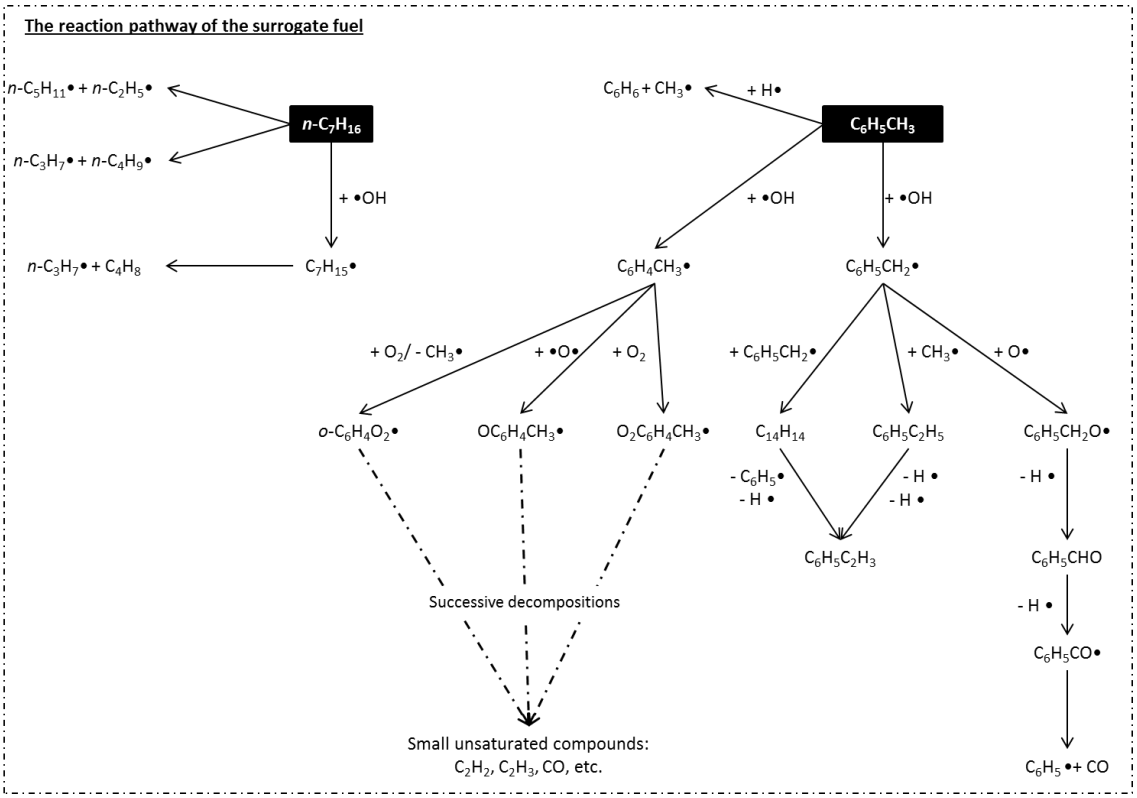

Figure 56: Reactions pathway of the surrogate fuel at 10 bar, Φ = 1, 1400 K.

n-Heptane follows exclusively the high temperature oxidation scheme. This compound forms *n*-propyl/ *n*-butyl radicals and *n*-pentyl/ ethyl radicals by unimolecular decompositions. Moreover, heptyl radicals formed by H-atom abstraction can undergo a β-scission to mainly form *n*-propyl radical and 1-butene. The reaction pathway of toluene is very different from one of *n*-heptane. During the initiation

step, toluene forms benzyl radical ($C_6H_5CH_2$) and methylphenyl radical ($C_6H_4CH_3$) by H-atom abstractions with OH radicals. Toluene forms also C_6H_6 and CH_3 by the ipso-addition with H atom. The fluxes of these reactions are similar. The formed methylphenyl radical reacts with O_2 and O atom to form oxygenated aromatic compounds as *o*-$C_6H_4O_2$, $OC_6H_4CH_3$, $O_2C_6H_4CH_3$. These oxygenated products then decompose by several reactions, which result in small unsaturated compounds as C_2H_2, C_2H_3, CO, etc. Similarly, benzyl radical reacts with O atom to form $C_6H_5CH_2O$ radical, which produces benzyl radical (C_6H_5) and CO by the release of two H atoms. Additionally, benzyl radical reacts in several reactions of termination to form bibenzyl ($C_{14}H_{14}$) and ethylbenzene ($C_6H_5C_2H_5$). These two products then undergo some decomposition reactions to form styrene ($C_6H_5C_2H_3$).

5.2.3 Laminar burning velocity of the surrogate fuel

Measurements of the laminar burning velocity of the surrogate fuel were conducted at atmospheric pressure. The initial temperature of gas flux was at 398 K. Figure 57 presents the laminar burning velocity of the surrogate fuel as a function of equivalence ratio. At the investigated experimental condition, the laminar burning velocity of the surrogate fuel varies from 30 to 60 cm/s and reaches its maximum value at Φ = 1.1 as observed in the case of other hydrocarbons [133]. According to the thermal theory developed by Mallard and Le Châtelier [201], laminar burning velocity (S_L) depends on thermal diffusivity (α) and chemical reaction rate (dξ/dt) as illustrated by the following formula $S_L \propto \sqrt{\alpha \times \frac{1}{d\xi/dt}}$. In lean condition (Φ < 1), S_L increases with Φ. When Φ becomes higher than 1, S_L decreases with Φ since the chemical reaction dominates the thermal diffusion. The maximum value of S_L would then be located at Φ = 1. In air, this value is found at Φ = 1.1. This happens because the combustion of fuel was carried in the present of an inert diluent, nitrogen. The heat produced by the combustion is partially captured by nitrogen. Consequently, the equilibrium of thermal diffusion and chemical reaction is displaced toward Φ = 1.1, i.e. the laminar burning velocity and the flame temperatures are maximum at this equivalence ratio.

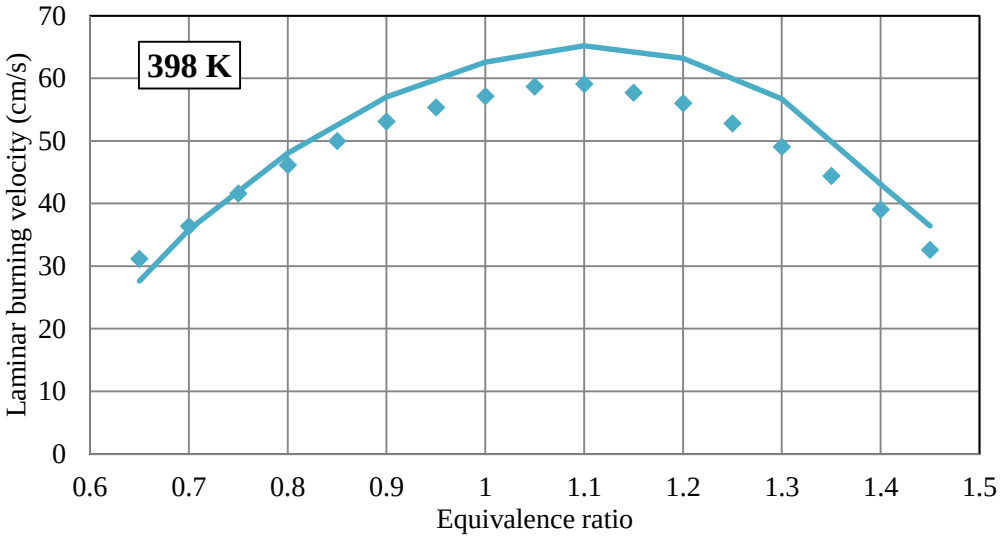

Figure 57: Laminar burning velocity of the surrogate fuel at atmospheric pressure and initial temperature of 398 K. Symbols: experiments. Lines: simulation

As observed in Figure 57, the simulation results are in good agreement with experiments. The kinetic model developed in this study well predicts the laminar burning velocity of the surrogate fuel in lean conditions (Φ < 0.9). As the equivalence ratio increases, the flame speeds of the surrogate fuel are slightly overestimated. The largest difference between simulation and experiments is about 5 cm/s.

ROP analyses, not shown here, highlight that the surrogate fuel undergoes the high temperature mechanism presented Figure 56.

5.2.4 Conclusion about the surrogate fuel reactivity

The IDT and laminar burning velocity measurements of the surrogate fuel were conducted in a ST, a RCM, and a flat flame burner. These experimental methods enabled the study of the surrogate fuel reactivity over a wide range of engine-relevant conditions.

RCM experiments were performed at 10 bar, Φ = 0.5 – 1, from 675 to 1000 K. Two-stage ignitions and NTC were observed. This helped to investigate the effect of the considered additives on these combustion phenomena. ST tests were conducted at 10 bar, Φ = 1, from 1350 to 1600 K. These ST conditions contributed to the study of the additives at high temperatures. As a result, the effects of the additives were experimentally investigated over a very wide range of temperatures.

Additionally, the laminar burning velocity of the surrogate fuel were carried out at an initial temperature of 398K, P = 1 atm, and Φ = 0.65 – 1.45. Flame velocity is an important property of fuel relating to engine power and undesired phenomena as knock and pre-ignition. The impact of the additives on the laminar burning velocity of the surrogate fuel is further presented.

In general, all experimental results are well simulated by the kinetic model. This confirms the performance of the surrogate fuel sub-mechanism in this model.

5.3 Effect of EHN

In this section, the effects of EHN on the IDT and the laminar burning velocity of the surrogate fuel are presented. The chemical effects of this additive are analyzed thanks to the validated kinetic model.

5.3.1 Ignition delay time of the surrogate fuel doped with EHN at T < 1000 K

5.3.1.a RCM experimental results

Table 27 summarizes the RCM operating conditions with the surrogate fuel doped with EHN. The doping levels of this additive were set to 0.1 and 1% mol.

Table 27: Experimental conditions of tests in the RCM performed with the surrogate fuel doped with EHN.

P (bar)	T (K)	Φ	Doping level of EHN (% mol.)	Composition of fuel gas mixture				
				Toluene (% mol.)	*n*-Heptane (% mol.)	EHN (ppm)	Oxygen (% mol.)	Nitrogen (% mol.)
10	675 - 1000	0.5	0.1	0.78	0.31	10.9	20.77	78.14
		0.5	1.0	0.77	0.30	108.6	20.77	78.14
		1.0	0.1	1.54	0.60	21.5	20.55	77.30
		1.0	1.0	1.53	0.59	214.9	20.55	77.30

Goldsborough et al. [40] demonstrated that under the considered RCM conditions (675 – 1025 K, 21 bar, Φ = 1), the gas mixtures doped with EHN released a remarkable heat during compression. A similar trend appears in this study. Under similar experimental conditions to those for the neat surrogate fuel and the surrogate fuel doped with 0.1 % mol. of EHN, a heat release before the end of the compression was recorded when the additive was used. This was characterized by a significant pressure increase compared to the measurement with the neat surrogate fuel. An evaluation of T_c by the calculation of the adiabatic compression for these experiments would lead to an important bias since the reaction heat release would be neglected. Due to this, T_c corresponding to the experiments with the undoped

fuel mixtures was also used to present the IDT of the EHN-doped surrogate fuel. Figure 58 illustrates the EHN effect on the surrogate fuel IDT at stoichiometric condition. Nevertheless, attention must be paid to understand this figure. For example, the real T_c reached by the compression of the surrogate fuel doped with 1% EHN at nominal conditions (T_c = 960 K, P_c = 10 bar) is higher than 960 K due to the exothermic reaction, but cannot be determined without numerical simulation by the adiabatic unreactive compression calculation.

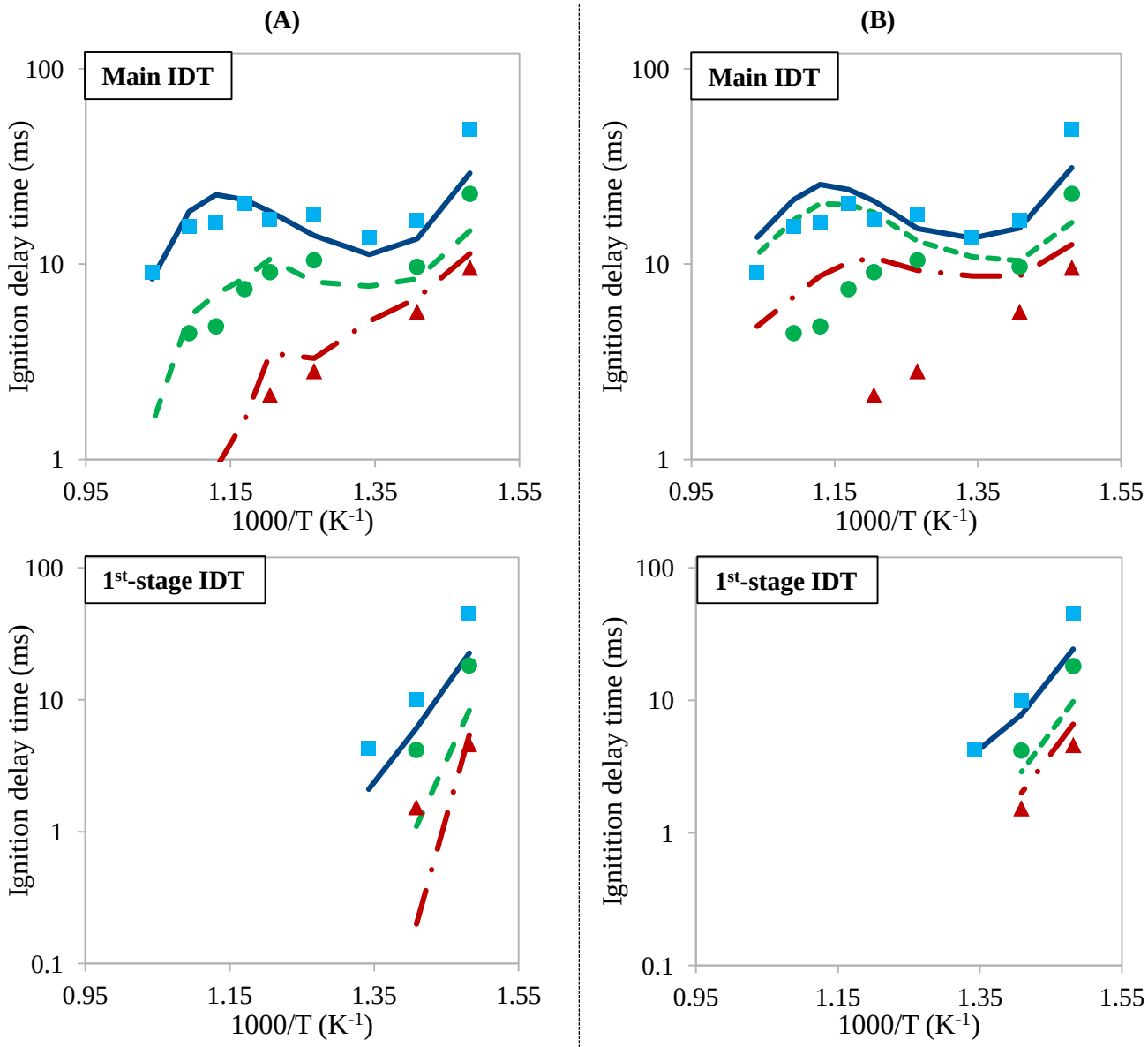

Figure 58: Measured and simulated 1st-stage and main IDT at 10 bar and Φ = 1: (A) Simulations with "all-simu" method. (B) Simulations with "frozen chemistry" method. Symbols refer to experimental data and lines are used to illustrate modeling work. The neat surrogate fuel results are illustrated with solid lines and square symbols. Doped fuels with 0.1% EHN is presented with dashed lines and circle symbols and 1% EHN with dash-dotted lines and triangle symbols.

At the investigated experimental conditions (10 bar, Φ = 1), EHN promotes the reactivity of the fuel at all examined T_c (675 – 960 K). A significant reduction of both 1st-stage IDT and main IDT of the surrogate fuel is observed in presence of EHN. This effect increases with EHN doping levels. The NTC behavior of the surrogate fuel is mitigated by the addition of EHN. At doping level of 1% mol., EHN suppresses totally the NTC behavior. The EHN promoting effect is minimum at T_c near 710 K and then increases with T_c. This feature agrees with the observation of Goldsborough et al. [40], which indicated that EHN had the weakest influence on the reactivity of the primary reference fuel (blend of *n*-heptane and

isooctane) of RON 91 and toluene reference fuel (blend of *n*-heptane, isooctane, and toluene) of RON 91 near 740 K.

As expected, the simulation method has a significant effect on the ignition delay modeling. At low temperature (T_c < 710 K), where a two-stage ignition is observed, both methods provide close results, which reasonably agree with the experimental data. However, as T_c increases, the "frozen chemistry" method underestimates largely the effect of EHN on the IDT of the surrogate. On the opposite, the "all-simu" method simulates correctly the reactivity of the doped fuel. This observation emphasizes the high reactivity of the doped fuel during the compression. Consequently, the "all-simu" method is confirmed to be more suitable than the "frozen chemistry" to simulate the RCM results for fuels doped with EHN, especially at T_c > 710 K.

In order to capture the early heat release due to EHN, the "all-simu" calculations were further analyzed. Figure 59 presents the simulated species profiles and the simulated pressure history during RCM tests at T_c = 675 K (A) and T_c = 915 K (B).

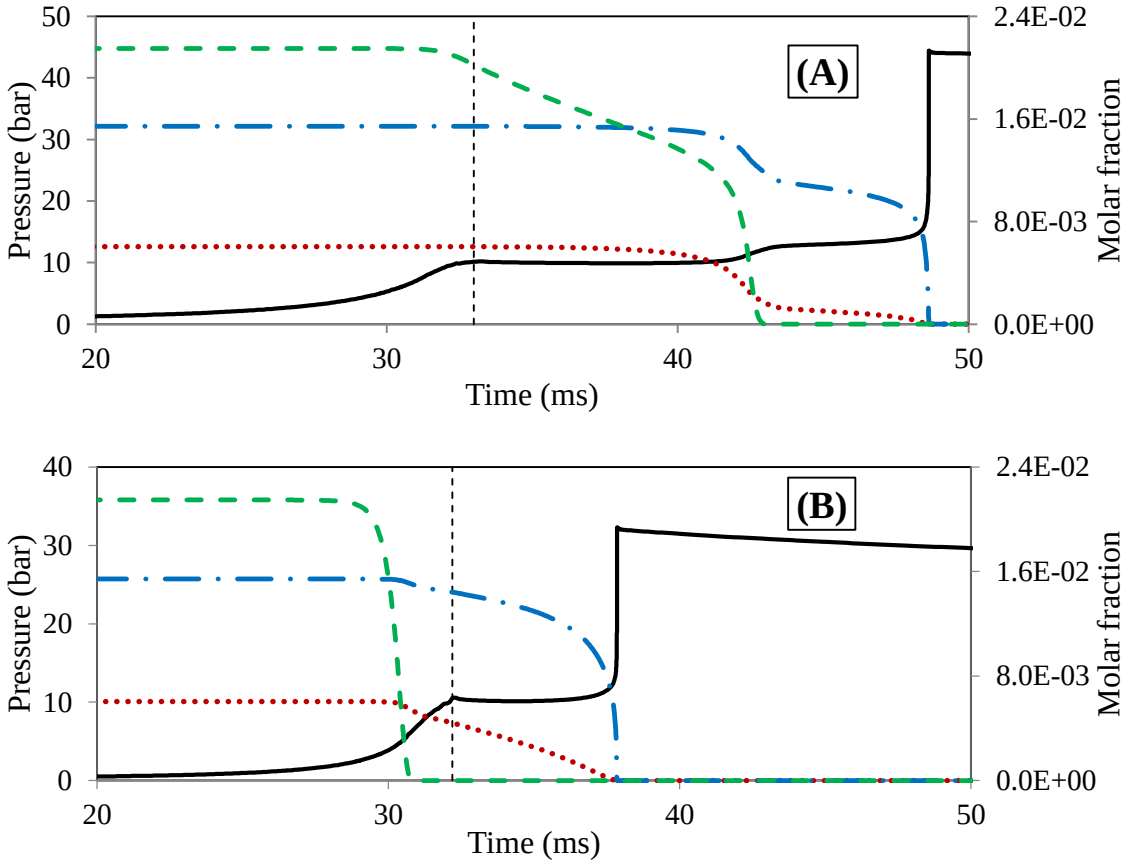

Figure 59 : Simulated species profiles of toluene (dashed lines), *n*-heptane (dash-dotted lines), EHN × 1000 (dotted lines) and simulated pressure histories (solid lines) of RCM experiments at P_c ≈ 10 bar, Φ = 1 and 0.1% mol. EHN. (A): T_c = 675 K and (B): T_c = 915 K. End of compression: vertical dashed lines.

At low T_c (675K), EHN decomposes slightly before the end of the compression. The decomposition of EHN progresses gradually until the 1st-stage ignition time where EHN is rapidly consumed. At high T_c (915 K), EHN decomposes totally before the end of piston movement. At T_c = 675 K, the gas mixture temperature increases gradually thanks to the heat release from the surrogate fuel oxidation after the end of the compression. However, for the condition T_c = 915 K, the compression increases the gas temperature leading to the full decomposition of EHN when the temperature reaches 830 K, before the piston stops. The reaction of the surrogate fuel, i.e. the toluene / *n*-heptane blend, is then initiated before the end of the compression, which results in an increase of P_c. This is validated thanks to the

simulation of pressure histories near the end of the compression of RCM experiments (see Figure 60). It was experimentally found that at T_c = 675 K, there is no P_c change between both the undoped and doped fuel tests. However, at T_c = 915 K, P_c increases remarkably in the presence of EHN 0.1% mol. These features are well captured by the kinetic model.

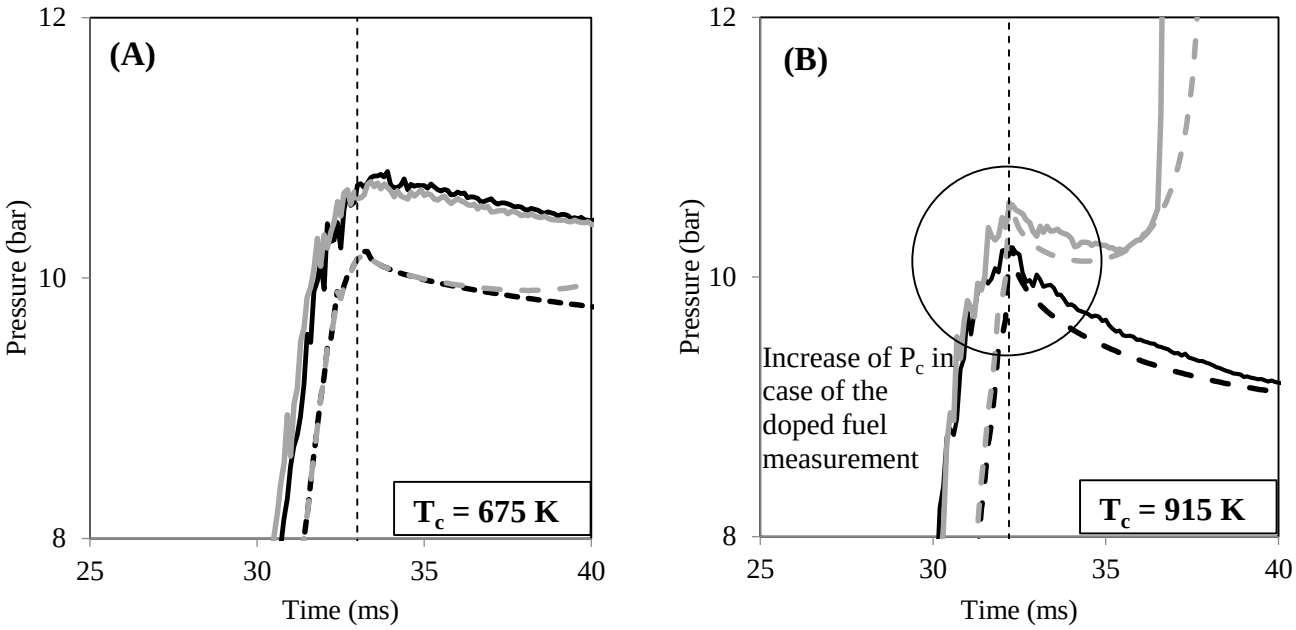

Figure 60: Measured (solid line) and simulated (dashed line) of pressure histories near the top dead center during RCM experiments at $P_c \approx 10$ bar, Φ = 1 of the neat surrogate fuel (black) and the surrogate fuel doped with EHN 0.1% mol (grey). (A): T_c = 675 K and (B): T_c = 915 K. End of compression: dashed black line.

As observed in Figure 58, the promoting effect of EHN evaluated in RCM tests rises with T_c. As T_c increases, EHN decomposes earlier during the compression. The chemical reactivity of the gas mixture during the compression is higher, which results in a shorter IDT. As a consequence, the EHN promoting effect is partly linked to the compression time. Consequently, a different RCM with another compression time would show a different effect of EHN on the surrogate fuel IDT.

Figure 61 presents the simulations of EHN promoting effect on the surrogate fuel at P_c = 10 bar and Φ = 0.5. The "all-simu" method was used to simulate RCM experiments and T_c in Figure 61 corresponding to the neat surrogate test. The kinetic mechanism simulates reasonably well the EHN promoting effect on main ignitions. The model, however, overestimates the EHN promoting effect on the 1st-stage ignition. Experimentally, the 1st-stage ignitions were observed in the case of the fuel doped with EHN 1% at two T_c: 675 K and 705 K. The measured 1st-stage IDT at these T_c are 15.8 and 3.1 ms respectively. Meanwhile, only 1st-stage ignition at T_c = 675 K was predicted (4.5 ms) by the kinetic model of this study. This may be related to the underestimation of the IDT regarding the neat surrogate fuel under these conditions.

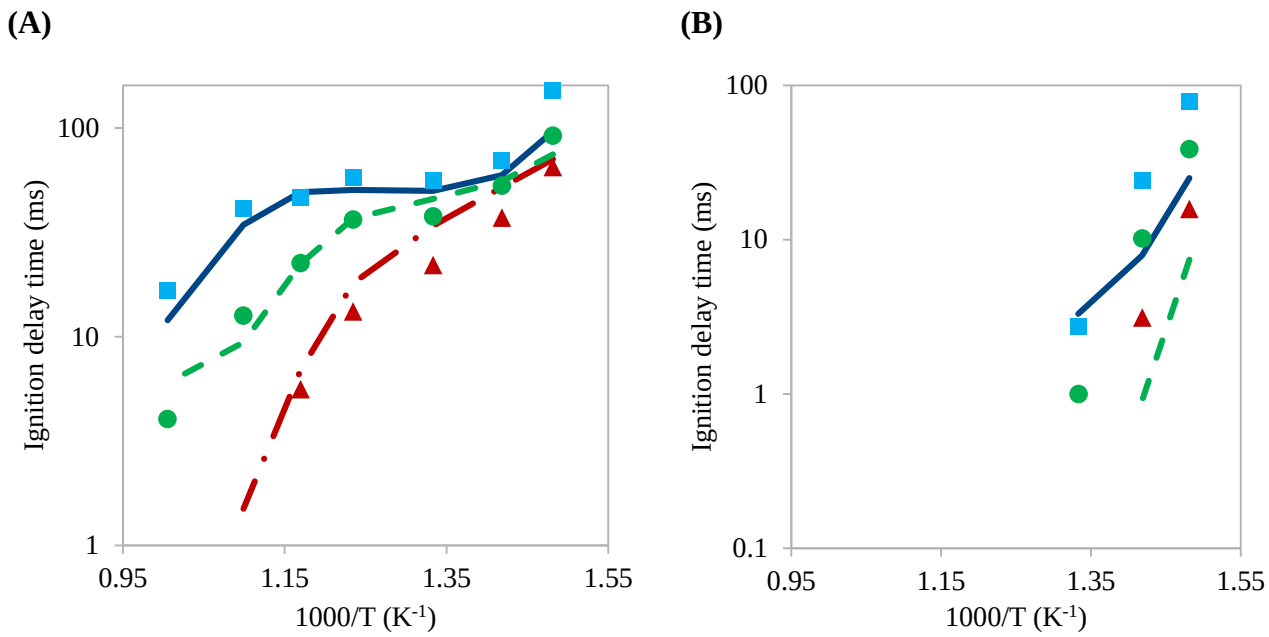

Figure 61: Measured (symbols) and simulated (lines) IDT of the neat surrogate fuel (solid lines and square symbols) and doped fuels with 0.1% EHN (dashed lines and circle symbols) and 1% EHN (dash-dotted lines and triangle symbols) at Pc = 10 bar, Φ = 0.5. (A) main IDT. (B) 1st-stage IDT.

Figure 62 shows the simulated relative effect (R_{eff}) of EHN (0.1% mol.) on the main ignition of the surrogate fuel at P_c = 10 bar, T_c = 675 - 915 K and two equivalence ratios: 0.5 and 1. R_{eff} for EHN is defined in Eq. 5. Higher R_{eff}, stronger is the EHN promoting effect. It is found that at two different equivalence ratios, the influence of EHN on fuel reactivity follows the same trend while T_c varies. The impact of EHN is the lowest at T_c near 740 K then increases with T_c. In the upper T_c range (> 850 K), EHN shows the same qualitative effect for the two equivalence ratios. However, the EHN promoting effect is significantly stronger (up to 5 times) at the lower range of T_c (< 800 K) for the stoichiometric mixtures. As discussed in section 4.2, EHN activity depends on its decomposition. At low T_c, EHN decomposes partly thanks to the heat released from the fuel oxidation. Under lean conditions (Φ = 0.5), the surrogate fuel is less reactive than at stoichiometric condition (Φ = 1). Consequently, the EHN decomposition is slower under lean condition implying a less pronounced additive effect.

$$R_{eff} = \frac{IDT_{undoped\ fuel} - IDT_{doped\ fuel}}{IDT_{undoped\ fuel}} \times 100\% \qquad (Eq.5)$$

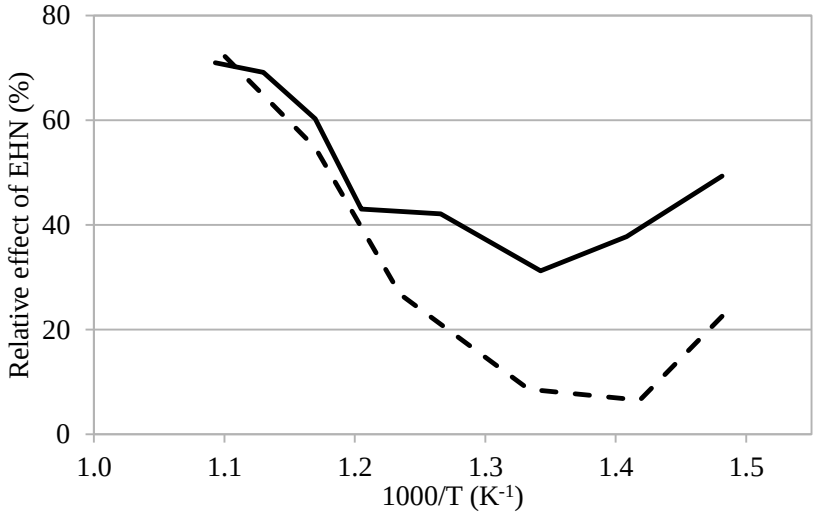

Figure 62: The simulated relative effect of EHN 0.1% mol. on the main IDT of the surrogate fuel at P_c = 10 bar and two equivalence ratios: Φ = 0.5 (dashed lines) and Φ = 1 (solid lines).

5.3.1.b Chemical effect of EHN

To understand the EHN chemical effect on the surrogate fuel, ROP analyses were carried out at three different T_c: 675 K, 745 K, and 915 K for EHN doping level of 0.1% mol. at P_c = 10 bar and Φ = 1 during the period of EHN decomposition. As EHN decomposes quickly, the additive affects the fuel decomposition through the initiation and propagation steps. Figure 63 illustrates the main reaction pathways of the surrogate fuel decomposition and analyses the chemical effect of EHN.

The effect of EHN lies in the chemical activity of its decomposition products C_7H_{15}-3 radical and NO_2. C_7H_{15}-3 radical follows the chemical scheme presented in Figure 54 to form OH radicals, which enhances the H-atom abstractions from fuel. NO_2 is able to enhance toluene reactivity. NO_2 reacts with benzyl radical to form benzoxyl radical (reaction R84 displayed in Figure 63). The last radical is more reactive than the benzyl peroxy radical since it can form phenyl radical (C_6H_5) and carbon monoxide (CO) by several H atom release steps. In addition to reaction R84, NO_2 can follow several H-abstraction reactions with small species such as HO_2 and CH_2CHO to form HONO (reaction R101, R102 respectively) at low T_c (675 K, 745 K). Especially, at T_c = 745 K, NO_2 is slightly stored in nitroethane ($C_2H_5NO_2$) because of reaction R103, which is the reverse reaction of R73 presented in Table 17 . This is the reason why the EHN promoting effect is lowest at T_c around 745 K.

$$NO_2 + HO_2 = O_2 + HONO \quad \textbf{(R101)}$$
$$NO_2 + CH_2CHO = CH_2CO + HONO \quad \textbf{(R102)}$$
$$NO_2 + C_2H_5 = C_2H_5NO_2 \quad \textbf{(R103)}$$

The nitric oxide (NO) formed by reaction R84 can react with peroxy radicals (reactions R80 – R83) to produce NO_2 and the corresponding alkoxy radicals. A cycle NO_2 – NO is then established. At intermediate temperature (T_c = 745 K), the reaction R83 competes with the HO_2 release reaction of the heptyl peroxy radicals. Consequently, the NTC behavior is mitigated.

EHN effect lies in interactions of NO_x with primary radicals derived from toluene and *n*-heptane. Consequently, it is suggested that the interaction between NO_x and fuel should be carefully considered to predict the EHN promoting effect on this fuel oxidation.

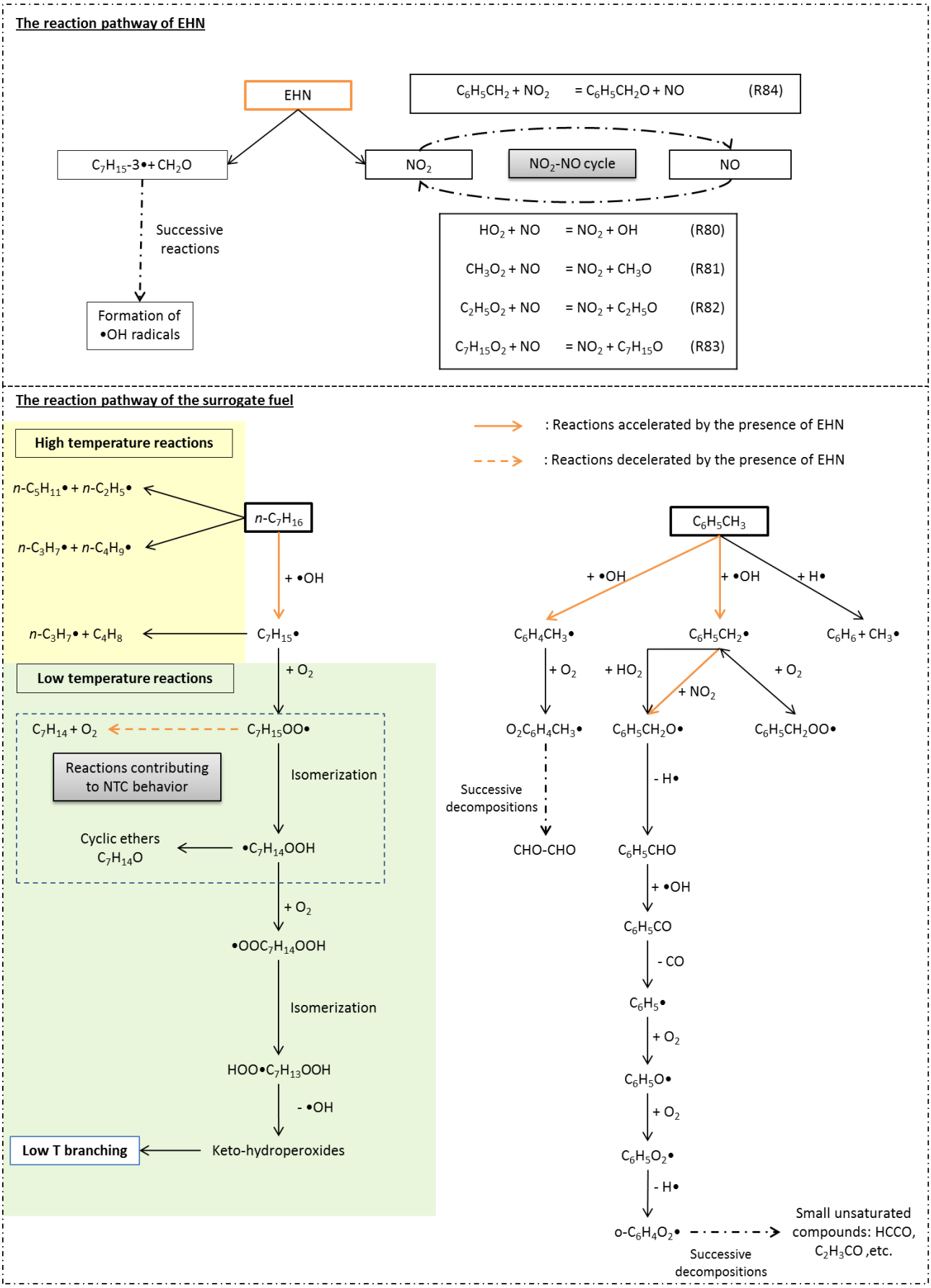

Figure 63: Reactions pathway of EHN and the surrogate fuel at 10 bar, Φ = 1 from 675 to 915 K.

In addition to ROP, sensitivity analyses on the formation of OH radical were conducted in the same conditions thanks to CHEMKIN-PRO [130]. These analyses evaluate how A-factor of each reaction in the kinetic model influences the formation of OH radical. The results analyses are given as sensitivity coefficients of reactions. A positive coefficient means that the relevant reaction has a promoting effect on the production of OH radical. On the other hand, a negative coefficient indicates the inhibiting effect of the relevant reaction on the production of OH radical. The result of the sensitivity analyses at 75 mol.% EHN decomposition is presented Figure 64. It is found that the reaction of EHN decomposition presents a high promoting effect on the production of OH radical in the early stage of combustion at all examined T_c. This reaction becomes less sensitive at the time of the total decomposition of EHN. According to the variation of T_c, the reaction of EHN decomposition is most sensitive at the highest temperature (T_c = 915 K). There is no other reaction of nitrogen chemistry being sensitive on the formation of OH radical.

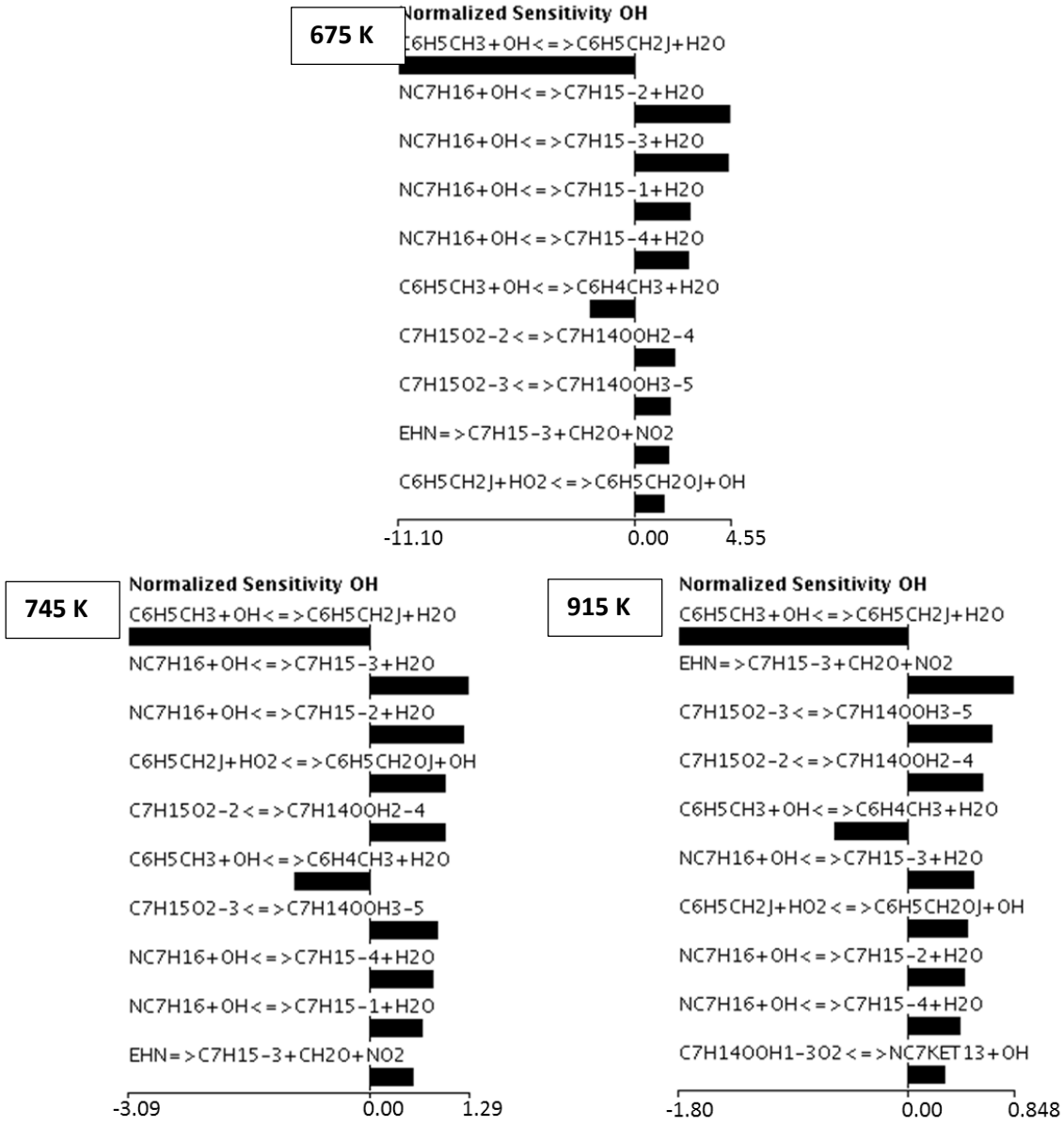

Figure 64: Results of sensitivity analyses on the formation of OH radical at 75 mol.% EHN decomposition at three different T_c: 675 K, 745 K, and 915 K for EHN doping level of 0.1% mol. at P_c = 10 bar and Φ = 1.

5.3.2 Ignition delay time of the surrogate fuel doped with EHN at T > 1000 K

5.3.2.a Shock tube experiments results

The experiments on the ST performed with the surrogate fuel doped with EHN were conducted at the same operating conditions that the surrogate fuel: 10 atm, Φ = 1, from 1350 to 1600 K. The doping level of EHN was set at 1% weight basis in the liquid-phase surrogate fuel. Table 28 presents the saturation vapor pressures of EHN, toluene, and *n*-heptane at 25°C. As EHN is much less volatile than two components of the surrogate fuel, the concentration of this additive in the surrogate fuel in the gas phase in the ST is much less than 1% weight basis. A calculation of molar composition of the EHN-doped fuel in the gas phase by UNIFAC model was not possible since no data for EHN were found. Table 29 summarizes the experimental condition investigated in the ST. The molar composition of the doped fuel was estimated by assuming the doping level of EHN in the gas phase was 1% weight basis.

Table 28: Saturation vapor pressure of compounds at 25 °C

Compound	Toluene	*n*-Heptane	EHN
Saturation vapor pressure (torr)	28.4	38.4	0.2[a]

[a]value at 20°C

Table 29: Experimental condition of tests on the ST performed with the surrogate fuel doped with EHN.

P (atm)	**T (K)**	**Φ**	**Doping level of EHN (% mass)**	**Composition of fuel gas mixture**				
				Toluene (% mol.)	*n*-Heptane (% mol.)	EHN (ppm)	Oxygen (% mol.)	Argon (% mol.)
10	1350 - 1600	1	1	0.28	0.22	27	4.78	94.71

Figure 65 illustrates the measured and simulated IDT of the neat and doped surrogate fuel. A significant effect of EHN on the reactivity of the target fuel was not observed at these conditions. The simulations performed with the kinetic model did not either present a remarkable effect of EHN. This agrees with the results of the study of Hartmann et al. [69]. These authors indicated that EHN showed its promoting effect on the combustion of *n*-heptane only at T < 900 K.

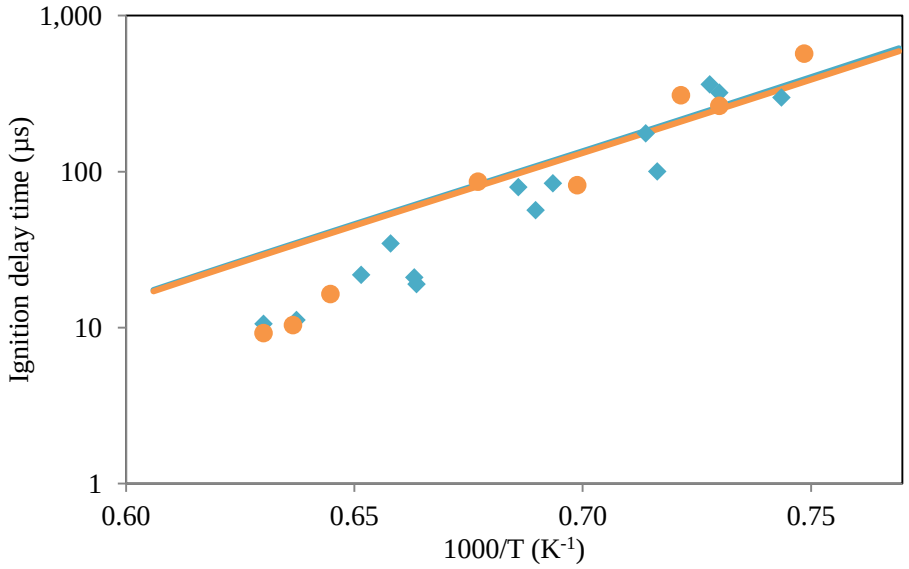

Figure 65: Ignition delay times of the neat surrogate fuel (blue) and the surrogate fuel doped with EHN (orange) at 10 atm, Φ = 1. The gas mixture composition is shown in Table 29. Symbols: experiments. Lines: simulations.

5.3.2.b Chemical effect of EHN

To clarify the little effect of EHN on the gas-phase reactivity of the surrogate fuel at high temperatures (T > 1300 K), ROP analyses were conducted at 1400 K, 10 atm, Φ = 1 for an EHN doping level of 1% mass. Simulations indicate that EHN totally decomposes in a very short time (less than 0.01 µs). In this condition, *n*-heptane undergoes exclusively C-C bond cleavage reactions forming small radicals including *n*-pentyl, *n*-butyl, *n*-propyl and ethyl as presented in Figure 56. The importance of the initiation and propagation steps on the combustion of the surrogate fuel at high temperatures (T > 1300) is negligible. As seen in Figure 63, EHN involves only in the initiation and propagation steps. For this reason, the effect of EHN is insignificant at high temperatures (T > 1300 K). In these conditions, NO_2 reacts in preference with alkyl radicals R (C_1-C_7) to produce the corresponding alkoxy radicals RO and NO.

5.3.3 Effect of EHN on the laminar burning velocity of the surrogate fuel

To evaluate the effect of EHN on the laminar burning velocity of the surrogate fuel, flat flame burner experiments were performed at atmospheric pressure and initial temperature at 398 K. Figure 66 illustrates the flame speed of the neat and EHN-doped surrogate fuel according to various equivalence ratios.

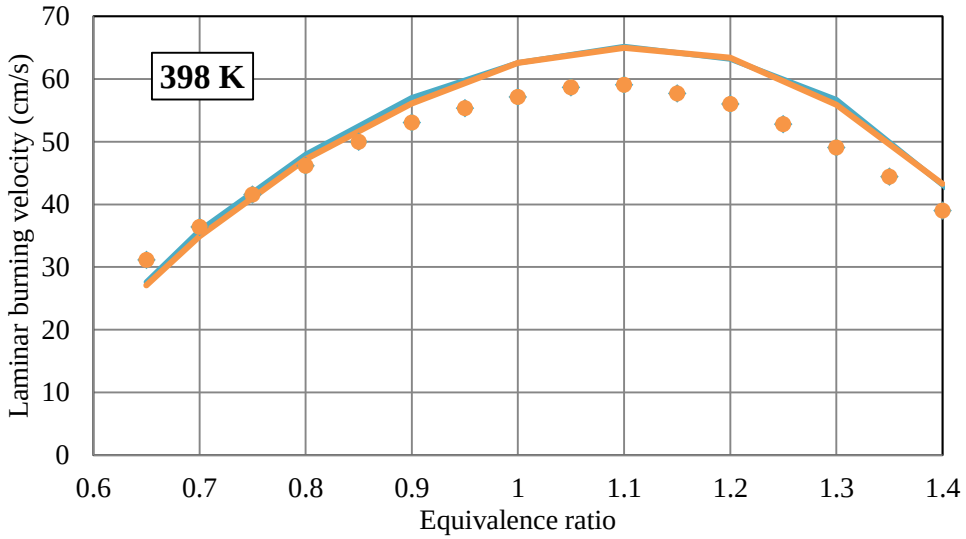

Figure 66: Laminar burning velocity of the neat surrogate fuel (blue) and the surrogate fuel doped with EHN 1% mass at atmospheric pressure and initial temperature of 398 K. Symbols: experiments. Lines: simulation.

Experimentally, EHN does not show any impact on the flame speed of the surrogate fuel. This observation is consistent with simulations.

5.4 Effect of ferrocene

In this section, the effects of ferrocene on the IDT and the laminar burning velocity of the surrogate fuel are presented. Improvements of the ferrocene sub-mechanism developed from literature data were carried out to better simulate experimental results. The chemical effect of this additive is revealed thanks to the new validated kinetic model.

5.4.1 Ignition delay time of the surrogate fuel doped with ferrocene at T < 1000 K

5.4.1.a RCM Experimental results

The effect of ferrocene on the IDT of the surrogate fuel is presented in Figure 67 for two equivalence ratios at 10 bar from about 675 K to almost 1000 K. The doping level of ferrocene was set at 0.01 and 0.1% mol. At doping level of 0.01% mol., the effect of ferrocene is negligible over almost the whole temperature range. Only a slight inhibiting effect of ferrocene is observed at T_c > 910 K. However, at a doping level of 0.1% mol., ferrocene shows a strong impact on the combustion of the surrogate fuel. While ferrocene does not show a remarkable effect on the 1st-stage ignition of the surrogate fuel, this additive presents a strong inhibiting effect on the main ignition. The latter effect increases with temperature. The main IDT of the doped fuel is up to four times longer than the one of the neat fuel at the highest examined temperatures (T_c > 900 K). In addition, ferrocene enhances the NTC behavior of the surrogate fuel. In lean conditions (Φ = 0.5), the doped fuel presents an NTC behavior from 750 K to 910 K which is not observed in the case of the surrogate fuel.

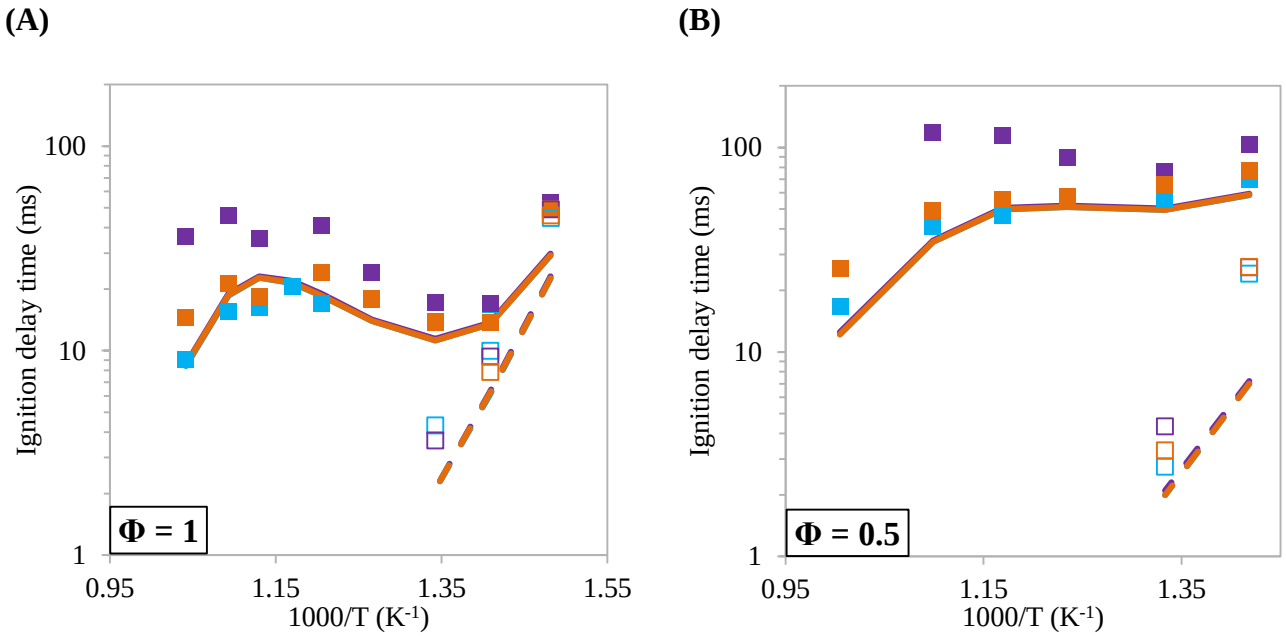

Figure 67: IDT of the neat surrogate fuel (blue) and the surrogate fuel doped with ferrocene at 0.01% mol. (orange) and 0.1% mol. (purple) at 10 bar. Experiments: filled symbols (main IDT) and empty symbols (1st-stage IDT). Simulations: solid lines (main IDT) and dashed lines (1st-stage IDT). (A) Φ = 1, (B) Φ = 0.5. Simulations employed the initial sub-mechanism of ferrocene reactions.

The kinetic model containing the initial sub-mechanism of ferrocene based on available data from the literature strongly underestimates the effect of this additive, as presented in Figure 67. This kinetic mechanism is limited to ferrocene and iron chemistry from Fenard et al. [75] and Rumminger et al. [188]. The rate constant of ferrocene decomposition was experimentally measured [185]. As a first approximation, the interactions of ferrocene with key combustion radicals (O, H, OH, HO_2) were estimated based on similar reactions of alkenes with these radicals [75]. The reactions of other iron

species were included from the model of Rumminger et al. [188] to simulate the very high temperature (T > 2000 K) reactivity, which is not relevant to the experimental conditions examined in this study. All above estimations are not reliable enough to describe the ferrocene effect under the conditions investigated in this work.

In order to propose a chemical reaction mechanism that can model the ferrocene behavior, improvements in its sub-mechanism were carried out. Quantum chemical calculations are powerful and provide a significant insight into key reaction properties including rate constant, products speciation and thermochemical data [140, 141]. However, it is challenging to employ this method to study iron chemistry as the element is a first-row transition metal. Iron is remarkably heavier than an atom of carbon, hydrogen, oxygen or nitrogen. Iron species, as well as other transition metal compounds, can present a multi-reference behavior. This implies that the non-dynamical correlation must be included in quantum calculations to get reliable results. This feature makes the calculations computationally expensive [202].

Another approach was applied in this study to improve the model. It was hypothesized that the effect of ferrocene may be due to reactions between iron species and radicals derived from hydrocarbon reactants. These coupling reactions should be included in the kinetic model to simulate the effect of ferrocene. Figure 68 presents the simulated profiles of iron species in conditions, in which ferrocene was experimentally found to be effective (see Figure 67), i.e. 10 bar, 830 K, Φ = 1, doping level of ferrocene at 0.1% mol. The most dominant iron species are $FeC_{10}H_{10}$, FeC_5H_5 and $Fe(OH)_2$. Their chemistry were assumed to be the most important to represent the inhibiting effect of ferrocene.

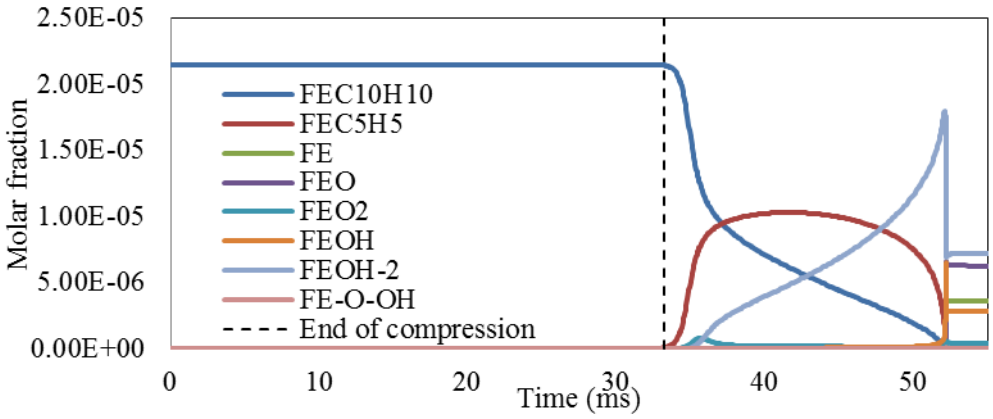

Figure 68: Simulated profiles of iron species during a RCM test at condition: 10 bar, 830 K, Φ = 1, surrogate fuel doped with 0.1% mol. ferrocene.

Rate constants of reactions of ferrocene with small radicals (H, O, OH, HO_2) are presented in Table 21 in section 4.3.2. Performing a brute sensitivity analysis, it was found that only reactions of $FeC_{10}H_{10}$ and FeC_5H_5 with HO_2 (R88 and R92 respectively) present a sensitive inhibiting effect at T_c < 885 K. Similar reactions (R104 – R109) were then included to represent the interactions of $FeC_{10}H_{10}$ and FeC_5H_5 and other important peroxy radicals (CH_3OO, C_2H_5OO, and $C_6H_5CH_2OO$). All these reactions produced the corresponding alcohols (CH_3OH, C_2H_5OH, and $C_6H_5CH_2OH$). At this step, the new model can simulate the effect of ferrocene at T_c < 885 K but not at T_c > 885 K. To extend the model performance, the chemistry of $Fe(OH)_2$ was updated because of its remarkable formation in the numerical study (see Figure 68). Thanks to the above proposed reactions of $FeC_{10}H_{10}$ and FeC_5H_5, the inhibiting effect of ferrocene is supposed to be due to the radical-consuming reactions producing low reactive species. Novel reactions between the radicals (OH, CH_3, C_2H_5, and $C_6H_5CH_2$) and $Fe(OH)_2$ forming the corresponding alcohols were thus included in the mechanism (R110 – R113). The added reactions were numerically proposed as the main source of the ferrocene inhibiting effect at T_c > 885 K. Table 30 summarizes the reactions involving $FeC_{10}H_{10}$, FeC_5H_5 and $Fe(OH)_2$. The activation energy and pre-

exponential factor estimations were based on the work of Rumminger et al. [188] in which the reference reactions of iron species were mostly barrierless. The proposed sub-mechanism captures the fuel additive effect suggesting that such inhibiting behavior could be a viable pathway to explain the ferrocene behavior in the tested operating conditions.

Table 30: Kinetic constant of reactions of new proposed reactions involving $FeC_{10}H_{10}$, FeC_5H_5 and $Fe(OH)_2$.

Reaction		A	n	E_a	Ref.
	Reactions of $FeC_{10}H_{10}$ and FeC_5H_5				
R88	$FeC_{10}H_{10} + HO_2 \rightarrow FeC_5H_5 + CYPDONE + H_2O$	1.0×10^{13}	0	100	
R104	$FeC_{10}H_{10} + CH_3O_2 \rightarrow FeC_5H_5 + CYPDONE + CH_3OH$	1.0×10^{13}	0	100	
R105	$FeC_{10}H_{10} + C_2H_5O_2 \rightarrow FeC_5H_5 + CYPDONE + C_2H_5OH$	1.0×10^{13}	0	100	
R106	$FeC_{10}H_{10} + C_6H_5CH_2O_2 \rightarrow FeC_5H_5 + CYPDONE + C_6H_5CH_2OH$	1.0×10^{13}	0	100	
R92	$FeC_5H_5 + HO_2 \rightarrow Fe + CYPDONE + H_2O$	1.0×10^{13}	0	100	
R107	$FeC_5H_5 + CH_3O_2 \rightarrow Fe + CYPDONE + CH_3OH$	1.0×10^{13}	0	100	This
R108	$FeC_5H_5 + C_2H_5O_2 \rightarrow Fe + CYPDONE + C_2H_5OH$	1.0×10^{13}	0	100	work
R109	$FeC_5H_5 + C_6H_5CH_2O_2 \rightarrow Fe + CYPDONE + C_6H_5CH_2OH$	1.0×10^{13}	0	100	
	Reactions of $Fe(OH)_2$				
R110	$Fe(OH)_2 + OH \rightarrow FeOH + H_2O$	2.0×10^{13}	0	100	
R111	$Fe(OH)_2 + CH_3 \rightarrow FeOH + CH_3OH$	2.0×10^{13}	0	100	
R112	$Fe(OH)_2 + C_2H_5 \rightarrow FeOH + C_2H_5OH$	2.0×10^{13}	0	100	
R113	$Fe(OH)_2 + C_6H_5CH_2 \rightarrow FeOH + C_6H_5CH_2OH$	2.0×10^{13}	0	100	

Rate expression: $k = AT^n \exp\left(\frac{-E_a}{RT}\right)$ in cm^3, mol, cal, s units.

Figure 69 illustrates the simulations obtained with the refined mechanism compared to the experimental data. In the stoichiometric condition, the inhibiting effect of ferrocene on the main IDT of the surrogate fuel over the whole temperature range at different doping levels is correctly captured. The model predicts an inhibiting effect on the 1st-stage IDT while this cannot be confirmed clearly experimentally. Overall, the proposed kinetic mechanism simulates reasonably well the experimental measurements at the two equivalence ratios investigated in this study.

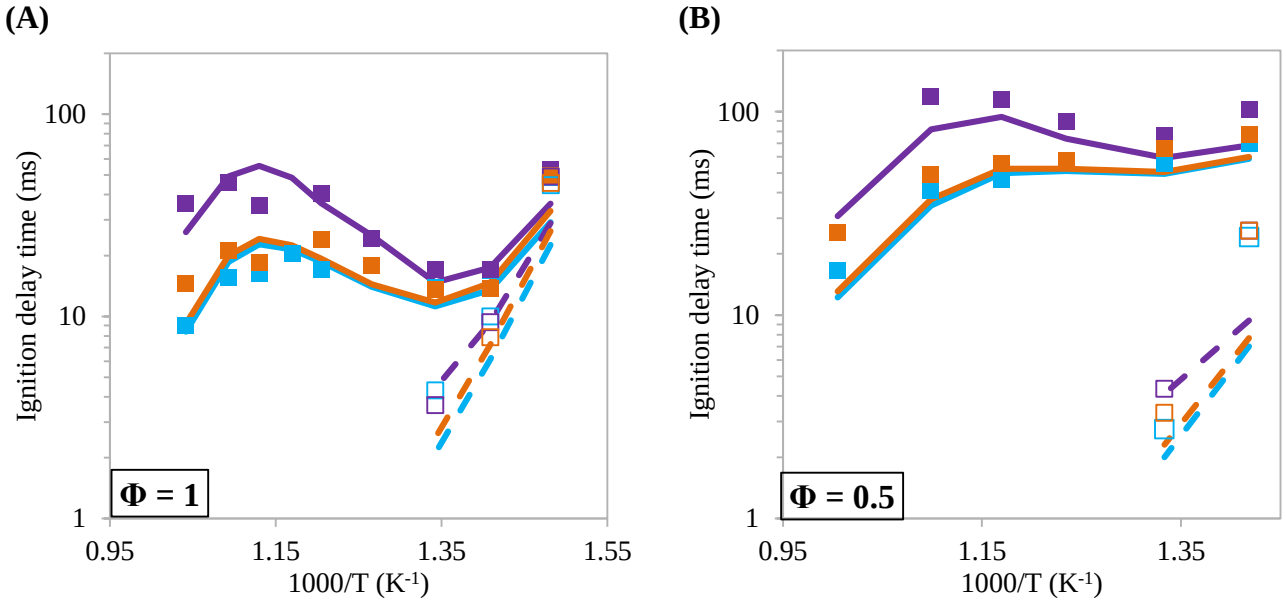

Figure 69: IDT of the neat surrogate fuel (blue) and of the surrogate fuel doped with ferrocene at 0.01% mol. (orange) and 0.1% mol. (purple) at 10 bar. Experiments: filled symbols (main IDT) and empty symbols (1st-stage IDT). Simulations: solid lines (main IDT) and dashed lines (1st-stage IDT). (A) Φ = 1, (B) Φ = 0.5. Simulations by the kinetic model employed the new sub-mechanism of ferrocene developed in this work.

5.4.1.b Chemical effect of ferrocene

While the use of additives to modify hydrocarbon reactivity has been investigated thoroughly in the past, discussions on the additive chemical effects are not frequent. Our kinetic model has the advantage to be developed for both iron involving species and nitrogen containing ones. More specifically, both the chemistries of an octane booster (ferrocene) and of a cetane booster (EHN) are included and validated. A comparison of the two additives is carried out to highlight the differences in chemical activities, which could be of interest for further additive development.

The first difference between the two additives is related to their reactivity during RCM tests. Simulations were performed at P_c = 10 bar, T_c = 915 K, Φ = 1 and the doping levels of EHN and ferrocene were set at 0.1% mol. in the surrogate fuel. It was observed that EHN decomposes before the end of compression while ferrocene remained nearly stable as presented in Figure 70. The early decay of EHN initiates the combustion of toluene and *n*-heptane and then increases P_c. Figure 71 presents the pressure histories near the end of compression of RCM tests with the neat and doped fuels. In the presence of EHN, P_c increases remarkably. The pressure histories of the neat and doped fuels are reasonably simulated. This also highlighted the correct behavior of the kinetic model.

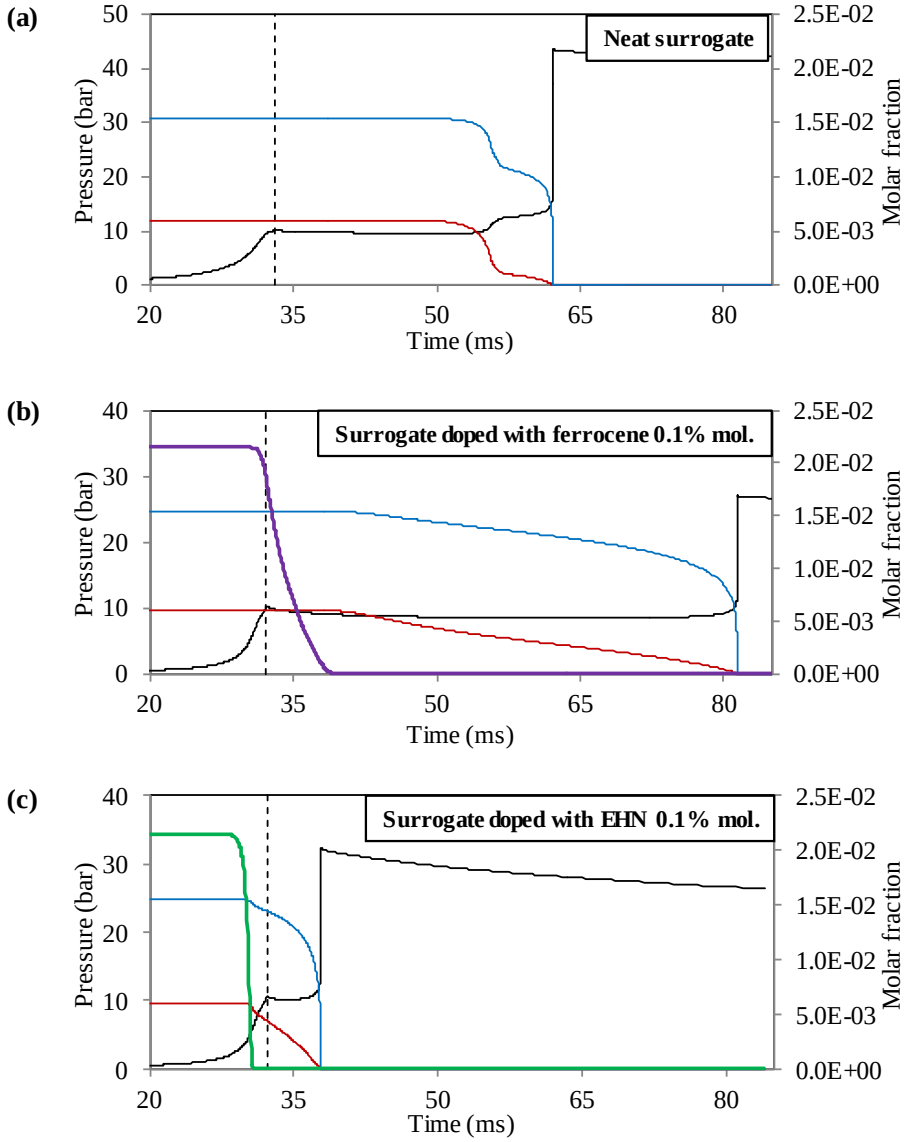

Figure 70: Simulated species profiles of toluene (blue solid line), *n*-heptane (red solid line), EHN x 1000 (green solid line), ferrocene x 1000 (violet line) and simulated pressure history (black solid line) of RCM experiments at P_c ≈ 10 bar, Φ = 1, T_c = 915 K. (a): neat surrogate. (b): surrogate fuel doped with ferrocene 0.1% mol. and (c): surrogate fuel doped with EHN 0.1% mol. End of compression: dashed black line.

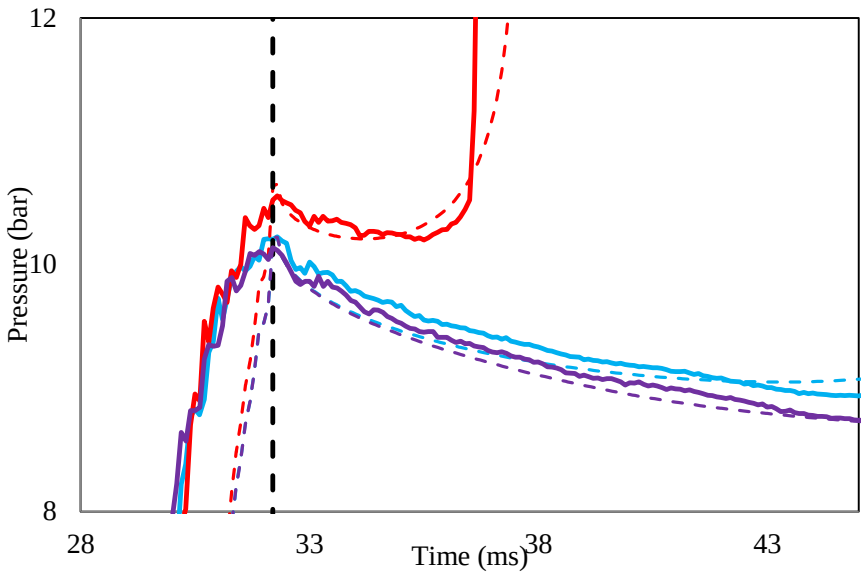

Figure 71: Measured (solid line) and simulated (dashed line) of pressure histories near the top dead center during RCM experiments at Pc ≈ 10 bar, Φ = 1, T_c = 915 K of the neat surrogate fuel (blue), the surrogate fuel doped with EHN 0.1% mol (red) and the surrogate fuel doped with ferrocene 0.1% mol.(purple).

The second difference between the two additives is related to their interactions with the fuel. Figure 72 illustrates how toluene reacts under the investigated conditions (10 bar, Φ = 0.5 – 1, 675 K – 1000 K). Toluene forms primarily benzyl radical ($C_6H_5CH_2$) by H-atom abstraction. This radical undergoes an O_2 addition to form benzyl peroxy radical ($C_6H_5CH_2OO$). This compound is much less reactive than heptyl peroxy radicals due to a limited intramolecular isomerization. As discussed previously, EHN decomposes very fast and forms NO_2, which can react with benzyl radical ($C_6H_5CH_2$) to produce NO and $C_6H_5CH_2O$ (reaction R84). This last radical is more reactive than $C_6H_5CH_2OO$ as it quickly decomposes into H-atom and benzaldehyde (C_6H_5CHO). This helps to enhance the reactivity of toluene in the presence of EHN. In the presence of ferrocene, this additive decelerates the toluene reactivity by a set of reactions (R106, R109, and R113): ferrocene and its derived compounds (FeC_5H_5, $Fe(OH)_2$) react with $C_6H_5CH_2$ and $C_6H_5CH_2OO$ radicals to produce the low reactivity benzylalcohol ($C_6H_5CH_2OH$).

The last difference between the two additives is their effect on the NTC behavior. It was found that EHN could mitigate the NTC behavior of the surrogate fuel. Conversely, the experimental results indicate that ferrocene enhances this phenomenon. The NTC behavior of the surrogate fuel comes from the chemistry of *n*-heptane. Figure 73 presents the reaction pathway of *n*-heptane at P_c = 10 bar, T_c = 830 K, Φ = 1 for three fuels: the neat surrogate fuel, the surrogate fuels doped with EHN 0.1 % mol. and with ferrocene 0.1% mol. The main reason for the NTC phenomenon involves the reactions of heptyl peroxy radicals ($C_7H_{15}OO$) and their isomer hydroperoxy heptyl radicals ($C_7H_{14}OOH$). At intermediate temperature (T_c = 830 K), the formation of conjugated alkenes and cyclic ethers from $C_7H_{15}OO$ and $C_7H_{14}OOH$ are favored compared to the second oxygen addition leading to the formation of ketohydroperoxides, which are branching agents. These reactions slow down the reactivity of *n*-heptane and the surrogate fuel. The formation of NO_2 from EHN also leads to the benzyl radical oxidation ($C_6H_5CH_2$) and produces NO and $C_6H_5CH_2O$. NO then reacts with $C_7H_{15}OO$ through reaction R83, which enhances the reactivity and restrains the NTC zone. Conversely, ferrocene enables the reactions R88 and R92 with HO_2. The consumption of HO_2 radicals released from $C_7H_{15}OO$ decomposition accelerates this latter reaction forming alkenes. Consequently, the NTC region is expanded.

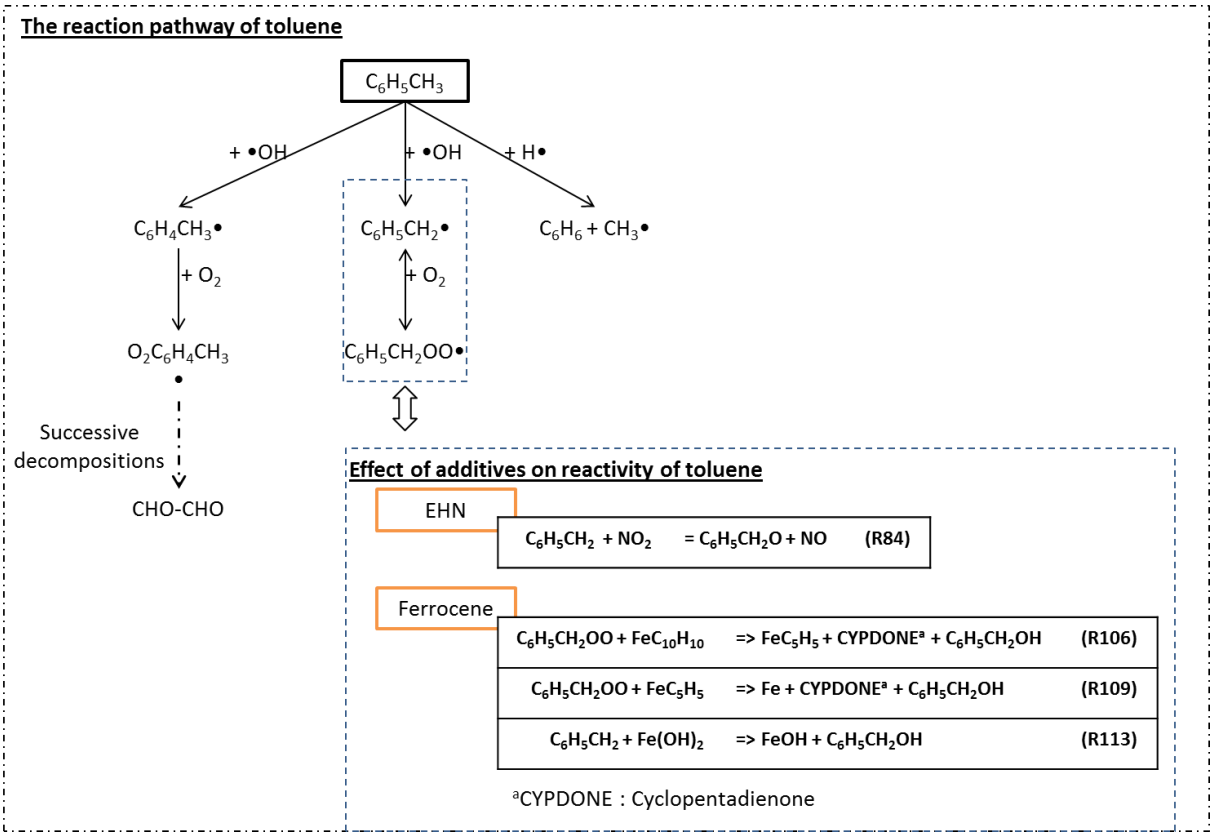

Figure 72: Reactions pathway of toluene at 10 bar, Φ = 0.5-1, 675 K – 1000 K and the reactions representing effects of EHN and ferrocene on toluene reactivity.

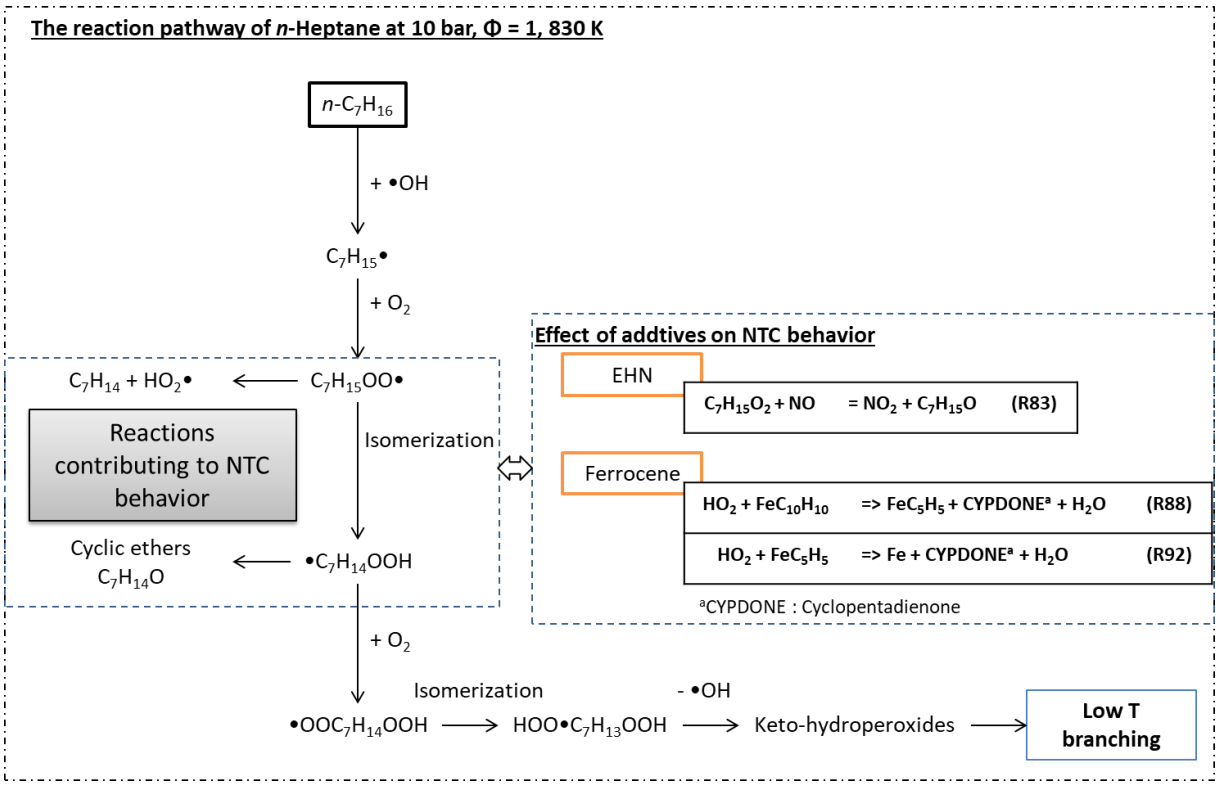

Figure 73: Reactions pathway of *n*-heptane at 10 bar, Φ = 1, 830 K and the chemical effects of EHN and ferrocene on NTC behavior.

To summarize, three main differences on two opposite additives regarding their effect on the surrogate fuel reactivity are described. They involve their stability, their impact on toluene reactivity and on the NTC behavior related to *n*-heptane.

To determine the most sensible reactions in ferrocene sub-mechanism, sensitivity analyses on the formation of OH radical were conducted at 10 bar, Φ = 1, at three T_c (675K, 830K, and 915K) thanks to CHEMKIN-PRO [130]. The result of the sensitivity analyses for a conversion of 75% of ferrocene is presented in Figure 74. As expected, there is no sensitive reaction belonging to ferrocene sub-mechanism at T_c = 675 K as this additive does not present an effect at this temperature. As T_c increases, some reactions of ferrocene with peroxides are found to be sensitive. The reactions of ferrocene with benzyl peroxy radical ($C_6H_5CH_2OO$) and with hydrogen peroxy radical (HO_2) present a strong inhibiting effect at 830 K and 915 K, respectively. There is no other reaction of iron chemistry being sensitive to the formation of OH radical. These results highlight again the importance of reactions of ferrocene with peroxy radicals on the inhibiting effect of ferrocene.

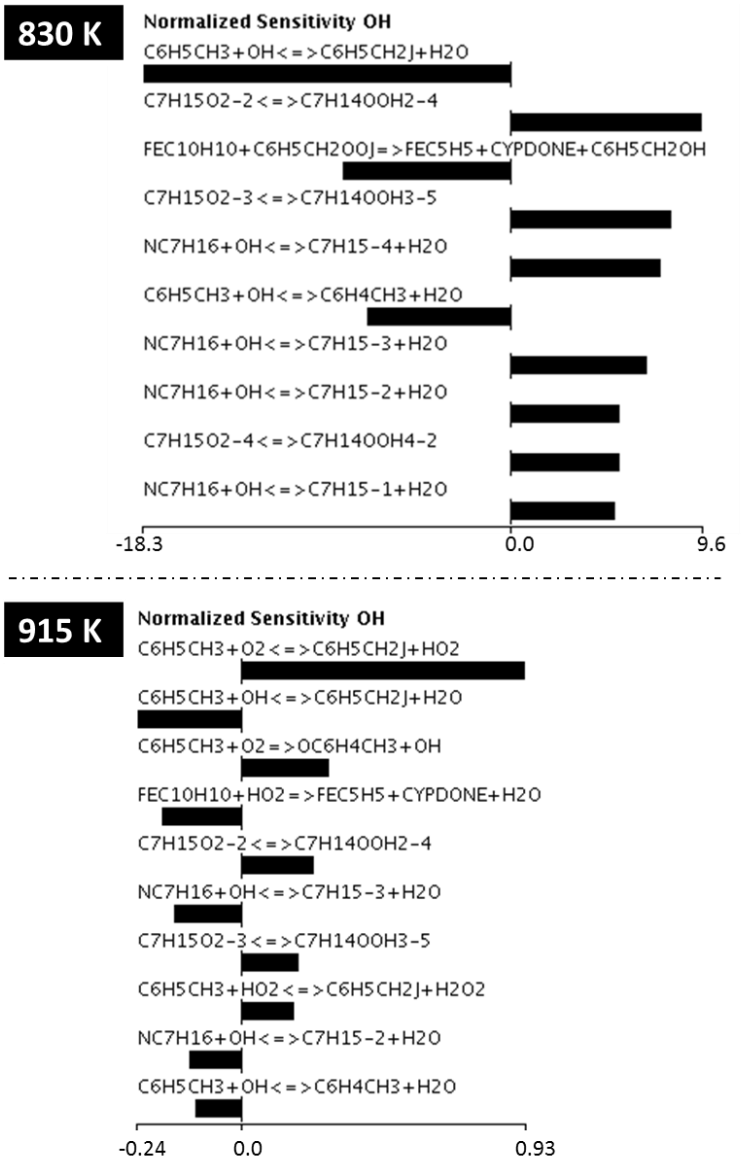

Figure 74: Results of sensitivity analyses on the formation of OH radical at 75 mol/% Ferrocene decomposition at two different T_c: 830 K, and 915 K for ferrocene doping level of 0.1% mol. at P_c = 10 bar and Φ = 1.

5.4.2 Ignition delay time of the surrogate fuel doped with ferrocene at T > 1000 K

5.4.2.a Shock tube experimental results

The effect of ferrocene on the IDT of the surrogate fuel at high temperature range was investigated in the ST. The experiments were performed at 10 atm, Φ = 1, from 1350 to 1600 K. The doping level of ferrocene was set at 0.1% weight basis in the liquid-phase surrogate fuel. Table 31 presents the saturation vapor pressures of ferrocene, toluene, and *n*-heptane at 25°C. As ferrocene is much less volatile than two components of the surrogate fuel, the real doping level of this additive in the surrogate fuel in the gas phase in the ST is much less than 0.1% weight basis. Similar to the case of EHN, a calculation of molar composition of the ferrocene-doped fuel in the gas phase by UNIFAC model was not performed since the data were found in the literature. Table 32 summarizes the experimental conditions investigated in the ST. The molar composition of the gas-phase doped fuel was estimated by assuming the doping level of ferrocene was 0.1% weight basis.

Table 31: Saturation vapor pressure of compounds at 25 °C

Compound	Toluene	*n*-Heptane	Ferrocene
Saturation vapor pressure (Torr)	28.4	38.4	7.4×10^{-3}

Table 32: Experimental condition of tests on the ST performed with the surrogate fuel doped with ferrocene.

P (atm)	**T (K)**	**Φ**	**Doping level of ferrocene (% mass)**	**Composition of fuel gas mixture**				
				Toluene (% mol.)	*n*-Heptane (% mol.)	Ferrocene (ppm)	Oxygen (% mol.)	Argon (% mol.)
10	1350 - 1600	1	0.1	0.28	0.22	3	4.78	94.71

Figure 75 illustrates the measured and simulated IDT of the neat and ferrocene-doped surrogate fuel. In these conditions, ferrocene does not show any effects. The simulations performed with the kinetic model did not either present a remarkable effect of ferrocene.

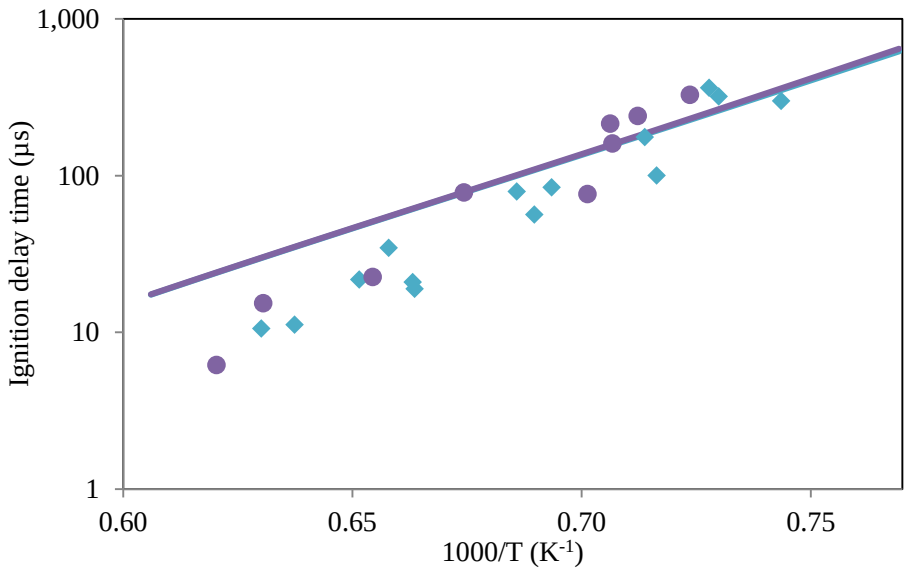

Figure 75 : Ignition delay times of the neat surrogate fuel (blue) and the surrogate fuel doped with ferrorence (purple) at 10 atm, Φ = 1. Gas mixture composition is shown in Table 32. Symbols: experiments. Lines: simulations.

5.4.2.b *Chemical effect of ferrocene*

At high temperatures (T > 1300 K), simulations show that ferrocene is principally consumed by the reaction with HO_2 as presented below:

$$FeC_{10}H_{10} + HO_2 \rightarrow FeC_5H_5 + CYPDONE + H_2O$$

$$FeC_5H_5 + HO_2 \rightarrow Fe + CYPDONE + H_2O$$

Different from conditions of low and intermediate temperatures (T < 1300 K) where chain-branching step depends strongly on HO_2 and primary radicals derived from parent fuels [203], the main reactions governing the fuel reactivity at high temperatures (T > 1300 K) [203] are :

$$H + O_2 = O + OH$$

$$O + H_2 = H + OH$$

$$OH + H_2 = H_2O + H$$

Any effect on the formation of HO_2 radicals do not affect the fuel reactivity at high temperatures (T > 1300 K). Consequently, ferrocene does not have a remarkable effect on the gas-phase reactivity of the surrogate fuel at high temperatures (T > 1300 K) as experimentally observed by ST tests.

5.4.3 Effect of ferrocene on the laminar burning velocity of the surrogate fuel

Flat flame burner experiments were performed at atmospheric pressure and initial temperature at 398 K to evaluate the effect of ferrocene on the laminar burning velocity of the surrogate fuel. Figure 76 illustrates the flame speed of the neat and EHN-doped surrogate fuel according to various equivalence ratios.

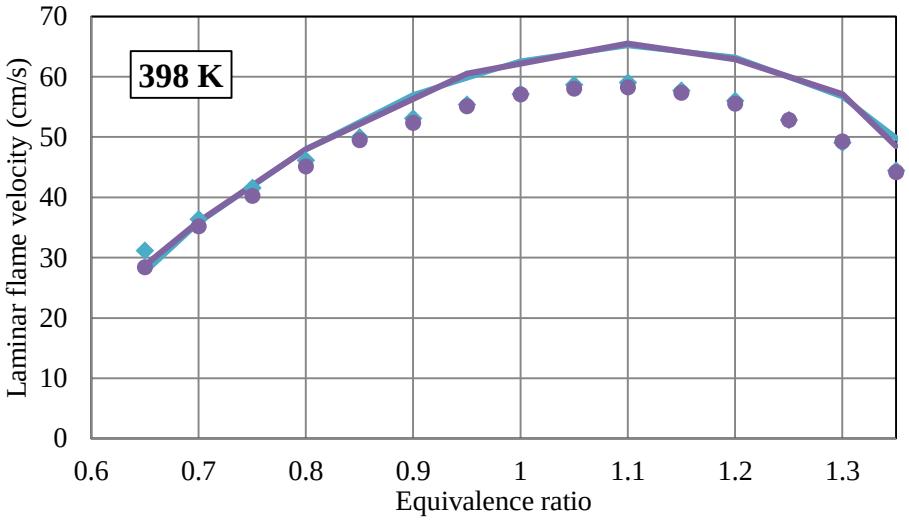

Figure 76: Laminar burning velocity of the neat surrogate fuel (blue) and the surrogate fuel doped with ferrocene 0.1% mass (purple) at atmospheric pressure and initial temperature of 398 K. Symbols: experiments. Lines: simulations.

It is experimentally observed that ferrocene does not affect the flame speed of the surrogate fuel in these operating conditions. The simulations results obtained by the kinetic model of this thesis agrees well with the experimental results.

5.5 Effect of 2,4-xylenol

In this section, the effects of 2,4-xylenol on the IDT and the laminar burning velocity of the surrogate fuel are presented.

5.5.1 Ignition delay time of the surrogate fuel doped with 2,4-xylenol at T < 1000 K

The effect of 2,4-xylenol on the IDT of the surrogate fuel in the RCM was examined at 10 bar, from 675 to 1000 K, at two equivalence ratios 0.5 and 1. Table 33 summarizes the operating conditions. The amount of this additive was set at 0.1 and 1% mol..

Table 33: Experimental condition of tests on the RCM performed with the surrogate fuel doped with EHN.

P (bar)	T (K)	Φ	Doping level of 2,4-xylenol (% mol.)	Composition of fuel gas mixture				
				Toluene (% mol.)	*n*-Heptane (% mol.)	2,4-Xylenol (ppm)	Oxygen (% mol.)	Nitrogen (% mol.)
10	675 - 1000	0.5	0.1	0.78	0.31	10.9	20.77	78.14
		0.5	1.0	0.77	0.30	108.6	20.77	78.14
		1.0	0.1	1.54	0.60	21.5	20.55	77.30
		1.0	1.0	1.53	0.59	214.9	20.55	77.30

Figure 77 presents the IDT of the doped and undoped surrogate fuel. Experimentally, it has been found that 2,4-xylenol does not show any remarkable effect on the reactivity of the surrogate fuel at both doping levels over the whole temperature range. The negligible effect of 2,4-xylenol in the considered condition may link to its low concentration. McCormick et al. [47] indicated that this additive increased the octane number of the target fuel from 85.8 up to 89 at a higher doping level of 2% vol. From another point of view, the use of 2,4-xylenol as an antioxidant is secured as this additive does not show side effects at a doping level below 1% mol. for a fuel having a tailored gas-phase reactivity.

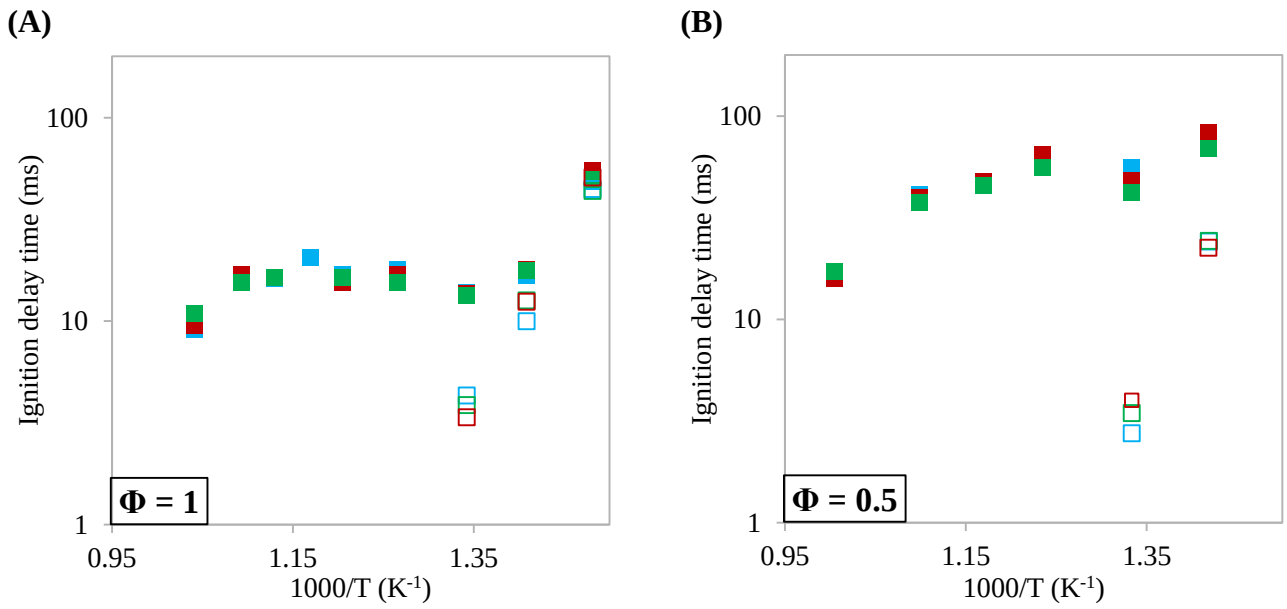

Figure 77: IDT of the neat surrogate fuel (blue) and the surrogate fuel doped with 2,4-xylenol at 0.1% mol. (green) and 1% mol. (red) at 10 bar. Experiments: filled symbols (main IDT) and empty symbols (1st-stage IDT). (A) Φ = 1, (B) Φ = 0.5.

Oxidation of 2,4-xylenol has been investigated by Zhang et al. [204]. A kinetic model of 2,4-xylenol was generated by using an automatic reaction mechanism generator (RMG) [205]. A RON increase of 1.7 was experimentally observed by incorporating 2% mol. of 2,4-xylenol into the neat *n*-butane. The model of Zhang et al. well predicted the octane-boosting effect of this additive. Regarding the

uncertainty in RON measurement was reported as 0.5, the inhibiting effect of 2,4-xylenol on the gas-phase reactivity was considered as low. The results of this thesis agree with the observation of Zhang et al..

5.5.2 Ignition delay time of the surrogate fuel doped with 2,4-xylenol at T > 1000 K

Similar to the case of EHN and ferrocene, the experiments on the ST performed with the surrogate fuel doped with 2,4-xylenol were conducted at 10 atm, Φ = 1, from 1350 to 1600 K. The doping level of 2,4-xylenol was set at 1% weight basis in the liquid-phase surrogate fuel. As the saturation vapor pressure at 25°C of 2,4-xylenol (0.1 Torr) is much less than ones of *n*-heptane (38.4 Torr) and toluene (28.4 Torr), the composition of the gas-phase 2,4-xylenol-doped fuel differs from that of this fuel prepared in the liquid phase. The molar composition of the 2,4-xylenol-doped fuel introduced into the shock tube was additionally estimated thanks to the UNIFAC model [199] in PRO II software [200]. The results of the calculations are presented in Table 34. The simulations of the IDT of the neat and 2,4-xylenol-doped surrogate fuel in Figure 78 were conducted with the calculated gas-phase. Table 35 summarizes the experimental condition investigated in the ST.

Table 34: Composition of the surrogate fuel doped with 2,4-xylenol.

Fuel		Surrogate fuel experimentally prepared in the liquid phase	Surrogate fuel numerically calculated in the gas phase at 25°C
Composition (% mol.)	Toluene	71.3	56.5
	n-Heptane	27.9	43.5
	2,4-Xylenol	0.8	9.4×10^{-3}

Table 35: Experimental condition of tests on the ST performed with the surrogate fuel doped with EHN.

P (atm)	**T (K)**	**Φ**	**Doping level of 2,4-xylenol (% mass)**	**Composition of fuel gas mixture**				
				Toluene (% mol.)	*n*-Heptane (% mol.)	2,4-xylenol (ppm)	Oxygen (% mol.)	Argon (% mol.)
10	1350 - 1600	1	1	0.28	0.22	0.5	4.78	94.71

Figure 78 illustrates the measured IDT of the neat and doped surrogate fuel. Similar to the observation at T < 1000 K, 2,4-xylenol does not impact the reactivity of the surrogate fuel. This could be related also to the low doping level of this additive.

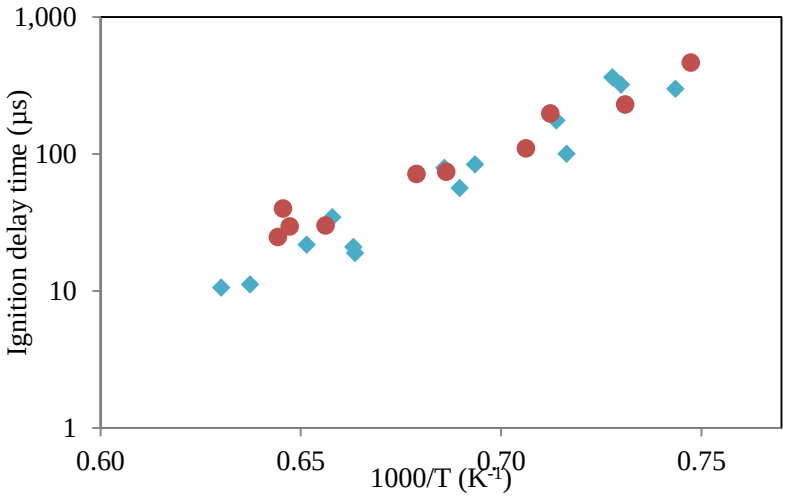

Figure 78 : Ignition delay times of the neat surrogate fuel (blue) and the surrogate fuel doped with 2,4-xylenol (red) at 10 atm, Φ = 1. The gas mixture composition is shown in Table 35.

5.5.3 Effect of 2,4-xylenol on the laminar burning velocity of the surrogate fuel

Figure 79 illustrates the measurements of the laminar burning velocity of the neat and 2,4-xylenol-doped surrogate fuel at atmospheric pressure, T_i = 398 K. The additive was set at 1 % mass. It is observed that 2,4-xylenol does not affect the flame speed of the surrogate fuel in these conditions.

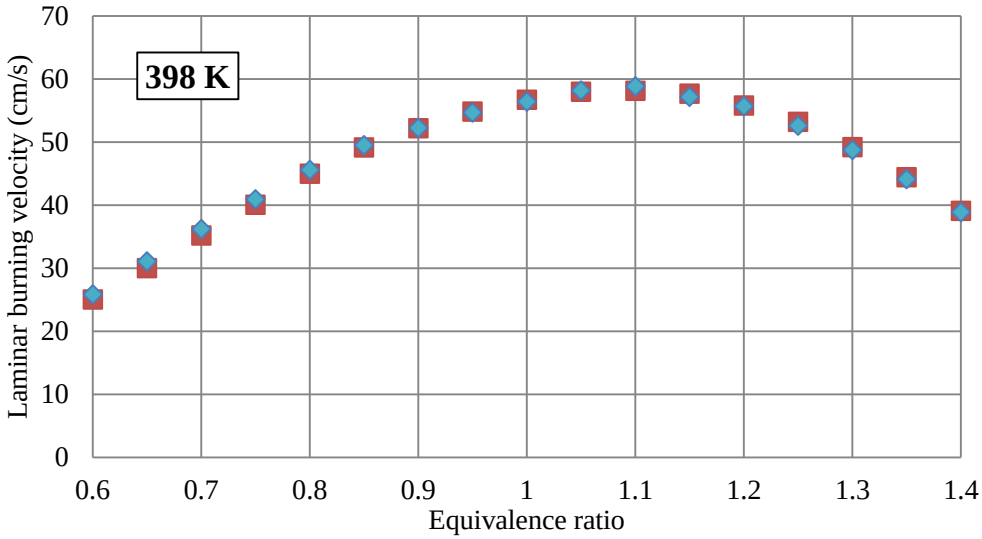

Figure 79: Measured laminar burning velocity of the neat surrogate fuel (blue) and the surrogate fuel doped with 2,4-xylenol 1% mass (red) at atmospheric pressure and initial temperature of 398 K.

5.6 Conclusions about the effect of additives

Experiments and modeling works were performed to investigate the chemical effect of three additives: EHN, ferrocene, and 2,4-xylenol. IDT of fuels were measured over a wide range of temperature from 675 to 1600 K thanks to a RCM and a ST. Both stoichiometric (Φ = 1) and lean (Φ = 0.5) mixtures were examined. Moreover, laminar flame velocities of fuels were investigated in a heat flux flat burner. The target surrogate fuel contains 65% toluene and 35% *n*-heptane by volume. The doping level of additives was limited at 1% (0.1% for ferrocene) weight basis for experiments in ST and flat flame burner and 1% molar basis for RCM experiments.

Figure 80 summarizes the effect of the three additives on the reactivity of the surrogate fuel as a function of temperature. 2,4-xylenol does not show any remarkable effect on the reactivity of the surrogate fuel in gas phase. EHN and ferrocene show reactivity-promoting effect and reactivity-inhibiting effect, respectively. However, these effects are observed exclusively at T lower than 1000 K. Moreover, this is consistent with the fact that the laminar burning velocity of the surrogate fuel is not affected by any additive. Chemical effect of each additive is further summarized in this chapter.

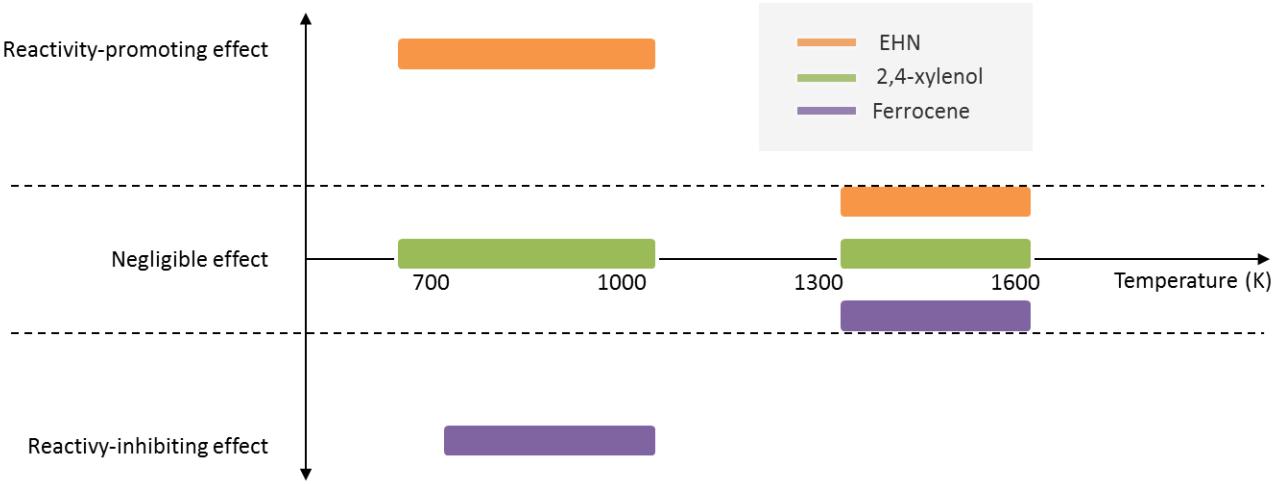

Figure 80: Simplified diagram representing the effect of EHN, 2,4-xylenol, and ferrocene on the reactivity of the surrogate fuel according to temperature.

5.6.1 Effect of EHN

In the experimental conditions of the RCM (10 bar, Φ = 0.5 and 1), it is observed that EHN has a promoting effect on the surrogate reactivity at all examined T_c (675 – 1000 K). This effect increases with EHN doping levels. The NTC behavior of the surrogate fuel is mitigated by the addition of EHN and at doping level of 1% mol., EHN inhibits the NTC phenomenon. The EHN promoting effect is found to be the lowest near 740 K and then increases with T_c.

A heat release during the compression process is observed in RCM tests of the doped fuels because of the rapid decomposition of EHN at T_c > 750 K. This implies that the measured EHN promoting effect in a RCM in this T_c range depends partly on the machine compression duration. Additionally, the chemical activity of gas fuel mixture during the compression process has to be carefully considered to get reliable simulation results.

Kinetic modeling shows a good coherence with experiments. The model reproduces properly the EHN promoting effect over the whole investigated temperature range and doping levels. EHN decomposition during the compression process is reasonably well simulated, which is validated by the pressure history modelling. By experiments in the RCM, it was found that EHN was less effective at low

T_c (< 800 K) in lean conditions than in stoichiometric condition because of its slower decomposition during the compression process.

The validation of the kinetic model against literature data was conducted. The results indicate that this kinetic model is able to simulate the EHN promoting effect in different fuels at various conditions.

Goldsborough et al. [40] indicated that EHN effect was linked to the formation of OH radicals by the two reactions: NO + HO_2 = NO_2 + OH and NO_2 + H = NO + OH. These authors stated that the reactions of hydrocarbon radicals and peroxy radicals with NO_x such as R + NO_2 = RO + NO and RO_2 + NO = RO +NO_2 could compete with the above reactions and then reduce the effect of EHN. The observation of Goldsborough et al. is somewhat different from the result of this study. Numerical analyses of this study indicate that EHN effect is due to the reactions of C_7H_{15}-3 radical and a NO_2-NO loop which contains reactions R + NO_2 = RO + NO and RO_2 + NO = RO + NO_2. OH radicals can be generated from the reactions of C_7H_{15}-3 radical and from the reaction NO + HO_2 = NO_2 + OH which is included in the NO_2-NO loop. In addition, in the NO_2-NO loop, NO_2 can react with benzyl radical ($C_6H_5CH_2$) to form $C_6H_5CH_2O$ radical and NO. This reaction enhances the toluene reactivity, i.e. the surrogate fuel reactivity. The reactions between NO and *n*-heptyl peroxy radicals are found to be the main cause of the EHN effect on the NTC region of the surrogate fuel oxidation. It is also found that the formation of nitroethane ($C_2H_5NO_2$), which trap the active NO_2 into a stable species, is the main reason, why EHN promoting effect is minimum around 740 K.

At higher temperatures (T > 1300 K) as the condition of ST and the flat flame burner, EHN does not show any experimental effect on the reactivity of the surrogate fuel.

5.6.2 Effect of ferrocene

In the condition of RCM experiments (10 bar, 675 -1000K, Φ = 0.5 and 1), it was found that ferrocene did not show a remarkable effect on the 1st-stage ignition of the surrogate fuel. However, ferrocene showed a strong inhibiting effect on the main ignition of the surrogate fuel at both equivalence ratios. This effect increases with T_c. Ferrocene enhances surrogate fuel NTC. The inhibiting effect of ferrocene increases with its concentration.

A kinetic model was developed based on a literature data assembly. This model failed to reproduce the effect of ferrocene emphasizing the need for an improved mechanism. Additional reactions involving the formation of low reactivity species from the reactions of iron species with radicals such as HO_2, $C_6H_5CH_2$, $C_6H_5CH_2OO$ were proposed. The developed model successfully simulated the inhibiting effect of ferrocene at both equivalence ratios within the whole temperature range.

Thanks to the validated kinetic model of ferrocene, the chemical effect of this additive on the fuel combustion is elucidated. Compared to EHN, which is a conventional reactivity enhancer, three differences are identified. The first difference is about the stability of the species as ferrocene is much more stable than EHN. The second is related to the additive chemical effect on the surrogate fuel. While EHN promotes the toluene oxidation with the interaction between NO_2 and benzyl radicals, ferrocene decreases the reactivity of toluene with the formation of alcohol. The reactions of benzyl and benzyl peroxy radicals with iron species enable this pathway. The last difference is the influence of these two additives on the NTC. EHN mitigates the NTC zone through the reaction of heptyl peroxy radicals with NO while ferrocene promotes the NTC phenomenon by consuming the HO_2 radical released from heptyl peroxy radicals.

As EHN, ferrocene does not affect the reactivity of the surrogate fuel at higher temperatures (T > 1300 K). This was highlighted with the ST and flat flame burner experiments. The modelling study suggested that ferrocene interacts exclusively with HO_2 radicals in these conditions. However, at high temperature, the main chain-branching reactions governing the fuel reactivity involve mainly H and O radicals.

5.6.3 Effect of 2,4-xylenol

2,4-xylenol does not show any effect on the gas-phase reactivity of the surrogate fuel considering the experiments performed in this study. The negligible effect of this additive may be due its low doping level considered. The obtained experimental results confirm that the utilization of 2,4-xylenol as an antioxidant at doping level below 1% mol. does not show any additional effects on the fuel gas-phase reactivity.

To our knowledge, no kinetic model has been developed for characterizing the antioxidant effect of 2,4-xylenol in the literature. Further experimental and numerical investigations of 2,4-xylenol impact on the liquid-phase reactivity are of interest.

5.7 Prediction of the effect of EHN and ferrocene in various conditions

Thanks to the mechanisms developed in this thesis, the effects of these additives are numerically explored in various fuels at different engine-relevant conditions.

As an effort to reduce greenhouse-gas emissions and the dependence on petroleum, biofuels are employed for transportation application. Ethanol is actually a widely used biofuel. The feature limiting the use of ethanol in LTC engines is its long ignition delay time. This issue can be fixed by the incorporation of EHN. The impact of EHN on the reactivity of ethanol is illustrated in this section. Furthermore, the effect of EHN and ferrocene on the RON value of different mixtures of toluene and *n*-heptane is investigated.

5.7.1 Effect of EHN on the reactivity of ethanol

Ethanol is a sustainable fuel for IC engines. It has been studied and successfully employed in engines for decades [206]. The advantages of ethanol on reducing combustion emissions, especially particulate matter, have been experimentally proved [207, 208]. Pure ethanol is a very low reactive fuel. Ethanol has a RON value of 109. Thanks to its properties, ethanol is usually blended with gasoline fuels to be used in SI engines [209, 210]. However, the application of ethanol in other prospective technologies, including LTC or with compression ignition is limited by its long ignition delay time. For example, a temperature of 1100 K is necessary to obtain a short ignition delay in adequation with operation in CI engines [211]. To solve this issue, an ignition improver, i.e. a cetane booster, can be used to enhance the ignition of ethanol. This method helps to avoid major engine modifications. For example, the fuel named ED95 contains 92% of hydrated ethanol (grade 95%), 5% cetane booster (polyethylene glycol (PEG) derivative, Beraid, Akzo Nobel), 2,8% denaturants (2.3% MTBE and 0.5% isobutanol) by weight [212]. This fuel is designed and commercialized by Scania to run a CI engine [213] for more than 30 years.

In this thesis, the effect of EHN on ethanol ignition is numerically investigated thanks to the validated kinetic model. The sub-mechanism of ethanol has been included in the reference model of LLNL [42], i.e. in the kinetic model of this thesis. All simulations were conducted with the closed homogeneous reactor model of CHEMKIN PRO [130].

The relative effect (R_{eff}) of EHN on reducing IDT of ethanol is defined in Eq.5. Higher R_{eff}, stronger is the EHN promoting effect.

Figure 81 illustrates the variation of EHN promoting effect on the reactivity of ethanol as a function of the temperature according to various doping levels. Simulations were conducted at 10 bar for stoichiometric mixtures. The amount of EHN varies from 0.1 to 1 % mol. It is found that the EHN effect

is most remarkable in the lowest temperature range (T < 1000 K) and decreases as temperature increases. The promoting effect of EHN is nearly stable at low temperature (T < 1000 K) then decreases sharply from 1000 to 1400 K and becomes almost stable at T > 1450 K. The promoting effect of EHN increases non linearly with doping levels.

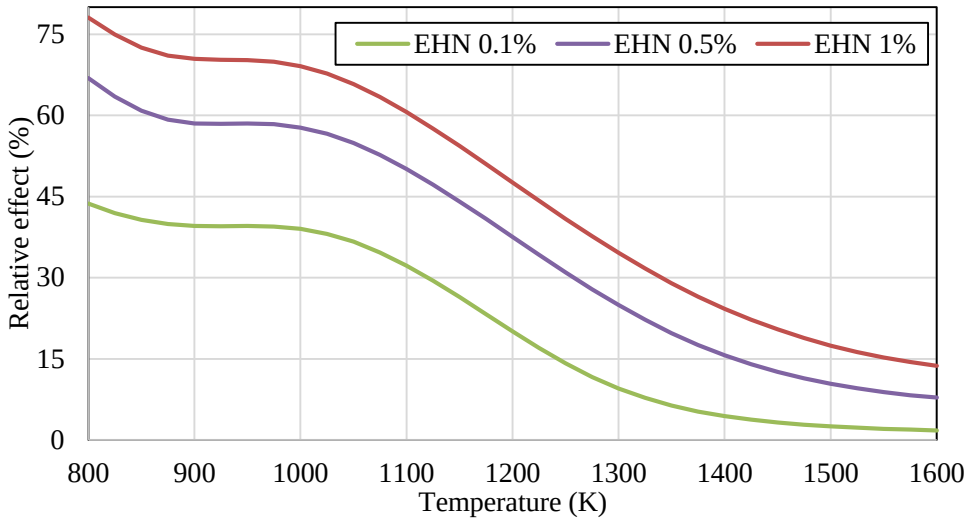

Figure 81: Simulated relative promoting effect of EHN on the combustion of ethanol at 10 bar and Φ = 1 for various doping levels of EHN.

The effects of equivalence ratio and pressure on the promoting effect of EHN were also numerically examined. The obtained results are respectively illustrated in Figure 82 and Figure 83. The pressure change does not affect the EHN promoting effect. The influence of equivalence ratios on the effect of EHN is not as sensitive as the impact of doping level on the effect of EHN.

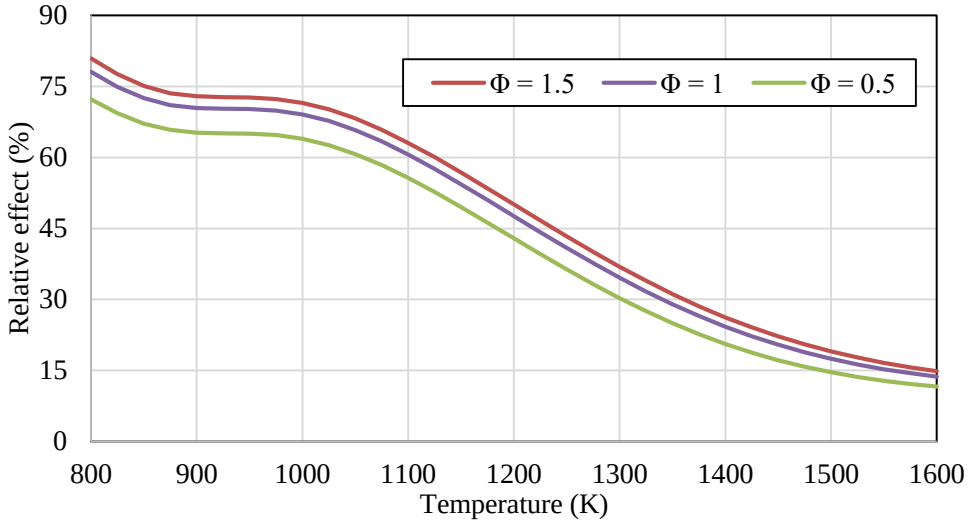

Figure 82: Simulated relative promoting effect of EHN (1% mol.) on the combustion of ethanol at 10 bar and at various equivalence ratios.

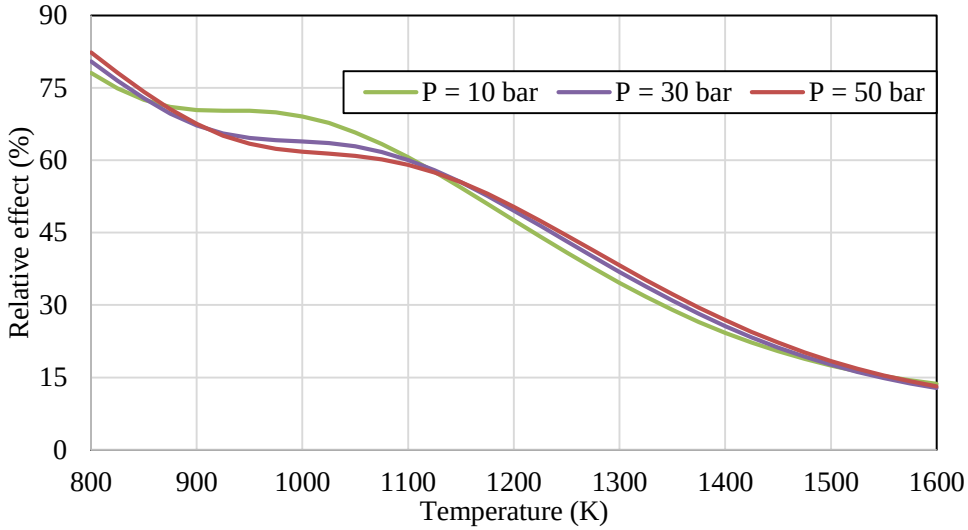

Figure 83: Simulated relative promoting effect of EHN (1% mol.) on the combustion of ethanol at Φ = 1 and at various pressures

To summarize, EHN can reduce IDT of ethanol. The promoting effect of EHN decreases with temperature This effect depends on EHN doping levels but not so much on pressure and equivalence ratio.

5.7.2 Effect of EHN and ferrocene on the RON value

As presented in the bibliography, the two conventional engines are SI engine and CI engine. While high-RON gasoline fuels (RON > 95) are employed in SI engine, diesel fuels having very low RON are used in CI engine. Actual LTC engines are being developed to operate with fuels having a wide range of RON [7] including fuels designed for CI and SI engines. To adjust the RON, additives can be employed.

Badra et al. [214] proposed five correlations between the simulated IDT of PRF and TRF fuels obtained by the reference model of LLNL [42] and their measured RON and MON. In this thesis, one of these correlations between RON and IDT is employed and presented below:

$$RON_{predicted} = 117.41654 - 17.99786 \times \exp\left(-\frac{IDT_{simu}}{22.0574}\right) - 41.40406 \times \exp\left(-\frac{IDT_{simu}}{1.7736}\right) - 184.6537 \times \exp\left(-\frac{IDT_{simu}}{0.30285}\right) \quad (Eq.6)$$

For the above correlation, IDT_{simu} were calculated using the reference model [42] in a constant volume reactor with CHEMKIN PRO [130] at condition 50 atm, 850 K, Φ = 1. Table 36 shows the measured RON of the mixtures of toluene and *n*-heptane used to validated the correlation. These RON measurements were conducted in a single-cylinder Cooperative Fuels Research (CFR) engine by Badra et al. [214]. The correlation was validated for a range of RON between 40 and 100. Figure 84 presents the prediction of measured RON of fuels shown in Table 36 by adopting the correlation Eq.6 with the IDT_{simu} calculations conducted with the kinetic model of this study.

Table 36: Measured RON of mixtures of toluene and *n*-heptane. Experimental data collected from [214].

Mixture	Molar composition (%)		Measured RON
	n-Heptane	Toluene	
1.	62.9	37.1	38.0
2.	52.1	47.9	51.4
3.	42.0	58.0	65.9
4.	34.4	65.6	75.6
5.	27.2	72.8	85.2
6.	23.7	76.3	89.3
7.	20.8	79.2	92.3
8.	16.0	84.0	97.7

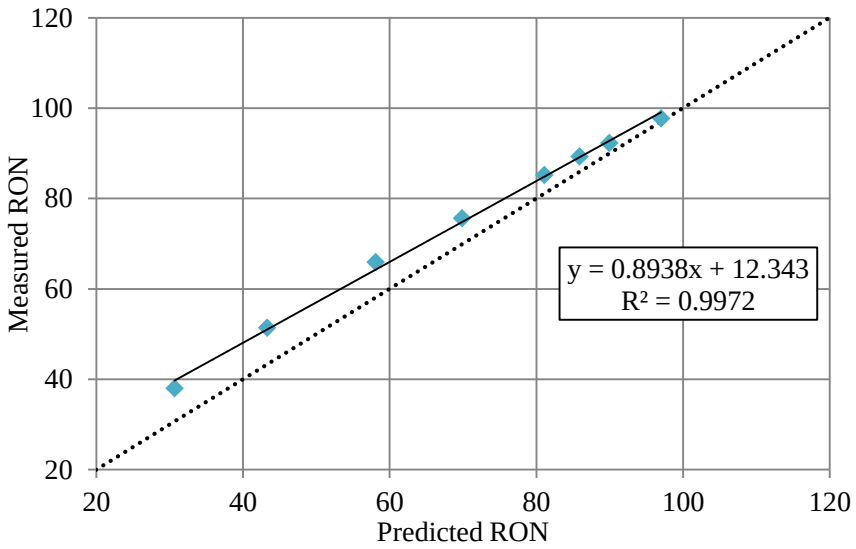

Figure 84: Comparison between measured RON and predicted RON by adopting the correlation Eq.6. The dashed line represents equation y = x.

The parity plot illustrated Figure 84 indicates that the correlation Eq.6 needs to be modified to be usable with the kinetic model of this study which is developed based on the reference model [42]. To do that, we introduce a new parameter named as $RON_{pseudo\text{-}predicted}$. The correlation Eq.6 is now modified as:

$$RON_{predicted} = a \times RON_{pseudo-predicted} + b \qquad (Eq.7)$$

With:

- $RON_{pseudo-predicted} = 117.41654 - 17.99786 \times \exp\left(-\frac{IDT_{simu}}{22.0574}\right) - 41.40406 \times \exp\left(-\frac{IDT_{simu}}{1.7736}\right) - 184.6537 \times \exp\left(-\frac{IDT_{simu}}{0.30285}\right)$
- IDT_{simu} (ms) is the simulated IDT of fuel in a constant volume reactor model at 50 atm, 850 K, and Φ = 1 obtained with the kinetic model developed in this work.

Two parameters a and b in Eq.7 are determined by a linear regression between the measured RON and $RON_{pseudo-predicted}$ of fuels shown in Table 36 . Consequently, the values of a and b are found as 0.89 and 12.34 respectively. Figure 85 represents the prediction of measured RON of fuels shown in Table

36 by adopting the correlation Eq.7 with the IDT_{simu} calculations conducted with the kinetic model of this study. The predicted RON agrees well with the measured ones. The largest difference between predicted and measured RON is about 1.7 which is similar to the experiment uncertainties of RON measurements.

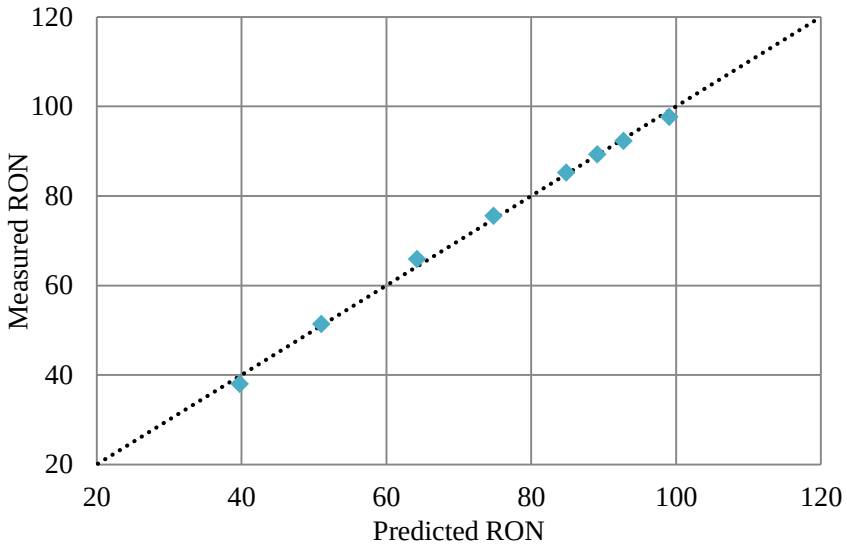

Figure 85: Comparison between measured RON and predicted RON. The dashed line represents equation y = x.

To evaluate the impact of EHN and ferrocene on RON of fuels, the correlation Eq.7 described above is employed. Figure 86 illustrates the effect of EHN on three different fuels comprising mixtures (3), (5), (8) listed in Table 36. EHN is found to reduce the RON value of these fuels. This effect increases non linearly with doping levels of EHN. It is observed that the RON-lowering effect of EHN is very sensible at very low concentration (< 0.1 % mol.) and then increases nearly linearly with higher concentrations (> 0.1 % mol.). Figure 87 shows the RON value decrease of the fuels by the incorporation of EHN. This additive shows the strongest influence for the most reactive fuel, i.e. the fuel having the lowest RON value. This result is in agreement with the experimental study of Ghosh et al. [39].

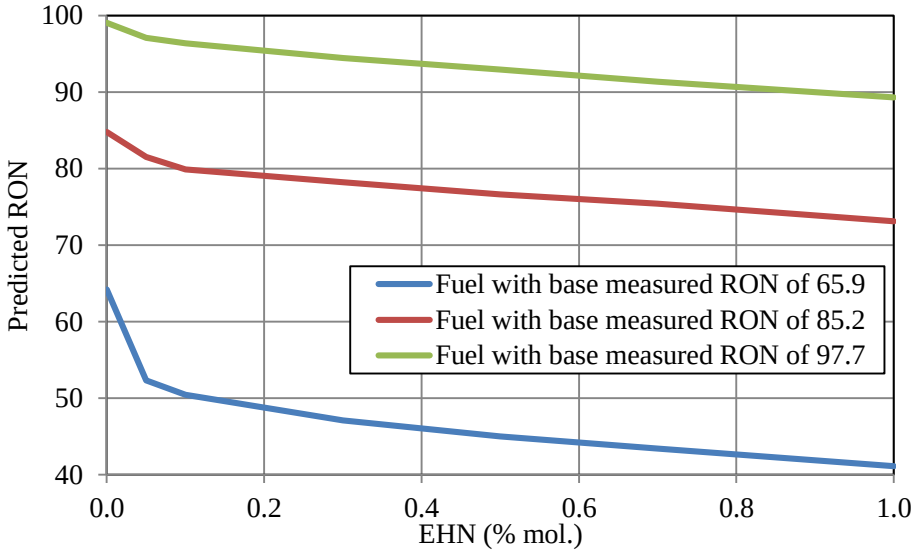

Figure 86: Prediction of impact of EHN on RON of fuels.

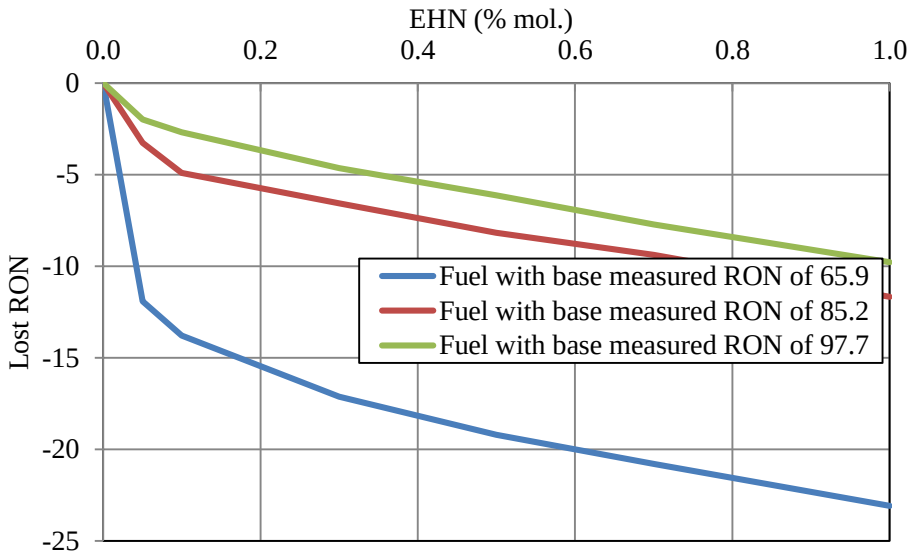

Figure 87: Prediction of lost RON value of the fuels by the incorporation of EHN.

Figure 88 presents the effect of ferrocene on three fuels including mixtures (1), (3), (5) listed in Table 36. The maximum examined doping level of ferrocene is 0.1%. It is found that the RON values of fuels are enhanced by the presence of ferrocene. The octane-boosting effect of ferrocene increases nearly linearly with doping level. This result is consistent with the experimental investigation of Fenard et al. [75]. Moreover, as shown in Figure 89, the octane-boosting effect of ferrocene is nearly independent of the initial RON value of the fuel.

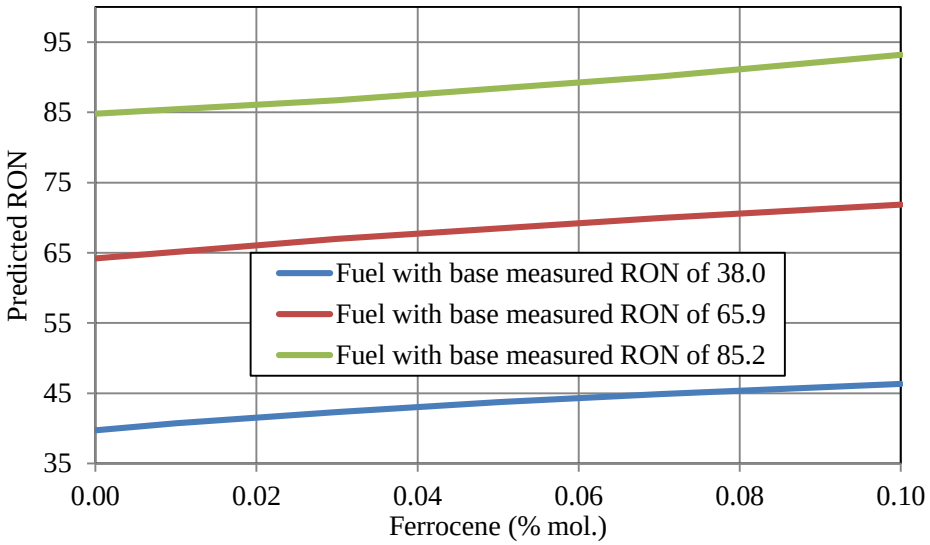

Figure 88: Prediction of ferrocene impact on RON of fuels

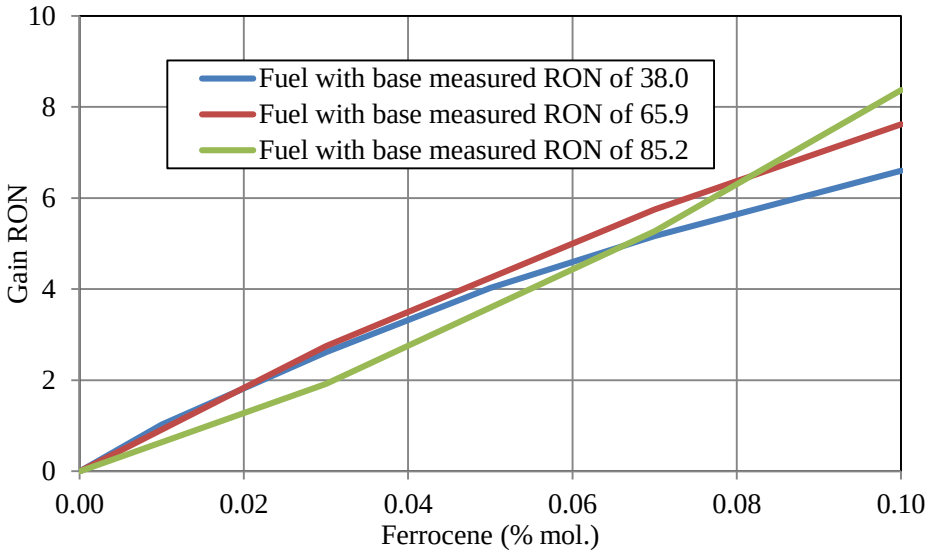

Figure 89: Prediction of variation of RON of fuels with ferrocene addition.

Briefly, this section describes how EHN and ferrocene affect the RON values of fuels containing toluene and *n*-heptane by numerical simulations. While EHN decreases the RON, this characteristic is enhanced by ferrocene. Moreover, the effects of these two additives are different. The octane-lowering effect of EHN depends on the initial RON value of fuel and increases nonlinearly with doping levels. Conversely, the reactivity of the base fuel does not affect the octane-boosting effect of ferrocene and this effect increases nearly linearly with the concentration of this additive.

The results presented in this section show the application of a detailed kinetic model in predicting effects of fuel additives on a standardized property of fuel. This enables to time and cost savings to reformulate fuels for a specific IC engine.

Chapter 6: Conclusions and future works

Environmental concerns urge researchers to improve internal combustion (IC) engines, which are dominantly used in the automotive industry. IC engines are required to operate more efficiently while reducing pollutants and greenhouse gases emission. Engine-fuel adequacy optimization is key to achieve this goal. Among the fuel parameters, the reactivity is the most important characteristic which needs to be carefully considered. Indeed, this feature is related to the fuel quality in the distribution system but also the combustion efficiency. Considering together the evolution of combustion systems (HCCI, SACI, GCI, etc.) and the incorporation of alternatives fuels (bio-sourced fuel, synthetic fuel, etc.), utilization of fuel additive is a required option to improve fuel-engine adequacy. In this context, the thesis aims to better understand the chemical effect of fuel additives on the gas-phase reactivity by experimental and numerical investigations. The chemical kinetic mechanisms developed will be dedicated to the evaluation of the potential effects of additives in various thermodynamic conditions and base fuels.

Thanks to the literature review, three additives are considered in this thesis: 2-ethylhexyl nitrate, ferrocene, and 2,4-xylenol. Their significant effect as a cetane booster, an octane booster, and an antioxidant, respectively, has been demonstrated in the literature. To understand the chemical effect of these additives, a surrogate fuel containing 35% *n*-heptane and 65% toluene by volume was adopted based on a literature study. This fuel belongs to the low-octane gasoline grade (RON = 84). The selection of this surrogate fuel was supported by available mechanisms of *n*-heptane and toluene, which facilitate the investigation of fuel additives. Furthermore, this surrogate allows to examine the effect of fuel additives on some specific combustion phenomena, such as two-stage ignition and negative coefficient temperature (NTC).

The impact of these additives on the gas-phase reactivity of the surrogate fuel was experimentally and numerically investigated in three devices including a shock tube (ST), a rapid compression machine (RCM), and a flat flame burner. This enables to explore the chemical effect of additives over a wide temperature range. From a modeling point of view, a detailed kinetic model was developed based on available recent literature data. This model consists of sub-mechanisms of combustion of *n*-heptane, toluene, nitrogen oxides, EHN and ferrocene. The new kinetic model was validated using a large set of experimental data. The validation confirms a good performance of the kinetic model to reproduce the reactivity of toluene and *n*-heptane mixtures, sensitizing effect of NO_x, and promoting effect of EHN.

In RCM experiments, the ignition delay times (IDT) of the neat and doped surrogate fuel were measured at 10 bar, T_c = 675 – 1000 K, at both lean (Φ = 0.5) and stoichiometric conditions. The doping levels of additives were set at 0.1 and 1% mol. For ferrocene, the concentration was set at 0.01 and 0.1 % mol. to avoid deposit formation. These concentrations are representative of doping levels identified in the literature. Two-stage ignitions and NTC were observed in the case of the neat surrogate fuel. EHN exhibits a promoting effect on the surrogate reactivity including 1^{st}-stage ignition and NTC regions. On the other hand, ferrocene shows an inhibiting effect. This effect is weak on the 1^{st}-stage ignition but significant on the main ignition of the surrogate fuel at both equivalence ratios. Ferrocene enhances the NTC region. The effects of both EHN and ferrocene increase with higher T_c and increasing doping level. Different from these two additives, 2,4-xylenol does not show any remarkable effect on the surrogate fuel reactivity under RCM conditions.

IDT measurements were also conducted at a high temperature range (1350 – 1600 K) in shock tube at 10 bar and Φ = 1. The doping levels were set at 1% weight basis for EHN and 2,4-xylenol and 0.1% weight basis for ferrocene in the liquid-phase surrogate fuel. The fuel gas mixtures were prepared at ambient temperature (near 25°C). It should be noticed that the experimental gas-phase doping levels

of additives were lower due to their lower vapor pressure in comparison with the components of the surrogate fuel. In the high-temperature conditions, no additives show a significant impact on the surrogate fuel reactivity.

The influence of additives on the laminar burning velocity of the surrogate fuel was examined in the heat flux burner. Experiments were performed at atmospheric pressure and an initial temperature of 398 K by Matieyendou Goussougli, an intern at Laboratoire Réaction et Génie des Procédés (LRGP) in Nancy, France. The doping levels of additives were fixed as same as in the ST experiments. It is found that the additives do not impact remarkably the laminar burning velocity of the surrogate fuel. Indeed, the measurements of laminar burning velocity involve the high-temperature chemistry of the surrogate fuel.

2,4-xylenol does not show any effect experimentally on the reactivity of the surrogate fuel. This tends to confirm that the utilization of 2,4-xylenol as an antioxidant at a doping level below 1% mol. does not show any side effect on the fuel gas-phase reactivity with the selected fuel surrogate.

All experimental results of the neat and doped surrogate fuel are well simulated by the developed kinetic model. For RCM simulations, the compression process has to be taken into account to reproduce properly the experimental results. By simulation, the promoting effect of EHN in the low temperature range (T < 1000 K) is linked to the reactions of C_7H_{15}-3 radical and to a NO_2-NO loop, which contains reactions R + NO_2 = RO + NO and RO_2 + NO = RO + NO_2. The reactions of C_7H_{15}-3 radical and the reaction NO + HO_2 = NO_2 + OH included in the NO_2-NO loop generate a supplementary source of OH radicals. In addition, NO_2 can react with benzyl radical ($C_6H_5CH_2$) to form $C_6H_5CH_2O$ radical and NO. This reaction enhances the toluene reactivity, i.e. the surrogate fuel reactivity. The reactions between NO and *n*-heptyl peroxy radicals are found to be the main cause of the EHN effect on the NTC region of the surrogate fuel oxidation. It is also found that the formation of nitroethane ($C_2H_5NO_2$), which traps the active NO_2 into a stable species, is the main reason of the minimum EHN promoting effect around 740 K.

To improve the performance of the ferrocene sub-mechanism, additional reactions of iron species with radicals such as HO_2, $C_6H_5CH_2$, $C_6H_5CH_2OO$, producing low reactivity species, were proposed to capture the inhibiting effect of ferrocene at both equivalence ratios within the lower temperature range (T < 1000 K). In comparison with EHN, ferrocene is much more stable. This thesis hypothesized that ferrocene chemical activity is related to alcohol formation. The reactions of benzyl and benzyl peroxy radicals with iron species enable this pathway. It is also found that ferrocene promotes the NTC phenomenon by consuming the HO_2 radicals released from the decomposition of heptyl peroxy radicals into heptenes.

The validated kinetic model was used to predict the effect of EHN and ferrocene on different fuels in various conditions. It is found for example that EHN can reduce IDT of pure ethanol. This effect is sensitive to the variation of EHN doping levels but not so much to the pressure variation and equivalence ratio. In addition, the influence of EHN and ferrocene on the RON of fuels containing toluene and *n*-heptane was numerically examined. As expected, EHN and ferrocene increase and decrease respectively the RON. The octane-lowering effect of EHN depends on the initial RON of the fuel and increases nonlinearly with doping levels. This is consistent with the experimental results of Ghosh et al. [39]. Conversely, the reactivity of the base fuel does not affect the octane-boosting effect of ferrocene and this effect increases nearly linearly with the concentration of this additive.

This thesis contributes to the fundamental understanding of the effect of additives on fuel reactivity. The validated kinetic model can efficiently help to investigate EHN promoting effect and ferrocene inhibiting effect in different engine simulations.

The current study suggests various future pathways including experimental and numerical works for a further exploration of fuel additives. Oxidation stability is an important fuel characteristic. Characterizing impact of the additives on the liquid-phase reactivity, which was not able to be performed in this work, is essential for their optimal uses in engines. In addition, some theoretical calculations dedicated to iron chemistry and experiments including RON and IDT measurements are of interest to improve the performance of the gas-phase kinetic model. The considering future works are described below:

- As shown in section 5.3.1, EHN is not thermally stable. EHN degradation could occur in the fuel distribution system and then impact the fuel oxidation stability. This aspect has been discussed in several studies. Hartikka et al. [215] indicated that EHN decreased the oxidation stability of a diesel fuel. However, this additive increased the oxidation stability of a biodiesel B20, as reported by Rashed et al. [216] and Ileri et al. [217]. The antioxidant effect of EHN depends on the chemistry of the base fuel. About 2,4-xylenol, this additive has been identified as an efficient antioxidant in the literature [47]. To our knowledge, no kinetic model has been developed in the literature to predict the impact of 2,4-xylenol on the liquid-phase reactivity. Similarly, the influence of ferrocene on the oxidation stability of fuels has not been experimentally and theoretically studied. Consequently, experiments and numerical studies concerning the liquid-phase oxidation are of interest to systematically explore the impact of EHN, 2,4-xylenol and ferrocene on the liquid-phase reactivity.

- This work provides an original set of experimental data combined with a first detailed kinetic model for ferrocene capable of modeling the additive behavior on the considered pressure, temperature and equivalence ratio range. Thanks to this methodology, this study highlights some potential sensitive types of reactions for the selected additive/fuel mixture. To better investigate these reactions, quantum calculations for iron species are suggested. This method is challenging but feasible. Though the available numerical data on iron containing species thermochemistry demonstrates important disparities, e.g. FeO_2 [202], quantum calculations would indeed help in characterizing the effect of a potential minor species not considered in the current model as well as other relevant pathways than the ones proposed in this thesis.

- Predictions of EHN and ferrocene effects on RON of fuels have been shown in section 5.7.2. To validate this approach, some RON experimental measurements of the neat and doped fuels should be conducted. Once validated, this method can be employed to efficiently reformulate fuels for specific engines.

- The effect of the additives on the gas-phase reactivity in the high temperature range ($T > 1300$ K) was investigated in the ST at LRGP in this work. As the vapor pressures of the compounds are different from each other, the main difficulty of the ST experiments was to obtain the desired gas mixture composition. Consequently, a heating system should be employed to ensure the total evaporation of compounds in the mixing tank. Once established, experiments in ST would be conducted to better characterize the effect of the additives in the high temperature range.

References

[1] International Energy Agency, “World Energy Outlook,” http://www.iea.org/weo/, February 18, 2018.

[2] Guibet, J.-C., “Carburants et moteurs,” Tome 1, Edition Technip, 1997.

[3] Vijayashree, G.V. (ed.), “A Comprehensive Review on Oxygenated Fuel Additive Options for Unregulated Emission Reduction from Diesel Engines,” In: Singh A., Sharma Y., Mustafi N., Agarwal A. (eds) Alternative Fuels and Their Utilization Strategies in Internal Combustion Engines., Energy, Environment, and Sustainability, Springer, Singapore, 2020.

[4] Dooley, S., Won, S.H., Heyne, J., Farouk, T.I. et al., “The experimental evaluation of a methodology for surrogate fuel formulation to emulate gas phase combustion kinetic phenomena,” *Combustion and Flame* 159(4):1444–1466, 2012, doi:10.1016/j.combustflame.2011.11.002.

[5] Agarwal, A.K., Singh, A.P., and Maurya, R.K., “Evolution, challenges and path forward for low temperature combustion engines,” *Progress in Energy and Combustion Science* 61:1–56, 2017, doi:10.1016/j.pecs.2017.02.001.

[6] Sharma, T.K., Rao, G.A.P., and Murthy, K.M., “Homogeneous Charge Compression Ignition (HCCI) Engines: A Review,” *Archives of Computational Methods in Engineering* 23(4):623–657, 2016.

[7] Kalghatgi, G. and Johansson, B., “Gasoline compression ignition approach to efficient, clean and affordable future engines,” *Proceedings of the Institution of Mechanical Engineers, Part D: Journal of Automobile Engineering* 232(1):118–138, 2017, doi:10.1177/0954407017694275.

[8] Reitz, R.D. and Duraisamy, G., “Review of high efficiency and clean reactivity controlled compression ignition (RCCI) combustion in internal combustion engines,” *Progress in Energy and Combustion Science* 46:12–71, 2015, doi:10.1016/j.pecs.2014.05.003.

[9] Manofsky, L., Vavra, J., Assanis, D.N., and Babajimopoulos, A., “Bridging the Gap between HCCI and SI: Spark-Assisted Compression Ignition,” SAE Technical Paper 2011-01-1179, 2011, doi:10.4271/2011-01-1179.

[10] U.S. Departement of Energy, “Co-Optimization of Fuels & Engines,” https://energy.gov/sites/prod/files/2016/06/f32/ft037_farrell_2016_o_web.pdf, February 12, 2018.

[11] Khodakov, A.Y., Chu, W., and Fongarland, P., “Advances in the Development of Novel Cobalt Fischer—Tropsch Catalysts for Synthesis of Long-Chain Hydrocarbons and Clean Fuels,” *ChemInform* 38(33):1692, 2007, doi:10.1002/chin.200733255.

[12] Bacha, K., “Etude de l’Interaction entre le Carburant Diesel et les Composants du Système d’Injection Diesel,” PhD Thesis, Université de Haute Alsace, 2016.

[13] Kuboyama, T., Moriyoshi, Y., and Morikawa, K., “Visualization and Analysis of LSPI Mechanism Caused by Oil Droplet, Particle and Deposit in Highly Boosted SI Combustion in Low Speed Range,” *SAE Int. J. Engines* 8(2):529–537, 2015, doi:10.4271/2015-01-0761.

[14] Chatelain, K., “Stabilité à l'oxydation des carburants en phase liquide,” PhD thesis, Université Paris-Saclay, 2016.

[15] Kim, D. and Lee, C., “Improved emission characteristics of HCCI engine by various premixed fuels and cooled EGR,” *Fuel* 85(5-6):695–704, 2006, doi:10.1016/j.fuel.2005.08.041.

[16] Wang, X., Zhang, H., Yao, B., Lei, Y. et al., “Experimental study on factors affecting lean combustion limit of S.I engine fueled with compressed natural gas and hydrogen blends,” *Energy* 38(1):58–65, 2012, doi:10.1016/j.energy.2011.12.042.

[17] Murta Valle, M.L., Leonardo, R.S., and Dweck, J., “Comparative study of biodiesel oxidation stability using Rancimat, PetroOXY, and low P-DSC,” *J Therm Anal Calorim* 116(1):113–118, 2014, doi:10.1007/s10973-014-3706-6.

[18] Machado, Y.L., Teles, U.M., Dantas Neto, A.A., Dantas, T.N.C. et al., "Determination of antioxidant depletion kinetics using ASTMD 7545 as the accelerated oxidation method," *Fuel* 112:172–177, 2013, doi:10.1016/j.fuel.2013.04.080.

[19] PTI/2, "Carburants pour automobiles. Carburant pour moteur diesel (gazole). Exigences et methodes d'essai," BS EN 590:2004, BSI, Rev. Aug. 2004.

[20] D02 Committee, "Specification for Diesel Fuel Oils," ASTM International, Rev. 2017.

[21] Suppes, G.J., Goff, M., Burkhart, M.L., Bockwinkel, K. et al., "Multifunctional Diesel Fuel Additives from Triglycerides," *Energy Fuels* 15(1):151–157, 2001, doi:10.1021/ef000122c.

[22] D02 Committee, "Test Method for Cetane Number of Diesel Fuel Oil," ASTM International, Rev. 2017.

[23] Beuth, "Testing of liquid fuels - Determination of ignition quality (cetane number) of Diesel fuels with the BASF-engine," Rev. 2010.

[24] D02 Committee, "Test Method for Determination of Ignition Delay and Derived Cetane Number (DCN) of Diesel Fuel Oils by Combustion in a Constant Volume Chamber," ASTM International, Rev. 2016.

[25] D02 Committee, "Test Method for Determination of Derived Cetane Number (DCN) of Diesel Fuel OilsFixed Range Injection Period, Constant Volume Combustion Chamber Method," ASTM International, Rev. 2016.

[26] D02 Committee, "Test Method for Determination of Derived Cetane Number (DCN) of Diesel Fuel OilsIgnition Delay and Combustion Delay Using a Constant Volume Combustion Chamber Method," ASTM International, Rev. 2017.

[27] Welling, O., Moss, J., Williams, J., and Collings, N., "Measuring the Impact of Engine Oils and Fuels on Low-Speed Pre-Ignition in Downsized Engines," *SAE Int. J. Fuels Lubr.* 7(1):1–8, 2014.

[28] Dahnz, C., Han, K.-M., Spicher, U., Magar, M. et al., "Investigations on Pre-Ignition in Highly Supercharged SI Engines," *SAE Int. J. Engines* 3(1):214–224, 2010, doi:10.4271/2010-01-0355.

[29] Kalghatgi, G.T. (ed.), "Fuel Anti-Knock Quality - Part I. Engine Studies," SAE Technical Paper Series, SAE International Fall Fuels & Lubricants Meeting & Exhibition, SEP. 24, 2001, SAE International400 Commonwealth Drive, Warrendale, PA, United States, 2001.

[30] Stradling, R., Rickeard, D., Hamje, H., Williams, J. et al., "Effect of Octane on the Performance of Two Gasoline Direct Injection Passenger Cars," *SAE 2015 World Congress & Exhibition*, SAE Technical Paper Series, APR. 21, 2015, SAE International400 Commonwealth Drive, Warrendale, PA, United States, 2015.

[31] D02 Committee, "Test Method for Research Octane Number of Spark-Ignition Engine Fuel," ASTM International, Rev. 2017.

[32] D02 Committee, "Test Method for Motor Octane Number of Spark-Ignition Engine Fuel," ASTM International, Rev. 2017.

[33] ATC-Technical Comitee of Petroleum Additive Manufacturers in Europe, "Fuel Additives: Use and Benefits," 2013.

[34] Nandi, M.K. and Jacobs, D.C. (eds.), "Cetane Response of Di-tertiary-butyl Peroxide in Different Diesel Fuels," SAE Technical Paper Series, 1995 SAE International Fall Fuels and Lubricants Meeting and Exhibition, OCT. 16, 1995, SAE International400 Commonwealth Drive, Warrendale, PA, United States, 1995.

[35] Nagpal, J.M., Joshi, G.C., and Rastogi, S.N., "Stability of cracked naphthas from thermal and catalytic processes and their additive response. Part I. Evaluation of stability and additive response," *Fuel* 74(5):714–719, 1995, doi:10.1016/0016-2361(95)91104-7.

[36] Battin-Leclerc, F., "Detailed chemical kinetic models for the low-temperature combustion of hydrocarbons with application to gasoline and diesel fuel surrogates," *Progress in Energy and Combustion Science* 34(4):440–498, 2008, doi:10.1016/j.pecs.2007.10.002.

[37] Robbins, W.E., Audette, R.R., and Reynolds, N.E., "Performance and Stability of Some Diesel Fuel Ignition Quality Improvers," *SAE Technical Paper 510200*, 1951.
[38] Howard, J.A. and K. U. Ingold, "The inhibited autoxidation of styrene: Part II. The relative inhibiting efficiencies of meta- and para-substituted phenols," *Canadian Journal of Chemistry* 41, 1963.
[39] Ghosh, P., "Predicting the Effect of Cetane Improvers on Diesel Fuels," *Energy Fuels* 22(2):1073–1079, 2008, doi:10.1021/ef0701079.
[40] Goldsborough, S.S., Johnson, M.V., Banyon, C., Pitz, W.J. et al., "Experimental and modeling study of fuel interactions with an alkyl nitrate cetane enhancer, 2-ethyl-hexyl nitrate," *Proc. Combust. Inst.* 35(1):571–579, 2015, doi:10.1016/j.proci.2014.06.048.
[41] Goussougli, M., "Délai d'Auto-Inflammation en Tube à Onde de Choc d'Additifs Améliorateurs d'Indice Octane des Essences," Master thesis, Université de Lorraine-Mines Nancy, 2019.
[42] Mehl, M., Pitz, W.J., Westbrook, C.K., and Curran, H.J., "Kinetic modeling of gasoline surrogate components and mixtures under engine conditions," *Proc. Combust. Inst.* 33(1):193–200, 2011, doi:10.1016/j.proci.2010.05.027.
[43] Moréac, G., Dagaut, P., Roesler, J.F., and Cathonnet, M., "Nitric oxide interactions with hydrocarbon oxidation in a jet-stirred reactor at 10 atm," *Combustion and Flame* 145(3):512–520, 2006, doi:10.1016/j.combustflame.2006.01.002.
[44] Gernigon, S., "Étude de la stabilité à l'oxydation des carburants liquides hydrocarbonés. Influence et comportement des antioxydants," Université Paris 7, Paris, 2010.
[45] D02 Committee, "Test Method for Oxidation Stability of Gasoline (Induction Period Method)," ASTM International, Rev. 2012.
[46] Diaby, M., Sablier, M., Le Negrate, A., and El Fassi, M., "Kinetic Study of the Thermo-Oxidative Degradation of Squalane (C30H62) Modeling the Base Oil of Engine Lubricants," *J. Eng. Gas Turbines Power* 132(3):32805, 2010, doi:10.1115/1.3155797.
[47] McCormick, R.L., Ratcliff, M.A., Christensen, E., Fouts, L. et al., "Properties of Oxygenates Found in Upgraded Biomass Pyrolysis Oil as Components of Spark and Compression Ignition Engine Fuels," *Energy Fuels* 29(4):2453–2461, 2015, doi:10.1021/ef502893g.
[48] Di Tommaso, S., Rotureau, P., Benaissa, W., Gruez, P. et al., "Theoretical and Experimental Study on the Inhibition of Diethyl Ether Oxidation," *Energy Fuels* 28(4):2821–2829, 2014, doi:10.1021/ef402508s.
[49] Zabarnick, S. and Mick, M.S., "Inhibition of Jet Fuel Oxidation by Addition of Hydroperoxide-Decomposing Species," *Ind. Eng. Chem. Res.* 38(9):3557–3563, 1999, doi:10.1021/ie990107z.
[50] Hirano, S., Yamashita, M., Fujimoto, K., and Kato, K., "Investigation of Engine Oil Effect on Abnormal Combustion in Turbocharged Direct Injection - Spark Ignition Engines (Part 2)," SAE Technical Paper Series, SAE/KSAE 2013 International Powertrains, Fuels & Lubricants Meeting, OCT. 21, 2013, SAE International400 Commonwealth Drive, Warrendale, PA, United States, 2013.
[51] Denisov, E. and Afanas'ev, I., "Oxidation and Antioxidants in Organic Chemistry and Biology," CRC Press, ISBN 978-0-8247-5356-6, 2005.
[52] Teixeira, L.S.G., Souza, J.C., dos Santos, H.C., Pontes, L.A.M. et al., "The influence of Cu, Fe, Ni, Pb and Zn on gum formation in the Brazilian automotive gasoline," *Fuel Processing Technology* 88(1):73–76, 2007, doi:10.1016/j.fuproc.2006.08.008.
[53] D02 Committee, "Test Method for Gum Content in Fuels by Jet Evaporation," ASTM International, Rev. 2001.
[54] Waynick, J.A., "The Development and Use of Metal Deactivators in the Petroleum Industry: A Review," *Energy Fuels* 15(6):1325–1340, 2001, doi:10.1021/ef010113j.
[55] Basha, J.S. and Anand, R.B., "An Experimental Study in a CI Engine Using Nanoadditive Blended Water–Diesel Emulsion Fuel," *International Journal of Green Energy* 8(3):332–348, 2011, doi:10.1080/15435075.2011.557844.

[56] Gumus, S., Ozcan, H., Ozbey, M., and Topaloglu, B., "Aluminum oxide and copper oxide nanodiesel fuel properties and usage in a compression ignition engine," *Fuel* 163:80–87, 2016, doi:10.1016/j.fuel.2015.09.048.

[57] Soukht Saraee, H., Jafarmadar, S., Alizadeh-Haghighi, E., and Ashrafi, S.J., "Experimental investigation of pollution and fuel consumption on a CI engine operated on alumina nanoparticles-Diesel fuel with the aid of artificial neural network," *Environ. Prog. Sustainable Energy* 35(2):540–546, 2016, doi:10.1002/ep.12233.

[58] Arul Mozhi Selvan, V., Anand, R.B., and Udayakumar, M., "Effects of cerium oxide nanoparticle addition in diesel and diesel-biodiesel-ethanol blends on the performance and emission characteristics of a CI engine," *ARPN Journal of Engineering and Applied Sciences* 4, 2009.

[59] Saxena, V., Kumar, N., and Saxena, V.K., "A comprehensive review on combustion and stability aspects of metal nanoparticles and its additive effect on diesel and biodiesel fuelled C.I. engine," *Renewable and Sustainable Energy Reviews* 70:563–588, 2017, doi:10.1016/j.rser.2016.11.067.

[60] Chatelain, K., Matrat, M., Catoire, L., and Bouchez, M., "Development of Kinetic Models for the Hybrid Fuels Combustion Containing Aluminum Particles," *Journal of Propulsion and Power* 35(2):443–450, 2019, doi:10.2514/1.B37201.

[61] Khrapkovskii, G.M., Shamsutdinov, T.F., Chachkov, D.V., and Shamov, A.G., "Energy of the O–NO2 bond dissociation and the mechanism of the gas-phase monomolecular decomposition of aliphatic alcohol nitroesters," *Journal of Molecular Structure: THEOCHEM* 686(1-3):185–192, 2004, doi:10.1016/j.theochem.2004.09.001.

[62] Sebbar, N., Bozzelli, J.W., and Bockhorn, H., "Comparison of RC(O)OOH, RC(O)OOH and R(CO)OOH bond dissociation energies with RCOOH, RCOOH and RCOOH, R as phenyl, vinyl and alkyl groups," *Chemical Physics Letters* 629:102–112, 2015, doi:10.1016/j.cplett.2015.03.040.

[63] Blanksby, S.J. and Ellison, G.B., "Bond dissociation energies of organic molecules," *Accounts of chemical research* 36(4):255–263, 2003, doi:10.1021/ar020230d.

[64] Suppes, G.J., Rui, Y., Rome, A.C., and Chen, Z., "Cetane-Improver Analysis and Impact of Activation Energy on the Relative Performance of 2-Ethylhexyl Nitrate and Tetraethylene Glycol Dinitrate," *Ind. Eng. Chem. Res.* 36(10):4397–4404, 1997, doi:10.1021/ie9702284.

[65] Russell, T.J., "Additives influencing diesel fuel combustion. Gasoline and Diesel Fuel Additives," *John Wiley and Sons*, 1989.

[66] Hashimoto, K., "Fuel Ignition Quality Control by Addition and Catalytic Decomposition of Cetane Improver," SAE Technical Paper 2006-01-3361, 2006, doi:10.4271/2006-01-3361.

[67] Rode, A.B., Chung, K., Kim, Y.-W., and Hong, I.S., "Synthesis and Cetane-Improving Performance of 1,2,4,5-Tetraoxane and 1,2,4,5,7,8-Hexaoxonane Derivatives," *Energy Fuels* 24(3):1636–1639, 2010, doi:10.1021/ef9013899.

[68] Yonei, T., Hashimoto, K., Arai, M., and Tamura, M., "Quantum Chemical Study of Cetane Improvers," *Energy Fuels* 17(3):725–730, 2003, doi:10.1021/ef020266m.

[69] Hartmann, M., Tian, K., Hofrath, C., Fikri, M. et al., "Experiments and modeling of ignition delay times, flame structure and intermediate species of EHN-doped stoichiometric n-heptane/air combustion," *Proc. Combust. Inst.* 32(1):197–204, 2009, doi:10.1016/j.proci.2008.06.068.

[70] Oxley, J.C., Smith, J.L., Rogers, E., Ye, W. et al., "Fuel Combustion Additives: A Study of Their Thermal Stabilities and Decomposition Pathways," *Energy Fuels* 14(6):1252–1264, 2000, doi:10.1021/ef000101i.

[71] Goodman, H., Gray, P., and Jones, D.T., "Self-heating during the spontaneous ignition of methyl nitrate vapor," *Combustion and Flame* 19(2):157–169, 1972, doi:10.1016/S0010-2180(72)80206-2.

[72] Seyferth, D., "The Rise and Fall of Tetraethyllead. 2," *Organometallics* 22(25):5154–5178, 2003, doi:10.1021/om030621b.

[73] Choi, S. and Seong, H., "Lube oil-dependent ash chemistry on soot oxidation reactivity in a gasoline direct-injection engine," *Combustion and Flame* 174:68–76, 2016, doi:10.1016/j.combustflame.2016.09.019.

[74] D'Andrea, T., "The addition of hydrogen to a gasoline-fuelled SI engine," *International Journal of Hydrogen Energy* 29(14):1541–1552, 2004, doi:10.1016/j.ijhydene.2004.02.002.

[75] Fenard, Y., Song, H., Dauphin, R., and Vanhove, G., "An engine-relevant kinetic investigation into the anti-knock effect of organometallics through the example of ferrocene," *Proc. Combust. Inst.* 37:547–554, 2019, doi:10.1016/j.proci.2018.06.135.

[76] Danilov, A.M., "Fuel additives: Evolution and Use in 1996-2000," *Chemistry and Technology of Fuels and Oils* 37(6):444–455, 2001, doi:10.1023/A:1014231230570.

[77] Bonczyk, P.A., "Effect of Ferrocene on soot in a prevaporized iso-octane/air diffusion flame," *Combustion and Flame* 87(3-4):233–244, 1991, doi:10.1016/0010-2180(91)90110-W.

[78] Hirasawa, T., Sung, C.-J., Yang, Z., Joshi, A. et al., "Effect of ferrocene addition on sooting limits in laminar premixed ethylene–oxygen–argon flames," *Combustion and Flame* 139(4):288–299, 2004, doi:10.1016/j.combustflame.2004.09.002.

[79] Koshiba, Y., Takahashi, Y., and Ohtani, H., "Flame suppression ability of metallocenes (nickelocene, cobaltcene, ferrocene, manganocene, and chromocene)," *Fire Safety Journal* 51:10–17, 2012, doi:10.1016/j.firesaf.2012.02.008.

[80] Reinelt, D. and Linteris, G.T., "Experimental study of the inhibition of premixed and diffusion flames by iron pentacarbonyl," *Symposium (International) on Combustion* 26(1):1421–1428, 1996, doi:10.1016/S0082-0784(96)80362-6.

[81] Linteris, G.T., "Inhibition of premixed methane flames by manganese and tin compounds," *Combustion and Flame* 129(3):221–238, 2002, doi:10.1016/S0010-2180(02)00346-2.

[82] Benson, S.W., "The Mechanism of Inhlbition of Knock by Lead Additives, a Chain Debranching Reaction," *Journal of Physical Chemistry* 92:1531–1533, 1988.

[83] Wlokas, I., Faccinetto, A., Tribalet, B., Schulz, C. et al., "Mechanism of Iron Oxide Formation from Iron Pentacarbonyl-Doped Low-Pressure Hydrogen/Oxygen Flames," *Int. J. Chem. Kinet.* 45(8):487–498, 2013, doi:10.1002/kin.20786.

[84] Cumming, W.M., Horn, J.A., and Ritchie, P.D., "Chromium hexacarbonyl. II. Chromium hexacarbonyl as a fuel additive," *J. Appl. Chem.* 5(1):39–52, 1955, doi:10.1002/jctb.5010050106.

[85] Awad, O.I., Mamat, R., Ibrahim, T.K., Hammid, A.T. et al., "Overview of the oxygenated fuels in spark ignition engine: Environmental and performance," *Renewable and Sustainable Energy Reviews* 91:394–408, 2018, doi:10.1016/j.rser.2018.03.107.

[86] Brown, J.E., Markley, F.X., and Shapiro, H., "Mechanism of Aromatic Amine Antiknock Action," *Ind. Eng. Chem.* 47(10):2141–2146, 1955, doi:10.1021/ie50550a034.

[87] Cullis, C.F., Holwill, J.M., and Pollard, R.T., "The influence of amines on the combustion of n-heptane," *Symposium (International) on Combustion* 13(1):195–203, 1971, doi:10.1016/S0082-0784(71)80023-1.

[88] Nilsson, P. and Otterstedt, J.-E., "Effect of composition of the feedstock on the catalytic cracking of heavy vacuum gas oil," *Applied Catalysis* 33(1):145–156, 1987, doi:10.1016/S0166-9834(00)80590-4.

[89] Burri, J., Crockett, R., Hany, R., and Rentsch, D., "Gasoline composition determined by 1H NMR spectroscopy," *Fuel* 83(2):187–193, 2004, doi:10.1016/S0016-2361(03)00261-8.

[90] Farrell, J.T., Cernansky, N.P., Dryer, F.L., Law, C.K. et al. (eds.), "Development of an Experimental Database and Kinetic Models for Surrogate Diesel Fuels," SAE Technical Paper Series, SAE World Congress & Exhibition, APR. 16, 2007, SAE International400 Commonwealth Drive, Warrendale, PA, United States, 2007.

[91] Westbrook, C.K., Warnatz, J., and Pitz, W.J., "A detailed chemical kinetic reaction mechanism for the oxidation of iso-octane and n-heptane over an extended temperature range and its application to analysis of engine knock," *Symposium (International) on Combustion* 22(1):893–901, 1989, doi:10.1016/S0082-0784(89)80098-0.

[92] Curran, H.J., Gaffuri, P., Pitz, W.J., and Westbrook, C.K., "A Comprehensive Modeling Study of n-Heptane Oxidation," *Combustion and Flame* 114(1-2):149–177, 1998, doi:10.1016/S0010-2180(97)00282-4.

[93] Zhang, K., Banyon, C., Bugler, J., Curran, H.J. et al., "An updated experimental and kinetic modeling study of n- heptane oxidation," *Combustion and Flame* 172:116–135, 2016, doi:10.1016/j.combustflame.2016.06.028.

[94] Poon, H.M., Ng, H.K., Gan, S., Pang, K.M. et al., "Evaluation and Development of Chemical Kinetic Mechanism Reduction Scheme for Biodiesel and Diesel Fuel Surrogates," *SAE Int. J. Fuels Lubr.* 6(3):729–744, 2013, doi:10.4271/2013-01-2630.

[95] Gustavsson, J. and Golovitchev, V.I. (eds.), "Spray Combustion Simulation Based on Detailed Chemistry Approach for Diesel Fuel Surrogate Model," SAE Technical Paper Series, 2003 JSAE/SAE International Spring Fuels and Lubricants Meeting, MAY. 19, 2003, SAE International400 Commonwealth Drive, Warrendale, PA, United States, 2003.

[96] Natelson, R.H., Kurman, M.S., Cernansky, N.P., and Miller, D.L., "Experimental investigation of surrogates for jet and diesel fuels," *Fuel* 87(10-11):2339–2342, 2008, doi:10.1016/j.fuel.2007.11.009.

[97] Puduppakkam, K., Naik, C.V., Meeks, E., Krenn, C. et al., "Predictive Combustion and Emissions Simulations for a High Performance Diesel Engine Using a Detailed Fuel Combustion Model," SAE Technical Paper 2014-01-2570, 2014, doi:10.4271/2014-01-2570.

[98] Pitz, W.J., Cernansky, N.P., Dryer, F.L., Egolfopoulos, F.N. et al. (eds.), "Development of an Experimental Database and Chemical Kinetic Models for Surrogate Gasoline Fuels," SAE Technical Paper Series, SAE World Congress & Exhibition, APR. 16, 2007, SAE International400 Commonwealth Drive, Warrendale, PA, United States, 2007.

[99] Gauthier, B.M., Davidson, D.F., and Hanson, R.K., "Shock tube determination of ignition delay times in full-blend and surrogate fuel mixtures," *Combustion and Flame* 139(4):300–311, 2004, doi:10.1016/j.combustflame.2004.08.015.

[100] Kim, Y., Min, K., Kim, M.S., Chung, S.H. et al. (eds.), "Development of a Reduced Chemical Kinetic Mechanism and Ignition Delay Measurement in a Rapid Compression Machine for CAI Combustion," SAE Technical Paper Series, SAE World Congress & Exhibition, APR. 16, 2007, SAE International400 Commonwealth Drive, Warrendale, PA, United States, 2007.

[101] Wang, H., Yao, M., Yue, Z., Jia, M. et al., "A reduced toluene reference fuel chemical kinetic mechanism for combustion and polycyclic-aromatic hydrocarbon predictions," *Combustion and Flame* 162(6):2390–2404, 2015, doi:10.1016/j.combustflame.2015.02.005.

[102] Kukkadapu, G., Kumar, K., Sung, C.-J., Mehl, M. et al., "Experimental and surrogate modeling study of gasoline ignition in a rapid compression machine," *Combustion and Flame* 159(10):3066–3078, 2012, doi:10.1016/j.combustflame.2012.05.008.

[103] Andrae, J.C.G. and Kovács, T., "Evaluation of Adding an Olefin to Mixtures of Primary Reference Fuels and Toluene To Model the Oxidation of a Fully Blended Gasoline," *Energy Fuels* 30(9):7721–7730, 2016, doi:10.1021/acs.energyfuels.6b01193.

[104] Atef, N., Kukkadapu, G., Mohamed, S.Y., Rashidi, M.A. et al., "A comprehensive iso-octane combustion model with improved thermochemistry and chemical kinetics," *Combustion and Flame* 178:111–134, 2017, doi:10.1016/j.combustflame.2016.12.029.

[105] Yuan, W., Li, Y., Dagaut, P., Yang, J. et al., "Investigation on the pyrolysis and oxidation of toluene over a wide range conditions. I. Flow reactor pyrolysis and jet stirred reactor oxidation," *Combustion and Flame* 162(1):3–21, 2015, doi:10.1016/j.combustflame.2014.07.009.

[106] Yuan, W., Li, Y., Dagaut, P., Yang, J. et al., "Investigation on the pyrolysis and oxidation of toluene over a wide range conditions. II. A comprehensive kinetic modeling study," *Combustion and Flame* 162(1):22–40, 2015, doi:10.1016/j.combustflame.2014.07.011.

[107] Westbrook, C.K., Pitz, W.J., Herbinet, O., Curran, H.J. et al., "A comprehensive detailed chemical kinetic reaction mechanism for combustion of n-alkane hydrocarbons from n-octane to n-hexadecane," *Combustion and Flame* 156(1):181–199, 2009, doi:10.1016/j.combustflame.2008.07.014.

[108] Zhang, Y., Somers, K.P., Mehl, M., Pitz, W.J. et al., "Probing the antagonistic effect of toluene as a component in surrogate fuel models at low temperatures and high pressures. A case study of toluene/dimethyl ether mixtures," *Proceedings of the Combustion Institute* 36(1):413–421, 2017, doi:10.1016/j.proci.2016.06.190.

[109] Hartmann, M., Gushterova, I., Fikri, M., Schulz, C. et al., "Auto-ignition of toluene-doped n-heptane and iso-octane/air mixtures: High-pressure shock-tube experiments and kinetics modeling," *Combustion and Flame* 158(1):172–178, 2011, doi:10.1016/j.combustflame.2010.08.005.

[110] Malliotakis, Z., Banyon, C., Zhang, K., Wagnon, S. et al., "Testing the validity of a mechanism describing the oxidation of binary n-heptane/toluene mixtures at engine operating conditions," *Combustion and Flame* 199:241–248, 2019, doi:10.1016/j.combustflame.2018.10.024.

[111] Herzler, J., Fikri, M., Hitzbleck, K., Starke, R. et al., "Shock-tube study of the autoignition of n-heptane/toluene/air mixtures at intermediate temperatures and high pressures," *Combustion and Flame* 149(1-2):25–31, 2007, doi:10.1016/j.combustflame.2006.12.015.

[112] Emel'yanov, V.E., Simonenko, L.S., and Skvortsov, V.N., "Ferrocene - A nontoxic antiknock agent for automotive gasolines," *Chemistry and Technology of Fuels and Oils* 37(4):224–228, 2001, doi:10.1023/A:1012391317921.

[113] Ortiz, A., Romero, J.L., Cueva, I., Jacobo, V.H. et al., "Spark plug failure due to a combination of strong magnetic fields and undesirable fuel additives," *Case Studies in Engineering Failure Analysis* 1(2):67–71, 2013, doi:10.1016/j.csefa.2013.04.004.

[114] Alfa Aesar, "Fiche de données de sécurité selon 1907/2006/CE, Article 31,"

[115] Fenard, Y., Dauphin, R., and Vanhove, G. (eds.), "Understanding the Anti-knock Effect of an Organometallic Additive: Ferrocene," Digital proceedings of the 8th European Combustion Meeting, Dubrovnik, Croatia, 18-21 April, 2017.

[116] Hanson, R.K. and Davidson, D.F., "Recent advances in laser absorption and shock tube methods for studies of combustion chemistry," *Progress in Energy and Combustion Science* 44:103–114, 2014, doi:10.1016/j.pecs.2014.05.001.

[117] Goldsborough, S.S., Hochgreb, S., Vanhove, G., Wooldridge, M.S. et al., "Advances in rapid compression machine studies of low- and intermediate-temperature autoignition phenomena," *Progress in Energy and Combustion Science* 63:1–78, 2017, doi:10.1016/j.pecs.2017.05.002.

[118] Bauge, J.-C., "Etude de l'oxydation de composés insaturés en réacteur parfaitement agité et en tube à onde de choc," PhD Thesis, Institut National Polytechnique de Lorraine, Nancy, 1998.

[119] Resler, E.L., Lin, S.-C., and Kantrowitz, A., "The Production of High Temperature Gases in Shock Tubes," *Journal of Applied Physics* 23(12):1390–1399, 1952, doi:10.1063/1.1702080.

[120] Heyberger, B., Belmekki, N., Conraud, V., Glaude, P.-A. et al., "Oxidation of small alkenes at high temperature," *Int. J. Chem. Kinet.* 34(12):666–677, 2002, doi:10.1002/kin.10092.

[121] Dayma, G., Glaude, P.-A., Fournet, R., and Battin-Leclerc, F., "Experimental and modeling study of the oxidation of cyclohexene," *Int. J. Chem. Kinet.* 35(7):273–285, 2003, doi:10.1002/kin.10127.

[122] Isufaj, F., "Experimental study of the oxidation of potential additives for HCCI engines," Master thesis, Université de Lorraine, 2016.
[123] Bradley, J.N., "Chemical applications of the shock tube,," Royal Institute of Chemistry, London, 1964.
[124] Falk, K.G., "The Ignition Temperatures of Hydrogen-Oxygen Mixtures," *J. Am. Chem. Soc.* 28(11):1517–1534, 1906, doi:10.1021/ja01977a001.
[125] Cassel, H., "Über Entflammung und Verbrennung von Sauerstoff–Wasserstoff-Gemischen," *Ann. Phys.* 356(23):685–704, 1917, doi:10.1002/andp.19173562302.
[126] Park, P. and Keck, J.C., "Rapid Compression Machine Measurements of Ignition Delays for Primary Reference Fuels," *SAE Technical Paper 900027*, 1990.
[127] Lee, D. and Hochgreb, S., "Rapid Compression Machines: Heat Transfer and Suppression of Corner Vortex," *Combustion and Flame* 114(3-4):531–545, 1998, doi:10.1016/S0010-2180(97)00327-1.
[128] Sung, C.-J. and Curran, H.J., "Using rapid compression machines for chemical kinetics studies," *Progress in Energy and Combustion Science* 44:1–18, 2014, doi:10.1016/j.pecs.2014.04.001.
[129] Pochet, M., Dias, V., Moreau, B., Foucher, F. et al., "Experimental and numerical study, under LTC conditions, of ammonia ignition delay with and without hydrogen addition," *Proc. Combust. Inst.* 37:621–629, 2019, doi:10.1016/j.proci.2018.05.138.
[130] Reaction Design, CHEMKIN-PRO (18.2), San Diego, 2017.
[131] Tanaka, S., Ayala, F., and Keck, J.C., "A reduced chemical kinetic model for HCCI combustion of primary reference fuels in a rapid compression machine," *Combustion and Flame* 133(4):467–481, 2003, doi:10.1016/S0010-2180(03)00057-9.
[132] Borghi, R. and Destriau, M., "La combustion et les flammes," Editions Technip, Paris, ISBN 2-7108-0684-3, 1995.
[133] Dirrenberger, P., "Étude Expérimentale et Théorique des Vitesses de Flammes Laminaires d'Hydrocarbures," Université de Lorraine, Nancy, 2014.
[134] Bell, J.B., Day, M.S., Rendleman, C.A., Woosley, S.E. et al., "Direct Numerical Simulations of Type Ia Supernovae Flames. II. The Rayleigh-Taylor Instabiblity," *Astrophysical Journal* 608(883-906), 2004.
[135] van Maaren, A., Thung, D.S., and de Goey, L. R. H., "Measurement of Flame Temperature and Adiabatic Burning Velocity of Methane/Air Mixtures," *Combustion Science and Technology* 96(4-6):327–344, 1994, doi:10.1080/00102209408935360.
[136] Dyakov, I.V., Konnov, A.A., Ruyck, J.D.E., Bosschaart, K.J. et al., "Measurement of Adiabatic Burning Velocity in Methane-Oxygen-Nitrogen Mixtures," *Combustion Science and Technology* 172(1):81–96, 2001, doi:10.1080/00102200108935839.
[137] Konnov, A.A. and Dyakov, I.V., "Experimental Study of Adiabatic Cellular Premixed Flames of Methane (Ethane, Propane) + Oxygen + Carbon Dioxide," *Combustion Science and Technology* 179(4):747–765, 2007, doi:10.1080/00102200601057550.
[138] Zhang, K., Banyon, C., Togbé, C., Dagaut, P. et al., "An experimental and kinetic modeling study of *n*-hexane oxidation," *Combustion and Flame* 162(11):4194–4207, 2015, doi:10.1016/j.combustflame.2015.08.001.
[139] Galimova, G.R., Azyazov, V.N., and Mebel, A.M., "Reaction mechanism, rate constants, and product yields for the oxidation of Cyclopentadienyl and embedded five-member ring radicals with hydroxyl," *Combustion and Flame* 187:147–164, 2018, doi:10.1016/j.combustflame.2017.09.005.
[140] Ghildina, A.R., Oleinikov, A.D., Azyazov, V.N., and Mebel, A.M., "Reaction mechanism, rate constants, and product yields for unimolecular and H-assisted decomposition of 2,4-cyclopentadienone and oxidation of cyclopentadienyl with atomic oxygen," *Combustion and Flame* 183:181–193, 2017, doi:10.1016/j.combustflame.2017.05.015.

[141] Oleinikov, A.D., Azyazov, V.N., and Mebel, A.M., "Oxidation of cyclopentadienyl radical with molecular oxygen: A theoretical study," *Combustion and Flame* 191:309–319, 2018, doi:10.1016/j.combustflame.2018.01.010.

[142] Klippenstein, S.J., Harding, L.B., and Georgievskii, Y., "On the formation and decomposition of C7H8," *Proceedings of the Combustion Institute* 31(1):221–229, 2007, doi:10.1016/j.proci.2006.08.045.

[143] Oehlschlaeger, M.A., Davidson, D.F., and Hanson, R.K., "Experimental investigation of toluene + H -- benzyl + H2 at high temperatures," *The journal of physical chemistry. A* 110(32):9867–9873, 2006, doi:10.1021/jp062567t.

[144] Bounaceur, R., Da Costa, I., Fournet, R., Billaud, F. et al., "Experimental and modeling study of the oxidation of toluene," *Int. J. Chem. Kinet.* 37(1):25–49, 2005, doi:10.1002/kin.20047.

[145] Seta, T., Nakajima, M., and Miyoshi, A., "High-temperature reactions of OH radicals with benzene and toluene," *The journal of physical chemistry. A* 110(15):5081–5090, 2006, doi:10.1021/jp0575456.

[146] Oehlschlaeger, M.A., Davidson, D.F., and Hanson, R.K., "Investigation of the reaction of toluene with molecular oxygen in shock-heated gases," *Combustion and Flame* 147(3):195–208, 2006, doi:10.1016/j.combustflame.2006.08.006.

[147] Keita, M., Nicolle, A., and Bakali, A.E., "A wide range kinetic modeling study of PAH formation from liquid transportation fuels combustion," *Combustion and Flame* 174:50–67, 2016, doi:10.1016/j.combustflame.2016.09.016.

[148] Narayanaswamy, K., Blanquart, G., and Pitsch, H., "A consistent chemical mechanism for oxidation of substituted aromatic species," *Combustion and Flame* 157(10):1879–1898, 2010, doi:10.1016/j.combustflame.2010.07.009.

[149] da Silva, G. and Bozzelli, J.W., "Kinetic modeling of the benzyl+HO2 reaction," *Proceedings of the Combustion Institute* 32(1):287–294, 2009, doi:10.1016/j.proci.2008.05.040.

[150] Brezinsky, K., Litzinger, T.A., and Glassman, I., "The high temperature oxidation of the methyl side chain of toluene," *Int. J. Chem. Kinet.* 16(9):1053–1074, 1984, doi:10.1002/kin.550160902.

[151] Murakami, Y., Oguchi, T., Hashimoto, K., and Nosaka, Y., "Theoretical study of the benzyl+O2 reaction: Kinetics, mechanism, and product branching ratios," *The journal of physical chemistry. A* 111(50):13200–13208, 2007, doi:10.1021/jp075369q.

[152] da Silva, G. and Bozzelli, J.W., "Benzoxyl radical decomposition kinetics: Formation of benzaldehyde + H, phenyl + CH2O, and benzene + HCO," *The journal of physical chemistry. A* 113(25):6979–6986, 2009, doi:10.1021/jp902458d.

[153] da Silva, G., Hamdan, M.R., and Bozzelli, J.W., "Oxidation of the Benzyl Radical: Mechanism, Thermochemistry, and Kinetics for the Reactions of Benzyl Hydroperoxide," *Journal of chemical theory and computation* 5(12):3185–3194, 2009, doi:10.1021/ct900352f.

[154] da Silva, G., Chen, C.-C., and Bozzelli, J.W., "Toluene combustion: Reaction paths, thermochemical properties, and kinetic analysis for the methylphenyl radical + O2 reaction," *J. Phys. Chem. A* 111(35):8663–8676, 2007, doi:10.1021/jp068640x.

[155] Alzueta, M.U., Glarborg, P., and Dam-Johansen, K., "Experimental and kinetic modeling study of the oxidation of benzene," *Int. J. Chem. Kinet.* 32(8):498–522, 2000, doi:10.1002/1097-4601(2000)32:8<498::AID-KIN8>3.0.CO;2-H.

[156] Altarawneh, M., Dlugogorski, B.Z., Kennedy, E.M., and Mackie, J.C., "Theoretical study of reactions of HO2 in low-temperature oxidation of benzene," *Combustion and Flame* 157(7):1325–1330, 2010, doi:10.1016/j.combustflame.2009.12.020.

[157] Wang, H. and Frenklach, M., "A detailed kinetic modeling study of aromatics formation in laminar premixed acetylene and ethylene flames," *Combustion and Flame* 110(1-2):173–221, 1997, doi:10.1016/S0010-2180(97)00068-0.

[158] Saggese, C., Frassoldati, A., Cuoci, A., Faravelli, T. et al., "A wide range kinetic modeling study of pyrolysis and oxidation of benzene," *Combustion and Flame* 160(7):1168–1190, 2013, doi:10.1016/j.combustflame.2013.02.013.

[159] Taatjes, C.A., Osborn, D.L., Selby, T.M., Meloni, G. et al., "Products of the benzene + O(3P) reaction," *The journal of physical chemistry. A* 114(9):3355–3370, 2010, doi:10.1021/jp9114145.

[160] Glarborg, P., Miller, J.A., Ruscic, B., and Klippenstein, S.J., "Modeling nitrogen chemistry in combustion," *Progress in Energy and Combustion Science* 67:31–68, 2018, doi:10.1016/j.pecs.2018.01.002.

[161] Fuller, M.E. and Goldsmith, C.F., "On the relative importance of HONO versus HNO2 in low-temperature combustion," *Proceedings of the Combustion Institute* 37(1):695–702, 2018.

[162] Zhang, K., Glarborg, P., Zhou, X., Zhang, L. et al., "Experimental and Kinetic Modeling Study of Nitroethane Pyrolysis at a Low Pressure: Competition Reactions in the Primary Decomposition," *Energy Fuels* 30(9):7738–7745, 2016, doi:10.1021/acs.energyfuels.6b01348.

[163] Zeldovich, J., "The Oxidation of Nitrogen in Combustion and Explosions: Acta," *Physiochem*, 1946.

[164] Zhang, K., Zhang, L., Xie, M., Ye, L. et al., "An experimental and kinetic modeling study of premixed nitroethane flames at low pressure," *Proceedings of the Combustion Institute* 34(1):617–624, 2013, doi:10.1016/j.proci.2012.06.010.

[165] Zhang, Y.-X. and Bauer, S.H., "Gas-Phase Pyrolyses of 2-Nitropropane and 2-Nitropropanol: Shock-Tube Kinetics," *J. Phys. Chem. A* 104(6):1207–1216, 2000, doi:10.1021/jp993204e.

[166] Anderlohr, J.M., Bounaceur, R., Pires Da Cruz, A., and Battin-Leclerc, F., "Modeling of autoignition and NO sensitization for the oxidation of IC engine surrogate fuels," *Combustion and Flame* 156(2):505–521, 2009, doi:10.1016/j.combustflame.2008.09.009.

[167] Zhao, H., Wu, L., Patrick, C., Zhang, Z. et al., "Studies of low temperature oxidation of n-pentane with nitric oxide addition in a jet stirred reactor," *Combustion and Flame* 197:78–87, 2018, doi:10.1016/j.combustflame.2018.07.014.

[168] Rasmussen, C.L., Rasmussen, A.E., and Glarborg, P., "Sensitizing effects of NOx on CH4 oxidation at high pressure," *Combustion and Flame* 154(3):529–545, 2008, doi:10.1016/j.combustflame.2008.01.012.

[169] Dagaut, P., Lecomte, F., Chevailler, S., and Cathonnet, M., "Mutual Sensitization of the Oxidation of Nitric Oxide and Simple Fuels Over an Extended Temperature Range: Experimental and Detailed Kinetic Modeling," *Combustion Science and Technology* 148(1-6):27–57, 1999, doi:10.1080/00102209908935771.

[170] Glaude, P.-A., Marinov, N., Koshiishi, Y., Matsunaga, N. et al., "Kinetic Modeling of the Mutual Oxidation of NO and Larger Alkanes at Low Temperature," *Energy Fuels* 19(5):1839–1849, 2005, doi:10.1021/ef050047b.

[171] Chen, Z., Zhang, P., Yang, Y., Brear, M.J. et al., "Impact of nitric oxide (NO) on n-heptane autoignition in a rapid compression machine," *Combustion and Flame* 186:94–104, 2017, doi:10.1016/j.combustflame.2017.07.036.

[172] Howard, C.J., "Kinetic Study of the Equilibrium HO2 + NO = OH + NO2 and the Thermochemistry of HO2," *J. Am. Chem. Soc.* 102(23):6937–6941, 1980, doi:10.1021/ja00543a006.

[173] Bardwell, M.W., Bacak, A., Teresa Raventos, M., Percival, C.J. et al., "Kinetics of the HO 2 + NO reaction: A temperature and pressure dependence study using chemical ionisation mass spectrometry," *Phys. Chem. Chem. Phys.* 5(11):2381–2385, 2003, doi:10.1039/B300842H.

[174] Chen, C., Shepler, B.C., Braams, B.J., and Bowman, J.M., "Quasiclassical trajectory calculations of the HO2 + NO reaction on a global potential energy surface," *Phys. Chem. Chem. Phys.* 11(23):4722–4727, 2009, doi:10.1039/B823031E.

[175] Bacak, A., Bardwell, M.W., Raventos, M.T., Percival, C.J. et al., "Kinetics of the Reaction of CH3O2 + NO: A Temperature and Pressure Dependence Study with Chemical Ionization Mass Spectrometry," *J. Phys. Chem. A* 108(48):10681–10687, 2004, doi:10.1021/jp047764b.

[176] Butkovskaya, N., Kukui, A., and Le Bras, G., "Pressure and temperature dependence of methyl nitrate formation in the CH3O2 + NO reaction," *The journal of physical chemistry. A* 116(24):5972–5980, 2012, doi:10.1021/jp210710d.

[177] Lesar, A., Hodoscek, M., Drougas, E., and Kosmas, A.M., "Quantum mechanical investigation of the atmospheric reaction CH3O2 + NO," *J. Phys. Chem. A* 110(25):7898–7903, 2006, doi:10.1021/jp0614244.

[178] Maricq, M.M. and Szente, J.J., "Kinetics of the Reaction between Ethylperoxy Radicals and Nitric Oxide," *J. Phys. Chem.* 100(30):12374–12379, 1996, doi:10.1021/jp9607935.

[179] Ranschaert, D.L., Schneider, N.J., and Elrod, M.J., "Kinetics of the C 2 H 5 O 2 + NO x Reactions: Temperature Dependence of the Overall Rate Constant and the C2H5ONO 2 Branching Channel of C2H5O2 + NO," *J. Phys. Chem. A* 104(24):5758–5765, 2000, doi:10.1021/jp000353k.

[180] Atkinson, R., Baulch, D.L., Cox, R.A., Hampson, R.F. et al. *J. Phys. Chem. Ref. Data* 21:1125, 1992.

[181] Xu, Z.F. and Lin, M.C., "Kinetics and mechanism for the CH2O + NO2 reaction: A computational study," *Int. J. Chem. Kinet.* 35(5):184–190, 2003, doi:10.1002/kin.10115.

[182] Bornemann, H., Scheidt, F., and Sander, W., "Thermal decomposition of 2-ethylhexyl nitrate (2-EHN)," *Int. J. Chem. Kinet.* 34(1):34–38, 2002, doi:10.1002/kin.10017.

[183] Morin, J. and Bedjanian, Y., "Thermal decomposition of n-propyl and n-butyl nitrates: Kinetics and products," *Journal of Analytical and Applied Pyrolysis* 124:576–583, 2017, doi:10.1016/j.jaap.2017.01.014.

[184] Pritchard, H.O., "Thermal decomposition of isooctyl nitrate," *Combustion and Flame* 75(3-4):415–416, 1989, doi:10.1016/0010-2180(89)90052-7.

[185] Lewis, K.E. and Smith, G.P., "Bond dissociation energies in ferrocene," *J. Am. Chem. Soc.* 106:4650–4651, 1984.

[186] Tsang, W., "Chemical Kinetic Data Base for Combustion Chemistry Part V. Propene," *Journal of Physical and Chemical Reference Data* 20:221, 1991, doi:10.1063/1.555880.

[187] Stark, M.S., "Addition of Peroxyl Radicals to Alkenes and the Reaction of Oxygen with Alkyl Radicals," *J. Am. Chem. Soc.* 122(17):4162–4170, 2000, doi:10.1021/ja993760m.

[188] Rumminger, M.D., Reinelt, D., Babushok, V., and Linteris, G.T., "Numerical study of the inhibition of premixed and diffusion flames by iron Pentacarbonyl," *Combustion and Flame* 116(1-2):207–219, 1999, doi:10.1016/S0010-2180(98)00033-9.

[189] Plane, J.M.C. and Rollason, R.J., "A study of the reactions of Fe and FeO with NO2, and the structure and bond energy of FeO2," *Phys. Chem. Chem. Phys.* 1(8):1843–1849, 1999, doi:10.1039/a809896d.

[190] Giesen, A., Herzler, J., and Roth, P., "High temperature oxidation of iron atoms by CO2," *Phys. Chem. Chem. Phys.* 4(15):3665–3668, 2002, doi:10.1039/b201822e.

[191] Wen, J.Z., Goldsmith, C.F., Ashcraft, R.W., and Green, W.H., "Detailed Kinetic Modeling of Iron Nanoparticle Synthesis from the Decomposition of Fe(CO) 5," *J. Phys. Chem. C* 111(15):5677–5688, 2007, doi:10.1021/jp066579q.

[192] Kim, D.H., Mulholland, J.A., Wang, D., and Violi, A., "Pyrolytic hydrocarbon growth from cyclopentadiene," *The journal of physical chemistry. A* 114(47):12411–12416, 2010, doi:10.1021/jp106749k.

[193] Butler, R.G. and Glassman, I., "Cyclopentadiene combustion in a plug flow reactor near 1150K," *Proceedings of the Combustion Institute* 32(1):395–402, 2009, doi:10.1016/j.proci.2008.05.010.

[194] Ristori, A., Dagaut, P., Bakali, A.E.L., Pengloan, G. et al., "Benzene Oxidation: Experimental Results in a JDR and Comprehensive Kinetic Modeling in JSR, Shock-Tube and Flame," *Combustion Science and Technology* 167(1):223–256, 2001, doi:10.1080/00102200108952183.

[195] Zhang, J., Burklé-Vitzthum, V., and Marquaire, P.-M., "NO2-promoted oxidation of methane to formaldehyde at very short residence time. Part I: Experimental results," *Chemical Engineering Journal* 189-190:393–403, 2012, doi:10.1016/j.cej.2012.02.046.

[196] Dubreuil, A., Foucher, F., Mounaïm-Rousselle, C., Dayma, G. et al., "HCCI combustion: Effect of NO in EGR," *Proceedings of the Combustion Institute* 31(2):2879–2886, 2007, doi:10.1016/j.proci.2006.07.168.

[197] Glänzer, K. and Troe, J., "Thermische Zerfallsreaktionen von Nitroverbindungen I: Dissoziation von Nitromethan," *HCA* 55(8):2884–2893, 1972, doi:10.1002/hlca.19720550821.

[198] Mathieu, O., Giri, B., Agard, A.R., Adams, T.N. et al., "Nitromethane ignition behind reflected shock waves: Experimental and numerical study," *Fuel* 182:597–612, 2016, doi:10.1016/j.fuel.2016.05.060.

[199] Prausnitz, J.M., Lichtenthaler, R.N., and Gomez de Azevedo, E., "Molecular thermodynamics of fluid-phase equilibria," 3rd ed., Prentice-Hall, ISBN 0-13-977745-8, 1999.

[200] Schneider-electric, PRO II, Process Engineering.

[201] Mallard, E. and Le Chatelier, H.L., "Thermal Model for Flame Propagation," *Annales des mines* 4(18):379–568, 1883.

[202] Nakazawa, T. and Kaji, Y., "A density functional theory investigation of the reactions of Fe and FeO2 with O2," *Computational Materials Science* 117:455–467, 2016, doi:10.1016/j.commatsci.2016.01.023.

[203] Curran, H.J., "Developing detailed chemical kinetic mechanisms for fuel combustion," *Proceedings of the Combustion Institute*, 2018, doi:10.1016/j.proci.2018.06.054.

[204] Zhang, P., Yee, N.W., Filip, S.V., Hetrick, C.E. et al., "Modeling study of the anti-knock tendency of substituted phenols as additives: An application of the reaction mechanism generator (RMG)," *Physical chemistry chemical physics : PCCP* 20(16):10637–10649, 2018, doi:10.1039/c7cp07058f.

[205] Gao, C.W., Allen, J.W., Green, W.H., and West, R.H., "Reaction Mechanism Generator: Automatic construction of chemical kinetic mechanisms," *Computer Physics Communications* 203:212–225, 2016, doi:10.1016/j.cpc.2016.02.013.

[206] Bergthorson, J.M. and Thomson, M.J., "A review of the combustion and emissions properties of advanced transportation biofuels and their impact on existing and future engines," *Renewable and Sustainable Energy Reviews* 42:1393–1417, 2015, doi:10.1016/j.rser.2014.10.034.

[207] Nord, K., Haupt, D., Ahlvik, P., and Egebäck, K., "Particulate Emissions From an Ethanol Fueled Heavy-Duty Diesel Engine Equipped With EGR, Catalyst and DPF," *SAE Technical Paper 2004-01-1987*, 2004.

[208] Rodríguez-Fernández, J., Tsolakis, A., Theinnoi, K., Snowball, J. et al., "Engine Performance and Emissions from Dual Fuelled Engine with In-Cylinder Injected Diesel Fuels and In-Port Injected Bioethanol," *SAE Technical Paper 2009-01-1853*, 2009.

[209] Foong, T.M., Morganti, K.J., Brear, M.J., Silva, G. et al., "The octane numbers of ethanol blended with gasoline and its surrogates," *Fuel* 115:727–739, 2014.

[210] Iodice, P., Langella, G., and Amoresano, A., "Ethanol in gasoline fuel blends: Effect on fuel consumption and engine out emissions of SI engines in cold operating conditions," *Applied Thermal Engineering* 130:1081–1089, 2018, doi:10.1016/j.applthermaleng.2017.11.090.

[211] Siebers, D. and Edwards, C., "Autoignition of Methanol and Ethanol Sprays under Diesel Engine Conditions," *SAE Technical Paper 870588*, 1987.

[212] Aakko-Saksa, P.T., Westerholm, M., Pettinen, R., Söderström, C. et al., "Renewable methanol with ignition improver additive for diesel engines," *Energy & fuels : an American Chemical Society journal*, 2019, doi:10.1021/acs.energyfuels.9b02654.

[213] "Scania is ready for the rise of ethanol," https://www.scania.com/group/en/scania-is-ready-for-the-rise-of-ethanol/, December 20, 2019.

[214] Badra, J.A., Bokhumseen, N., Mulla, N., Sarathy, S.M. et al., "A methodology to relate octane numbers of binary and ternary n-heptane, iso-octane and toluene mixtures with simulated ignition delay times," *Fuel* 160:458–469, 2015, doi:10.1016/j.fuel.2015.08.007.

[215] Hartikka, T., Kiiski, U., Kuronen, M., and Mikkonen, S., "Diesel Fuel Oxidation Stability: A Comparative Study," SAE Technical Paper Series, SAE/KSAE 2013 International Powertrains, Fuels & Lubricants Meeting, OCT. 21, 2013, SAE International400 Commonwealth Drive, Warrendale, PA, United States, 2013.

[216] Rashed, M.M., Masjuki, H.H., Kalam, M.A., Alabdulkarem, A. et al., "A comprehensive study on the improvement of oxidation stability and NO x emission levels by antioxidant addition to biodiesel blends in a light-duty diesel engine," *RSC Adv* 6(27):22436–22446, 2016, doi:10.1039/C5RA26271B.

[217] İleri, E. and Koçar, G., "Experimental investigation of the effect of antioxidant additives on NOx emissions of a diesel engine using biodiesel," *Fuel* 125:44–49, 2014, doi:10.1016/j.fuel.2014.02.007.

Résumé étendu

Les préoccupations environnementales incitent les chercheurs à travailler à l'amélioration des moteurs à combustion interne (CI), qui sont principalement utilisés dans l'industrie automobile. Les moteurs CI sont tenus de fonctionner plus efficacement tout en réduisant les émissions polluantes et de gaz à effet de serre. L'optimisation de l'adéquation moteur-carburant est essentielle pour atteindre cet objectif. Parmi les paramètres physico-chimiques des carburants, la réactivité est la principale caractéristique qui doit être considérée. Cette caractéristique impacte non seulement l'efficacité de la combustion mais aussi le comportement du carburant dans le système de distribution. Compte tenu de l'évolution des systèmes de combustion et de l'incorporation de carburants alternatifs (carburants biosourcés, carburants synthétiques, etc.), l'utilisation d'additifs est une méthode efficace pour améliorer l'adéquation entre moteurs et carburants. Dans ce contexte, cette thèse vise à mieux comprendre l'effet chimique des additifs sur la réactivité en phase gazeuse des carburants en effectuant des études expérimentales et numériques. Le modèle cinétique développé permet l'évaluation des effets potentiels des additifs dans diverses conditions et pour divers carburants de base.

Grâce à une étude bibliographique, trois additifs ont été sélectionnés dans cette thèse : le 2-éthylhexyl nitrate (EHN), le ferrocène, et le 2,4-xylénol. Leur effet significatif comme booster de cétane, booster d'octane, et antioxydant en phase liquide, respectivement, a été démontré dans la littérature. La structure chimique des additifs est présentée dans la Figure R-1.

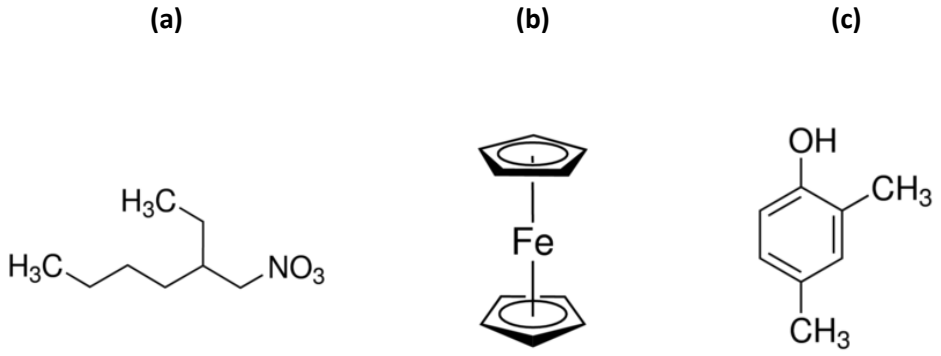

Figure R-1 : Structure chimique des additifs étudiés : (a) 2-éthylhexyl nitrate, (b) ferrocène, (c) 2,4-xylénol.

Pour comprendre l'effet chimique de ces additifs, un carburant modèle contenant 35% de *n*-heptane et 65% de toluène en volume a été adopté. Son indice d'octane (RON) est de 84. La définition de ce carburant modèle a été soutenue par la disponibilité de mécanismes de *n*-heptane et de toluène dans la littérature, ce qui facilite l'étude ultérieure des additifs par simulation. En outre, ce carburant permet d'examiner l'effet des additifs sur certains phénomènes spécifiques de la combustion, tels que les flammes froides et le coefficient négatif de température (« Negative Temperature Coefficient », NTC en anglais), domaine de température dans lequel la réactivité des hydrocarbures diminue tandis que la température augmente.

Un modèle cinétique détaillé a été développé dans cette thèse pour simuler l'effet des additifs sur la réactivité du carburant modèle. Ce modèle se compose de trois sous-mécanismes contenant des réactions d'oxydation du carburant modèle, des oxydes d'azote et des additifs. La structure du modèle est résumée graphiquement dans la Figure R-2.

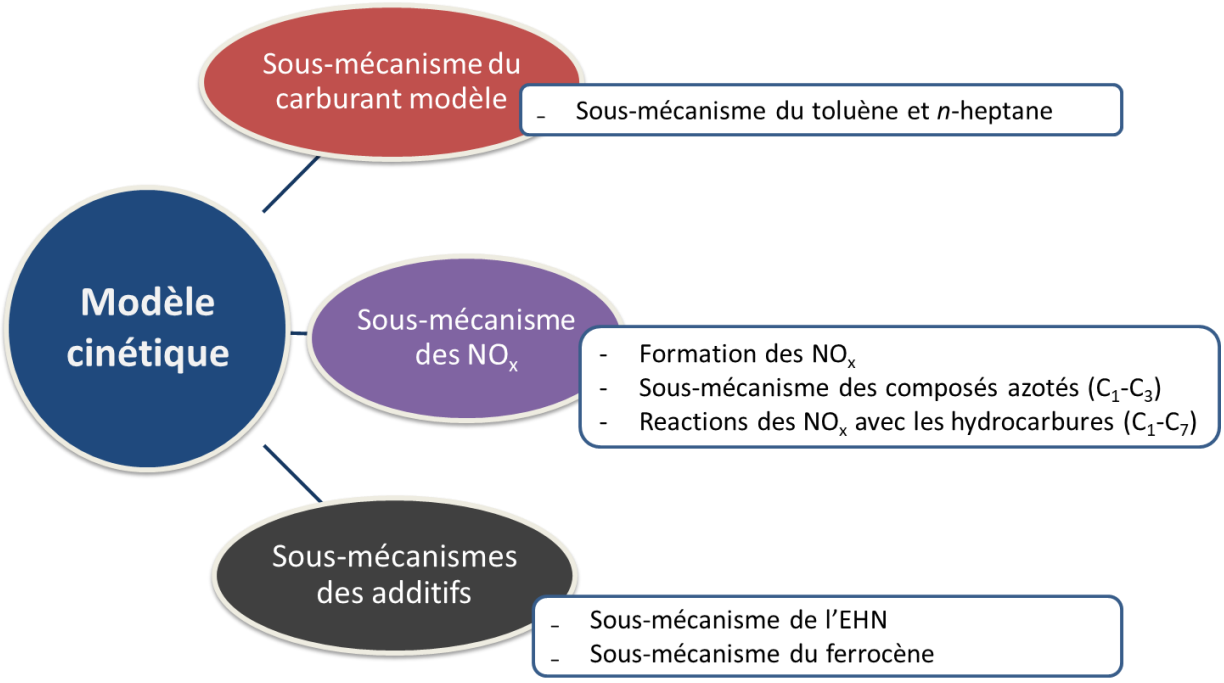

Figure R-2 : Structure du modèle cinétique développé dans cette thèse.

Le sous-mécanisme du carburant modèle a été adopté à partir du modèle du Laboratoire National du Lawrence Livermore (LLNL) [1], qui contient une chimie détaillée de l'oxydation du toluène et du *n*-heptane. Le sous-mécanisme du toluène a ensuite été mis à jour à l'aide des études récentes des molécules aromatiques publiées par Yuan et al. [2] et Keita et al. [3]. Les réactions mises à jour comprennent celles du toluène et de des radicaux et des molécules qui en dérivent, par exemple, les radicaux phényle, benzyle, méthylphényle, et le phénol, le crésol et les petits composés insaturés en C_2-C_4. L'importance des réactions du 1,3-cyclopentadiene (C_5H_6) et du radical cyclopentadiényle (C_5H_5) sur la réactivité du toluène a été soulignée par Yuan et al. [2]. Par conséquent, le sous-mécanisme du C_5H_6 a été mis à jour à l'aide des données récentes proposées par l'équipe de Mebel [4-6].

Le sous-mécanisme des NO_x a été développé grâce à des données de la littérature. Les réactions de formation des NO_x et de petits composés azotés (C_1-C_2) ont été adoptées à partir de la revue récente de Glarborg et al. [7]. Les réactions du nitroéthane proposées par Zhang et al. [8] ont été incluses dans le modèle. Un schéma similaire de réaction a été employé pour décrire la réactivité des deux isomères du nitropropane (1-nitropropane et 2-nitropropane). Les réactions des NO_x avec les hydrocarbures plus lourds (C_4-C_7) ont été prises dans le travail d'Anderlorh et al. [9].

Les produits de décomposition de l'EHN sont le radical 3-heptyle (C_7H_{15}-3), le formaldéhyde (CH_2O) et NO_2. La constante de vitesse de cette réaction est estimée selon les travaux expérimentaux de Pritchard et al. [10] et Bornemann et al. [11]. Les réactions de C_7H_{15}-3 et de CH_2O ont été incluses dans le modèle de référence [1].

Le sous-mécanisme du ferrocène ($FeC_{10}H_{10}$) a été construit en se basant sur les données de la littérature. La décomposition de cet additif a été décrite comme une décomposition en deux étapes. Tout d'abord, $FeC_{10}H_{10}$ libère le radical C_5H_5 et produit FeC_5H_5. La constante de vitesse de cette réaction a été adoptée à partir de travail de Lewis et al. [12]. La deuxième étape est la dissociation de FeC_5H_5 produisant Fe et C_5H_5. La cinétique de cette réaction a été estimée par Hirasawa et al. [13]. Le modèle contient des réactions des petits radicaux (H, OH, HO_2) avec le ferrocène estimées par Fenard et al. [14]. Des réactions du fer (Fe), d'oxydes de fer (FeO, FeO_2), d'hydroxides de fer (FeOH, $Fe(OH)_2$) et

d'autres composés contenant du fer (FeOOH, FeH) ont été adoptées à partir de travail de Rumminger et al. [15].

La validation du modèle développé est faite grâce aux données expérimentales disponibles dans la littérature. Les expériences considérées sont effectuées dans des conditions expérimentales différentes (température, pression) et avec plusieurs types de réacteur tels que les réacteur fermés (tube à onde de choc, machine à compression rapide), le réacteur parfaitement agité ou le réacteur à écoulement piston. La comparaison a été effectuée afin de valider les différents sous-mécanismes : la réactivité des composés aromatiques, y compris le toluène, le benzène et le 1,3-cyclopentadiene [2, 16-18], la réactivité des mélanges du toluène et *n*-heptane [19, 20], la chimie des composés azotés [8, 21-28] et l'effet promoteur de l'EHN [29]. L'étape de validation démontre un accord simulation-expérience satisfaisant concernant l'ensemble des données utilisées.

La Figure R-3 présente tous les dispositifs expérimentaux utilisés dans cette thèse pour étudier l'effet chimique des additifs sur la combustion du carburant. En effet, la réactivité en phase gazeuse d'un carburant peut être caractérisée notamment par les deux paramètres que sont le délai d'auto-inflammation et la vitesse de flamme.

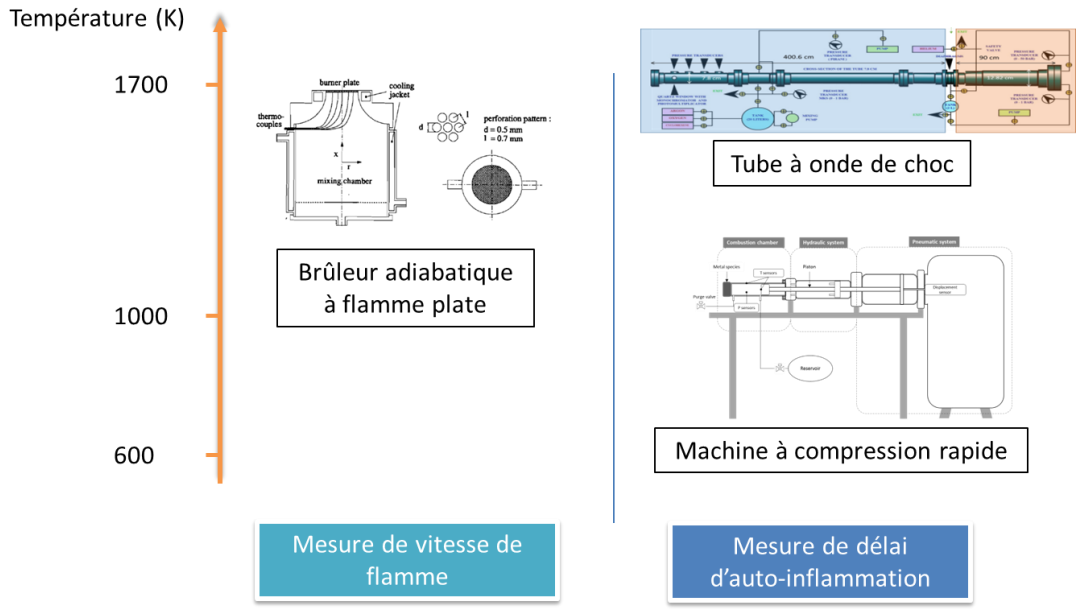

Figure R-3 : Présentation des dispositifs expérimentaux employés dans cette thèse avec l'intervalle de température de fonctionnement correspondant.

Un tube à onde de choc et une machine à compression rapide (MCR) ont été utilisés pour mesurer des délais d'auto-inflammation sur une large plage de température (600 à 1700 K). Le principe de fonctionnement de ces équipements est de compresser un mélange gazeux de carburant et de combustible jusqu'à une condition thermodynamique désirée (P, T). Dans un tube à onde de choc, la compression se fait par une onde de choc induite par une différence de pression. Dans le cas d'une MCR, le mouvement d'un piston compresse mécaniquement le mélange gazeux. Une fois que le carburant est amené dans les conditions thermodynamiques (P, T, Φ) dans lesquelles les réactions de combustion débutent, il faut un certain temps jusqu'à ce que le carburant s'enflamme, c'est-à-dire qu'une une forte augmentation de la pression et de température soit observée. Cette période définit le délai d'auto-inflammation d'un carburant dans une condition considérée. Ce délai dépend notablement de la température et de la pression, ainsi que de la nature du combustible et du mélange réactif caractérisé par la richesse et la dilution. Dans la pratique, la valeur absolue du délai d'auto-

inflammation est définie spécifiquement selon chaque méthode expérimentale. Alors qu'un tube à onde de choc est utilisé pour mesurer la réactivité du carburant à haute température (T > 900 K) [30], une MCR permet de caractériser l'auto-inflammation d'un carburant dans une plage de température plus basse (T < 900 K) [31]. Dans les conditions des expériences en tube à onde de choc, les réactions de décomposition unimoléculaire sont favorisées. D'autre part, la chimie des peroxydes pilote la réactivité à basse température d'un carburant dans des expériences d'un MCR. A des températures intermédiaires (750 < T < 900 K), certains phénomènes particuliers de combustion d'un carburant apparaissent, comme le NTC et l'apparition de flammes froides suivie d'une auto-inflammation de deuxième stade. L'impact des additifs sur ces phénomènes peut être étudié dans ce dernier appareillage. Cet aspect est encore peu discuté dans la littérature.

La vitesse de flamme est une propriété importante d'un carburant qui permet de contrôler la combustion dans les moteurs. Dans cette thèse, l'impact des additifs sur la vitesse de flamme du carburant modèle a été étudié dans un brûleur adiabatique à flamme plate prémélangée. La méthode du flux de chaleur est employée dans ce brûleur pour mesurer la vitesse de flamme dans des conditions de flammes stabilisées adiabatiques.

Les données obtenues à partir de ces équipements expérimentaux sont à la fois fondamentales et essentielles pour valider le modèle cinétique développé. Ensuite, le modèle validé permet d'analyser et de comprendre l'effet chimique des additifs et par la suite de prédire leur impact dans des conditions différentes. Les expériences en tube à onde de choc ont été effectuées au Laboratoire Réactions et Génie des Procédés (LRGP) à Nancy. En outre, les expériences avec le brûleur adiabatique à flamme plate ont été effectuées au LRGP par Matieyendu Goussougli [32] pendant son stage de Master. Enfin, les expériences en MRC ont été menées au laboratoire Pluridisciplinaire de Recherche en Ingénierie des Systèmes, Mécanique, Énergétique (PRISME) à Orléans.

Dans les expériences en MCR, les délais d'auto-inflammation des carburants ont été mesurés à 10 bar, T_c = 675 à 1000 K (T_c : température atteinte dans la chambre en fin de compression), à richesses pauvre (Φ = 0.5) et stœchiométrique. Les concentrations des additifs ont été fixées à 0,1 et 1% mol. Pour le ferrocène, sa concentration a été imposée à 0,01 et 0,1 % mol. pour éviter la formation de dépôts. Ces concentrations sont représentatives des niveaux de dopage des additifs identifiés dans la littérature. Des flammes froides et un NTC ont été observés dans le cas du carburant modèle pur, sans additifs. L'EHN montre un effet promoteur sur la réactivité du carburant modèle, y compris sur le délai de flamme froide et la zone du NTC. Un dégagement de chaleur pendant le processus de compression, avant que le piston n'atteigne le point mort haut, est observé dans les expériences avec les carburants dopés par l'EHN en raison de la décomposition rapide de ce composé à des températures T_c supérieures à 750 K. Cela implique que la réaction chimique du mélange gazeux pendant le processus de compression doit être soigneusement prise en compte pour obtenir des simulations fiables. D'autre part, le ferrocène montre un effet inhibiteur. Cet effet est faible sur le délai de flamme froide, mais significatif sur l'auto-inflammation principale du carburant modèle, quelle que soit la richesse. Le ferrocène renforce le NTC. Cet additif provoque une variation plus importante de la réactivité entre le maximum et le minimum de la réactivité. L'effet de l'EHN et du ferrocène augmente avec la température et leur concentration. Contrairement à ces deux additifs, le 2,4 xylénol n'influence pas notablement la réactivité du carburant modèle dans les conditions de la MCR.

La mesure des délais d'auto-inflammation a également été effectuée sur une plage de hautes températures (de 1350 à 1600 K) dans le tube de choc sous 10 bars et à la stœchiométrie. Les concentrations des additifs ont été fixés à 1% massique pour l'EHN et le 2,4-xylénol et à 0,1% massique pour le ferrocène lors de la préparation des carburants dans la phase liquide. Les mélanges gazeux de

carburant pour les mesures ont été préparés à température ambiante (≈ 25°C). Il convient de noter que les concentrations des additifs en phase gazeuse des additifs étaient plus faibles que celles en phase liquide en raison de leur pression de vapeur plus faible que celles des composants du carburant modèle. Les concentrations des phases gazeuses obtenues à 25°C ont été évaluées par simulation thermodynamique de l'équilibre de phases. Dans les conditions à haute température, aucun additif n'a un impact significatif sur la réactivité du carburant modèle.

L'influence des additifs sur la vitesse de flamme du carburant modèle a été examinée dans le brûleur adiabatique à flamme plate prémélangée. Des expériences ont été menés à la pression atmosphérique et à une température initiale de 398 K. Les concentrations des additifs ont été fixées comme dans les expériences sur le tube à onde de choc. Il est constaté que les additifs n'ont pas d'impact remarquable sur la vitesse de flamme du carburant modèle. En effet, les mesures de la vitesse de flamme impliquent la chimie à haute température du carburant modèle, sur laquelle les additifs montrent peu d'influence.

Le 2,4-xylénol ne montre aucun effet expérimental sur la réactivité du carburant modèle. Ceci tend à confirmer que l'utilisation de 2,4-xylenol comme antioxydant à une concentration inférieure à 1% mol. ne donne aucun effet secondaire sur la réactivité en phase gazeuse.

Tous les résultats expérimentaux du carburant modèle sans et avec additif sont bien simulés par le modèle cinétique développé dans ce travail. Pour les simulations de la MCR, le processus de compression est pris en compte pour reproduire correctement les résultats expérimentaux. Par simulation, l'effet promoteur de l'EHN dans le domaine de basse température (T à 1000 K) apparait lié aux réactions chimiques du radical heptyle C_7H_{15}-3 et à une boucle des espèces NO_2-NO, qui met en jeu les réactions R + NO_2 = RO + NO et RO_2 + NO = RO + NO_2. Les réactions du radical C_7H_{15}-3 et la réaction NO + HO_2 = NO_2 + OH génèrent une source supplémentaire de radicaux OH. En outre, NO_2 peut réagir avec le radical benzyle ($C_6H_5CH_2$) pour former le radical $C_6H_5CH_2O$ radical et NO. Cette réaction augmente la réactivité du toluène, et aussi la réactivité globale du carburant modèle. Les réactions entre NO et les radicaux $C_7H_{15}OO$ sont l'origine principale de l'effet promoteur de l'EHN dans la région du NTC. Il est également constaté que la formation de nitroéthane ($C_2H_5NO_2$), qui transforme le NO_2 actif en une espèce stable, réduit l'effet promoteur de l'EHN autour de 740 K.

Pour améliorer la performance du modèle du ferrocène, des réactions supplémentaires entre des espèces contenant du fer et des radicaux tels que HO_2, $C_6H_5CH_2$, $C_6H_5CH_2OO$ produisant des composés peu réactifs, ont été proposées pour reproduire l'effet inhibiteur du ferrocène à toutes les richesses (Φ = 0,5 et 1) dans la plage de basse température (T < 1000 K). En comparaison avec l'EHN, le ferrocène est beaucoup plus stable. Cette thèse émet l'hypothèse que l'effet chimique du ferrocène est liée à la formation d'alcools. Les réactions des radicaux $C_6H_5CH_2$, $C_6H_5CH_2OO$ avec des espèces contenant du fer permettent cette voie. Il est aussi constaté que le ferrocène entraîne une variation plus importante de la réactivité entre le maximum et le minimum de la réactivité dans la région du NTC en consommant les radicaux HO_2 produits par la décomposition des radicaux $C_7H_{15}OO$ en heptènes (C_7H_{14}).

Le modèle cinétique validé a été utilisé pour prédire l'effet de l'EHN et du ferrocène sur différents carburants dans diverses conditions. Il est observé que l'EHN peut réduire les délais d'auto-inflammation de l'éthanol. Cet effet est sensible à la variation de concentration de l'EHN, mais peu dépendant de la pression et de la richesse. De plus, l'influence de l'EHN et du ferrocène sur le RON des carburants contenant du toluène et du *n*-heptane a été examinée numériquement. Comme prévu, l'EHN et le ferrocène augmentent et diminuent respectivement le RON. L'effet de l'EHN dépend du RON initial du carburant et augmente non linéairement avec sa concentration. Cela est cohérent avec les résultats expérimentaux de Ghosh et al. [33]. Inversement, la réactivité du carburant de base

n'affecte pas l'amplitude de l'effet du ferrocène et cet effet augmente quasiment linéairement avec la concentration de cet additif.

Cette thèse contribue à la compréhension fondamentale de l'effet des additifs sur la réactivité du carburant. Le modèle cinétique validé peut aider efficacement à étudier l'effet promoteur de l'EHN et l'effet inhibiteur du ferrocène dans différentes simulations de moteur.

Cette étude permet de proposer des perspectives, y compris des travaux expérimentaux et numériques, pour une exploration plus poussée des additifs de carburant. La stabilité à l'oxydation est une caractéristique importante du carburant. Caractériser l'impact des additifs sur la réactivité en phase liquide, qui n'a pas pu être effectuée dans ce travail, est essentiel pour garantir leur utilisation optimale dans les moteurs. De plus, des calculs théoriques consacrés à la chimie du ferrocène et de ses produits de décomposition et des expériences en moteur comprenant les mesures de RON et de délai d'auto-inflammation, sont nécessaires pour améliorer la performance du modèle cinétique en phase gazeuse. Les travaux envisagés sont décrits ci-dessous :

- L'EHN n'est pas thermiquement stable. La dégradation de l'EHN pourrait se produire dans le système de distribution de carburant et avoir un impact sur la stabilité à l'oxydation du carburant. Cet aspect a été discuté dans plusieurs études. Hartikka et coll. [34] ont indiqué que l'EHN a diminué la stabilité à l'oxydation d'un carburant diesel. Cependant, cet additif a augmenté la stabilité à l'oxydation d'un biodiesel B20 rapporté par Rashed et al. [35] et Ileri et al. [36]. L'effet antioxydant de l'EHN dépend de la chimie du carburant de base. Dans le cas du 2,4-xylenol, cet additif a été identifié comme un antioxydant efficace dans la littérature [37]. À notre connaissance, aucun modèle cinétique n'a été développé dans la littérature pour prévoir l'impact du 2,4-xylenol sur la réactivité liquide-phase. De même, l'influence du ferrocène sur la stabilité à l'oxydation des carburants n'a pas été étudiée expérimentalement et théoriquement. Par conséquent, les expériences et les études numériques concernant l'autoxydation sont essentielles pour explorer systématiquement l'impact de l'EHN, du 2,4-xylénol et du ferrocène sur la réactivité en phase liquide et le vieillissement des carburants.

- Ce travail fournit un ensemble original de données expérimentales combinées à un premier modèle cinétique détaillé pour le ferrocène capable de modéliser le comportement de cet additif sur la plage considérée de pression, de température et de richesse. Grâce à cette méthodologie, cette étude met en évidence certains types de réactions sensibles à l'effet promoteur du ferrocène. Pour mieux étudier ces réactions, des calculs quantiques pour les espèces contenant du fer sont prévues. Cette méthode est difficile mais réalisable. Bien que les données numériques disponibles sur la thermochimie des espèces du fer montrent d'importantes disparités, par exemple pour FeO_2 [38], les calculs quantiques aideraient en effet à caractériser l'effet potentiel d'une espèce mineure potentielle non considérée dans le modèle actuel ainsi que d'autres voies pertinentes que celles proposées dans cette thèse.

- Les prédictions des effets de l'EHN et du ferrocène sur le RON des carburants ont été effectuées à l'aide du modèle cinétique développé. Pour valider cette approche, certaines mesures expérimentales de RON des carburants devraient être réalisées en banc moteur. Une fois validée, cette méthode peut être utilisée pour reformuler efficacement les carburants pour des moteurs spécifiques.

- L'effet des additifs sur la réactivité en phase gazeuse à haute température (T > 1300 K) a été étudié dans le tube à onde de choc à LRGP dans ce travail. Comme les pressions de vapeur des composés sont différentes, la principale difficulté des expériences sur le tube à onde de choc

était d'obtenir la composition souhaitée des mélanges gazeux. Par conséquent, un système de chauffage devrait être employé pour assurer l'évaporation totale des composés dans le réservoir de préparation des mélanges. Une fois établies, des expériences sur le tube à onde de choc seraient menées pour mieux caractériser l'effet des additifs à haute température.

Références du résumé étendu

[1] Mehl, M., Pitz, W.J., Westbrook, C.K., and Curran, H.J., "Kinetic modeling of gasoline surrogate components and mixtures under engine conditions," *Proc. Combust. Inst.* 33(1):193–200, 2011, doi:10.1016/j.proci.2010.05.027.

[2] Yuan, W., Li, Y., Dagaut, P., Yang, J. et al., "Investigation on the pyrolysis and oxidation of toluene over a wide range conditions. II. A comprehensive kinetic modeling study," *Combustion and Flame* 162(1):22–40, 2015, doi:10.1016/j.combustflame.2014.07.011.

[3] Keita, M., Nicolle, A., and Bakali, A.E., "A wide range kinetic modeling study of PAH formation from liquid transportation fuels combustion," *Combustion and Flame* 174:50–67, 2016, doi:10.1016/j.combustflame.2016.09.016.

[4] Galimova, G.R., Azyazov, V.N., and Mebel, A.M., "Reaction mechanism, rate constants, and product yields for the oxidation of Cyclopentadienyl and embedded five-member ring radicals with hydroxyl," *Combustion and Flame* 187:147–164, 2018, doi:10.1016/j.combustflame.2017.09.005.

[5] Ghildina, A.R., Oleinikov, A.D., Azyazov, V.N., and Mebel, A.M., "Reaction mechanism, rate constants, and product yields for unimolecular and H-assisted decomposition of 2,4-cyclopentadienone and oxidation of cyclopentadienyl with atomic oxygen," *Combustion and Flame* 183:181–193, 2017, doi:10.1016/j.combustflame.2017.05.015.

[6] Oleinikov, A.D., Azyazov, V.N., and Mebel, A.M., "Oxidation of cyclopentadienyl radical with molecular oxygen: A theoretical study," *Combustion and Flame* 191:309–319, 2018, doi:10.1016/j.combustflame.2018.01.010.

[7] Glarborg, P., Miller, J.A., Ruscic, B., and Klippenstein, S.J., "Modeling nitrogen chemistry in combustion," *Progress in Energy and Combustion Science* 67:31–68, 2018, doi:10.1016/j.pecs.2018.01.002.

[8] Zhang, K., Glarborg, P., Zhou, X., Zhang, L. et al., "Experimental and Kinetic Modeling Study of Nitroethane Pyrolysis at a Low Pressure: Competition Reactions in the Primary Decomposition," *Energy Fuels* 30(9):7738–7745, 2016, doi:10.1021/acs.energyfuels.6b01348.

[9] Anderlohr, J.M., Bounaceur, R., Pires Da Cruz, A., and Battin-Leclerc, F., "Modeling of autoignition and NO sensitization for the oxidation of IC engine surrogate fuels," *Combustion and Flame* 156(2):505–521, 2009, doi:10.1016/j.combustflame.2008.09.009.

[10] Pritchard, H.O., "Thermal decomposition of isooctyl nitrate," *Combustion and Flame* 75(3-4):415–416, 1989, doi:10.1016/0010-2180(89)90052-7.

[11] Bornemann, H., Scheidt, F., and Sander, W., "Thermal decomposition of 2-ethylhexyl nitrate (2-EHN)," *Int. J. Chem. Kinet.* 34(1):34–38, 2002, doi:10.1002/kin.10017.

[12] Lewis, K.E. and Smith, G.P., "Bond dissociation energies in ferrocene," *J. Am. Chem. Soc.* 106:4650–4651, 1984.

[13] Hirasawa, T., Sung, C.-J., Yang, Z., Joshi, A. et al., "Effect of ferrocene addition on sooting limits in laminar premixed ethylene–oxygen–argon flames," *Combustion and Flame* 139(4):288–299, 2004, doi:10.1016/j.combustflame.2004.09.002.

[14] Fenard, Y., Song, H., Dauphin, R., and Vanhove, G., "An engine-relevant kinetic investigation into the anti-knock effect of organometallics through the example of ferrocene," *Proc. Combust. Inst.* 37:547–554, 2019, doi:10.1016/j.proci.2018.06.135.

[15] Rumminger, M.D., Reinelt, D., Babushok, V., and Linteris, G.T., "Numerical study of the inhibition of premixed and diffusion flames by iron Pentacarbonyl," *Combustion and Flame* 116(1-2):207–219, 1999, doi:10.1016/S0010-2180(98)00033-9.

[16] Kim, D.H., Mulholland, J.A., Wang, D., and Violi, A., "Pyrolytic hydrocarbon growth from cyclopentadiene," *The journal of physical chemistry. A* 114(47):12411–12416, 2010, doi:10.1021/jp106749k.

[17] Butler, R.G. and Glassman, I., "Cyclopentadiene combustion in a plug flow reactor near 1150K," *Proceedings of the Combustion Institute* 32(1):395–402, 2009, doi:10.1016/j.proci.2008.05.010.

[18] Ristori, A., Dagaut, P., Bakali, A.E.L., Pengloan, G. et al., "Benzene Oxidation: Experimental Results in a JDR and Comprehensive Kinetic Modeling in JSR, Shock-Tube and Flame," *Combustion Science and Technology* 167(1):223–256, 2001, doi:10.1080/00102200108952183.

[19] Hartmann, M., Gushterova, I., Fikri, M., Schulz, C. et al., "Auto-ignition of toluene-doped n-heptane and iso-octane/air mixtures: High-pressure shock-tube experiments and kinetics modeling," *Combustion and Flame* 158(1):172–178, 2011, doi:10.1016/j.combustflame.2010.08.005.

[20] Herzler, J., Fikri, M., Hitzbleck, K., Starke, R. et al., "Shock-tube study of the autoignition of n-heptane/toluene/air mixtures at intermediate temperatures and high pressures," *Combustion and Flame* 149(1-2):25–31, 2007, doi:10.1016/j.combustflame.2006.12.015.

[21] Moréac, G., Dagaut, P., Roesler, J.F., and Cathonnet, M., "Nitric oxide interactions with hydrocarbon oxidation in a jet-stirred reactor at 10 atm," *Combustion and Flame* 145(3):512–520, 2006, doi:10.1016/j.combustflame.2006.01.002.

[22] Zhang, Y.-X. and Bauer, S.H., "Gas-Phase Pyrolyses of 2-Nitropropane and 2-Nitropropanol: Shock-Tube Kinetics," *J. Phys. Chem. A* 104(6):1207–1216, 2000, doi:10.1021/jp993204e.

[23] Rasmussen, C.L., Rasmussen, A.E., and Glarborg, P., "Sensitizing effects of NOx on CH4 oxidation at high pressure," *Combustion and Flame* 154(3):529–545, 2008, doi:10.1016/j.combustflame.2008.01.012.

[24] Dagaut, P., Lecomte, F., Chevailler, S., and Cathonnet, M., "Mutual Sensitization of the Oxidation of Nitric Oxide and Simple Fuels Over an Extended Temperature Range: Experimental and Detailed Kinetic Modeling," *Combustion Science and Technology* 148(1-6):27–57, 1999, doi:10.1080/00102209908935771.

[25] Zhang, J., Burklé-Vitzthum, V., and Marquaire, P.-M., "NO2-promoted oxidation of methane to formaldehyde at very short residence time. Part I: Experimental results," *Chemical Engineering Journal* 189-190:393–403, 2012, doi:10.1016/j.cej.2012.02.046.

[26] Dubreuil, A., Foucher, F., Mounaïm-Rousselle, C., Dayma, G. et al., "HCCI combustion: Effect of NO in EGR," *Proceedings of the Combustion Institute* 31(2):2879–2886, 2007, doi:10.1016/j.proci.2006.07.168.

[27] Glänzer, K. and Troe, J., "Thermische Zerfallsreaktionen von Nitroverbindungen I: Dissoziation von Nitromethan," *HCA* 55(8):2884–2893, 1972, doi:10.1002/hlca.19720550821.

[28] Mathieu, O., Giri, B., Agard, A.R., Adams, T.N. et al., "Nitromethane ignition behind reflected shock waves: Experimental and numerical study," *Fuel* 182:597–612, 2016, doi:10.1016/j.fuel.2016.05.060.

[29] Hartmann, M., Tian, K., Hofrath, C., Fikri, M. et al., "Experiments and modeling of ignition delay times, flame structure and intermediate species of EHN-doped stoichiometric n-heptane/air combustion," *Proc. Combust. Inst.* 32(1):197–204, 2009, doi:10.1016/j.proci.2008.06.068.

[30] Hanson, R.K. and Davidson, D.F., "Recent advances in laser absorption and shock tube methods for studies of combustion chemistry," *Progress in Energy and Combustion Science* 44:103–114, 2014, doi:10.1016/j.pecs.2014.05.001.

[31] Goldsborough, S.S., Hochgreb, S., Vanhove, G., Wooldridge, M.S. et al., "Advances in rapid compression machine studies of low- and intermediate-temperature autoignition phenomena," *Progress in Energy and Combustion Science* 63:1–78, 2017, doi:10.1016/j.pecs.2017.05.002.

[32] Goussougli, M., "Délai d'Auto-Inflammation en Tube à Onde de Choc d'Additifs Améliorateurs d'Indice Octane des Essences," Manuscrit de master, Université de Lorraine-Mines Nancy, 2019.

[33] Ghosh, P., "Predicting the Effect of Cetane Improvers on Diesel Fuels," *Energy Fuels* 22(2):1073–1079, 2008, doi:10.1021/ef0701079.

[34] Hartikka, T., Kiiski, U., Kuronen, M., and Mikkonen, S., "Diesel Fuel Oxidation Stability: A Comparative Study," SAE Technical Paper Series, SAE/KSAE 2013 International Powertrains, Fuels & Lubricants Meeting, OCT. 21, 2013, SAE International400 Commonwealth Drive, Warrendale, PA, United States, 2013.

[35] Rashed, M.M., Masjuki, H.H., Kalam, M.A., Alabdulkarem, A. et al., "A comprehensive study on the improvement of oxidation stability and NO x emission levels by antioxidant addition to biodiesel blends in a light-duty diesel engine," *RSC Adv* 6(27):22436–22446, 2016, doi:10.1039/C5RA26271B.

[36] İleri, E. and Koçar, G., "Experimental investigation of the effect of antioxidant additives on NOx emissions of a diesel engine using biodiesel," *Fuel* 125:44–49, 2014, doi:10.1016/j.fuel.2014.02.007.

[37] McCormick, R.L., Ratcliff, M.A., Christensen, E., Fouts, L. et al., "Properties of Oxygenates Found in Upgraded Biomass Pyrolysis Oil as Components of Spark and Compression Ignition Engine Fuels," *Energy Fuels* 29(4):2453–2461, 2015, doi:10.1021/ef502893g.

[38] Nakazawa, T. and Kaji, Y., "A density functional theory investigation of the reactions of Fe and FeO2 with O2," *Computational Materials Science* 117:455–467, 2016, doi:10.1016/j.commatsci.2016.01.023.

Appendix

A1. Kinetic model validation

Experiments conducted in plug flow reactors

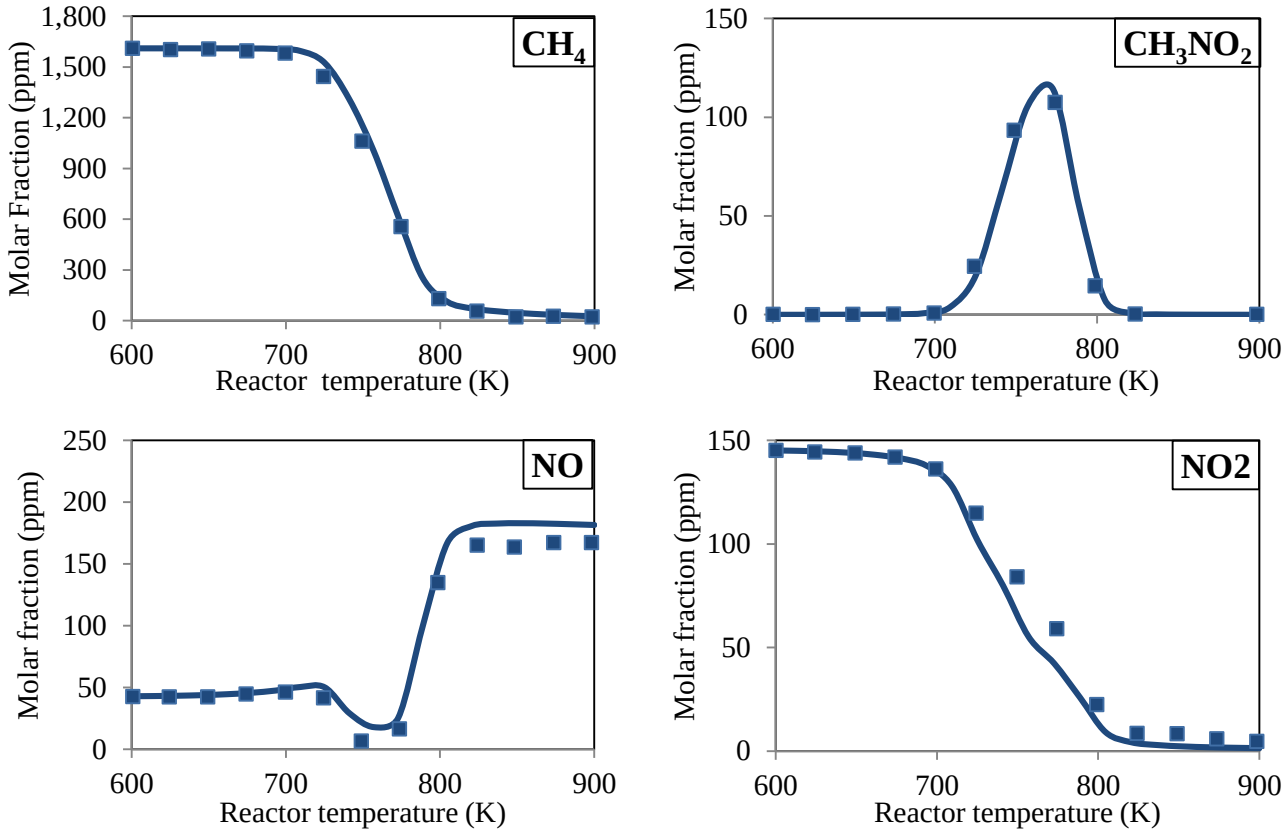

Figure A-1: Species profiles of CH_4, CH_3NO_2, NO and NO_2 at 50 atm, Φ = 1.15, from 500 to 900 K. Symbols: experimental results. Lines: simulations results. Initial fuel mixture: CH_4 (1610 ppm)/ NO (43 ppm)/ NO_2 (145 ppm)/ O_2 (2798 ppm)/ N_2 (99.54% mol.). Experiments conducted by Rasmussen et al.[168].

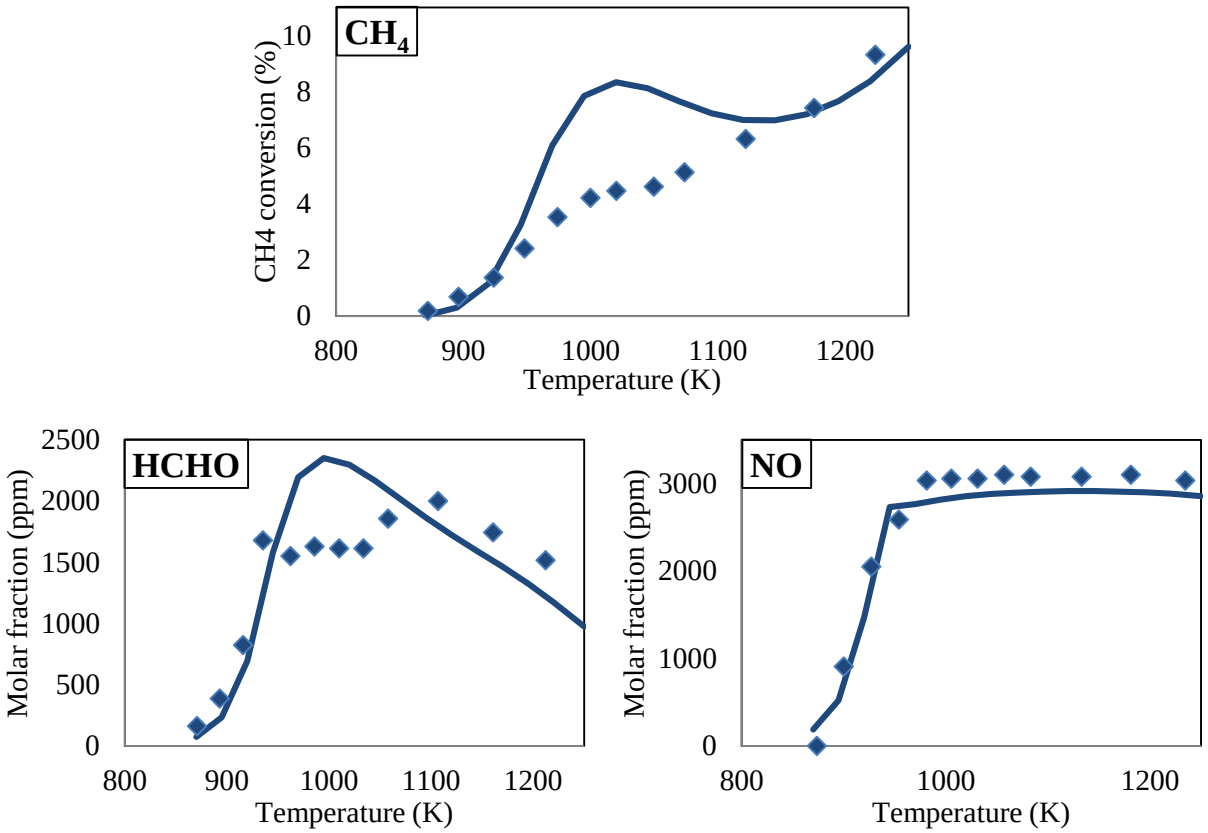

Figure A-2: CH_4 conversion and concentrations of HCHO and NO as a function of reactor temperature. Experimental conditions: 2 bar, Φ = 4. Symbols: experimental results. Lines: simulations results. Initial fuel mixture: CH_4 (6667 ppm)/ NO_2 (300 ppm)/ O_2 (3.3% mol.)/ Ar (89.7% mol.). Experiments conducted by Zhang et al.[195].

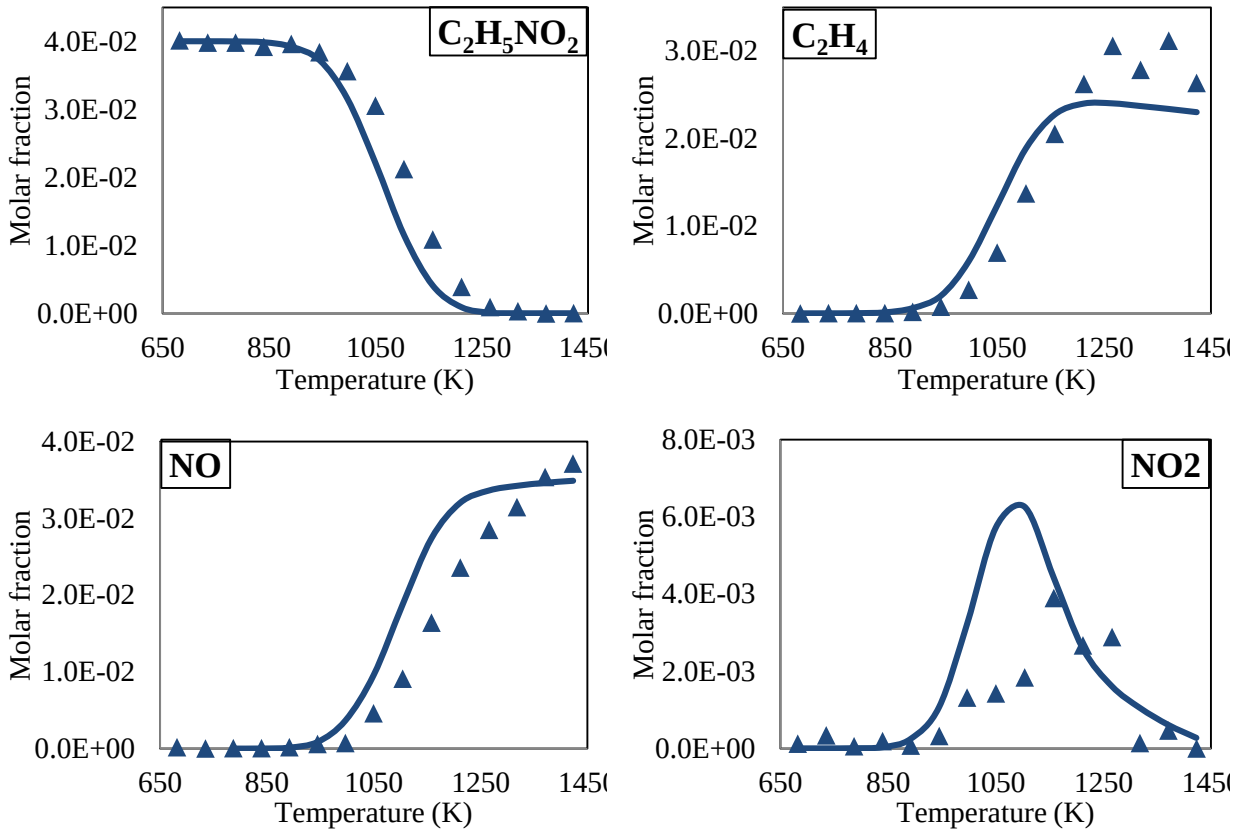

Figure A-3: Species profiles of $C_2H_5NO_2$, C_2H_4, NO and NO_2 as a function of reactor temperature during $C_2H_5NO_2$ pyrolysis. Experimental conditions: 5 torr, from 650 to 1450 K. Symbols: experimental results. Lines: simulations results. Initial fuel mixture: $C_2H_5NO_2$ (4% mol.)/ Ar (96% mol.) Experiments conducted by Zhang et al.[162].

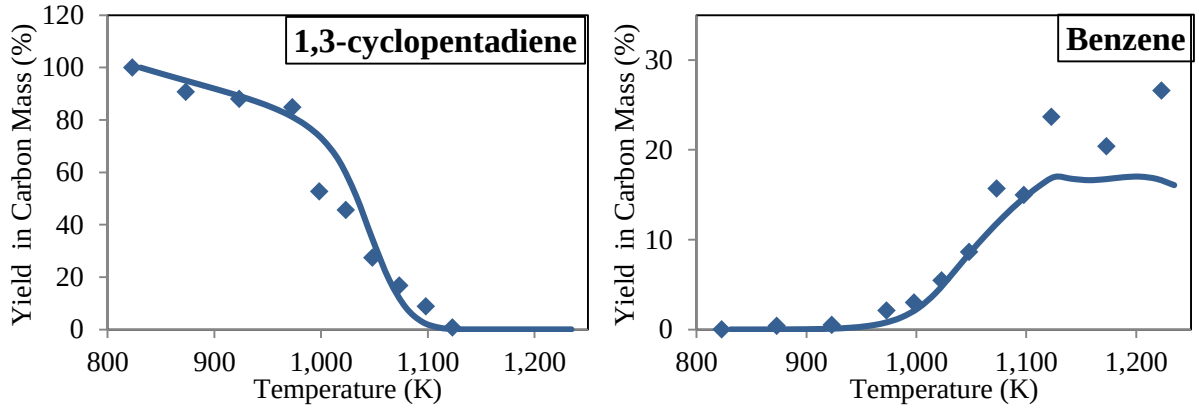

Figure A-4: Conversion of 1,3-cyclopentadiene and benzene as afunction of reactor temperature during 1,3-cyclopentadiene pyrolysis at 1 atm, reisdence time of 3 s, from 800 to 1200 K. Symbols: experimental results. Lines: simulations results. Initial fuel mixture: 0.7 % mol. of 1,3-cyclopentadiene in N_2. Experiments conducted by Kim et al.[192].

Experiments conducted in perfectly stirred reactors

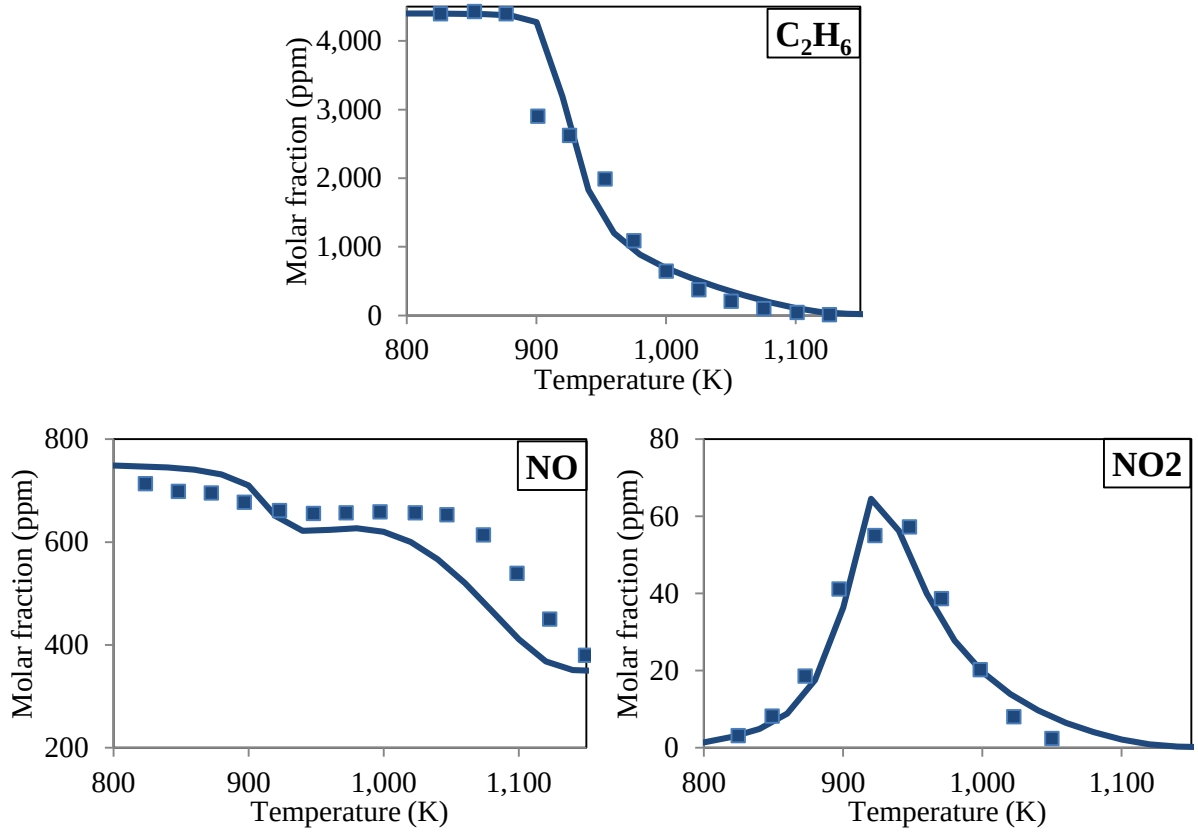

Figure A-5: Species profiles of C_2H_6, NO, NO_2 as a function of reactor temperature. Experimental conditions: 1 atm, Φ = 1, residence time: 0.13 s. Symbols: experimental results. Lines: simulations results. Initial fuel mixture: C_2H_6 (4400 ppm)/ NO (750 ppm)/ O_2 (1.54% mol.)/ N_2 (97.95% mol.) . Experiments conducted by Dagaut et al.[169].

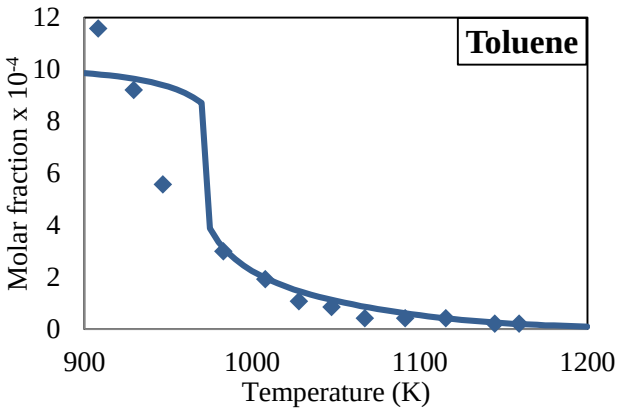

Figure A-6: Species profiles of toluene as a function of reactor temperature. Experimental conditions: 10 atm, Φ = 1, residence time: 0.6 s. Symbols: experimental results. Lines: simulations results. Initial fuel mixture: toluene (0.1 % mol.), O_2 (0.9 % mol.) in N_2. Experiments conducted by Yuan et al.[105].

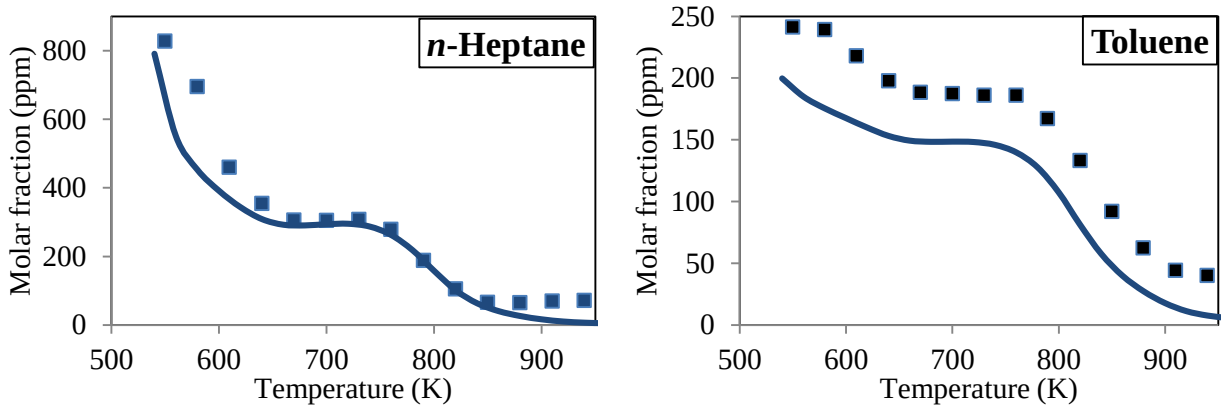

Figure A-7: Species profiles of *n*-heptane and toluene as a function of reactor temperature. Experimental conditions: 10 atm, Φ = 0.2, residence time: 0.5 s. Symbols: experimental results. Lines: simulations results. Initial fuel mixture: *n*-heptane (800 ppm)/ toluene (200 ppm)/ NO (50 ppm)/ O_2 (5.3% mol.)/ N_2 (94.6% mol.) . Experiments conducted by Dubreuil et al.[196].

Experiments conducted in shock tubes

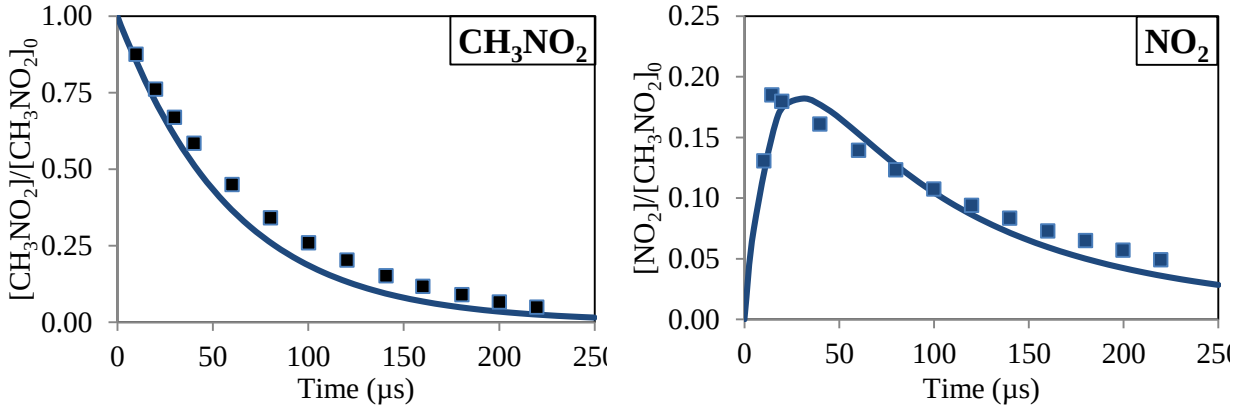

Figure A-8: Species profiles of CH_3NO_2 and NO_2 as a function of time. Experimental conditions: 5.95 atm, T = 1180 K. Symbols: experimental results. Lines: simulations results. Initial fuel mixture: 370 ppm CH_3NO_2 in Argon. Experiments conducted by Glänzer and Troe [197].

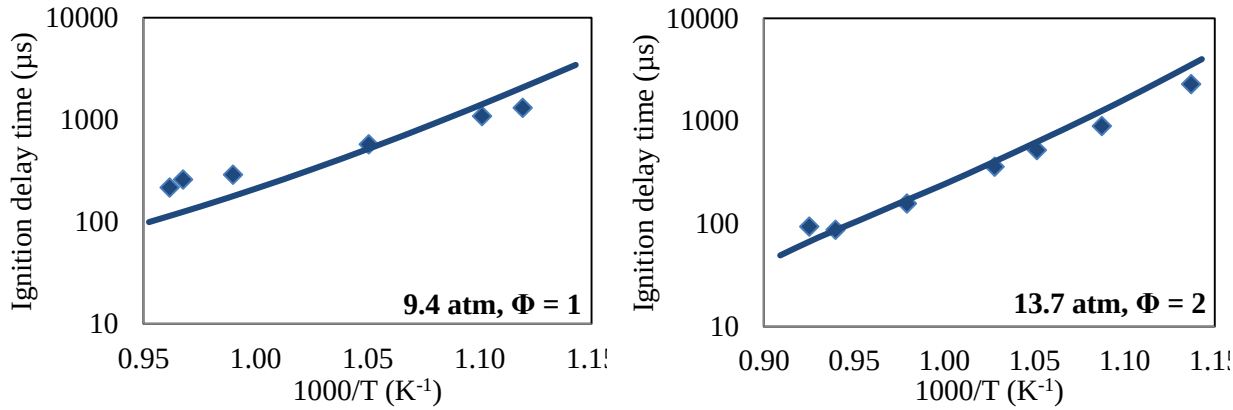

Figure A-9: Ignition delay time of nitromethane (CH_3NO_2) at different pressures and equivalence ratios. Symbols: experimental results. Lines: simulations results. Experiments conducted by Mathieu et al.[198].

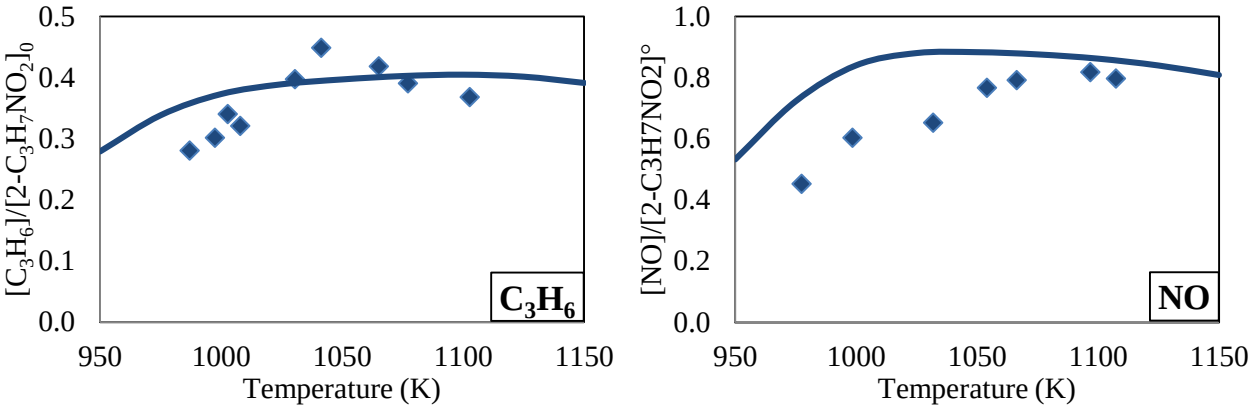

Figure A-10: Species profiles of C_3H_6 and NO as a function of temperature. Experimental conditions: 5 atm, reaction time: 1.3 ms. Symbols: experimental results. Lines: simulations results. Initial fuel mixture: 6500 ppm 2-nitropropane (2-$C_3H_7NO_2$) in Argon. Experiments conducted by Zhang et al.[165].

A2. Determination of condition of gas in a shock tube

In a shock tube, it is assumed that the gases are ideal, non-viscous, non-conductive and the wall effects are negligible. We can write the equations of conservation of mass (Eq.10), momentum (Eq.11) and energy (Eq.12) for a constant cross-section tube of gases passed by the incident shock wave as:

$$\rho_1 u_1 = \rho_2 u_2 \quad (Eq.10)$$

$$\rho_1 u_1^2 + P_1 = \rho_2 u_2^2 + P_2 \ (Eq.12)$$

$$\frac{1}{2}u_1^2 + H_1 = \frac{1}{2}u_2^2 + H_2 \ (Eq.13)$$

P, ρ, H, and u refer respectively to the pressure, the density, the enthalpy per unit of mass and the velocity of the gas linked to the shock front. Indexes 1 and 2 correspond to the front and back of the shock front. The Hugoniot equation (Eq. 14) which is a characteristic equation of a shock wave is then obtained:

$$H_2 - H_1 = \frac{1}{2}(P_2 - P_1)\left(\frac{1}{\rho_1} + \frac{1}{\rho_2}\right) \ (Eq.14)$$

In the case of an ideal gas, P=ρRT, the Hugoniot equation becomes:

$$H_2 - H_1 = \frac{R}{2}(\rho_2 T_2 - \rho_1 T_1)\left(\frac{1}{\rho_1} + \frac{1}{\rho_2}\right) \ (Eq.15)$$

A new parameter is introduced $\rho_{21} = \rho_2/\rho_1$. A solution of u_1 is obtained:

$$u_1 = \sqrt{\frac{R(\rho_{21}T_2 - T_1)}{1 - \frac{1}{\rho_{21}}}} \qquad (Eq.16)$$

By introducing the Mach number (M), which is the ratio of gas flow velocity to the speed of sound:

$$M_1 = \frac{u_1}{a_1} \ avec \ a = \sqrt{\gamma RT} \ et \ \gamma = \frac{c_p}{c_v}$$

We obtain the condition of gases linked to the shock front:

$$\rho_{21} = \frac{\rho_2}{\rho_1} = \frac{(\gamma+1)M_1^2}{(\gamma+1)M_1^2 + 2} \qquad (Eq.17)$$

$$\frac{P_2}{P_1} = \frac{2\gamma M_1^2 - (\gamma - 1)}{(\gamma + 1)} \qquad (Eq.18)$$

A3. Experimental results

Rapid compression machine experiments

Table A-1: Measured ignition delay time (IDT) of the neat surrogate fuel at P_c = 10 bar, Φ = 0,5 and 1 .

Φ = 1					
P_i (mbar)	**T_i (K)**	**Compression time (ms)**	**T_c (K)**	**1st-stage IDT (ms)**	**Main IDT (ms)**
0.612	333.15	33.0	670	44.5	48.8
0.612	353.15	33.9	710	10.0	16.8
0.380	328.15	34.7	745	4.3	13.8
0.360	353.15	31.8	790		17.8
0.227	323.15	33.2	830		16.9
0.227	338.15	31.8	855		20.5
0.227	353.15	32.7	885		16.2
0.227	368.15	32.2	915		15.6
0.227	393.15	32.7	960		9.0
Φ = 0.5					
P_i (mbar)	**T_i (K)**	**Compression time (ms)**	**T_c (K)**	**1st-stage IDT (ms)**	**Main IDT (ms)**
0.54	313.15	34.3	675	78.3	150.5
0.54	328.15	34.1	705	24.2	69.9
0.55	353.15	33.2	750	2.8	55.8
0.38	343.15	34.1	810		57.8
0.36	363.15	34.1	855		46.4
0.36	393.15	33.3	910		41.0
0.215	378.15	31.6	995		16.6

Table A-2: Measured ignition delay time (IDT) of the surrogate fuel doped with EHN at P_c = 10 bar, Φ = 0,5 and 1 .

Φ = 1							
				EHN 1% mol.		**EHN 0.1% mol.**	
P_i (mbar)	**T_i (K)**	**Compression time (ms)**	**T_c (K)**	**1st-stage IDT (ms)**	**Main IDT (ms)**	**1st-stage IDT (ms)**	**Main IDT (ms)**
0.612	333.15	33.0	670	4.6	9.6	18.1	22.9
0.612	353.15	33.9	710	1.5	5.7	4.2	9.7
0.380	328.15	34.7	745		-		-
0.360	353.15	31.8	790		2.8		10.5
0.227	323.15	33.2	830		2.1		9.1
0.227	338.15	31.8	855		-		7.4
0.227	353.15	32.7	885		-		4.8
0.227	368.15	32.2	915		-		4.4
0.227	393.15	32.7	960		-		-
Φ = 0.5							
				EHN 1% mol.		**EHN 0.1% mol.**	
P_i (mbar)	**T_i (K)**	**Compression time (ms)**	**T_c (K)**	**1st-stage IDT (ms)**	**Main IDT (ms)**	**1st-stage IDT (ms)**	**Main IDT (ms)**
0.54	313.15	34.3	675	15.80	64.90	38.5	91.77
0.54	328.15	34.1	705	3.13	37.17	10.2	52.93
0.55	353.15	33.2	750		22.07	1	37.67
0.38	343.15	34.1	810		13.20		36.37
0.36	363.15	34.1	855		5.60		22.57
0.36	393.15	33.3	910				12.63
0.215	378.15	31.6	995				4.03

Table A-3: Measured ignition delay time (IDT) of the surrogate fuel doped with ferrocene at P_c = 10 bar, Φ = 0,5 and 1.

Φ = 1							
				Ferrocene 0.1% mol.		**Ferrocene 0.01% mol.**	
P_i (mbar)	**T_i (K)**	**Compression time (ms)**	**T_c (K)**	**1st-stage IDT (ms)**	**Main IDT (ms)**	**1st-stage IDT (ms)**	**Main IDT (ms)**
0.612	333.15	33.0	670	49.2	53.1	45.8	49.4
0.612	353.15	33.9	710	9.3	17.1	7.9	13.7
0.380	328.15	34.7	745	3.6	17.1		13.6
0.360	353.15	31.8	790		24.1		17.9
0.227	323.15	33.2	830		40.6		24.0
0.227	353.15	32.7	885		35.4		18.4
0.227	368.15	32.2	915		45.9		21.2
0.227	393.15	32.7	960		36.0		14.5
Φ = 0.5							
				Ferrocene 0.1% mol.		**Ferrocene 0.01% mol.**	
P_i (mbar)	**T_i (K)**	**Compression time (ms)**	**T_c (K)**	**1st-stage IDT (ms)**	**Main IDT (ms)**	**1st-stage IDT (ms)**	**Main IDT (ms)**
0.54	328.15	34.1	705	26.0	102.8	26.0	77.1
0.55	353.15	33.2	750	4.3	76.2	3.3	65.6
0.38	343.15	34.1	810		89.6		57.7
0.36	363.15	34.1	855		114.7		55.8
0.36	393.15	33.3	910		118.9		48.9
0.215	378.15	31.6	995		-		25.5

Table A-4: Measured ignition delay time (IDT) of the surrogate fuel doped with 2,4-xylenol at P_c = 10 bar, Φ = 0,5 and 1 .

Φ = 1							
				2,4-xylenol 1% mol.		**2,4-xylenol 0.1% mol.**	
P_i (mbar)	**T_i (K)**	**Compression time (ms)**	**T_c (K)**	**1st-stage IDT (ms)**	**Main IDT (ms)**	**1st-stage IDT (ms)**	**Main IDT (ms)**
0.612	333.15	33.0	670	50.7	54.7	43.6	49.4
0.612	353.15	33.9	710	12.5	17.8	12.6	17.7
0.380	328.15	34.7	745	3.4	13.7	3.9	13.3
0.360	353.15	31.8	790		16.9		15.5
0.227	323.15	33.2	830		15.5		16.3
0.227	353.15	32.7	885		16.3		16.3
0.227	368.15	32.2	915		16.9		15.5
0.227	393.15	32.7	960		9.5		10.9
Φ = 0.5							
				2,4-xylenol 1% mol.		**2,4-xylenol 0.1% mol.**	
P_i (mbar)	**T_i (K)**	**Compression time (ms)**	**T_c (K)**	**1st-stage IDT (ms)**	**Main IDT (ms)**	**1st-stage IDT (ms)**	**Main IDT (ms)**
0.54	328.15	34.1	705	22.5	83.6	24.4	69.2
0.55	353.15	33.2	750	4.0	48.3	3.5	42.2
0.38	343.15	34.1	810		64.6		56.1
0.36	363.15	34.1	855		47.8		45.6
0.36	393.15	33.3	910		39.9		37.4
0.215	378.15	31.6	995		15.8		17.1

Shock tube experiments

Table A-5: Measured ignition delay time of the neat surrogate fuel at 10 atm, Φ = 1. The gas mixture composition is presented in Table 25.

P_5 (atm)	**T_5 (K)**	**Igniton delay time (µs)**
8.3	1345	299
10.1	1370	320
10.3	1374	363
10.3	1396	100
10.1	1401	176
10.3	1442	84
10.0	1450	57
10.4	1458	79
9.5	1507	19
9.8	1508	21
10.5	1520	34
10.8	1535	22
9.9	1569	11
9.9	1587	10

Table A-6: Measured ignition delay time of the surrogate fuel doped with EHN at 10 atm, Φ = 1. The gas mixture composition is presented in Table 29.

P_5 (atm)	T_5 (K)	Igniton delay time (µs)
9.9	1336	570
10.2	1370	264
10.4	1386	309
9.9	1431	82
10.9	1477	86
9.6	1551	16
10.1	1571	10
9.8	1587	9

Table A-7: Measured ignition delay time of the surrogate fuel doped with ferrocene at 10 atm, Φ = 1. The gas mixture composition is presented in Table 32.

P_5 (atm)	T_5 (K)	Igniton delay time (µs)
10.3	1382	328
10.6	1404	240
9.9	1415	160
10.5	1416	214
9.8	1426	76
9.8	1483	78
9.3	1528	23
9.7	1586	15
9.8	1612	6

Table A-8: Measured ignition delay time of the surrogate fuel doped with 2,4-xylenol at 10 atm, Φ = 1. The gas mixture composition is presented in Table 35.

P_5 (atm)	T_5 (K)	Igniton delay time (µs)
9.9	1338	465
10.1	1368	230
10.5	1404	197
10.0	1416	110
10.2	1457	74
10.1	1473	72
9.4	1524	30
10.0	1545	30
9.3	1549	40
9.4	1552	25

Heat flux burner experiments

Table A-9: Measured burning velocity of the neat and doped surrogate fuels at P = 1 atm and T_i = 398 K.

Equivalence ratio	Burning velocity (cm/s)			
	Neat surrogate	EHN 1% mass	Ferrocene 1% mass	2,4-Xylenol 1% mass
0.65	31.08	28.4	28.4	29.99
0.7	36.21	35.2	35.2	35.18
0.75	40.89	40.24	40.24	40.06
0.8	45.59	45.15	45.15	44.98
0.85	49.47	49.49	49.49	49.12
0.9	52.21	52.36	52.36	52.17
0.95	54.68	55.14	55.14	54.8
1	56.41	57.09	57.09	56.69
1.05	58.16	58.02	58.02	57.99
1.1	58.84	58.26	58.26	58.15
1.15	57.16	57.35	57.35	57.68
1.2	55.7	55.57	55.57	55.79
1.25	52.6	52.81	52.81	53.22
1.3	48.74	49.26	49.26	49.2
1.35	44.11	44.2	44.2	44.4
1.4	38.87	39.21	-	-
1.45	32.68	-	-	-

List of figures

List of tables

Study of additive's chemical structure effect on the control of fuel reactivity

Abstract

Modern societies require cleaner and more efficient internal combustion engines. This constraint has involved a significant evolution in the combustion systems and fuel formulation. Engine-fuel adequacy is the key item to be optimized to achieve this goal. Among adjustable parameters, the reactivity of the fuel is the most important characteristic to be considered. This leads to an increasing use of additives that allows fuel to meet various combustion requirements. However, the design and the use of additives still faces a lack of comprehension regarding their effect. In this context, this thesis aims to better understand the chemical effect of additives on the fuel gas-phase reactivity. Three additives including a cetane booster, an octane booster, and a free radical scavenger are considered: 2-ethylhexyl nitrate, ferrocene, and 2,4-xylenol, respectively. The chemical effect of these additives on the reactivity of a surrogate fuel containing 35% *n*-heptane and 65% toluene by volume was experimentally and numerically investigated. Experiments were conducted in three devices: a shock tube, a rapid compression machine, and a heat flux burner. The use of these experimental devices allows to explore the reactivity over a wide range of engine-relevant conditions. For simulations, a detailed kinetic model was developed based on recent literature data. The satisfactory agreement between experiments and simulations enables to propose several hypothesis regarding the chemical effect of the additives.

Keywords: Fuel additives, 2-ethylhexyl nitrate, ferrocene, nitrogen oxides chemistry, low temperature combustion, kinetic modelling.

Etude de l'influence de la structure chimique des additifs sur le contrôle de la réactivité des carburants

Résumé

Les sociétés modernes ont besoin de moteurs à combustion interne plus propres et plus efficaces. Cette contrainte entraîne une évolution significative des systèmes de combustion et de la formulation de carburants. L'adéquation moteur-carburant est l'élément clé à optimiser pour atteindre cet objectif. Parmi les paramètres en jeu, la réactivité du carburant est une caractéristique de premier ordre. C'est l'une des raisons en lien avec l'utilisation des additifs. Ils permettent au carburant d'améliorer l'ensemble de ses propriétés notamment vis-à-vis de la combustion. Cependant, le choix et l'utilisation des additifs se heurte encore à un manque de compréhension de leur mécanisme d'action. Dans ce contexte, cette thèse vise à mieux comprendre l'effet chimique des additifs sur la réactivité dans la phase gazeuse. Trois additifs, dont un booster de cétane, un booster d'octane et un antioxydant sont considérés : le 2-ethylhexyl nitrate (EHN), le ferrocène et le 2,4 xylénol respectivement. L'effet chimique de ces additifs sur la réactivité d'un carburant modèle contenant 35 % de *n*-heptane et 65 % de toluène en volume a fait l'objet d'une étude expérimentale et numérique. Des expériences ont été menées à l'aide de trois équipements : un tube de choc, une machine de compression rapide et un brûleur à flamme plate. L'utilisation de ces équipements permet d'explorer la variation de la réactivité dans des conditions variables représentatives du fonctionnement des moteurs. En parallèle, un modèle cinétique détaillé a été élaboré en s'appuyant sur des données récentes de la littérature. L'accord satisfaisant entre les expériences et les simulations permet de proposer des hypothèses quant à l'effet chimique des additifs.

Mots clés : Additifs pour carburant, 2-ethylhexyl nitrate, ferrocène, chimie de l'oxydes d'azote, combustion à basse température, modélisation cinétique.